

THE ROLE OF RHOE IN REGULATING GLIOBLASTOMA

by

MAIHAFIZAH BINTI MOHD ZAHARI

A thesis submitted to

The University of Birmingham

for the degree of

DOCTOR OF PHILOSOPHY

School of Biosciences

College of Life and Environmental Sciences

The University of Birmingham

July 2018

UNIVERSITY OF
BIRMINGHAM

University of Birmingham Research Archive

e-theses repository

This unpublished thesis/dissertation is copyright of the author and/or third parties. The intellectual property rights of the author or third parties in respect of this work are as defined by The Copyright Designs and Patents Act 1988 or as modified by any successor legislation.

Any use made of information contained in this thesis/dissertation must be in accordance with that legislation and must be properly acknowledged. Further distribution or reproduction in any format is prohibited without the permission of the copyright holder.

ABSTRACT

Glioblastoma is a malignant form of brain cancer. This type of tumour is resistant to medical treatment and often yields a poor prognosis. It is important to understand the molecular basis of glioblastoma for developing new therapies. This study used U87 human glioblastoma cells for the investigation. The glioma cell line displayed the hallmarks of a tumour cell and corresponded on various cellular functions that are regulated by Rho family GTPases. This study intended to analyse the role of one member from this family - RhoE in U87 cells. RNA interference (RNAi) method was applied to knock down RhoE. The result showed that the loss of RhoE expression is associated with the decrease in cell cycle progression and increase apoptosis in U87 cells. Endogenous RhoE was found localised to the nucleus in U87 cells. RhoE is known can interact with serine/threonine kinases called ROCK1 and PKC α . The application of RNAi that knocks down ROCK1 has led to the stabilisation of RhoE expression in U87 cells. Y27632 was used to inhibit ROCK1 whereas Gö6976 blocked the function of PKC α . Both pharmacological inhibitors prevent individual interaction with RhoE. The activation of novel PKC α by PMA exhibit an increased the upper band of RhoE (29kD) and it remains more in the nucleus consistent with the active conventional PKC during ROCK1 inhibition. A co-immunoprecipitation (Co-IP) technique was used to pull down FLAG-RhoE from the transfected U87 cells with wild-type construct. As a result, the translocation of RhoE to the nucleus was facilitated by the interaction with importin β (Imp β). A bioinformatics study on protein-protein interactions using DAVID on mass spectrometry data elucidated that RhoE could be indirectly bound to nuclear proteins. In conclusion, RhoE plays a pivotal role in regulating glioblastoma at the post-translational level.

DEDICATION

This thesis is dedicated to my late mother - Jawishah binti Itam Serah who kept praying for my success whilst she still alive, my beloved sister Mairazilla binti Mohd Zahari who consistently offers emotional support and my husband - Abul 'As bin Abdul Raffar, who is faithful and loves me unconditionally. These remarkable people have devoted themselves to provide me with the opportunity to study abroad. They had persistently stayed by my side through good and bad time, just to ensure that I survive this ordeal and gain this invaluable life experience!

ACKNOWLEDGEMENT

This research project was supported by the Ministry of Health Malaysia together with the Federal Training Reward Scheme – Biochemist with a fully paid salary (HLP-CBBP). It is impossible to complete this work without the enormous help and guidance from numerous individuals at University of Birmingham, including School of Biosciences and Institute for Biomedical Research (IBR), School of Medicine, College of Medical and Dental Sciences. I would like to specifically acknowledge Professor John K. Heath, Susan Brewer and Dr Mellisa Grant who kindly allowed me to use most of the equipment, chemicals and sometimes some tissue culture reagents in the laboratory on the 5th Floor, Tower, School of Biosciences to accomplish my laboratory work.

Second, I would also like acknowledge Professor Roy Bicknell and Professor Francesco Falciani in allowing me to visit their lab in IBR to obtain the U87 human glioblastoma cells that are mainly used in most of my research work. Besides that, I would love to thank Sarah Durant, who guided me on the protocols of RNA interference (RNAi), immunoprecipitation and microarray. It will be impossible for me to perform the mass spectrometry sample preparation, analysis and sequencing of the peptide without the generous help from Cleidi and Debbie, who patiently answered my endless questions.

I am also grateful for receiving generous ideas in relation to the upgrade of experimental design on nuclear and chromatin-bound protein preparation from Tijs and Trushar. I also appreciated Kamil and Wei Zheng help in introducing useful software like Image J. Besides, I give credit to Nicola for her initial guide on epifluorescence microscope as well as Shrikant Johndale, Jenson Lim and Lizzie for their guidance on confocal laser

scanning microscope handling. I also received tremendous help from Sylwia, Byron, Akilu and Izabel for protocol refining on immunostaining as well as microscopic data extraction and interpretation. I would also like to thank Byron for his patience and generosity in sharing his opinion and continuously helping me to improve my presentation skills.

My deepest appreciation then goes to my main Ph.D. supervisor – Dr Neil A. Hocthin, who has provided me with strong support and guidance throughout my study. I have spent nearly eight years working with him, and he has provided me with all the opportunities to develop myself in different aspects. He has also convinced and inspired me to become an independent researcher. I would never imagine myself to progress this far without his support. I also want express my gratitude to Professor Dr. Kevin Chipman, who is my second supervisor, for his guidance and support throughout my PhD study for the countless discussions and invaluable advices for each project including his suggestion to proofread my thesis.

I am indebted to all my friends who have supported me during these four years. It is impossible to acknowledge everyone that has contributed to my joyful life in Birmingham. Nevertheless, I would like to particularly acknowledge Nurul Iman, Mei Ann Lim, Gloria and Katherine, who have always been there for me on sharing every moment of my life for both happy and sad. Thank you for the great friendship! I am also grateful to Nick, Muhammad, Hong Yang, Shabana, Roy and Adil for their care, encouragements and motivation. I hope that our friendship will last beyond the duration of this study. I would also like to thank all the members at the 5th and 6th Floor, Tower, School of Biosciences for their kindness during my stay there.

TABLE OF CONTENT

THE ROLE OF RHOE IN REGULATING GLIOBLASTOMA	i
ABSTRACT	iii
DEDICATION	iv
ACKNOWLEDGEMENT	v
TABLE OF CONTENT	vii
LIST OF FIGURES	xv
LIST OF TABLES	xxix
LIST OF ABBREVIATIONS	xxx
CHAPTER 1	1
INTRODUCTION AND LITERATURE REVIEW	1
1.1 Research Background.....	1
1.2 Glioma.....	3
1.3 Small GTPases	8
1.3.1 Rho GTPase Family	8
1.3.1.1 Subfamily of Rho GTPase.....	8
1.3.1.2 Regulators of Small GTPases	11

1.3.1.3	Effector Molecules of Rho GTPases	14
1.3.2	The Role of Rho GTPases in Mammalian Cells	18
1.3.2.1	Rho GTPases in Cell Cycle.....	18
1.3.2.2	Rho GTPases in Apoptosis	22
1.3.2.3	Rho GTPases in Cancer	25
1.3.3	Small GTPase in Nucleocytoplasmic Transport.....	28
1.4	RhoE/Rnd3	33
1.4.1	Definition, Structure and Characteristics of RhoE.....	33
1.4.2	Function of RhoE	37
1.4.2.1	RhoE in Reorganisation of Actin and Stress Fibre.....	37
1.4.2.2	RhoE and Cell Cycle Progression	38
1.4.2.3	RhoE in Cell Differentiation	42
1.4.3	Regulation of RhoE	42
1.4.3.1	Regulation of RhoE at Transcriptional Level	42
1.4.3.2	Regulation of RhoE via Phosphorylation for Stabilisation.....	44
1.4.3.3	RhoE Is Not Regulated by ROCK2.....	51
1.4.3.4	Regulation of RhoE via Farnesylation to Induce Translocation	52

1.4.3.5 Regulation of RhoE via Ubiquitination to Promote Proteosomal Degradation	57
1.4.4 RhoE in Cancer.....	57
1.5 The Aim of This Project.....	59
CHAPTER 2	62
MATERIALS AND METHODS	62
2.1 Materials	62
2.1.1 General Laboratory Reagents	62
2.1.2 Media and Other Reagents for Cell Culture	62
2.1.3 DNA Constructs	63
2.1.4 Primers.....	63
2.1.5 Antibodies.....	67
2.2 Methods	70
2.2.1 General Laboratory Procedure.....	70
2.2.1.1 Cell Culture	70
2.2.1.2 Cell Lysis	71
2.2.1.3 Purification of Plasmid DNA.....	71

2.2.1.4	Quantification of DNA Concentration	72
2.2.1.5	Western Blotting	72
2.2.1.6	Immunoblotting.....	72
2.2.1.7	Image Scanning.....	75
2.2.1.8	Densitometry Analysis	75
2.2.1.9	Preparation of Glass Cover Slips for Cell Culture	75
2.2.1.10	Fixation of U87 Human Glioblastoma Cell Lines on Coverslips.....	76
2.2.1.11	Permeabilisation	76
2.2.1.12	Immunofluorescence Staining.....	76
2.2.1.13	Immunofluorescence Staining for FLAG and Confocal Microscopy	77
2.2.2	Experimental Design	78
2.2.2.1	RNAi Transfection for Knocking Down RhoE	78
2.2.2.2	Bromodeoxyuridine (BrdU) Uptake	80
2.2.2.3	Optimisation of Apoptosis Assay	80
2.2.2.4	Translocation of RhoE to the Nucleus by the Effect of Serine/ Threonine Kinase.....	83
2.2.2.5	Localisation of RhoE in U87 Cells via Export-import Mechanism.....	85

2.2.2.6 Transient Transfection of RhoE Constructs into U87 Cells	86
2.2.2.7 Immunoprecipitation Followed by Mass Spectrometry Analysis.....	87
2.2.2.8 Bioinformatics Analysis on The List of Genes Found from RhoE Pulled-down Assay	87
2.3 Statistical analysis	88
CHAPTER 3	89
RHOE REGULATES CELL CYCLE AND APOPTOSIS IN U87 HUMAN GLIOBLASTOMA CELLS	89
3.1 Introduction	89
3.2 Results	91
3.2.1 RhoE Regulates the Cell Cycle of U87 Cells.....	91
3.2.2 RhoE Regulates Apoptosis in U87 Cells.....	95
3.2.3 RhoE Regulates Apoptosis but Independent ROCK1	98
3.2.4 RhoE is Essential in Attenuating Genotoxic Stress in Glioma.....	107
3.3 Discussion.....	113
CHAPTER 4.....	117
LOCALISATION OF RHOE TO THE NUCLEUS OF U87 CELLS IS INDEPENDENT ROCK1	117

4.1 Introduction.....	117
4.2 Results	119
4.2.1 The Localisation of Endogenous RhoE to the Nucleus of Glioblastoma..	119
4.2.2 Confirmation of Endogenous RhoE Localisation to the Nucleus of U87 Cells.....	124
4.2.3 The Expression of RhoE in the Nucleus of U87 cells is ROCK1 Independent	127
4.2.4 ROCK1 Interaction is Not Solely Required for Nuclear Localisation of RhoE.....	132
4.2.5 Localisation of RhoE to the Nucleus is Alternatively Dependent on PKC α	134
4.2.6 Nucleocytoplasmic Transport is Essential for the Localisation of RhoE.....	142
4.3 Discussion.....	153
CHAPTER 5.....	159
IDENTIFICATION OF NOVEL RHOE INTERACTING PROTEINS.....	159
5.1 Introduction.....	159
5.2 Results	162
5.2.1 Overexpressed RhoE in the U87 Cells.....	162

5.2.2	Confocal Analysis Confirmed RhoE Localised to the Nucleus of U87 Cells.....	168
5.2.3	Bioinformatics Analysis on RhoE Pull-Down Assay.....	171
5.2.3.1	Immunoprecipitation Followed by Mass-Spectrometry Analysis	171
5.2.3.2	Manipulating Bioinformatics Tools to Identify Novel RhoE Binding Partners.....	174
5.2.4	RhoE Involves in DNA Replication of U87 Glioblastoma Cells	184
5.3	Discussion.....	189
CHAPTER 6.....		193
CONCLUDING REMARKS AND FUTURE DIRECTIONS		193
6.1	Conclusion.....	193
6.2	Model Postulation on the Role of RhoE in Glioblastoma	196
6.3	Suggestions for Future Work.....	199
6.3.1	Microarray Analysis of RhoE Function in U87 Human Glioblastoma Cell Line.....	199
6.3.2	Phosphorylation Status of RhoE.....	200
6.2.4	Chromatin Immunoprecipitation (ChIP) of RhoE with DNA Helicase Protein.....	201

APPENDIX 1	202
SEQUENCE AND ALIGNMENT OF PLASMID RhoEWT (TRANSFECTED INTO 293T/U87 CELLS)	202
APPENDIX 2	207
SEQUENCE AND ALIGNMENT OF EMPTY VECTOR PLASMID (TRANSFECTED INTO 293T/U87 CELLS).....	207
APPENDIX 3	213
PHOSPHORYLATION SITES PREDICTED IN RHOE.....	213
APPENDIX 4	215
NUCLEAR EXPORT SIGNAL (NES) PREDICTED IN RHOE.....	215
APPENDIX 5	216
NUCLEAR LOCALISATION SIGNAL (NLS) PREDICTED IN RHOE.....	216
APPENDIX 6	217
LIST OF GENES FROM RHOE PULL DOWN ASSAY	217
REFERENCES.....	232

LIST OF FIGURES

Figure 1: Immunohistochemistry (IHCC) of cells from the lesion tissue compared to the normal brain cells. (A) Glioblastoma showing extensive proliferation; (B) Normal brain tissue; (C) GBM cross section. Images are reproduced from College of American Pathologists (2011) and Sathornsumetee et al. (2007).....	7
Figure 2: The Rho phylogeny of 20 members of Rho proteins and the presence of eight subgroups that are distributed into four distinct clusters using ClustalX Neighbour-Joining (NJ) and ProMaximum-Likelihood (ML). The numbers that appeared in primary and secondary branches show the bootstrap repetition of NJ values. This chart is reproduced from Boureux et al. (2007).....	10
Figure 3: The Rho GTPase cycle. The cycling of Rho GTPase between inactive GDP-bound and active-GTP bound states. Table 1 shows the examples of downstream effector of the Rho family.....	13
Figure 4: Activated Rho binding to ROCK or caspase cleavage in response to genotoxic stress to activate the kinase (Adapted from Coleman and Olson 2002; Croft and Olson 2011).....	24
Figure 5: Rho GTPases and major function in tumour that is relevant at cellular and molecular level. (Adapted from Karlsson et al. 2009; Senoo and Iijima 2013).	26

Figure 6: Nuclear transporters (importin and exportin) through nuclear pore complex (NPC) and facilitated via GTP hydrolysis by Ran. The blue arrows show different localisation of Ran-GTP in the nucleus and Ran-GDP in the cytosol (Adapted from Alberts et al. 2008).30

Figure 7: The high-resolution structure of RhoE in human (pdb: 1M7B) was visualised in PyMOL Molecular Visualisation and it was retrieved in a PNG file format. RhoE consists of six (6) β -sheet strands (five parallel, one antiparallel) that are surrounded by five (5) α -helices connected by a loop and an insert helix.....34

Figure 8: The sequence of RhoE protein established in FASTA format (UniProt, 2011), RhoE is structurally different than RhoA due to the different coordination of GTP for GTP binding site that allows contact between additional water molecule to invariant Ala¹⁷⁹ of the ¹⁷⁷CSAL-motive as well as carbonyl oxygen of the base. Additional stabilisation of RhoE by Asp¹⁰³ is at the Lys¹³⁶ of the ¹³⁵CKSD-motive whereas RhoA is at the Ser⁸⁵36

Figure 9: The schematic diagram on the regulation of cell cycle progression by RhoE. Phosphatase PP2A dephosphorylates 4EBP1. The presence of RhoE deactivates the extracellular signal-regulated kinase (ERK) pathway. Sequentially, eIF4A blocks protein kinase; mamalian target of rapamycin (mTOR) from phosphorylating 4EBP1, as well as ruling out its binding to 4EBP1. RhoE reduces 4EBP1 phosphorylation and prevents eIF4E from inducing the translations of genes that are required for cell cycle progression and stop at G₁ phase (Adapted from Riou et al. 2010).40

Figure 10: RhoE regulates the cell cycle progression in normal cell type by blocking the cell cycle progression at either G₁/S or G₂/M phases. Cyclin D1 and its kinase partners, CDK4 and CDK6, are consistently decrease in the presence of RhoE. The cell cycle regulator, Cyclin D1,

in associating either CDK4 or CDK6 is required for the S-phase entry to mediate the phosphorylation of pocket proteins (e.g.: retinoblastoma, pRb). The presence of RhoE also attenuates E2F transcription factors and sequentially prevents the translational activity of CDKs. However, information regarding the rest of cell cycle regulators (Cyclin A and E that associate with CDK2 or Cyclin B that associates with CDK1) that are relevant to RhoE is quite limited. (Adapted from Kolupaeva and Janssens 2012).....41

Figure 11: The schematic diagram shows the seven phosphorylation sites on RhoE. ROCK1 phosphorylates one site on threonine (Thr²¹⁴) and six sites on serine residues (Ser⁷, Ser¹¹, Ser²¹⁰, Ser²¹⁸, Ser²²², Ser²⁴⁰) that are located in the N- and C-termini regions, outside the core-GTP-binding domain in RhoE. (Adapted from Riento et al. 2005b; Riou et al. 2013)..... 45

Figure 12: The high-resolution structure of RhoE in complex with the ROCK1 kinase domain. The structure of dimerisation domain between RhoE-ROCK1 and ROCK1-RhoE is visualised by Protein Data Bank (pdb: 2V55) using - PyMOL Molecular Visualisation and that can be retrieved in PNG file format. Each subunit of the ROCK1 dimer binds with one molecule of RhoE.47

Figure 13: A diagram for the flow of interaction between ROCK1 and RhoE. **(A)** Molecular structure of ROCK1 comprised a sequence of kinase domain that is located at the amino terminus of the protein, followed by a coiled-coil region containing the Rho Binding Domain (RBD) and a Plextrin Homology domain (PH) with a cysteine-rich domain (CRD). **(B)** ROCK1 is activated when it interacts with RhoA bound GTP. **(C)** ROCK1 is inactivated when it interacts with RhoE, particularly when C-terminus of ROCK binds to the N-terminal region of the kinase, forming autoinhibitory loop. (Adapted from Loirand et al. 2006; Chen et al. 2010; Tu et al. 2011).....50

Figure 14: The high-resolution structure of 14-3-3 (pdb: 4BG6) interaction with prenyl-phosphorylation motif that upstream to the residues 232-241 of the CAAX box. Crystal structure of 14-3-3 (zeta/delta) indicated by homodimers of blue helices. The farnesylated peptide (olive stick – KDKAK) bound to each 14-3-3 monomer at Cys²⁴¹ and anchor residue that is indicated by red stick. The homodimers of 14-3-3 at diagonal position are visualised to expose the farnesylated peptide in RhoE..... 54

Figure 15: The interaction of RhoE with ROCK1 and PKC and post-translational modification via farnesylation. 14-3-3 inhibits RhoE-induced cell rounding by translocating it from the plasma membrane to the cytosol and facilitated via phosphorylation of RhoE at Ser²¹⁸ and Ser²⁴⁰ by ROCK1 and Ser²¹⁰ by protein kinase C (PKC). (Adapted from Riou et al. 2013). .. 56

Figure 16: The map of the mammalian expression vector-pCMV5 that was predicted to have RhoE construct in between *EcoRI* and *HindIII* (highlighted in blue). The position of the nearest primers namely CMV_fwd_primer and pCEP_fwd_primer are highlighted in yellow. These primers are mapped adjacent to the multiple cloning sites (MCS) (Adapted from Brewer 2011; Chubet and Brizzard 1996; Riento et al. 2003). 65

Figure 17: Knock down RhoE of U87 cells using oligo RhoE A (**A**) and oligo RhoE B (**B**) in comparison with control oligo (non-silencing control) over time. The depletion of RhoE was prolonged until at least 96 h. 79

Figure 18: Schematic diagram of optimised apoptosis experiment indicating critical time for the addition (+) of apoptotic inducer (cisplatin) and ROCK inhibitor (Y-27632). 82

Figure 19: Schematic diagram for the procedure of investigating the translocation of RhoE to the nucleus using pharmacological compound - ROCK inhibitor (Y27632), PKC inhibitor

(Gö6976) and novel PKC activator (PMA). The verification of the experiment was determined by the localisation of endogenous RhoE in U87 cells in the control condition. ... 84

Figure 20: Less cell number entered S-phase indicated by the green fluorescence of BrdU in RhoE depleted U87 cells (RhoE oligos, A and B) compared to the cells with the presence of RhoE (Control oligo). The cell nuclei were stained with DAPI where the same field is observed for BrdU uptake. The images represent the three separate experiments ($n = 3$)..... 93

Figure 21: The loss of RhoE expression in U87 cells has resulted in the decreased number of cells entering the S-phase. The percentage of U87 cells in S-phase was analysed and the mean values are presented. The error bars show the standard error of the mean (S.E.M) for each datasets of three separate experiments ($n = 3$), where 250 cells were counted in each of the three coverslips. The differences are significant between the silencing RhoE and control oligo (*) ($p < 0.05$). The statistical analysis was performed using ANOVA single factor..... 94

Figure 22: Preliminary results on apoptosis show that RhoE depleted U87 cells are more sensitive to cisplatin. There is no result of RhoE blot for the condition without cisplatin due to shortage of sample. For the condition with cisplatin treatment, RhoE was almost entirely depleted using RhoE oligo B whereas RhoE oligo A reached approximately quarter knockdown. 97

Figure 23: The occurrence of apoptosis was detected based on the intrinsic pathway, where caspase 9 functions as the initiator of caspase cascade; and caspase 3 for the execution phase of caspase cascade. 102

Figure 24: The densitometry analysis of late-stage apoptotic marker (execution pathway); the caspase 3 using Image J. (A) Semi-quantitative analysis to compare full-length caspase 3

between siRhoE and NSiC when increasing the concentration of cisplatin with and without the presence of ROCK inhibitor, Y27632. There were no significant difference for the full length caspase 3 (ns) ($p > 0.05$); except during the titration of 0Y50C and 5Y50C (**) ($0.001 < p < 0.01$). The siRhoE was severely affected by cisplatin though in the presence of Y27632 for the titration 5Y50C if compared to 5Y25C (**) ($0.001 < p < 0.01$).

(B) Semi-quantitative analysis to compare cleaved caspase 3 between siRhoE and the NSiC when increasing the concentration of cisplatin with and without the presence of ROCK inhibitor, Y27632. The difference between NSiC and siRhoE as well as the increased concentration of cisplatin compared to without cisplatin were considered statistically significant for cleaved caspase 3 with (****) $p < 0.0001$. These data are representatives for three separate experiments ($n = 3$)..... 106

Figure 25: RhoE is essential in attenuating genotoxic stress in glioma. RhoE also reflects the stability of ROCK1 expression at 160 kD in control condition. Cisplatin could induce the expression of RhoE in U87 cells but it did not happen in RhoE knockdown condition. The ROCK1 blot in RhoE knockdown condition presented with smaller molecular weight at approximately 130 kD that represents the caspase-cleaved form of ROCK1..... 109

Figure 26: The evaluation of nuclear condensation in U87 cells with the presence of RhoE (NSiC) and in RhoE depleted U87 cells (siRhoE). The U87 cells were observed under DAPI fluorescence and the percentage (%) of condensed nuclei was calculated by counting the number of cells that appeared condensed at the nucleus, which is then divided by the total number of cells grown on coverslips. The difference between NSiC and siRhoE were considered statistically significant for condensed nuclei, since (*) $p < 0.05$ or (**) $p < 0.01$. These data are representatives for three separate experiments ($n = 3$)..... 111

Figure 27: Localisation of endogenous RhoE in U87 cells. U87 cells were lysed in a buffer containing Nonidet P-40. Nuclear and cytoplasmic fractions were prepared, separated by SDS-PAGE and immunoblotted with an antibody against RhoE. The effective isolation of nuclear and cytoplasmic fractions was confirmed using antibodies against Lamin A/C and α -tubulin respectively. These blots represent the results of three separate experiments ($n = 3$)..... 120

Figure 28: The relative distribution of endogenous RhoE in U87 cells. A semi-quantitative analysis was conducted using Image J to quantify the RhoE intensity for the blot in Figure 4.1. It was also used to determine the distribution of the different forms of RhoE (27 kD and 29 kD). A statistical analysis was done on paired datasets (29kD and 27 kD) of each fraction using Welch Two Sample t -test. These data represent results for the three separate experiments ($n = 3$), and the difference are significant with the p value is below than 0.05 (*) ($p < 0.05$). Error bars indicate the standard error of the mean (S.E.M) and they are shown alongside the histogram of each mean value..... 121

Figure 29: Localisation of RhoE in multiple types of cell lines. Each cell lines were lysed in a buffer containing Nonidet P-40. Then, nuclear and cytoplasmic fractions were prepared, separated by SDS-PAGE and immunoblotted with an antibody against RhoE. An effective isolation of nuclear and cytoplasmic fractions was confirmed using antibodies against Lamin A/C and α -tubulin respectively. Glioma Type 11 and 21 are cell lines that represent brain tumour at Stage IV, whereas HaCaT represents normal cell type..... 123

Figure 30: The localisation of endogenous RhoE to the nucleus of U87 cells was confirmed using RNAi. U87 cells were knockdown for 48 h and cells were harvested from the 6 wells plate. U87 cells were lysed in buffer containing Nonidet P-40. Next, nuclear and cytoplasmic

fractions were prepared, separated by SDS-PAGE and immunoblotted with an antibody against RhoE. An effective isolation of nuclear and cytoplasmic fractions was confirmed using antibodies against α -tubulin. These blots represent the results of three (3) separate experiments ($n = 3$)..... 125

Figure 31: Immunostaining of U87 cells (A) U87 cell of non-silencing control using control oligo, (B) RhoE depleted U87 cells using RhoE oligo A (C) RhoE depleted U87 cells using RhoE oligo B. U87 cells were cultured for 24h on coverslips and observed under epifluorescence microscope at 40 x magnification. (a) U87 cells staining for F-actin observed at 900 ms exposure under Texas Red isothiocyanate (TRITC) filter (b) U87 cells staining for nuclear observed at 100 ms exposure under DAPI filter (c) U87 cells staining for Rnd3/RhoE observed at 400 ms exposure under FITC filter (d) U87 cells' merged image of three (3) different fluorescence filters (TRITC/DAPI/FITC). 126

Figure 32: The localisation of RhoE to the nucleus is not regulated by ROCK1. U87 cells were lysed in a buffer containing Nonidet P-40. Next, nuclear and cytoplasmic fractions were prepared, separated by SDS-PAGE, and immunoblotted with an antibody against RhoE. The effective isolation of nuclear and cytoplasmic fractions was confirmed using antibodies against SSRPI and α -tubulin, respectively..... 129

Figure 33: The acceleration of 29 kD RhoE in the nuclear proportionate to 27 kD of RhoE in cytoplasm were observed in ROCK1 depleted U87 cells. The densitometry of RhoE using Image J in ROCK1 depleted U87 cells using both oligos were compared to the control condition. The intensity unit for nuclear and cytoplasmic RhoE from each condition is arbitrary and it was respectively normalised either to SSRPI or to α -tubulin as the loading control. Error bars indicate standard error of the mean (S.E.M) of each data set according to

U87 cells conditions. This study employed statistical analysis using Tukey Kramer procedure on one factor ANOVA for the whole dataset from four replicated independent experiments ($n = 4$) ($p < 0.01$). 130

Figure 34: Immunostaining of U87 cells show the interaction of ROCK1 is not solely required for the RhoE localisation to the nucleus. (A) U87 cell of non-silencing control (NSiC) using control oligo, (B) ROCK1 depleted U87 cells (siROCK1) using ROCK1 oligo 7. U87 cells were cultured for 48h on coverslips and observed under epifluorescence microscope at 40 x magnification. (a) U87 cells staining for F-actin observed at 900 ms exposure under Texas Red iso-thiocyanate (TRITC) filter (b) U87 cells staining for nuclear observed at 100 ms exposure under DAPI filter (c) U87 cells staining for RhoE observed at 400 ms exposure under FITC filter (d) Merged image of U87 cells at three different fluorescence filters (TRITC/DAPI/FITC). 133

Figure 35: Localisation RhoE to the nucleus is alternatively dependent on PKC α without the assistance of ROCK1. RhoE (29kD) almost completely lost from the nucleus by the stimulation of conventional PKC α with or without RhoE interaction to ROCK1. A clean separation of the nuclear RhoE from the cytoplasm was confirmed based on the empty α -tubulin blot and the appearance of each individual band at the SSRPI blot. Y27632 used to inhibit the interaction of ROCK1 to RhoE, enabled individual interaction with PKC α . Gö6976 prevented the interaction of PKC α to RhoE, allowed a sole interaction with ROCK. 136

Figure 36: Histogram of nuclear RhoE intensity according to the treatment of pharmacological inhibitor in U87 cells. RhoE almost completely lost from the nucleus by the stimulation of conventional PKC α with or without RhoE interaction to ROCK1. The activation of novel PKC α by PMA exhibit an increased the upper band of RhoE (29kD) and it

remains more in the nucleus consistent with the active conventional PKC during ROCK1 inhibition. The intensity unit for nuclear RhoE (29 kD) from each condition was normalised to SSRPI as the nuclear loading control. The RhoE intensity was compared between U87 cells treated with pharmacological inhibitors, (+) Y27632 or/and (+) Gö6976 for 3 h (▨) and the activation of PKC with the addition of PMA in U87 cells (□). The statistical analysis for two factor ANOVA with replication involving multiple comparisons uses Tukey's HSD procedure to identify the difference within the whole datasets of three independent experiment ($n = 3$) (****) ($p < 0.0001$)..... 137

Figure 37: Immunoblot of cytoplasmic fraction of U87 cells post 24 h culture. Cells were treated with pharmacological inhibitors either ROCK1 or/and PKC α using Y27632 (10 μ M) and Gö6976 (2.5 μ M) for 3 h. Then, the activation of PKC was applied using PMA (100 nM) for 15 min. U87 cells were lysed in a buffer containing Nonidet P-40. Then, nuclear and cytoplasmic fractions were prepared, separated by SDS-PAGE and immunoblotted with an antibody against Rnd3/RhoE. α -tubulin blot detected at 55 kD is a loading control for cytoplasm that represents equal protein loaded for each sample from the cytoplasmic fraction. A clean separation of the cytoplasm is shown from the empty SSRPI blot..... 138

Figure 38: (A) Data presents the mean of cytoplasmic RhoE intensity as determined from triplicate experiment ($n = 3$) of western blotting of the cytoplasm. The intensity unit of cytoplasmic RhoE (29 and 27 kD) was normalised to α -tubulin as the loading control. The RhoE intensity was compared between U87 cells treated with pharmacological inhibitors, (+) Y27632 or/and (+) Gö6976 for 3 h (▨) and the activation PKC with the addition of PMA in U87 cells (□). A statistical analysis using two factor ANOVA with replication involving

multiple comparisons uses Tukey's HSD procedure to identify the difference within the whole datasets of three independent experiment ($n = 3$)..... 139

Figure 39: NES predicted in human RhoE (pdb: 1M7B) is visualised at different orientations. The high resolution structure of RhoE that appears with the NES was visualised in PyMOL Molecular Visualisation and retrieved in PNG file format. The predicted NES (TQRIEL⁷³SL⁷⁵) in RhoE was indicated with labelled of amino acids, and the position in 3D is visualised at different directions. (A) NES sequence view at vertical axis (B) NES sequence view at diagonal direction (C) NES sequence view at skew position. 144

Figure 40: The RhoE expression in U87 cells is unaffected by the inhibition of NES. After 6 h treatment with the increased concentration of Leptomycin B (LepB) (0.0-15.0 nM), U87 cells were lysed in a buffer containing Nonidet P-40. Nuclear and cytoplasmic fractions were prepared, separated by SDS-PAGE and immunoblotted with an antibody against Rnd3/RhoE. The effective isolation of nuclear and cytoplasmic fractions was confirmed using antibodies against SSRPI and α -tubulin respectively. These blots represent the result of only a single experiments ($n = 1$)..... 148

Figure 41: Overexpressed RhoE in U87 cells (RhoE^{WT}) shows high affinity to Imp β , indicating that the nuclear localisation signal (NLS) existed in RhoE. RhoE wild type (RhoE^{WT}) and RhoE double mutants (RhoE^{T173R/V192R}) with FLAG-tagged RhoE epitope were transfected into U87 cells. Overexpression vectors containing empty vector (EV) were also applied for the control of the experiment using construct plasmid pCMV5 EV FLAG. Co-Immunoprecipitation (Co-IP) technique was used to pull-down RhoE from a combination of nuclear and cytoplasmic fractions of the transfected U87 cells. At the same time, negative control for the Co-IP experiment was also conducted using the reagent blank without

candidate protein sample. Then, yields from Co-IP pulled down assay went through SDS-PAGE and immunoblotted with antibodies against Imp β , Rnd3/RhoE, FLAG-RhoE and α -tubulin. These blots represent the results of a single experiment ($n = 1$). 152

Figure 42: The overexpressed RhoE in U87 cells shows that RhoE was localised to the nucleus and cytoplasm in double mutants RhoE. **(A)** U87 cells transfected with pCMV Empty Vector. **(B)** U87 cells transfected with pCMV5 FLAG-RhoE^{WT} **(C)** U87 cells transfected with pCMV5 FLAG-RhoE^{T173R/V192R} 164

Figure 43: The immunoblot of FLAG confirmed that the double mutants RhoE (RhoE^{T173R/V192R}) overexpressed in the U87 cells and localised to the nucleus and cytoplasm..... 166

Figure 44: The localisation of RhoE to the nucleus of U87 cells at 42 hours post-transfection. The immunostaining of U87 cells was conducted for FLAG to detect RhoE. The primary antibody used an anti-FLAG which was raised in a mouse to detect RhoE. On the other hand, the secondary antibody used an anti-mouse with conjugated Alexa Fluor 488nm, which was raised in a goat that has green fluorescence. Laser acquisition and vertical sectioning were applied within multiple layers of U87 cells towards a region of interest (ROI) on the coverslips until up to 100 layers via Z-Stack experiment. The thickness of the layers on each selected ROI is fixed to create an accurate overlapping between channels (bright field and 488 nm laser). **(A)** Confocal image of RhoE wild-type (RhoE^{WT}) and **(B)** Confocal image of RhoE double mutants (RhoE^{T173R/V192R}). **(1)** Arrow indicates nuclei of U87 cells; **(2)** Arrow indicates cytoplasm of U87 cells. 169

Figure 45: The high-resolution structure of RhoE interacts with ROCK1 (pdb: 2V55) - heterodimer was visualised in PyMOL Molecular Visualisation and retrieved in PNG file format. Localisation of single mutant or double mutant RhoE interfacing ROCK1 lead to disruption of RhoE: ROCK1 interaction. Each mutated residue is shown in blue stick within folding protein structure. 170

Figure 46: The immunoprecipitation of RhoE wild-type (RhoE^{WT}) and RhoE double mutants (RhoE^{T173R/V192R}) that are compared to the Empty Vector. The individual lane shows distribution of monomeric protein after 2-D separation via electrophoresis through SDS-PAGE followed by staining with Coomassie blue. The fade FLAG-RhoE band was only found in RhoE^{WT} and RhoE^{T173R/V192R} but none could be found in Empty Vector. 173

Figure 47: Bio-Ven – a web application for the comparison and visualisation of biological list using area-proportional Venn diagrams. ID Set X represents a total of 65 GO term list found in U87 cells transfected with RhoE^{WT} whereas ID Set Y represents a total of 51 GO term list found in U87 cells transfected with RhoE^{T173R/V192R}. The total overlapping between ID Set Y with ID set X is 44 GO term list. This is equals to 68% similarity shared between RhoE double mutants with the wild-type. 183

Figure 48: The immunoblots of MCM3 accumulation in U87 cells with and without the presence of RhoE. U87 cells were lysed in a buffer containing Nonidet-P 40 and nuclear. Cytoplasmic fractions were prepared, separated by SDS-PAGE, and immunoblotted with an antibody against MCM3. An effective isolation of nuclear and cytoplasmic fractions was confirmed using antibodies against Lamin A/C and a-tubulin, respectively (result not shown). These data are representative of three separate experiments ($n = 3$). 185

Figure 49: Densitometry analysis using Image J for the semi-quantification of the MCM3 intensity in U87 cells with and without the presence of RhoE from three separate experiments ($n = 3$). Data were statistically evaluated using Welch Two Sample t -test used for paired samples, (*) (p value < 0.05). The error bars show the standard error of the mean (S.E.M) for each datasets of three separate experiments ($n = 3$). 187

Figure 50: MCM3 is a novel interacting partner for RhoE. Depletion of RhoE promotes the localisation of MCM3 to the nucleus. (A) MCM3 in control condition; (B) MCM3 in siRhoE using RhoE oligo A; (C) MCM3 in siRhoE using oligo B. Right: Nuclear visualisation using DAPI at 300ms exposure, 40 x magnification. Left: Black and white image of MCM3 showing exact localisation of MCM3 using MCM3 antibody at 900ms exposure, 40 x magnification. 188

Figure 51: Model of the localisation of RhoE to the nucleus. The activation of PKC α led to increasing the upper band of RhoE (29kD) and triggered translocation of RhoE to the nucleus even though without the assistance of ROCK1. The presence of nuclear localisation signal (NLS) in RhoE promotes the recognition by the nucleocytoplasmic transporter (Importin, Imp α/β) and directs RhoE: PKC α complex to enter the nucleus, interacts with helicase loading (MCM3 and MCM5 as well as ORC3L), and regulates the cell cycle. 198

LIST OF TABLES

Table 1: List of Effector Proteins for Rho Family – RhoA, Rac1 and Cdc42	16
Table 2 : Contribution of Rho GTPases in cell cycle (Adapted from Hall 2009).....	19
Table 3: Phosphorylation of Rho Signalling Proteins by Mitotic Kinases (Reproduced from David et al. 2012)	20
Table 4: Interaction between RhoE and ROCK1 (Adapted from Komander et al. 2008).....	49
Table 5: Primers for RT-PCR of RhoE Sequence	66
Table 6: List of antibodies used in immunoblotting (IB) and immunocytochemistry (ICC) ...	68
Table 7: Immunoblotting protocols	73
Table 8: The data are the mean ratio that listed along with standard error of the mean (S.E.M) from four replicated independent experiment ($n = 4$).	131
Table 9: Mutagenesis of ROCK1: RhoE Interface (Adapted from Komander et al. 2008) ...	161
Table 10: Functional annotation chart showing RhoE (Rnd3) and its binding partners that are clustered into molecular function (MF) and biological processes (BP) in the U87 cells transfected with pCMV5 FLAG-RhoE ^{WT}	176
Table 11: Functional annotation chart showing RhoE (Rnd3) and its binding partners that are clustered into molecular function (MF) and biological processes (BP) in U87 cells transfected with pCMV5 FLAG-RhoE ^{T173R/V192R}	179

LIST OF ABBREVIATIONS

A5	Annexin-V
7AAD	7-Amino-actinomycin D
AES	Amino-terminal enhancer of split
ATM	Ataxia telangiectasia mutated protein
ATR	ATM-and Rad3-related protein
Bad	BCL2-associated antagonist of cell death
Baiap2	Brain specific angiogenesis inhibitor 1-associated protein 2
Bcl2	B-cell lymphoma 2
BrdU	Bromodeoxyuridine
CAF1	Chromatin assembly factor 1
CAM	Chick chorioallantoic membrane
CDK	Cyclin dependent kinase
Cdk1	Cyclin dependent kinase-1
DMF	Dimethylformamide
DTT	Dithiothreitol
EC	Endothelial cell
ECM	Extracellular matrix
Ect2	Epithelial cell transforming 2
eIF4E	Eukaryotic translation initiation factor 4E

ERK	Extracellular signal regulated kinase
4EBP1	eIF4E-binding protein 1
EST	Expressed sequence tag
FBS	Foetal bovine serum
Fc γ R	Fragment crystallisable gamma receptor
GAP	GTPase activating protein
GAPDH	Glyceraldehyde-3-phosphate dehydrogenase
GBM	Glioblastoma multiforme
GDI	Guanine nucleotide dissociation inhibitor
GDP	Guanosine diphosphate
GEF	Guanine nucleotide exchange factor
GG	Geranylgeranylation
GTP	Guanosine triphosphate
HaCaT	Human keratinocyte
IAP	Inhibitor of apoptosis protein
IB	Immunoblotting
ICC	Immunocytochemistry
IgG	Immunoglobulin
Imp α	Importin alpha
Imp β	Importin beta

ITF	Invasive tumour front
KPN	Karyopherin
M	Mitosis
MAPK	Mitogen activator protein kinase
MCM3	Minichromosomal maintenance protein 3
MCM5	Minichromosomal maintenance protein 5
MLC	Myosin light chain
MLCK	Myosin light chain kinase
MLCP	Myosin light chain phosphatase
MRCK	Myotonic dystrophy kinase-related CDC42-binding kinase
NES	Nuclear Export Signal
NF- κ B	Nuclear factor kappa B
NLS	Nuclear Localisation Signal
NPC	Nuclear Pore Complex
NTR	Nuclear Transport Receptor
PAK	p21 activated kinase protein
Par6	Partitioning Defective Protein 6
PBS	Phosphate buffered saline
PBST	Phosphate buffered saline with Tween-20
PH	Pleckstrin homology

PKC	Protein Kinase C
PKC α	Protein Kinase C – alpha
Plk-1	Polo like kinase-1
PMA	Phorbol myristate acetate
PP2A	Protein phosphatase 2A
pRB	Retinoblastoma pocket protein
PS	Phosphatidyl serine
RBD	Rho-binding domain
ROCK1	Rho-associated coiled kinase 1
SDS	Sodium dodecyl sulphate
SDS-PAGE	Sodium dodecyl sulphate –polyacrylamide gel electrophoresis
siRNA	small interfering RNA
Skp2	S-phase kinase-associated protein 2
Smac	Second mitochondria derived activator of caspase
SSRPI	Structure specific recognition protein 1
TBS	Tris buffered saline
TBST	Tris buffered saline with Tween-20
TNF	Tumour necrosis factor
Wasp	Wiskott-Aldrich syndrome protein

CHAPTER 1

INTRODUCTION AND LITERATURE REVIEW

1.1 Research Background

The origins of tumours are diverse and heterogeneous and almost all tumours have the ability to perform excessive proliferation compared to normal tissue. The imbalance between cell growth, differentiation and apoptosis could affect the net number of cells in the body, and the dysregulation of these processes extend a great risk of tumours (Ulrich et al. 2014). The cells in normal tissue proliferate to reproduce new and healthy two daughter cells. Extensive DNA damage in cell can occur during proliferation or cell division that result in apoptosis (Pecorino 2008). Thus, the starting point for the formation of all tumours is the anomaly in the regulation of cell proliferation and cell survival (Evan and Vousden 2001).

The characterisation of the difference between normal cell and tumour cell phenotype is essential in monitoring cell proliferation and apoptosis (Pecorino 2008). It is crucial to study Rho GTPases since uncontrolled cell proliferation and suppression of apoptosis are central to tumours formation and both processes are dependent on the role of these small GTP-binding proteins (Cinti et al. 2003). These signalling proteins are important for various cellular processes such as cell cycle progression (Ras), dynamics of the cytoskeleton (Rho and Rac), membrane trafficking (Arf and Rab), and nucleocytoplasmic transport (Ran) (Williams and Rottner 2010). They are also implicated in multiple physiological processes, including

embryogenesis, reorganisation and maintenance of polarity, cell-cell adhesion and migration as well as differentiation of numerous cell types (Symons 2003).

On the other hand, small GTPases are involved in numerous pathological human conditions, such as uncontrolled cell proliferation, metastasis or angiogenesis during tumour development, inflammation and vascular diseases, mental retardation and infections (William and Rottner 2010). It is not surprising that there is the involvements of small GTPases in the abnormality of pathological features as signalling proteins play the pivotal roles in numerous normal and developmentally regulated processes of living cells. As an example, Rho GTPase signalling in glioma cell could implicate invasion and tumour progression (Fortin Ensign et al. 2013). One of the criticisms on the existed literature to date is the poor explanation on how small Rho GTPases regulate brain cancer (Liacini et al. 2014; Poch et al. 2007).

Poch et al. (2007) demonstrated that RhoE has the ability to regulate cell proliferation in U87 cells in the two different stages of cell cycle. One of the limitations in their work is that they did not disclose a specific regulation for either G₁/S phase due to the loss of RhoE or G₂/M phase during the overexpression of RhoE. Their finding's main weaknesses are the precise function of RhoE and the reason it switches between these two phases - G₁/S or G₂/M respectively. Moreover, it was observed that RhoE regulates apoptosis via promoting the expression of p53 target genes that inhibit membrane blebbing via antagonising the function of ROCK1 (Ongusaha et al. 2006). Therefore, this study intended to analyse the role for one of the members of Rho GTPases family - RhoE in glioma. Both findings will provide a significant framework in resolving intermediates and identifying pathways that are involved in both processes. It is assumed that, analysing the protein-protein interactions between RhoE

and potential tumour marker would be advantageous. This approach would reveal the mechanism and signalling pathway that are involved and used for exertive therapy.

1.2 Glioma

In general, glioma is a tumour of glial cell, which is a supportive cell that does not transmit impulse in the central nervous system (CNS). Glial cells comprised variety cell type in the brain including oligodendrocytes, astrocytes, ependymal cells, Schwann cells, microglia and satellite cells except neuronal cells. Approximately, 45 out of 100 (45%) of the primary brain tumours are gliomas. The incidence rate for new primary brain tumours that was diagnosed in the United Kingdom has reached 4 500 cases per year (NHS 2013). Brennan et al. (2013) reported that 2 to 3 per 100 000 population in the United States of America and European countries were diagnosed with brain tumour. It is known that, glioblastoma multiforme (GBM) is the most common and lethal primary brain tumours in adults (TCGA 2008). Glioblastoma is associated with poor prognosis and the typical survival duration after diagnosis is less than two years (Holmberg et al. 2011).

Brain tumours are classified based on glial cell growth efficiency. Pathologists had classified glioma into four groups, Grades 1 to 4 based on microscopic examination (NHS 2013). Typically, the lower grade glioma is referred as slower growing brain tumour that is slightly similar to healthy cells. A higher grade of the glioma relies on the degree of phenotype abnormality and efficiency of the brain tumour formation (Soffietti et al. 2010).

The first group is Grade 1, a benign glioma that is characterised by pilocytic astrocytoma with the slowest growing brain tumours. The second group is low-grade glioma

(LGG) that has multiple types of glioma, including astrocytoma, oligodendroglioma and oligoastrocytoma. Both Grade 3 and Grade 4 are malignant and the most aggressive form of glioma (CRUK 2013). These two malignant gliomas can be differentiated by their morphologies. Grade 3 has distinct morphologies including anaplastic astrocytoma, anaplastic oligodendroglioma and anaplastic mixed oligoastrocytoma whereas Class 4 is an unspecified glioma or glioblastoma multiforme (GBM).

Recently, it was found that GBM has multiple sub-types phenotypes that respond differently to aggressive therapies, making treatment extremely difficult and challenging (Kong et al. 2013; Verhaak et al. 2010). The sub-types include Proneural, Neural, Classical and Mesenchymal that are differentiated based on their gene signatures as well as somatic mutations and aberration of DNA copy number. As a result, the National Institute of Health under The Cancer Genome Atlas (TCGA) Research Network (2008) decided to select GBM as the first brain tumour to be sequenced as a part of their effort to map the genomes, instead of other types of cancer (Robbins et al. 2013).

GBM is developed from the progenitors of star-shaped glial cells, called astrocytes that support nerve cells (Kong et al. 2013) and it developed primarily in the cerebral hemispheres that spread to other brain compartment, brainstem or spinal cord (NHS 2013). There is a high probability that each glioma could reoccur after surgery, even if it is completely removed. However, GBMs rarely metastasise outside the central nervous system (CNS). All gliomas have tentacle-like projections morphology that can directly invade nearby brain tissue (Li et al. 2007). Although low-grade astrocytoma is less harmful, it can spread to another region of the brain or spinal cord due to the lack of invasive barrier in the tissue

(Fortin Ensign 2013). Thus, recurrence after initial treatment is common, and the options of spreading to other brain sections or spinal cord is relatively high (Brennan et al. 2013).

On the other hand, radiotherapy and chemotherapy are sometimes used to treat benign tumours which are similarly used in treating malignancies. The treatment for brain tumour is more complicated compared to other types of tumour from various parts of the human body. The key problem of this explanation is its lack of detail regarding why the treatment process is difficult, whereby benign tumour can cause severe symptoms and be deadly if it occurs in a significant part of the brain (Kunz et al. 2011).

Figure 1 shows a glioblastoma lesion in the brain tissue and the defects in cell morphology. The appearance of deep blue-purple colour of nuclei is due to complex formation during staining of hematoxylin with nucleic acids; whereas eosin is pink and it non-specifically stains proteins in the cytoplasm. These stains are commonly used in recognising various types of tissue and morphologic changes. In the pathology laboratory, hematoxylin is used to diagnose and determine between healthy cell type or cancer-type-specific patterns based on the condensation of heterochromatin (Fischer et al. 2008).

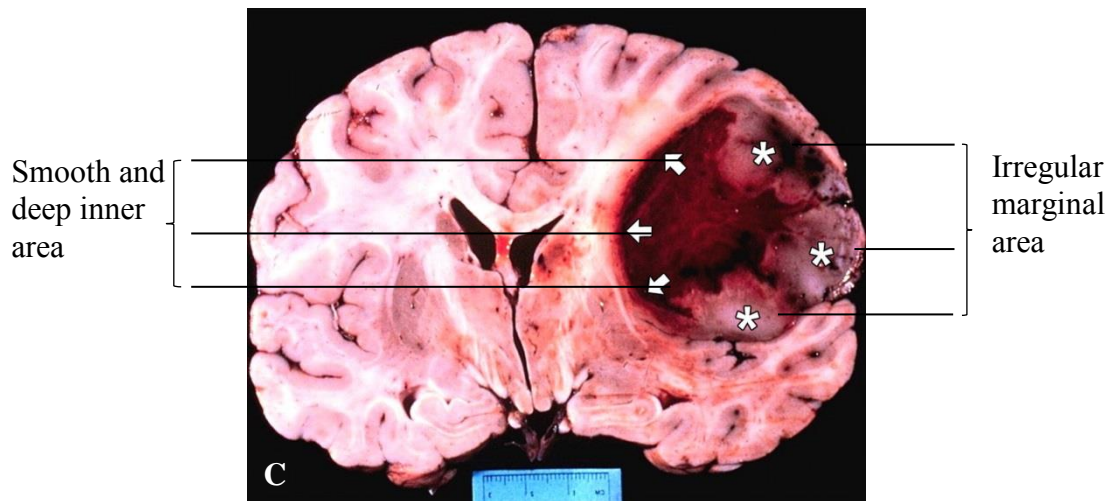
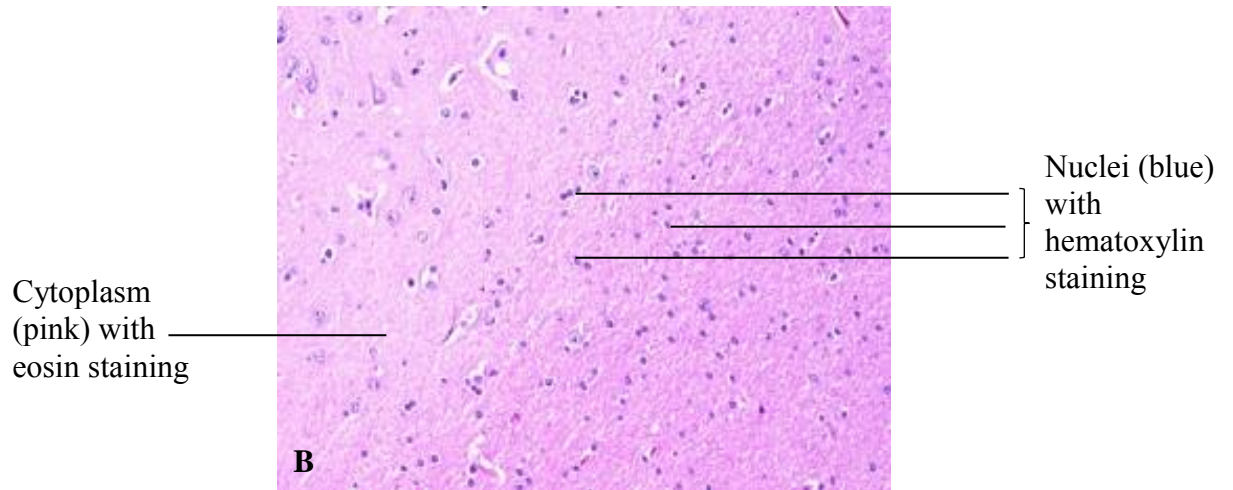
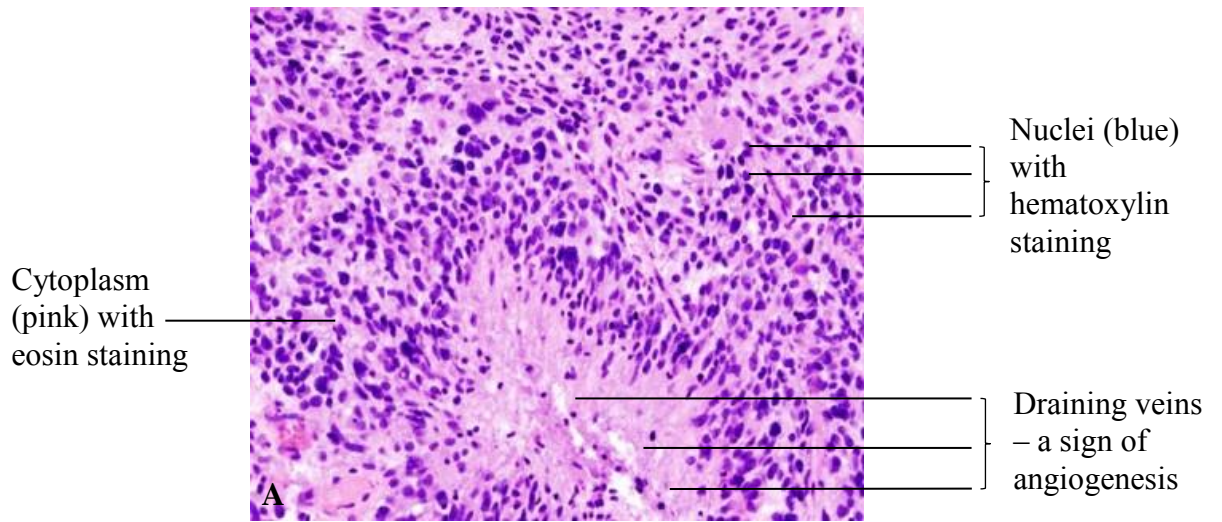


Figure 1: Immunohistochemistry (IHCC) of cells from the lesion tissue compared to the normal brain cells. (A) Glioblastoma showing extensive proliferation; (B) Normal brain tissue; (C) GBM cross section. Images are reproduced from College of American Pathologists (2011) and Sathornsumetee et al. (2007).

1.3 Small GTPases

1.3.1 Rho GTPase Family

1.3.1.1 Subfamily of Rho GTPase

The Rho family of GTPases is a family of small signalling G proteins with low molecular weight (21-28 kD) and it is also a subfamily of the Ras superfamily. A phylogenetic analysis using bioinformatics tools demonstrated the classification for 20 members of Rho proteins in mammals (Dellinger 2006). Although the Rho family is composed of 20 members, but only RhoA, Rac1 and Cdc42 were best characterised (McCormack et al. 2013). Figure 2 illustrates the Rho proteins that are structured into eight subgroups; (i) Rnd1, Rnd2, Rnd3/RhoE; (ii) RhoA, RhoB, RhoC; (iii) RhoD, Rif; (iv) Rac1, Rac2, Rac3, RhoG; (v) Cdc42, RhoQ/TC10, RhoJ/TCL, RhoV/Chp, RhoU/Wrch2; (vi) RhoH/TTF; (vii) RhoBTB1; and (viii) RhoBTB2/DBC-2. They are then distributed into four distinct clusters based on the expressed sequence tag (EST) databases for Rho GTPases using TBlastN or BlastP (v2.2.13) algorithms (Boureaux et al. 2007).

In a recent study, Saad et al. (2014) stipulated an advance evolutionary study on Ras superfamily and subfamily. The Ras superfamily consists of five major families including Ras, Rho, Arf, Ran and Rab. However, their work was restricted to Ras superfamily, as well as Rho and Rab subfamilies. These proteins in particular are involved in signal transduction pathway whereas Arf and Ran were poorly studied. The evolutionary of small GTPase and the signalling pathway that is involved in cancer and other developmental diseases can be exploited for a better drug design (Saad et al. 2014). Cook et al. (2014) also agreed on the fact that the abnormalities of Rho family small GTPases in

humans has a huge impact in cancer and other diseases as well as affecting cancer signalling pathway.

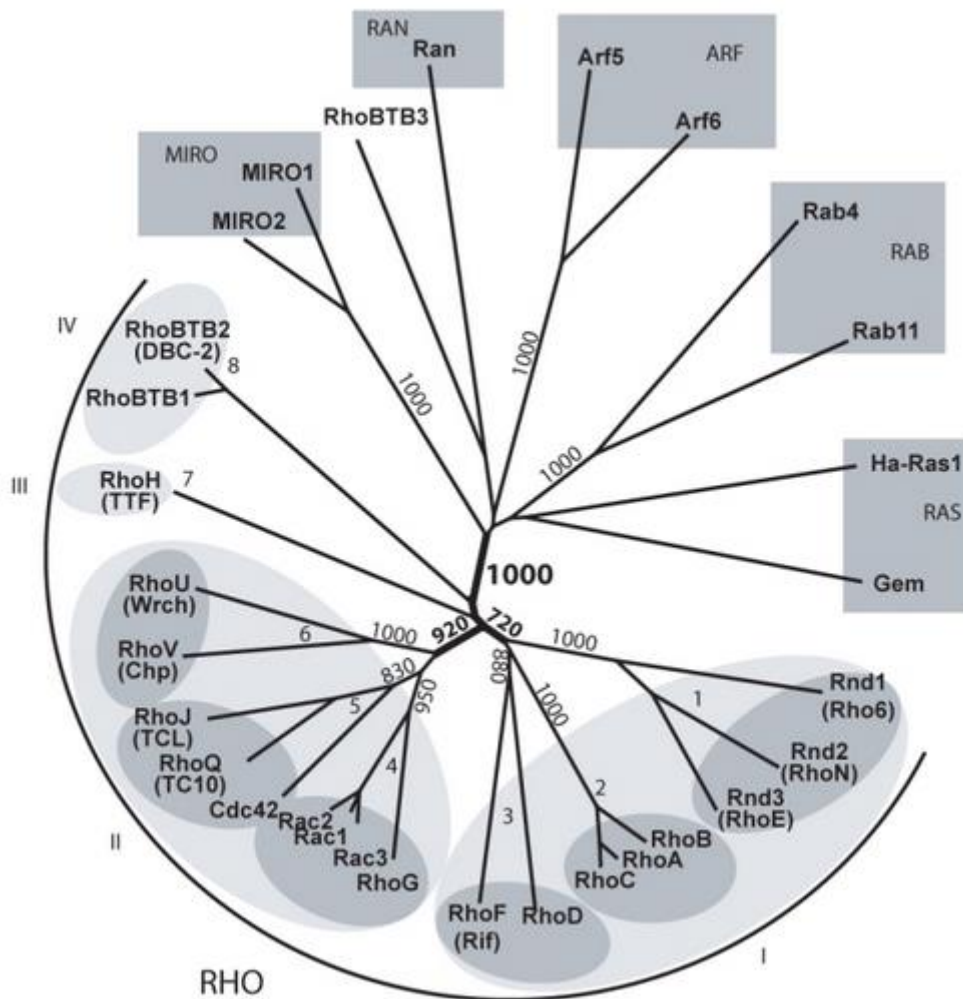


Figure 2: The Rho phylogeny of 20 members of Rho proteins and the presence of eight subgroups that are distributed into four distinct clusters using ClustalX Neighbour-Joining (NJ) and ProMaximum-Likelihood (ML). The numbers that appeared in primary and secondary branches show the bootstrap repetition of NJ values. This chart is reproduced from Boureux et al. (2007).

1.3.1.2 Regulators of Small GTPases

The deformity of Ras homolog related to Rho family GTPases was recently identified as an indicator of cancer and other human diseases (Cook et al. 2014). In relation with the cancerous indication, Spiering and Hodgson (2011) explained that the function of Rho GTPases as molecular switches and they figured out the interaction via its downstream effector molecules. They have manipulated the work of Machacek et al. (2009) in examined the coordination of RhoGTPase during cell migration and rearrangement of the cytoskeleton. RhoA synchronises the leading edge by initiating the protrusion and retraction of the cell. At the end of the protrusion, Rac1 and Cdc42 block the advancement of cell edge by inhibiting the function of RhoA. One of the limitations for this explanation is its lack of clarification whether RhoE acts accordingly or against other Rho GTPase during cell migration.

Each movement of the cell propagates the signal transduction in their activated GTP-bound state. The intrinsic phosphatase activity hydrolyses the GTP to GDP that turns the protein to become inactive. In this context, Cherfils and Zeghouf (2013) affirmed that the switch is positively controlled by guanine nucleotide exchange factors (GEFs) that catalyse the replacement of GDP by GTP besides being negatively regulated by GTPase activating proteins (GAPs) that facilitate the exchange of GDP to GTP via intrinsic activity of GTPase. In other words, Rho GTPases switches are respectively turned on and off by GEF and GAP.

Fortin Ensign et al. (2013) have validated whether guanine nucleotide dissociation inhibitors proteins (GDIs) are important in regulating homoeostasis of the Rho GTPases by preventing protein degradation. The GTPases function as binary switches in cell signalling

that initially bind to GDP and localise in cytosol in an inactive form, and they are associated with membranes and converted into an active-GTP bound state in the place of effector target (Dermardirossian and Bokoch 2005).

Figure 3 shows a comprehensive cycle of the Rho GTPase in which Rho GTPase shifts between inactive GDP-bound and active-GTP bound states. Typically, Rho proteins carry either farnesyl or geranylgeranyl lipid at their C-terminus and localise them to the cellular membranes (Cook et al. 2014). However, GDI shielding for the hydrophobic tails of the canonical Rho proteins allows diffusion into the cytosol and prevents the activated Rho-GTP anchoring to the membrane (Boulter et al. 2010).

Cherfils and Zeghouf (2013) discovered the regulations of small GTPases using advanced mechanisms that are not dependent on GEF, GAP and GDI, and they are controlled by themselves. It is known that the GTPases in humans could deliver cellular signals and build up specific cell responses including rearrangement of autoinhibition, GTPase activating feedback loops, synchronise signalling between regulators and effectors and provide phosphorylation site for GDI. In addition, these small GTPase regulators (GEF, GAP and GDI) are vulnerable to biochemical aberrancy due to mutational diseases as well as bacterial infection that could invade the host regulatory system and intimidate the host cell (Cook et al. 2014; Lemichez and Aktories 2013).

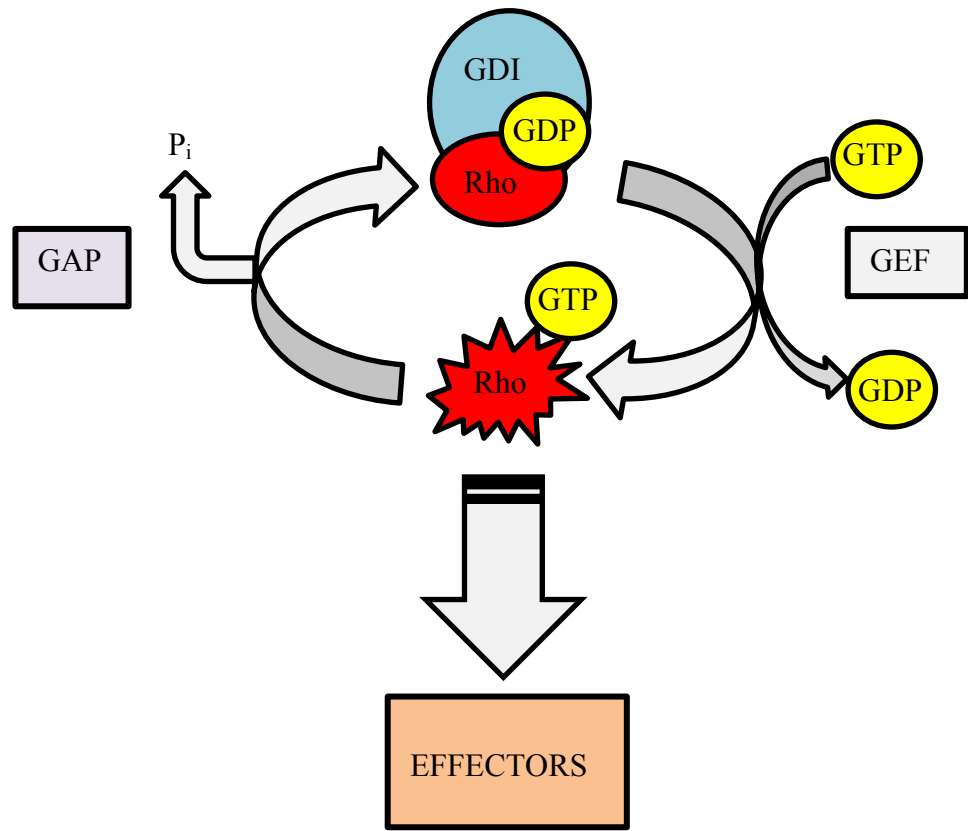


Figure 3: The Rho GTPase cycle. The cycling of Rho GTPase between inactive GDP-bound and active-GTP bound states. Table 1 shows the examples of downstream effector of the Rho family.

1.3.1.3 Effector Molecules of Rho GTPases

The Rho family members consisting of RhoA, Rac1 and Cdc42 are well characterised as the regulators of the actin cytoskeleton and they promote stress fibre formation, lamellipodia or filopodia. These regulators have specific interaction towards downstream effectors as listed in Table 1. Depending on particular signalling pathway involving RhoA, Rac1 or Cdc42, the downstream effector will correspond to a pertinent individual biological action (Arulanandam et al. 2010). Occasionally, Rho proteins interact with downstream effector molecules that are engaged to specific signalling cascades in coordinating various cellular processes, including cytoskeletal reorganization, vesicle trafficking, cell cycle progression, cell polarity, and transcription (Stengel and Zheng 2011).

The effector's regulatory mechanisms are divided into catalytic and non-catalytic proteins. Bustelo et al. (2007) had discussed the multiple types of effector proteins such as p21 activated kinase protein (PAK), Rho-associated coiled-coil containing protein kinase (ROCK) and protein kinase N (PKN) that serve as catalytic proteins. The non-catalytic effector proteins function as an adaptor protein that include Diaphanous, Wiskott-Aldrich syndrome protein (Wasp) and Brain specific angiogenesis inhibitor 1-associated protein 2 (Baiap2). Bustelo et al. (2007) emphasised that both class of proteins either catalytic or non-catalytic play a role as the effector for members of the Rho family, specifically for Cdc42. These effectors use distinct residues within switch I and switch II regions of the regulatory protein to identify the recognition site. Hence, the variant between residues is essential to make it visible, in creating docking between both proteins - Rho and downstream effector.

Stengel and Zheng (2011) suggested a number of catalytic proteins, particularly kinases that interact with Cdc42 such as p21 protein (Cdc42/Rac)-activated kinases (PAKs), mixed lineage kinases (MLKs) and Myotonic dystrophy protein kinase-like (MRCK). In addition, there are also other scaffolding proteins that are associated with Cdc42, including Partitioning Defective Protein 6 (Par6), Wiskott-Aldrich syndrome protein (WASP) and IQ motive containing GTPase-activating protein (IQGAP). Recently, Fortin Ensign et al. (2013) disclosed that the downstream effectors of RhoGTPase could promote invasiveness and glioma cell survival. As an example, Rac1 and Cdc42 share an overlapping set of downstream effectors such as signalling pathway via activation of PAK and MAPK during the process of cell migration. Table 1 described the comprehensive details about effector proteins for Rho family involving RhoA, Rac1 and Cdc42.

Table 1: List of Effector Proteins for Rho Family – RhoA, Rac1 and Cdc42

Effector	Type of protein	Upstream GTPase	Main Biological Action	Reference
Pard6, A, G	Scaffold protein (Par6, α,γ)	Rac1, Cdc42	Cell polarity, links GTPases and atypical PKCs	Bustelo et al. (2007)
IQGAP1, 2	RhoGAP and scaffold protein	Rac1, Cdc42	Regulator of the cytoskeleton, cell-cell contacts and proliferation	Fortin Ensign et al. (2013)
c-Cbl	Ubiquitin Ligase	Cdc42	EGFR degradation	Stengel and Zheng (2011)
Cit	Serine/threonine kinase (Citron)	RhoA	Cytokinesis	Bustelo et al. (2007)
Pkn1,2	Serine/threonine kinase (Prk)	RhoA	Vesicle recycling, cell cycle regulation, Pld1 activation	Bustelo et al. (2007)
ROCK 1, 2	Serine/threonine kinase (ROCK α,β)	RhoA	Cytoskeleton, cytokinesis, blockage of cell contact inhibition	Croft and Olson (2011)
Pak1-7	Serine/threonine kinase	Rac1, Cdc42	Cytoskeletal organization, activation of kinase cascades	Bastos et al. (2012)
Map3K11	Serine/threonine (Mlk3)	Rac1, Cdc42	Activation in kinase cascades	Bustelo et al. (2007)
PrkcA	Serine/threonine kinase (PKC α)	RhoE, RhoA, Rac1, Cdc42	Signal transduction	Sathornsumetee et al. (2007)
Cdc42bpgA,B	Serine/threonine kinase (MRCK α,β)	Rac1, Cdc42	Cytoskeletal regulation	Bustelo et al. (2007)

Effector	Type of protein	Upstream GTPase	Main Biological Action	Reference
Rps6kB1	Serine/threonine kinase (p70 ^{S6k} , S6K1)	Cdc42	Regulation of translation, cell cycle	Bustelo et al. (2007)
Map3K10	Serine/threonine kinase (Mlk2)	Cdc42	Activation of kinase cascades	Fortin Ensign et al. (2013)
Map3K4	Serine/threonine kinase (Mekk4)	Cdc42	Activation of Jnk route	Fortin Ensign et al. (2013)
Tnk2	Tyrosine kinase (Ack)	Cdc42	Signal transduction, activation of GEFs	Bustelo et al. (2007)
Ppplr12A	Regulatory subunit of phosphatase1	RhoA	Myosin light chain inactivation, cytoskeletal regulation	Bustelo et al. (2007)
Fml1	Formin-like molecule	Rac1	Cytoskeletal organization, cell polarity and cytokinesis	Bustelo et al. (2007)
Fhod1	Formin-like molecule	Rac1	Cytoskeletal and transcriptional regulation	Bustelo et al. (2007)
Cyfip1	Actin binding protein	Rac1	Cytoskeletal organisation	Bustelo et al. (2007)
FlnA	Actin binding protein	RhoA, Rac1, Cdc42	Cytoskeletal regulation, actin filament crosslinking	Bustelo et al. (2007)
TubA1	Tubulin	Rac1	Integral component of microtubule	Bustelo et al. (2007)
Stat3	Transcriptional factor	Rac1, Cdc42	Transcription	Arulanandam et al. (2010)
Smurf2	E3 Ubiquitin protein ligase 2	Rac1	Smad and RhoA ubiquitination, TGFβ receptor signalling	Stengel and Zheng (2011)

1.3.2 The Role of Rho GTPases in Mammalian Cells

1.3.2.1 Rho GTPases in Cell Cycle

To date, cell cycle is closely associated with cancer cell motility and invasive properties (Kagawa et al. 2013). The Rho family GTPases - Rho, Rac and Cdc42 in particular, have important roles in regulating the cell cycle (David et al. 2012). The division of cells have four main phases including G1, S (DNA replication), G2 and M (mitosis) and they are almost all regulated by either Rho, Rac or Cdc42 (Hall 2005). In agreement with this fact, Hall (2009) explained that the function of Rho GTPase subfamilies is specifically based on the individual phases of the cell cycle, and Table 2 shows their functions. Specifically, Rho plays a major role by controlling every phase and sub-phase of the checkpoints in cell cycle compared to Rac and Cdc42 (Hall 2009). Besides that, Rho GTPases are also involved in cell mitosis for the activation of Rho-associated kinase (ROCK), where the effector of RhoA mediated the cortical retraction during mitotic cell rounding (Villalonga and Ridley 2006).

Regarding the function of Rho in cell cycle, mitotic Rho regulatory pathway could directly affect cell proliferation (David et al. 2012). Moreover, mitotic kinases could also control the activity of phosphorylation and regulate cell cycle machinery including the processes of transcriptional activation, ubiquitylation and proteosomal degradation. David et al. (2012) summarised the examples of the mitotic kinases and their specific functions in regulating the cell cycle. Some of the kinases were picked up as they might be relevant in targeting Rho and the signalling pathways are also antagonising RhoE. Table 3 shows the list of mitotic kinases and the important functions in cell cycle that closely related to RhoE.

Table 2 : Contribution of Rho GTPases in cell cycle (Adapted from Hall 2009)

Level of Cell Cycle	Phases for Checkpoints in Cell Cycle	Role of Rho GTPases Family
G ₁	Cell size	Cyclin D1 transcription by Rho/Rac/Cdc42
	Levels of nutrients / growth factor	Cyclin D1 mRNA translation by Rac
	DNA damage	Cyclin D/CDK inhibitor p21/p27 expression by Rho
S	S Phase entry	Delay for problems in replication by Rho/Rac/Cdc42
G ₂	Cell size DNA damage	Assessment and G ₂ /M progression by Rho/Rac
M	Prophase	Cell rounding by Rho Centrosome position by Rho
	Prometaphase	Kinetochore attachment by Cdc42/Rho
	Metaphase	Asymmetric spindle positioning by Cdc42
	Anaphase	-
	Telophase	-
	Cytokinesis	Contractile ring abscission by Rho

Table 3: Phosphorylation of Rho Signalling Proteins by Mitotic Kinases (Reproduced from David et al. 2012)

Mitotic Kinases	Target	Residues of Rho	Cell Cycle Machinery
Cdk1	Ect2	Thr ⁴¹²	Required for Ect/Plk-1 interaction Increases GEF activity Induces excessive membrane blebbing
	GEF-H1	Ser ⁹⁵⁹	Inhibits GEF activity Dephosphorylation prior to cytokinesis
	p190 RhoGAP	NR	Downregulates GAP activity
Plk-1	ROCK2	Thr ⁹⁶⁷ , Ser ¹⁰⁹⁹ , Ser ¹¹³³ , Ser ¹³⁷⁴ , Thr ⁴⁸⁹	Plk-1 dependent ROCK2 phosphorylation activates ROCK2
Aurora A	GEF-H1	Ser ⁸⁸⁵	Inhibits GEF activity Dephosphorylation prior to cytokinesis Allows interaction with 14-3-3
Aurora B	MacRacGAP	Ser ³⁸⁷	From telophase to cytokinesis Renders the GAP active on RhoA

*NR : Not reported

According to the list of mitotic kinases in Table 3, Cdk1 is shown having critical function in phosphorylating Rho signalling protein including epithelial cell transforming 2 (Ect2), Guanine nucleotide exchange factor-H1 (GEF-H1), and p190 RhoGAP. David et al. (2012) also denoted that there are various substrates that are phosphorylated by Cdk1 including histones, nuclear lamins, proteins that interact with microtubules, condensation of chromosomes, nuclear envelope and spindle assembly. Regarding to the detail in Table 2, both cell assessment and G₂/M progression by Rho/Rac are essential to define cell size and DNA damage (Hall 2009). At this checkpoint, Cdk1 activation occurs during the transition phase to allow cell progression into mitotic phase. Beforehand, Cdk1 has to be initially executed by Cdc25 phosphatase via dephosphorylation at residue threonine 14 (Thr¹⁴) and tyrosine 15 (Tyr¹⁵) to enable its function (David et al. 2012).

Cytokinesis is coordinated on each cell cycle during late mitosis. Su et al. (2003) have examined multiple phenotypes within cells when p190 Rho GAP was overexpressed. It was observed that the increased level of exogenous p190 RhoGAP expression has led to the formation of multinucleation in the nuclear region, abnormal positioning of cleavage furrow specification site, unequal daughter cell partitioning and faulty furrow contraction. Besides that, endogenous p190 RhoGAP – a Rho family GTPase-activating protein, basically regulates cell proliferation, as well as having a close link to the completion of cytokinesis and generating viable cell progeny (Su et al. 2003).

In summary, cell cycle is mainly regulated by Rho GTPases in G₁ progression and M phases. The extracellular matrix (ECM) acts as elicit signals via integrins and actin cytoskeleton during the progression of cells from G₁ entering S-Phase. Rho GTPases also control both assembly and disassembly of actin filament and these processes are necessary

for microtubule and actin filament reorganisation during mitosis. This study is interested to further investigate cell cycle by focusing on RhoE representing Rho GTPases. It is hoped that this effort would disclose more detailed explanations in characterising the role of Rho GTPase in cell cycle.

1.3.2.2 Rho GTPases in Apoptosis

The common characteristics of apoptosis are cell shrinkage, membrane blebbing and budding, chromatin condensation, and precise fragmentation at the end that led to cell disposal (Wickman et al. 2013). The subfamily of Rho GTPases that is listed in Section 1.3.1.1 commonly acts as molecular switches in intracellular signal transduction pathways. Cinti et al. (2003) affirmed that one of the promising therapeutic targets in eliminating cancer cells is targeting components of pro-survival signal transduction pathways which involve Ras superfamily such as Ras, Rho, Arf/Sar, Ran, and Rab. It is known that this signalling pathway may contribute to intrinsic or inducible drug resistance. For instance, small molecule inhibitors of phosphoinositide-3-kinase (PI3K) kinase/Akt and farnesyltransferases are necessary in the activity of Ras that could induce apoptosis (Leverrier and Ridley 2001). It is advantageous to block this pathway as it is non-carcinogenic to the normal cell besides annihilating the tumour.

Moreover, Coleman and Olson (2002) discussed that Rac1 and Cdc42 signalling pathway could encourage cell survival. Both of these Rho GTPases interact with p21 activated kinase protein (PAK) in enabling phosphorylation of BCL2-associated antagonist of cell death (Bad). Besides that, it was found that Rho GTPases including RhoA, Rac1 and Cdc42 could activate the transcription factor; whereas necrosis factor-kappa B (NF-

κ B) could block apoptosis (Perona et al. 1997). Effective activation of NF- κ B by Rho GTPases has the ability to induce translocation of this transcription factor into the nucleus. As a result, cell survival is maintained by DNA transcription and cytokine production by NF- κ B (Perona et al. 1997).

On the other hand, the signalling downstream of Rho GTPases has contributed to actin reorganisation. As an example, cleavage of Cdc42 and Rac1 lead to the termination of downstream signalling. During apoptosis, Cdc42 and Rac1 eliminate actin filament, followed by ROCK1 that promotes actin-myosin II contractility. As a result, Cdc42 and Rac1 are cleaved at the end of the apoptotic process. For clearer description, Coleman and Olson (2002) agreed with Croft and Olson (2011) on a proposed mechanism of ROCK activation which is shown in Figure 4. This figure explains the loss of autoinhibition by Rho binding and caspase cleavage that led to ROCK activation. It was found that activated ROCK1 could aid the contraction and membrane blebbing during the late execution phase of apoptosis (Samuel and Olson 2010).

Section 1.3.2.1 previously described that Rho GTPases interact with multiple functions in cell cycle. However, aberrant yield from the cell cycle has to be eliminated and this has made apoptosis an important mechanism in demolishing insignificant revenue. It was found that Rho GTPases - Rac1 and Cdc42 in particular regulate apoptotic cell uptake. An earlier research by Leverrier and Ridley (2001) demonstrated that the signalling pathways in regulating apoptotic cell phagocytosis and fragment crystallisable gamma receptor (Fc γ R)-mediated phagocytosis share a common requirement for Rho GTPases including Rac1 and Cdc42, excluding Rho.

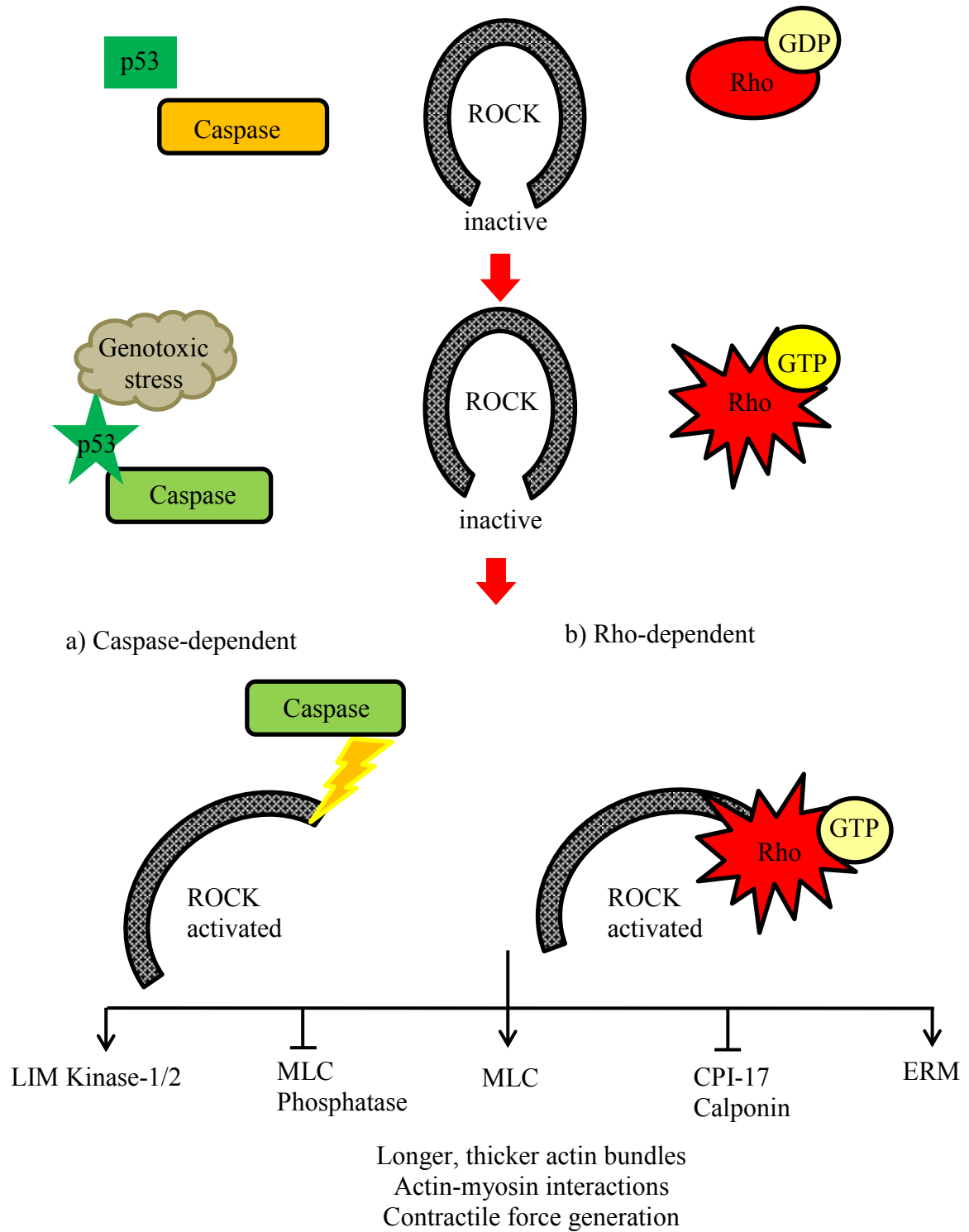


Figure 4: Activated Rho binding to ROCK or caspase cleavage in response to genotoxic stress to activate the kinase (Adapted from Coleman and Olson 2002; Croft and Olson 2011).

Recently, Ohgushi et al. (2010) demonstrated that apoptotic cell uptake requires Rho. They claimed that the inhibition of endogenous Rho GTPases has blocked apoptosis and cell phagocytosis. This blockage occurs in a dose-dependent manner where apoptosis is dependent on the type of kinase inhibitors that are being used for that particular experiment. Regarding this argument, they clarified that Rac1 and Cdc42 were not only required during apoptosis as well as cell phagocytosis but these processes were enhanced via Rho depletion (Ohgushi et al. 2010).

1.3.2.3 Rho GTPases in Cancer

It was observed that tumour cells display uncontrolled proliferation, altered interactions with neighbouring cells and the surrounding ECM, as well as enhanced migratory properties. Senoo and Iijima (2013) reported that the proteins of the Rho GTPase family play important roles in regulating various uncontrolled processes in the cancer cells *in vitro* as well as in humans. Karlsson et al. (2009) also presumed that there is the involvement of proteins that regulate Rho GTPases and other effectors of Rho GTPases. For example, the differentiation between GDP-GTP bound forms of Rho requires the recognition of conformational changes by downstream effector proteins (Riento et al. 2003). As a family of 20 small G proteins, Rho GTPases regulate the cytoskeleton and other cellular functions, including cell cycle, cell polarity and cell migration. Figure 5 shows a diagram of Rho GTPase and the major function in tumour that is relevant at cellular and molecular level.

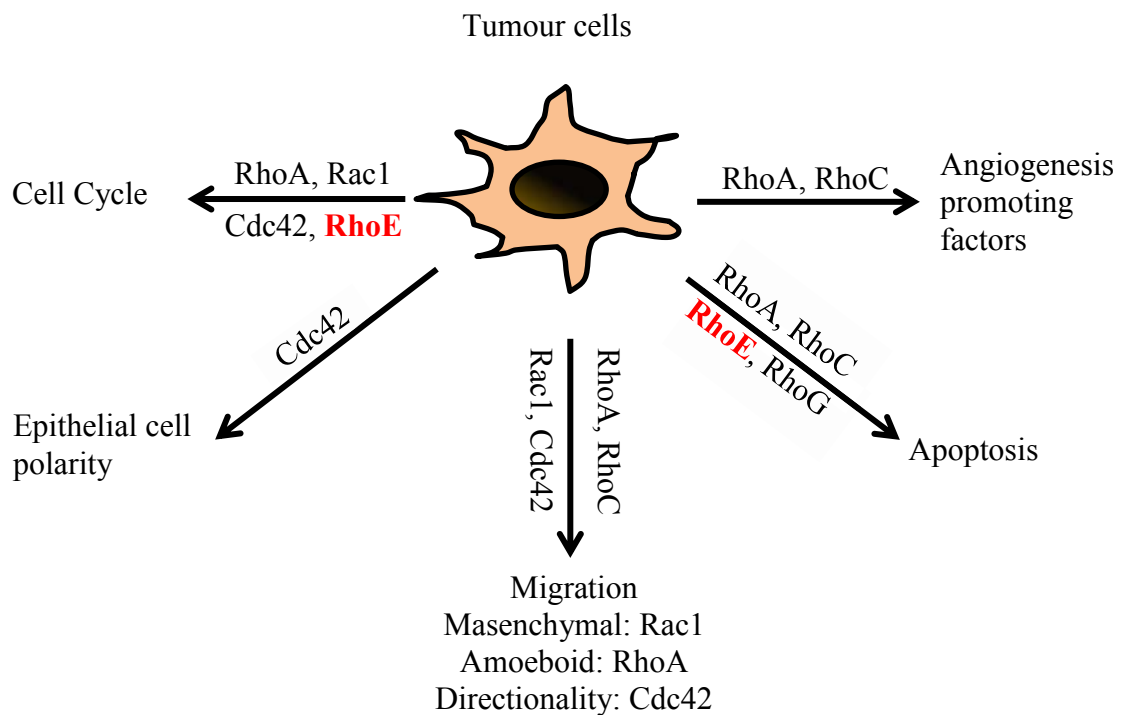


Figure 5: Rho GTPases and major function in tumour that is relevant at cellular and molecular level. (Adapted from Karlsson et al. 2009; Senoo and Iijima 2013).

Figure 5 shows that Rho GTPases regulate different cellular processes and they are important for tumour growth and progression *in vitro*. This study focused on the role of one member of this family, RhoE, which has the ability to regulate apoptosis and cell cycle in human cells. The summarised processes show the importance of Rho GTPases in cancer development. For example, Rac1 and RhoA promote G₁-S transition by increasing the amount of cyclin D1 in cell cycle. On the other hand, for an experimental study that uses fibroblast, RhoE inhibits the cell cycle progression, upstream of the pRB checkpoint by blocking the expression of cyclin D1 at the posttranslational level when it binds to GTP (Poch et al. 2007). In addition, RhoE inhibits vincristine-induced apoptosis by reducing expression of BCL2-associated X protein (Bax) and promotes tumour cell survival albeit RhoA and RhoC by inducing the upregulation of Bax that led to apoptosis (Karlsson et al. 2009).

1.3.3 Small GTPase in Nucleocytoplasmic Transport

The most important molecular processes are transcription and translation that require an exchange between the cytoplasm and the nucleus. The exchange process predominantly occurs through large protein channel in the nuclear envelope (NE), which is particularly across the nuclear pore complex (NPC) (Kodiha and Stochaj 2012). However, the aberrant activity during DNA transcription in the nucleus can occur at a particular point due to the presence of excessive transcription factors. At that point, nuclear trafficking via NPC, could affect nuclear protein transport. This potential abnormality happens when uncontrolled protein is trafficking whilst the transportation of the translated protein traverses the NPC. The post-translational modification via phosphorylation at serine and threonine, as well as tyrosine, may direct the translocation of protein to the nucleus (Mihlan et al. 2013).

In general, NPC is spanned for the means of either passive or active. Macromolecules exchange throughout NPC is restricted and sometimes dependent on nucleocytoplasmic machinery (Mingot et al. 2004) and commonly mediated by karyopherins (KPNs), which is the nuclear transport protein. KPN is a family of transport receptors that bind to their cargoes via recognition of nuclear localisation signal (NLS) for nuclear import or nuclear export signal (NES) during formation of transportation cargo complex. This recognition process enables transient interaction between KPN with the NPC component.

The import-export mechanisms are predominant nucleocytoplasmic machinery that regulates protein transport between the cytoplasm and the nucleus. Ran GTPase (Ras-related nuclear protein) controls the interaction of karyopherin (KPN) with their cargoes

during nucleocytoplasmic transports (Sorokin et al. 2007). In addition, Bilokapic and Schwartz (2012) clarified that nuclear transport receptors (NTR) mediate the transport of proteins between the nucleus and the cytoplasm; similar function with KPN, the importin and exportin, but so-called with an alternative name. They also revealed a detailed description regarding NPC structure, NLS and NES, as well as the model of classic Ran-dependent transport (Bilokapic and Schwartz 2012).

Figure 6 shows an example of nucleocytoplasmic transport model and it suggests that the GTP hydrolysis by Ran in the cytosol facilitates the function of nuclear transporters (NTR/KPN) to traverse the NPC. This model is reproduced from Alberts et al. (2008) in explaining the recognition of NLS on a larger size protein that is mediated by either importin alpha subunit ($\text{Imp}\alpha$) or importin alpha and beta heterodimer ($\text{Imp}\alpha/\beta$) or by using importin beta ($\text{Imp}\beta$) alone or one of its many homologues (Alberts et al. 2008).

For the principle, Chang et al. (2013) suggested that the NLS residue has to be recognised by the adaptor molecule of import receptor, which is $\text{Imp}\alpha$ (Chang et al. 2013). Then, this cargo is linked to the carrier molecule or intermediate that is called importin-beta ($\text{Imp}\beta$). The complex of cargo protein ($\text{RhoE-Imp}\alpha\text{-Imp}\beta$) translocates into the nucleus by crossing the nuclear pore within the nuclear envelope (Marfori et al. 2011). Besides that, the $\text{Imp}\beta$ subunit mediates the docking of complex at the NPC, followed by translocation to the nucleoplasm. This model is also accepted by Xu et al. (2012) that established a similar conception for transient interaction which is specific for cargo delivery by nuclear transporter (NTR/KPN) (Xu et al. 2012).

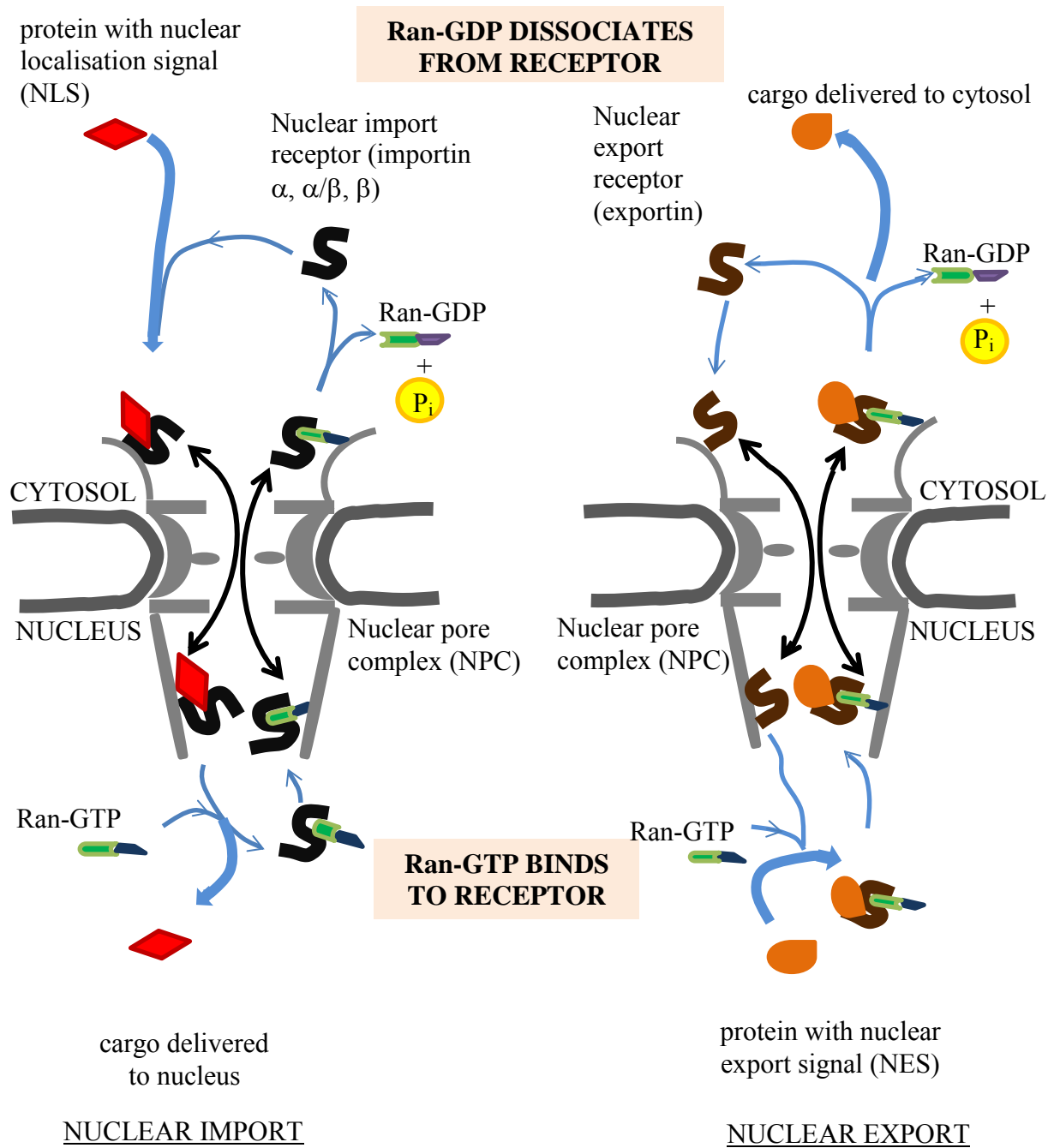


Figure 6: Nuclear transporters (importin and exportin) through nuclear pore complex (NPC) and facilitated via GTP hydrolysis by Ran. The blue arrows show different localisation of Ran-GTP in the nucleus and Ran-GDP in the cytosol (Adapted from Alberts et al. 2008).

The cycles between Ran-GTP associates importin in the nucleus and Ran-GDP dissociates exportin in the cytosol are designated for cargo delivery across the NPC. However, the directionality of the transport process is maintained by the establishment of a Ran gradient (blue arrows, in Figure 6), whereby Ran-GDP is predominantly found in the cytoplasm and Ran-GTP is located in the nucleus. The transport process is sustained through the actions of the cytoplasmic Ran GTPase-activating protein (Ran-GAP), and the chromatin-bound Ran GDP-GTP exchange factor (Ran-GEF), respectively. In addition, Figure 6 also indicates the dissociation of the complex inside the nucleus, which is affected by the binding of guanine nucleotide-binding protein Ran in its GTP-bound form (Ran-GTP) to Imp β , thereby displacing Imp α . After the dissociation is completed, the importins are cycled back to the cytoplasm and they are ready for another round of import (black arrow in Figure 6).

Moore (1998) affirmed that nuclear carriers for most proteins depend on transporters of Imp β group. Family members of Imp β interact with their cargo directly or through an adaptor protein. In addition, phosphorylation and other post-translational modifications can also change the transport of individual cargos (Moore 1998). Nuclear export occurs in an analogous fashion, in which the proteins inside the nucleus containing a nuclear export signal (NES) are recognised by exportins, followed by a complex formation with Ran-GTP. In the cytoplasm, the hydrolysis of Ran-GTP to Ran-GDP dissociates the complex. In addition, a critical function of small G protein-Ran which is a member of RAS oncogene family can be indicated by Ran Binding Protein 2 (RanBP2) based on the work carried out by (Hamada et al. 2011). The process of GTP binding nuclear protein is essential to capture the recycling Ran GTP–importin- β complexes at the cytoplasm to allow adequate recognition for NLS-mediated cargo import. Furthermore,

RanBP2 or also known as Nup358, is the major component of cytoplasmic filaments for nuclear pore complex (NPC). It is known that RanBP2 is essential in sustaining cell viability and providing strong evidence that the apoptosis of cell is associated with transport defects rather than mitotic failure (Hamada et al. 2011).

Usually, the permeability of NPC is selective and dependent on cell trafficking properties in controlling composition of macromolecules that are transported between the nucleus and the cytoplasm (Mingot et al. 2004). In this case, the small molecules are effectively transported via passive diffusion but the object exceeding 45kD and it has to be transported through facilitated mean. The conventional nuclear import for larger proteins requires recognition from nuclear localisation signal (NLS). Poon and Jans (2005) also clarified on how NLS with larger size protein can be recognised. The short sequence of basic amino acids either alone (monopartite) or separated by a linker region of 10–12 amino acids (bipartite), that are located in the cargo protein, should be visible and detected by the members of the importin superfamily (Poon and Jans 2005).

Overall, proteins that are lower than 45 kD should be able to efficiently diffuse across the nuclear envelope including RhoE (27-29 kD). Hence, there is still the requirement of transient interaction with NTR/KPN if RhoE is bound to its interacting protein partners and formed complexes that are larger than 45 kD. Moreover, there is a recent development in the field of nucleocytoplasmic transport that importin and Ran-dependent transport are not the only mechanisms that enter the nucleus. As an alternative, pathways that are independent of transporter molecules, RanGTPase, or energy are essential (Kodiha and Stochaj 2012). Thus, retention or accumulation of RhoE proteins in the nucleus offers a flip side of investigation for nucleocytoplasmic transport.

1.4 RhoE/Rnd3

1.4.1 Definition, Structure and Characteristics of RhoE

RhoE is predominantly a membrane-associated protein that has several synonyms such as Rho8, Rnd3 as well as Rho family GTPase 3. Besides that, RhoE is a small GTP-binding protein that belongs to the Ras Superfamily (Riou et al. 2013). This signalling protein is also a member of the Rnd subfamily. In general, Rnd proteins are unique, and they are originally identified by making the cells round up when expressed. To date, three Rnd proteins were identified including Rnd1, Rnd2 and Rnd3/RhoE (Cao and Buck 2011).

Komander et al. (2008) stated that RhoE is not stimulated by the conventional shift of GTP-binding configuration like other Rho family members. Although this protein is a small G-protein that belongs to the member of Rnd family for Rho GTPases, RhoE exhibits unusual properties through undetectable GTPase activity, and it does not bind to GDP. For instance, like other small G-proteins, RhoE binds to GTP, unlike other G-proteins, RhoE does not hydrolyse GTP to GDP (Fiegen et al. 2002).

The molecular structure of RhoE is visualised using the three-dimensional individual proteins - PyMOL Molecular Visualisation. To date, the data available in PDB Europe (<http://www.ebi.ac.uk/pdbe>) provides four ID codes that are related to the well-established RhoE crystallisation work including 4BG6 (RhoE and interaction with 14-3-3 for prenyl and phosphorylation motif), 2V55 (RhoE and interaction with ROCK1 for multi-site phosphorylation), 1M7B (RhoE and its functional implication in human), and 1GWN (homodimer and core domain for constitutively activated RhoE). The code of 1M7B is portrayed in the following figure that mimics the character of RhoE in human. Figure 7 shows the high-resolution structure of RhoE image.

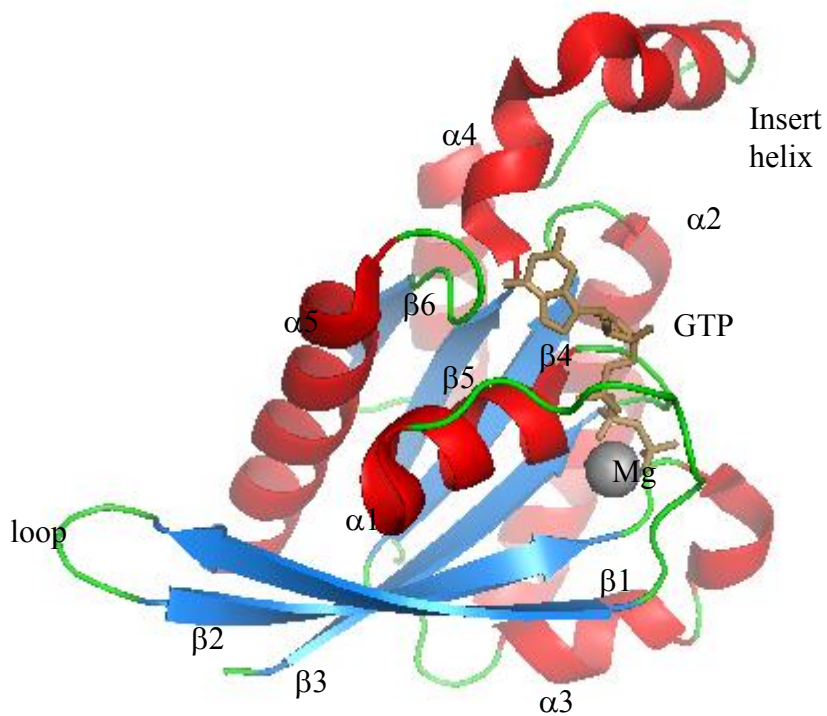


Figure 7: The high-resolution structure of RhoE in human (pdb: 1M7B) was visualised in PyMOL Molecular Visualisation and it was retrieved in a PNG file format. RhoE consists of six (6) β -sheet strands (five parallel, one antiparallel) that are surrounded by five (5) α -helices connected by a loop and an insert helix.

Referring to the 3D image that visualises the folding structure of RhoE, Figure 8 shows a linear amino acid sequence of RhoE. This protein has a unique GTP binding site in the GTP coordination where additional water molecule contacts invariant Ala¹⁷⁹ of the ¹⁷⁷CSAL-motive and the carbonyl oxygen of the base, which are structurally different than RhoA. Additional stabilisation of RhoE by Asp¹⁰³ is at the Lys¹³⁶ of the ¹³⁵CKSD-motive, whereas in RhoA is at the Ser⁸⁵ (Garavini et al. 2002).

Fiegen et al. (2002) mentioned that RhoE looks quite similar to RhoA in terms of sequence homology. Although the proteins share conserved regions and RhoE reproduces the essential structural features of RhoA that bind to the regulators or effectors, RhoE is differently regulated. RhoE does not utilise GDI, GAP and GEF, which regulate the activity of the most of small GTPases (Fiegen et al. 2002).

Foster et al. (1996) had initially disclosed that RhoE proteins are unable to hydrolyse GTP and they are resistant to GAP activity. In addition, RhoE is resistant to RhoGAP activity because due to the absence of a catalytically competent glutamine; Ser⁸¹ and the steric clash of the arginine finger (RhoGAP) with Ser³² (Guasch et al. 1998). As a consequence, the G-domain of RhoE is also completely unable to hydrolyse GTP in the absence or the presence of RhoGAP (Foster et al. 1996). Furthermore, Fiegen et al. (2002) also found that the alterations of four amino acids - Ser³² and Gln³³ (P-loop region), Ser⁷⁹ and Ser⁸¹ (Switch II region) are responsible for the RhoE GTPase deficiency (Fiegen et al. 2002).

```

      10      20      30      40      50      60
MKERRASQKL SSKSIMDPNQ NVKCKIVVVG DSQCGKTALL HVFAKDCFPE NYVPTVFENY

      70      80      90     100     110     120
TASFEIDTQR IELSLWDTSG SPYDNRPL SYPDSDAVLI CFDISRPETL DSVLKKWKGE

     130     140     150     160     170     180
IQEFCPNTKM LLVGCKSDLR TDVSTLVELS NHRQTPVSYD QGANMAKQIG AATYIE CSAL
                Lys136                                Ala179

     190     200     210     220     230     240
QSENSVRDIF HVATLACVNK TNKNVKNKS QRATKRISHM PSRPELSAVA TDLRKDKAKS

244
CTVM

```

Figure 8: The sequence of RhoE protein established in FASTA format (UniProt, 2011), RhoE is structurally different than RhoA due to the different coordination of GTP for GTP binding site that allows contact between additional water molecule to invariant Ala¹⁷⁹ of the ¹⁷⁷CSAL-motive as well as carbonyl oxygen of the base. Additional stabilisation of RhoE by Asp¹⁰³ is at the Lys¹³⁶ of the ¹³⁵CKSD-motive whereas RhoA is at the Ser⁸⁵.

1.4.2 Function of RhoE

1.4.2.1 RhoE in Reorganisation of Actin and Stress Fibre

RhoE involves in the reorganisation of actin cytoskeleton and loss of stress fibres followed by the decreased of contractility in various cell types (Riou et al. 2010). Normally, RhoE effect antagonises RhoA/ROCK1 mediated actomyosin contractility. Consequently, RhoE activity affects cell migration, contraction of the smooth muscle and neurite extension (Pacary et al. 2011). For instance, the dynamics of actin cytoskeleton in vertebrate is crucial in maintaining cell shape, enabling cell motility, as well as regulating cell cycle progression and mitosis (David et al. 2012). Thus, RhoE is a critical regulator that controls cell dynamic as it induces cell rounding.

Besides that, Gottesbühren et al. (2012) revealed that RhoE induces the increase in stress fibres and paxillin-containing focal adhesion. This effect was found to be non-canonical as it is solely applied to endothelial cells (EC) in blood vessels and not for other cell type. Moreover, an experimental study using murine cerebral cortex demonstrated that p190 RhoGAP and PlexinB2 to be competing for RhoE binding (Azzarelli et al. 2014). In principle, RhoE function antagonises RhoA but the existence of PlexinB2 in the cerebral cortex inhibits the function of RhoE and physical interaction with other proteins. Hence, RhoA activity is elevated. In this context, both physical and functional interaction between RhoE and PlexinB2 receptor enable the stimulation of RhoA activity during the migration of cortical neurons (Jie et al. 2015).

1.4.2.2 RhoE and Cell Cycle Progression

RhoE has an important role in the regulation of cell cycle. Lonjedo et al. (2013) investigated the RhoE expression level during cell proliferation and mechanisms for the regulation of cell cycle. They affirmed that RhoE is immediately accumulated when cells are entering the G₁ phase, particularly during inhibition of cell-cell contact and when exiting the cell cycle. They also found that RhoE is rapidly degraded during the G₁/S transition that is dependent on Akt (also known as protein kinase B/PKB) (Lonjedo et al. 2013).

Akt plays an important role in controlling both growth and neurotrophic factors; thus, commonly suppressing neuronal cell death. It is important to considering the Akt pathway in neuronal progression, as the role of RhoE is relevant in regulating the proliferation activity of the brain tumour cells. Glioma is also classified as the tumour of CNS and it is closely related with the abnormality of neuronal cells. Thus, the degradation of RhoE dependent on Akt pathway during the G₁/S transition may reveal an explanation on how RhoE deregulates the cell cycle systems and promotes uncontrolled proliferation of the glioblastoma.

In addition, Poch et al. (2007) explained that RhoE level will decrease immediately at the G₁/S transition and prolong towards the end of the cell cycle in several cell types. Besides that, RhoE also regulates cell cycle in normal cell type (Villalonga et al. 2004). They also revealed that RhoE inhibits cell cycle progression at G₁ phase in NIH3T3 cells. Nevertheless, the overexpression of RhoE could lead to the accumulation of cells in G₂. The presence of RhoE inhibits cell proliferation, particularly via the deactivation of extracellular signal-regulated kinase (ERK) pathway (Poch et al. 2007).

Riou et al. (2010) also explained that the mechanism of cell cell cycle progression is regulated by RhoE via suppressing translation of the cell cycle regulators, which are cyclin D1 and c-Myc. For instance, the recognition of 5' cap mRNA of cyclin D1 and c-Myc by eukaryotic translation initiation factor 4E (eIF4E) is necessary to promote the translation of these genes before proceeding to G₁ phase. However, the function of eIF4E is dependent on the phosphorylation status of translational regulator, 4EBP1 that is specifically phosphorylated by the protein kinase, mTOR (Villalonga et al. 2009). Most importantly, the phosphorylation of 4EBP1 by mTOR is also essential in promoting cell growth. Besides that, RhoE enables dephosphorylation of 4EBP1 via activation of protein phosphatase 2A (PP2A). Hence, RhoE promotes the binding between eIF4E to 4EBP1 and indirectly disrupt the cell cycle progression at G₁ phase. Figure 9 shows the schematic diagram of RhoE action in regulating the cell cycle progression.

Retinoblastoma tumour suppressor (pRB) has been studied as an attenuator of cell cycle progression through the interaction with E2F family of the transcription factors (McCabe et al. 2005). It was observed that cyclin D1 and its kinase partners, CDK4 and CDK6 consistently decreased in the presence of RhoE. The cell cycle regulators are required for the S-phase entry to mediate the phosphorylation of pocket proteins including retinoblastoma (pRb) (Kolupaeva and Janssens 2013). In general, the key function of pocket protein is to modulate E2F-regulated genes during the progression of cell cycle. The deactivation of E2F transcription factors could attenuate cyclin D1 and block the cell cycle progression (Cobrinik 2005). Consequently, the overexpression of RhoE leads to cell cycle arrest at the G₁ phase. Figure 10 shows the particular points that RhoE would interfere in the cell cycle progression of a normal cell type.

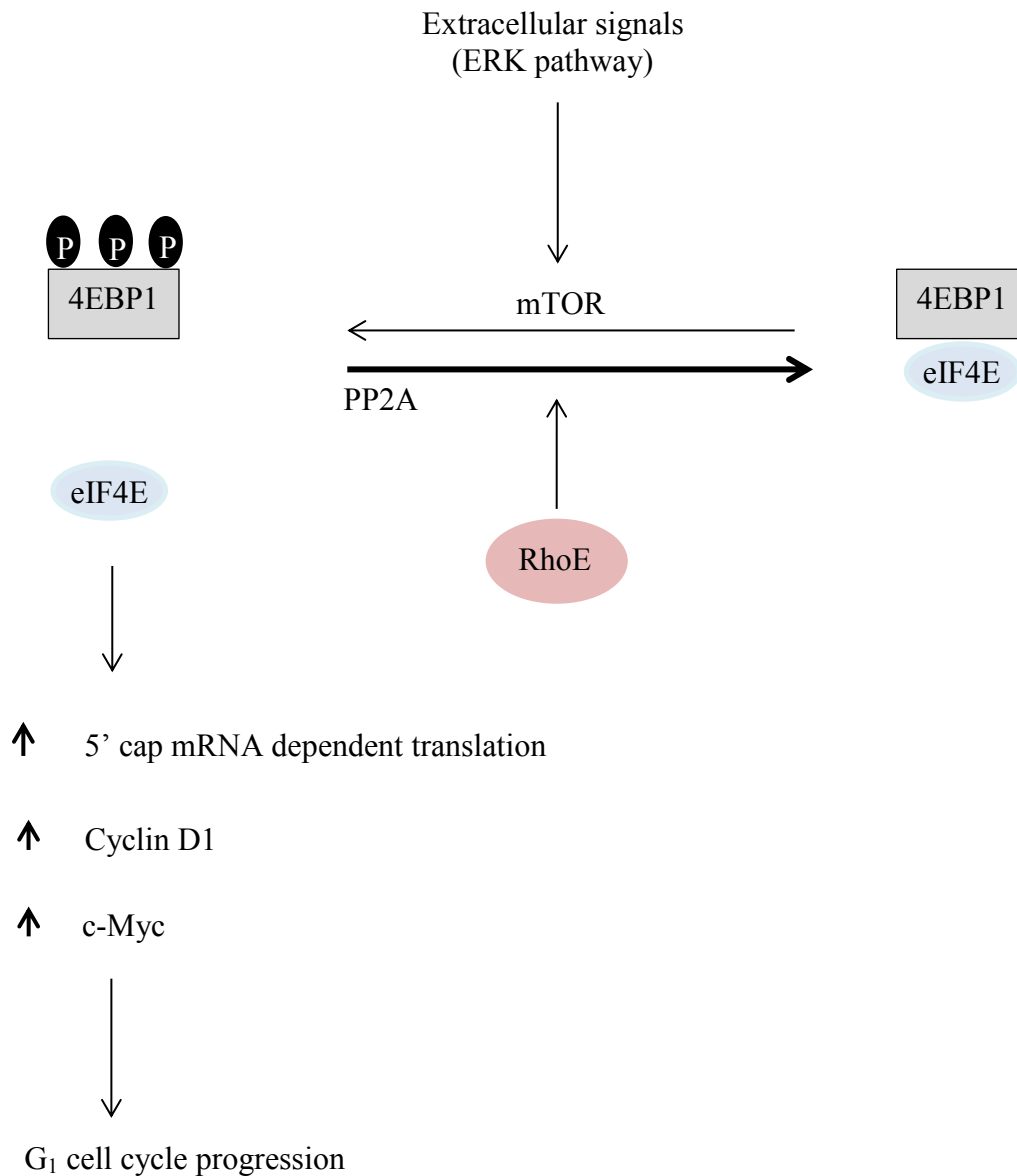


Figure 9: The schematic diagram on the regulation of cell cycle progression by RhoE. Phosphatase PP2A dephosphorylates 4EBP1. The presence of RhoE deactivates the extracellular signal-regulated kinase (ERK) pathway. Sequentially, eIF4A blocks protein kinase; mamalian target of rapamycin (mTOR) from phosphorylating 4EBP1, as well as ruling out its binding to 4EBP1. RhoE reduces 4EBP1 phosphorylation and prevents eIF4E from inducing the translations of genes that are required for cell cycle progression and stop at G₁ phase (Adapted from Riou et al. 2010).

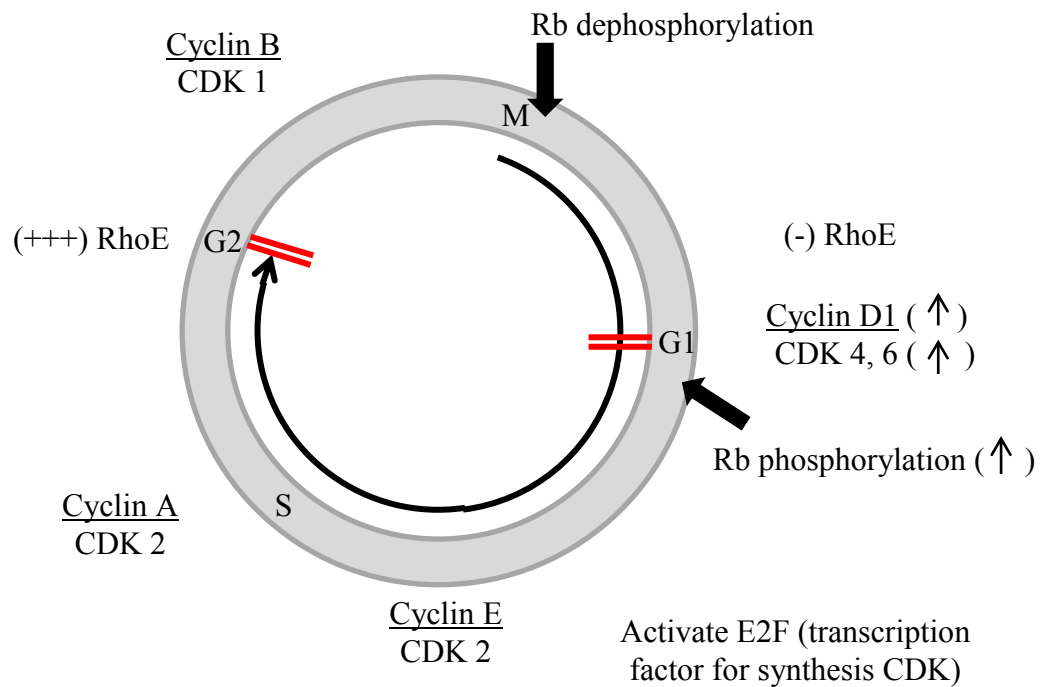


Figure 10: RhoE regulates the cell cycle progression in normal cell type by blocking the cell cycle progression at either G₁/S or G₂/M phases. Cyclin D1 and its kinase partners, CDK4 and CDK6, are consistently decrease in the presence of RhoE. The cell cycle regulator, Cyclin D1, in associating either CDK4 or CDK6 is required for the S-phase entry to mediate the phosphorylation of pocket proteins (e.g.: retinoblastoma, pRb). The presence of RhoE also attenuates E2F transcription factors and sequentially prevents the translational activity of CDKs. However, information regarding the rest of cell cycle regulators (Cyclin A and E that associate with CDK2 or Cyclin B that associates with CDK1) that are relevant to RhoE is quite limited. (Adapted from Kolupaeva and Janssens 2012).

1.4.2.3 RhoE in Cell Differentiation

Occasionally, the healthy cells stop dividing and they are no longer preceded into the cell cycle. Instead, the cells undergo differentiation. Riou et al. (2010) reported that RhoE is transiently up-regulated during keratinocyte differentiation. Corresponding to the higher expression of RhoE, the cells will exit from the cell cycle. In contrast, when RhoE is down-regulated, hyperproliferation of cells was observed (Liebig et al. 2009). Similarly, Ryan et al. (2012) also investigated a similar study and discovered the function of RhoE in controlling epithelial cell polarity and differentiation of keratinocytes. They also discovered that the knockdown of RhoE could induce hyperproliferation and overexpression of RhoE in increasing differentiation, which is indicated by the stratification layers of keratinocytes (Ryan et al. 2012).

1.4.3 Regulation of RhoE

1.4.3.1 Regulation of RhoE at Transcriptional Level

It was discovered that RhoE is not regulated by GTP hydrolysis, but instead the regulation of this protein is at multiple stages, including the transcription activity in the nucleus. A few evidence showed that it was activated at the level of transcription by diverse stimulants (Riou et al. 2010). Besides that, Chen et al. (2011) had carried out an experiment that used the inhibitor of histone deacetylation, Trichostatin A (TSA). This pharmaceutical product particularly blocks histone deacetylases (HDAC) by intercepting the elimination of acetyl groups from histones as well as modifying the functional gene synthesis. As a result, this modification promotes the accessibility of transcription factors

entering the DNA molecules inside chromatin. They revealed that acetylation of histone could elevate the activity of RhoE promoter, as well as RhoE mRNA and protein expression level (Chen et al. 2011). In contrast, they also discovered that DNA methylation has no effect on RhoE promoter based on the treatment with 5'-Aza-2'-deoxycytidine (5-Aza-dC), which is a DNA methylation inhibitor. There is yet a study that reveals the effect of RhoE expression on other cell types. These two different kinds of promoter inhibitor - HDAC and 5-Aza-dC were only applied in gastric cancer cells.

Besides, amino-terminal enhancer of split (AES) also enhances the activity of RhoE promoter. Although AES does not have a DNA binding site, it could regulate the transcriptional activity via interaction with transcriptional factors. Xia et al. (2013) investigated the expression level of RhoE when AES was knocked down via RNA interference. The results showed that mRNA of RhoE, as well as protein level, were down-regulated in MDA-MB-231 and HepG2, two types of cancer cell lines when AES is depleted. The overexpress AES had significantly increases the activity of RhoE promoter (Xia et al. 2013).

On the other hand, Pacary et al. (2011) discovered that RhoE is a direct transcriptional target of *Ascl1*, which is the proneural factor. *Ascl1* is required for neurogenesis and proper neuronal migration in the embryonic cortex. The manipulation of the gene expression using microarrays indicated that RhoE was significantly down-regulated in the embryonic cortex of mutant embryos when *Ascl1* was depleted and up-regulated in the ventral telencephalon of embryos that were overexpressing *Ascl1*. These results showed that *Ascl1* regulates RhoE expression in the embryonic mice cortex by the direct regulation of E1 enhancer region and also other elements in the RhoE locus.

1.4.3.2 Regulation of RhoE via Phosphorylation for Stabilisation

RhoE is a multifunctional protein where localisation and actions are commonly regulated by phosphorylation (Riento et al. 2005a). One of the most important aspects of RhoE regulation via phosphorylation is its interaction with ROCK1. Fiegen et al. (2002) discovered that α -helix of RhoE is profound with hydrophobic residues. There was also comparison being made with other small G-proteins such as the interaction between α -5 and ROCK1 α -G helix which was completely hydrophobic. As previously mentioned in Section 1.4.1, the specific sites of RhoE that interacts with ROCK1 do not exist in Rnd1 and Rnd2, which led to disabling the specific interaction with ROCK1. Therefore, RhoE is designed as a substrate for ROCK1.

The stable localisation of RhoE protein is increased via ROCK1 phosphorylation. Riento et al. (2003) stated that ROCK1 serine/threonine protein kinase promotes the formation of actin stress fibres and integrin-based focal adhesion by integrating the function of RhoA. The phosphorylation of RhoE by ROCK1 on multiple N and C termini has led to the stabilisation of RhoE. As a result, this modification reduces the stress fibre assembly, which contradicts to the function of RhoA (Riento et al. 2005a). Moreover, ROCK1 is also known to phosphorylate RhoE at seven sites (Riento et al. 2005b). Figure 11 shows the schematic diagram for the seven domains of phosphorylation on RhoE. These seven domain sequences are located in the N- and C-termini regions of RhoE, outside the core GTP-binding site. Amongst all seven phosphorylation sites, only S²⁴⁰ is modified by farnesylation and this phenomenon will be further discussed in Section 1.4.3.4. This site is adjacently located at the C-terminal cysteine.

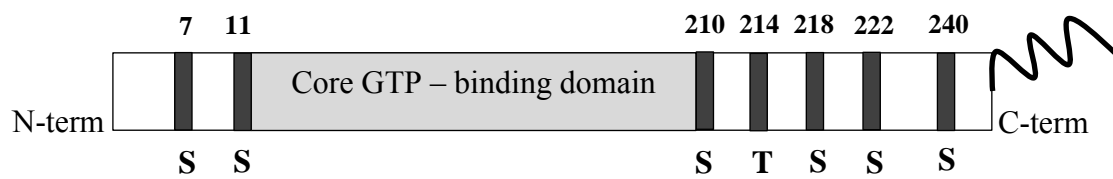


Figure 11: The schematic diagram shows the seven phosphorylation sites on RhoE. ROCK1 phosphorylates one site on threonine (Thr²¹⁴) and six sites on serine residues (Ser⁷, Ser¹¹, Ser²¹⁰, Ser²¹⁸, Ser²²², Ser²⁴⁰) that are located in the N- and C-termini regions, outside the core-GTP-binding domain in RhoE. (Adapted from Riento et al. 2005b; Riou et al. 2013).

RhoE interacts with ROCK1 through binding at the kinase domain (Sebti and Der 2003). Komander et al. (2008) conducted crystal diffraction analysis and revealed that RhoE interacts with ROCK1, specifically at the C-lobe of α -G helix domains. In particular, this area is adjacent to the catalytic site of ROCK1 that is located at N and C termini, but far from RhoE effector region (Komander et al. 2008). Moreover, the same working group showed that a high-resolution structure of RhoE in complex with ROCK1 kinase domain was found as a diverse phosphorylation site. Figure 12 shows the overview of ROCK1: RhoE complex.

Riento et al. (2005a) demonstrated that the phosphorylation status of ROCK1 by RhoE could promote the function of RhoE in regulating the cell cycle progression. When stress fibres are disassembled, phosphorylated RhoE can be seen. Simultaneously, the dephosphorylation of RhoE is also reciprocated with the formation of stress fibres. Although RhoE activity is regulated by ROCK1 phosphorylation, a study by Riento and co-workers (2005b) discovered that unphosphorylated RhoE is not involved in the reorganisation of actin filaments. Moreover, Riento et al. (2003) also priorly claimed that RhoE interaction with ROCK1 is essential in the process of cell migration.

Despite that disruption of ROCK1-RhoE interface eliminates RhoE phosphorylation, but it still maintaining disassembly of actin stress fibres. The defect at RhoE effector region causes the loss of stress fibres and disorganisation of actin cytoskeleton. As a result, RhoE forces the dysfunctional of ROCK1 specifically by blocking its interaction with effector region (Komander et al. 2008).

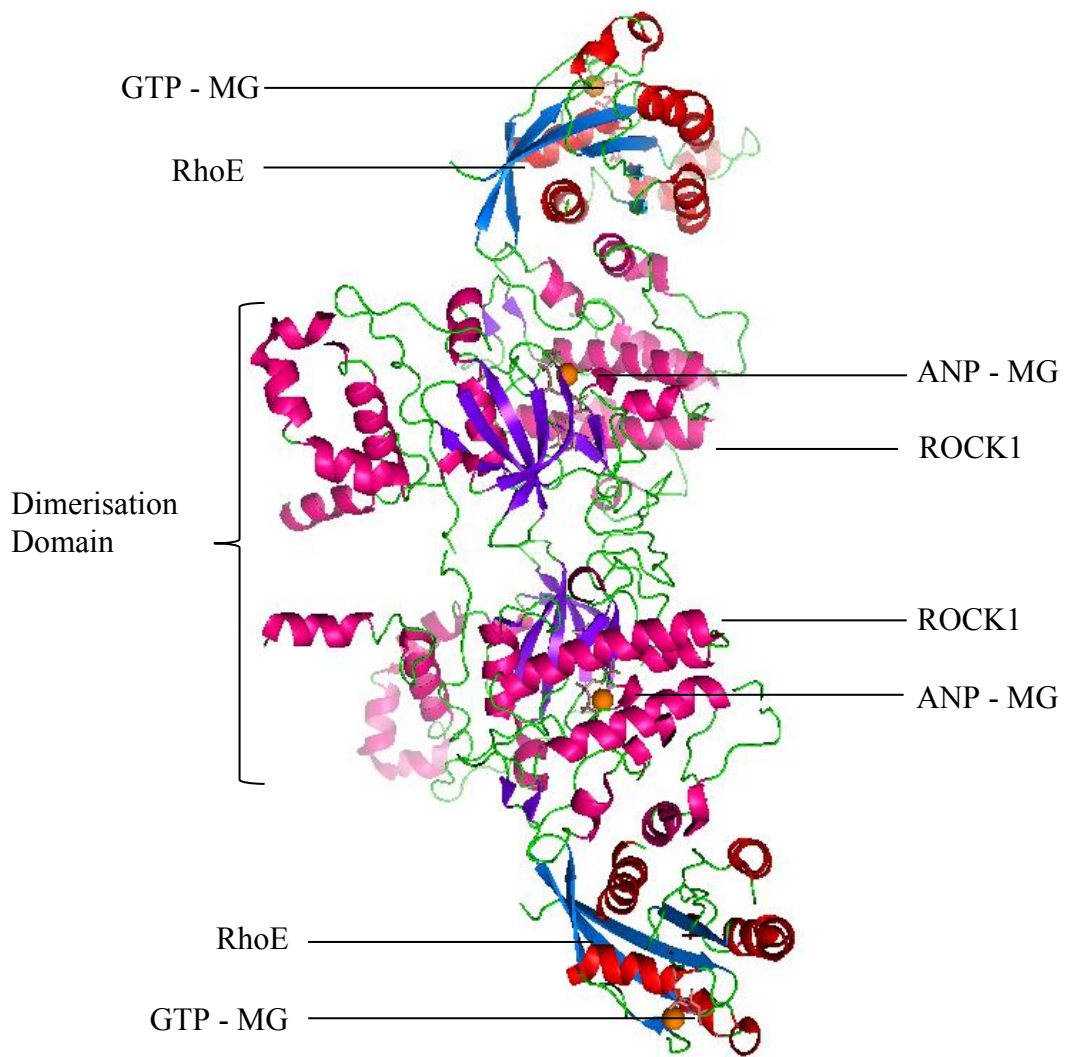


Figure 12: The high-resolution structure of RhoE in complex with the ROCK1 kinase domain. The structure of dimerisation domain between RhoE-ROCK1 and ROCK1-RhoE is visualised by Protein Data Bank (pdb: 2V55) using - PyMOL Molecular Visualisation and that can be retrieved in PNG file format. Each subunit of the ROCK1 dimer binds with one molecule of RhoE.

In brief, Komander et al. (2008) summarised the crystal diffraction work in Table 4. The list differentiates the interaction between RhoE and ROCK1 by means of ROCK1 residues that are exposed to RhoE interfacing RhoE residues interacted with ROCK1. In principle, the part of a feedback loop in RhoA signalling is regulated by ROCK1 phosphorylation of RhoE (Komander et al. 2008). RhoE antagonistically reacts with RhoA by inducing the loss of stress fibre formation, specifically at a part that binds to RhoA downstream kinase Rho-associated kinase (ROCK1) that resulted in the formation of a complex phosphorylated RhoE. This antagonist action prevents ROCK1 activation and inhibits downstream signalling (Loirand et al. 2006). Figure 13 shows a diagram for the flow of interaction between ROCK1 and RhoE.

Table 4: Interaction between RhoE and ROCK1 (Adapted from Komander et al. 2008)

Residue of ROCK1 exposed to RhoE	Residue of RhoE interacted with ROCK1
α G helix (Val ²⁸⁴ , Tyr ²⁸⁷ , Met ²⁹¹) α EF helix (Leu ²⁴⁶) additional contact: (Gln ²⁴⁹ - amide side chain)	α 5 helix (Val ¹⁹² and Leu ¹⁹⁵) additional contacts: (His ¹⁹¹ - imidazole side chain) (Arg ¹⁸⁷ - guanidium side chain)
α G helix (Ser ²⁸⁸)	β 6 strand (Thr ¹⁷³)
α G helix (Asn ²⁹² - amide side chain at C terminus)	α 4 strand (Tyr ¹⁵⁹ – hydroxyl group of side chain at the N terminus)
α EF/ α F loop (Gln ²⁴⁹ – amide side chain; and Ala ²³⁴ - amide main chain)	β 2/ β 3 loop (Asp ⁶⁷ – side chain)
α EF/ α F loop (Gln ²⁴⁹) - conformational shift	β 2/ β 3 loop (Asp ⁶⁷) α 5 helix (His ¹⁹¹)

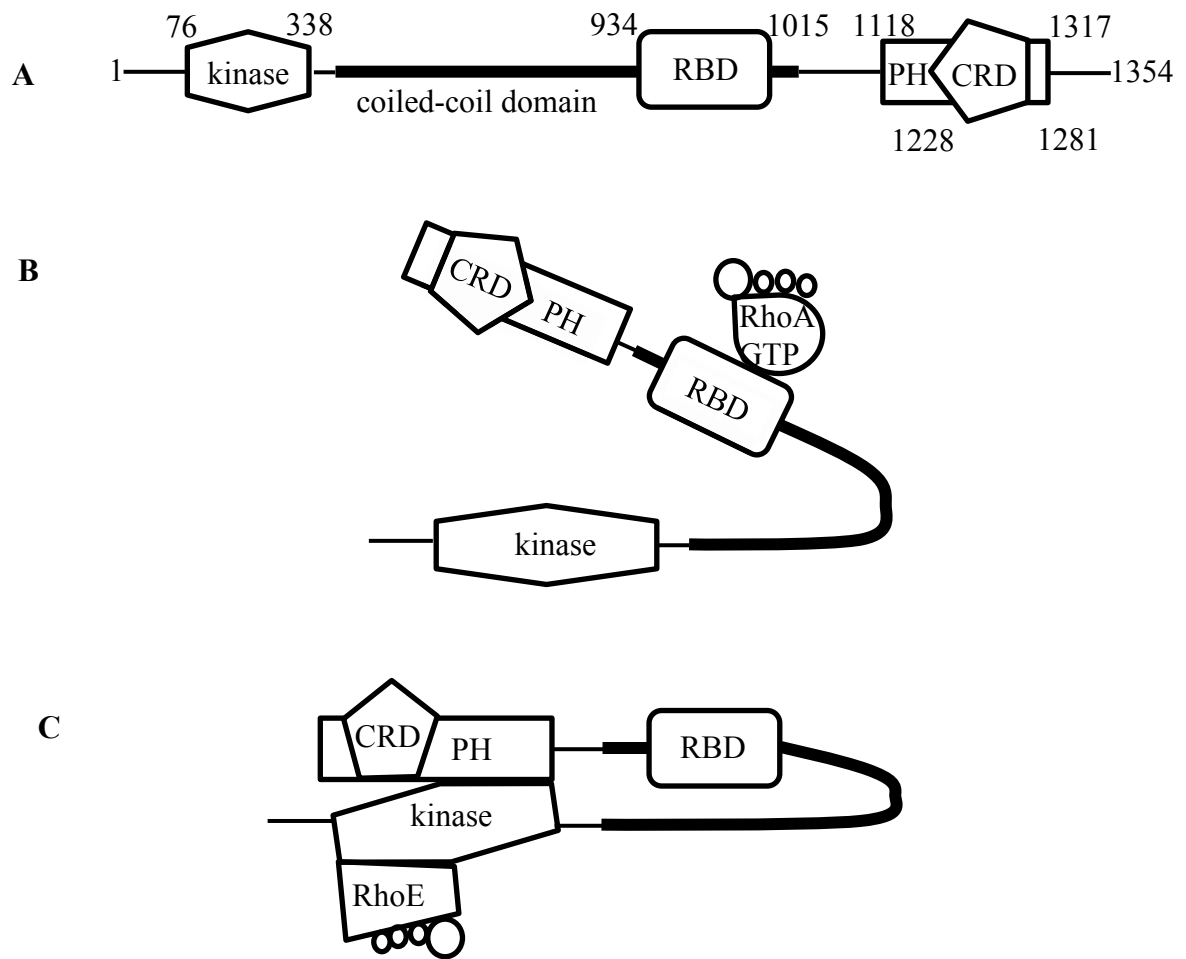


Figure 13: A diagram for the flow of interaction between ROCK1 and RhoE. **(A)** Molecular structure of ROCK1 comprised a sequence of kinase domain that is located at the amino terminus of the protein, followed by a coiled-coil region containing the Rho Binding Domain (RBD) and a Plextrin Homology domain (PH) with a cysteine-rich domain (CRD). **(B)** ROCK1 is activated when it interacts with RhoA bound GTP. **(C)** ROCK1 is inactivated when it interacts with RhoE, particularly when C-terminus of ROCK binds to the N-terminal region of the kinase, forming autoinhibitory loop. (Adapted from Loirand et al. 2006; Chen et al. 2010; Tu et al. 2011).

1.4.3.3 RhoE Is Not Regulated by ROCK2

ROCK1 and ROCK2 are two ROCK isoforms found in humans. ROCKs are not identical to other protein kinases, and they are usually differentiated by the serine or threonine kinase domains. The N- and C-termini extension segments are both required for the catalytic activity. The N-terminal enables the combination of two ROCK kinase domains to form homodimers. The formation of ROCK dimer via homophilic interactions occurs at the coiled-coil domains. However, the conformation of the coiled-coil domain in ROCK is not permanent whereby the amino acids could be replaced or conserved between ROCK1 and ROCK2 (Morgan-Fisher et al. 2013).

The properties of kinase domain have also led to the formation of autoinhibitory loops. Furthermore, the inactivation of kinase activity occurs when it binds to the C-terminal Rho Binding Domain (RBD) and Plextrin Homology (PH). Recent research by Chuang et al. (2012) revealed that autophosphorylation of ROCK2 is at Ser¹³⁶⁶. The specific site of phosphorylation is subjected to the activation status of the kinase (Chuang et al. 2012). Nevertheless, there is yet to be any cited literature on the statement that autophosphorylation at this site corresponds to the kinase activity status. Thus, more studies should be done to identify the effect of phosphorylation, particularly on protein targeting or protein-protein interactions.

One critic is not enough to explain on ROCK2 regarding the reason that RhoE is not meant to be its substrate. As mentioned in Section 1.4.3.2, residue α G helix (Ser²⁸⁸) of ROCK1 allows the interaction of β 6-strand (Thr¹⁷³) of RhoE. Although, ROCK1 and ROCK2 are both reflecting amino acid Serine, they are subjected to activate their kinase domain. However, the reasons given on why RhoE is not designated as a downstream effector for ROCK2 is questionable.

1.4.3.4 Regulation of RhoE via Farnesylation to Induce Translocation

Signal transduction can be amplified by membrane association to allow protein-protein interaction (Tamanoi et al. 2001). For instance, the post-translational modification of RhoE by prenylation can activate the membrane function of this protein (Foster et al. 1996). Prenylation is required in cycling the localisation of RhoE between cytoplasm and plasma membrane. Besides that, Riou et al. (2010) also reported that Rho protein, RhoE in particular can be prenylated with the addition of 15-carbon farnesyl group at C-terminus. Other Rho proteins such as RhoA, Rac1 and Cdc42 are prenylated with the addition of 20 carbon of geranylgeranyl isoprenoid group. The prenylation process utilises a precursor of either geranylgeranyl or farnesyl isoprenoid, and the hydrophobic molecule is added to a cysteine to anchor and attach them to the membrane (Visvikis et al. 2010).

During prenylation, geranylgeranylation (GG) and farnesylation are similar processes that occur in Ras superfamily protein, but both of them are specifically for Rab and Ras only. RhoE in particular contains the sequence of CTVM at the C-terminal, thus making it vulnerable to lipid modification. RhoE is unlike other Rho protein in lipid modification by GG, instead by the farnesylation because it has methionine at the carboxy-terminal box, which is similar with Ras protein (Foster et al. 1996).

14-3-3 is a scaffold protein that specifically binds to serine/threonine kinases (Linch et al. 2014). The function of 14-3-3 as an adapter which might change the configuration of other proteins or mask a part of the physical features of the binding partners before initiate various signalling cascades in cells. For example, Riou et al. (2013) have successfully used the novel farnesylation protein hybrid mode III/IV 14-3-3 binding to RhoE. The mode III is defined as 14-3-3 binds to N terminal residue of RhoE, whereas

mode IV is defined when C terminal of RhoE binds to two isoprenyl units. This hybrid mode can be manipulated to engage the C-terminal farnesyl group synchronously with the adjacent phosphorylated serine residues that are characterised in RhoE. Figure 14 shows the visualisation on 3D of 14-3-3 hybrid binding to RhoE.

In brief, Figure 14 shows the high-resolution structure of the interaction at prenyl-phosphorylation motif. The farnesylated peptide (KDKAK) is located upstream to the residues 232-241 of the CAAX box of RhoE, anchored by 14-3-3 at residue Cys²⁴¹. Linch et al. (2014) stated that the disposition of RhoE from cytoplasm to the membrane requires farnesylation of isoprenoid protein, 14-3-3. However, RhoE prenylation process is dependent on dual phosphorylation, by PKC (Ser²¹⁰) and ROCK1 (Ser²⁴⁰ and Ser²¹⁸) dependent (Linch et al. 2014).

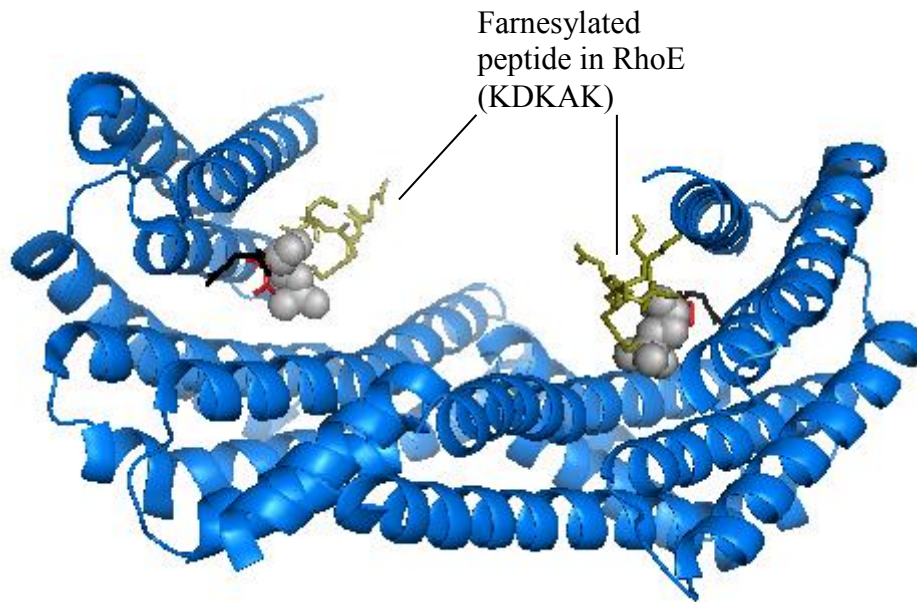


Figure 14: The high-resolution structure of 14-3-3 (pdb: 4BG6) interaction with prenyl-phosphorylation motif that upstream to the residues 232-241 of the CAAX box. Crystal structure of 14-3-3 (zeta/delta) indicated by homodimers of blue helices. The farnesylated peptide (olive stick – KDKAK) bound to each 14-3-3 monomer at Cys²⁴¹ and anchor residue that is indicated by red stick. The homodimers of 14-3-3 at diagonal position are visualised to expose the farnesylated peptide in RhoE.

Figure 15 shows a proposed mechanism during RhoE farnesylation that requires phosphorylation by ROCK1 and PKC. 14-3-3 inhibits RhoE-induced cell rounding by translocating this protein from the plasma membrane to the cytosol and it is facilitated via phosphorylation of RhoE at Ser²¹⁸ and Ser²⁴⁰ by ROCK1 and Ser²¹⁰ by protein kinase C (PKC). Riou et al. (2013) stated that Ser²⁴⁰ is a consensus site with PKC and the position of this amino acid is upstream to the CAAX prenylation motif at C-terminal hypervariable membrane-targeting domain of RhoE.

Madigan (2008) has investigated the modulation of PKC by using bryostatin-1, phorbol myristate acetate (PMA) and ionomycin that caused the loss of RhoE from the plasma membrane. In contrast, RhoE was found to be enriched in the cytosol and internal membranes when PKC was activated. Subsequently, Madigan et al. (2009) suggested that PKC agonist enables phosphorylation of RhoE to direct intracellular localisation. ROCK1 and PKC are both members of AGC kinase family that require dual phosphorylation and they are responsible for C-terminal site modification (Flynn et al. 2000). Overall, the complex formation of RhoE protein to the farnesyl group from 14-3-3 besides the additional phosphate from PKC and ROCK1 could influence RhoE function in the plasma membrane.

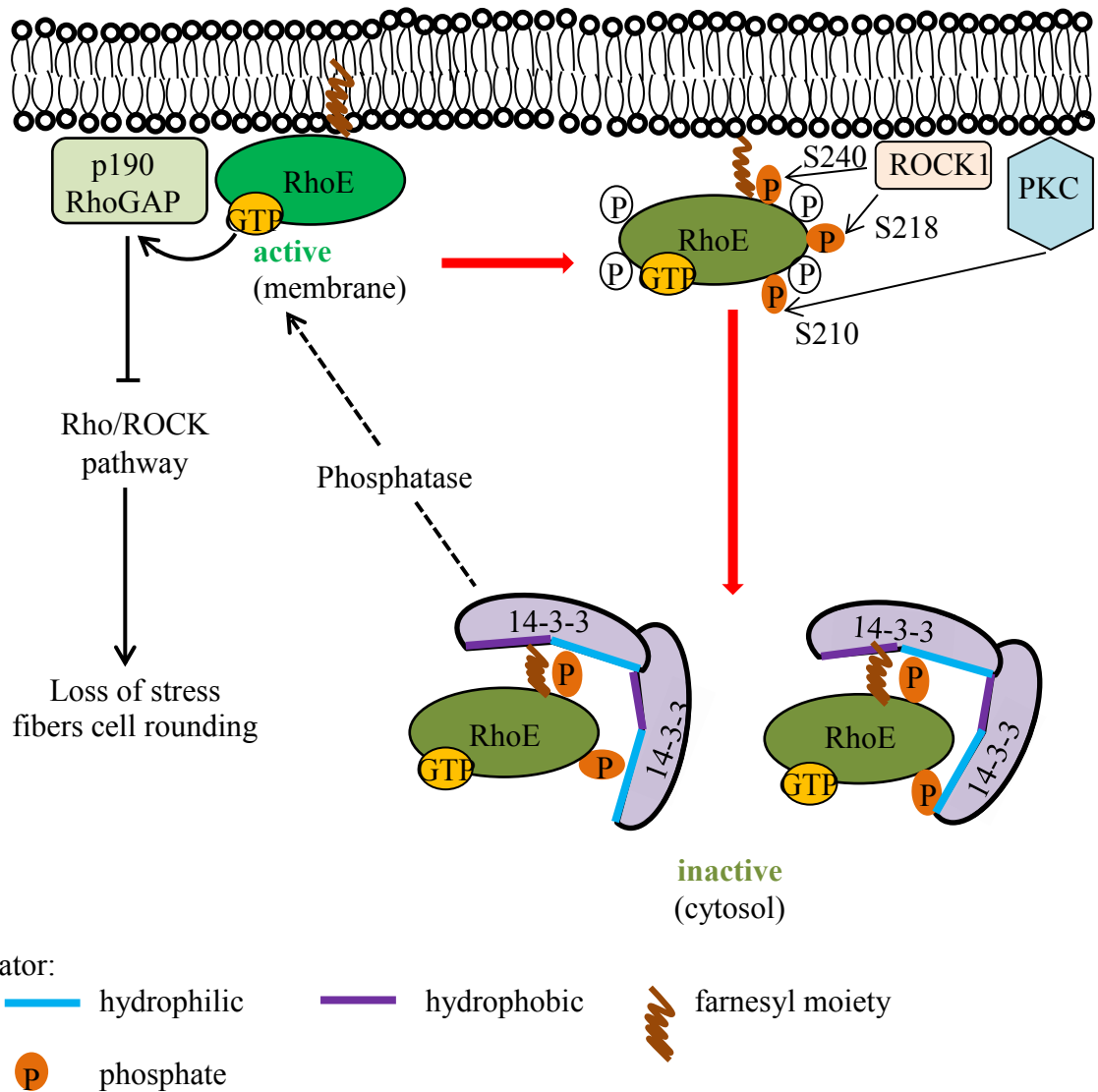


Figure 15: The interaction of RhoE with ROCK1 and PKC and post-translational modification via farnesylation. 14-3-3 inhibits RhoE-induced cell rounding by translocating it from the plasma membrane to the cytosol and facilitated via phosphorylation of RhoE at Ser²¹⁸ and Ser²⁴⁰ by ROCK1 and Ser²¹⁰ by protein kinase C (PKC). (Adapted from Riou et al. 2013).

1.4.3.5 Regulation of RhoE via Ubiquitination to Promote Proteosomal Degradation

Lonjedo et al. (2013) have identified a region between amino acids 231 and 240 of RhoE as the S-phase kinase-Associated Protein 2 (Skp2), E3 Ubiquitin Protein Ligase (Skp2-interacting domain) and Lys²³⁵ for the substrate of ubiquitylation. They proposed the mechanism by investigating which proteasomal degradation of RhoE by Skp2 that regulates its protein levels to control cellular proliferation.

In principle, proteasomal degradation of RhoE requires the interaction with Skp2 at C-terminal domain and ubiquitylation of Lys²³⁵. Due to the RhoE mutant lacking of C-terminal domain, it becomes more stable when compared to wild-type protein. The mutated residues of either Lys⁴⁵ or Lys²³⁵ increase the half-life of RhoE. Based on these findings, these residues are modified under specific conditions or responded to different stimuli. Besides that, it was discovered that the half-life of RhoE is shorter than other Rho proteins. Thus, proteasomal degradation by ubiquitination is involved in regulating the level expression of RhoE (Lonjedo et al. 2013).

1.4.4 RhoE in Cancer

During the overexpression of several members in Rho family of GTPases, it was observed that their upstream regulators or downstream effectors cause various malignancies, including pancreatic, breast, brain and prostate cancer. The negative regulation of p190 RhoGAP has the ability to negatively control the tumour growth, transformation, metastasis, invasion and angiogenesis, suggesting that Rho protein may function as a tumour suppressor *in vivo* (Vega and Ridley 2008). Prolonged inactivation of

Rho can result in apoptosis; however, reports are contrary regarding which apoptotic signalling pathways are activated. Furthermore, the cell transformation status was not clearly defined during the activation of signalling pathway (Ludwig and Parsons 2011).

Vega and Ridley (2008) reported that RhoE has multiple effects on cancer cell proliferation of either inhibiting of cell cycle via Ras-induced transformation or enhancing cancer progression by acting as a pro-survival factor induced by p53 depending genotoxic stress. Similarly, a recent report by Pacary et al. (2011) inferred that RhoE involved in neuronal tumour formation. However, the study did not completely examine the exact role of RhoE in inducing neurite outgrowth during the migration of neurones. An extended study by Peris et al. (2012) revealed the role of RhoE in neuronal polarisation by examining neurite and axon outgrowth. It was discovered that down-regulation of RhoE could lead to neuronal alterations and activate the signalling pathway of RhoA/ROCK1 /LIMK/Cofilin (Peris et al. 2012).

RhoE has an important role regarding cancer by regulating apoptosis and the function of this protein is to antagonise p190 RhoGAP (Poch et al. 2007). Ludwig and Parsons (2011) demonstrated that p190 RhoGAP levels can regulate the apoptotic response in breast cancer cell lines with docetaxel, which is a chemotherapy drug for breast cancer that uses the regulation of Rho. They suggested that p190 RhoGAP is also a regulator of apoptosis. The formation of intermediates for apoptosis such as multinucleation and dendritic phenotypes suggested that this process is mediated by p190 RhoGAP and its downstream effectors, including caspases. In addition, they also affirmed that elevated levels of p190 RhoGAP can sensitise breast cancer cells to docetaxel-induced apoptosis, which functions as a tumour suppressor. Since RhoE function is antagonising p190

RhoGAP, RhoE-deactivated cell death may function as a tumour enhancer. Thus, the depletion of RhoE could assist apoptosis, and it can be manipulated for cytoskeletal-based chemotherapeutics.

Ma et al. (2013) found a suppress profiling of RhoE that is closely related to tumourigenesis and metastasis of hepatocellular carcinoma cells (HCC). They observed that the decreased expression of RhoE in patients with hepatic tumours is significantly correlated with short survival after diagnosis. Moreover, a liver graft transplant model had demonstrated that RhoE depletion promotes local invasion of cancerous cells in the hepatic tissue of a nude mice *in vivo*. The immunity-inhibited mice exhibit the increase of angiogenesis including invasive tumour front (ITF) and formation of a large amount of draining veins in the liver.

1.5 The Aim of This Project

Peris et al. (2012) demonstrated that RhoE protein signature is consistent with the development of neuron. The knockdown of RhoE has led to suppressing both neurite and axon outgrowth as well as delaying the process of impulse transmission between neurons. RhoE depletion also induces neuronal alterations which involves in the activation of signalling pathway of RhoA/ROCK1 /LIMK/Cofilin. Regarding the work by Peris and co-workers (2012), it can be suggested that the examination for the role of RhoE can be extrapolated. This research should consider examining the function of RhoE in U87 human glioblastoma cell since this glioma cell line is derived from a stage IV tumour of CNS that is closely related to neurons.

Soulet et al. (2010) conducted preliminary studies using the chick chorioallantoic membrane (CAM) model *in vivo*. They implanted U87 cells into the CAM and mRNA samples, which are prepared at regular intervals after the implantation and the samples are analysed using microarrays. The result from the bioinformatics analysis of microarray data from U87 cells implicates nuclear RhoE in tumour development. Subsequently, Falciani and collaborators (2011) found that a number of nuclear RhoE interacting proteins are up-regulated 2-3 days after implantation (result unpublished).

The U87 human glioblastoma cell line is manipulated to study the function and regulation of RhoE *in vitro* for cell cycle and apoptosis, which is highly beneficial due to its ability to express RhoE at a consistent level. This is a collaboration work with Prof. Falciani and S. Durant from Molecular Angiogenesis Group at the IBR, School of Medicine, College of Medical and Dental Sciences, University of Birmingham, United Kingdom. Ryan (2010) has conducted an experiment using 293T cells that were generated preliminary data from the mass spectrometry analysis (result unpublished). The researcher has identified several novel protein partners in the nucleus that could potentially interact with RhoE including MCM3, MCM5, SSRPI, ORC3L and CAF1.

The rationale of investigating the nuclear RhoE interacting proteins for this project is to understand the mechanism and signalling pathway that are involved at the molecular level during the formation and development of brain tumour particularly glioma. By referring to the work done by Soulet et al. (2010) and the preliminary result by Ryan (2010), I intended to extend the research to determine the role of RhoE in regulating glioblastoma.

I will use the U87 human glioblastoma cell line *in vitro* for this research. The following are the individual aims of the experiments:

Aim 1: Analyse the role of RhoE in cell proliferation and apoptosis

Aim 2: Investigate whether the localisation of RhoE to the nucleus is dependent on serine/threonine kinases

Aim 3: Identify a novel RhoE interacting protein partners in the nucleus

CHAPTER 2

MATERIALS AND METHODS

2.1 Materials

2.1.1 General Laboratory Reagents

Cisplatin (cis-DDP or cis-diamminedichloroplatinum (II)) was supplied by Calbiochem, (Catalogue No. 232120). Y27632 was produced by GlaxoSmithKline under the license from Welfide Corporation. Gö6976 was supplied by Cell Signalling (Catalogue No: 12060). Phorbol myristate acetate (PMA) was obtained from Merk Millipore (Catalogue No: 52440). Other salts were obtained from either Fischer Scientific or Sigma Aldrich or other suppliers that are stated in the text. This study has used acids that were analytical grade and they were supplied by Fischer Scientific whereas all bases were supplied by Sigma Aldrich. Besides that, all solvents were analytical grade and they were purchased from Fisher Scientific, except acetonitrile that was provided by Scientific Laboratory Supplies with HPLC grade.

2.1.2 Media and Other Reagents for Cell Culture

Dulbecco Modified Eagle Medium (DMEM), Trypsin-EDTA (1X) and Optimem were purchased from Gibco (Life Technologies) whereas Eagle's Minimum Essential Medium (EMEM) was obtained from Lonza (BioWhittaker).

2.1.3 DNA Constructs

The overexpression vectors containing wild-type (WT) mouse RhoE and empty vector (EV) control, (pCMV5 RhoE Flag and pCMV5 EV Flag) and five (5) mutant constructs (pCMV5 Flag RhoE^{V56Y}, pCMV5 Flag RhoE^{T173R/V192R}, pCMV5 Flag RhoE^{F57Y}, pCMV5 Flag RhoE^{Y60A}, pCMV5 Flag RhoE^{V192R}) were received courtesy of Professor Ridley (King's College London) (Komander et al. 2008). Both recombinant RhoE wild-type (RhoE^{WT}) and RhoE point mutants were expressed as FLAG-tagged fusion proteins in *E. coli*. Recombinant FLAG was used as a control. Komander et al. (2008) generated all these constructs using the mutagenesis kit and they were cloned into the pCMV5 FLAG vector to produce FLAG epitope-tagged proteins. The wild-type and empty vector constructs were confirmed by DNA sequencing (Appendix 1 and Appendix 2).

2.1.4 Primers

Primers for real-time polymerase chain reaction (RT-PCR) targeted for RhoE sequence were designed according to personal discussion with Dr Sue Brewer (Brewer 2011). The appropriate primer was determined according to the nearest promoter adjacent to the multiple cloning sites (MCS). The gene of interest (RhoE) is usually inserted into the MCS of the vector via recombinant technology.

Riento et al. (2003) supported this presumption when they generated expression vector encoding FLAG-RhoE by inserting full-length mouse cDNA between *Eco*RI and *Hind*III sites of pCMV5-FLAG. A plasmid vector - pCMV5 was used in this experiment. The description of mammalian expression vector was adapted from Chubet and Brizzard (1996) and Figure 16 shows the prediction of RhoE construct as well as the nearest primers. For the transient

transfection experiment, two primers were selected which are CMV_fwd_primer and pCEP_fwd_primer as these primers are mapped adjacent to the MCS, that notably starts at *EcoRI*. These primers were then purchased from AltaBioscience, University of Birmingham, United Kingdom. Table 5 shows the details of these primers.

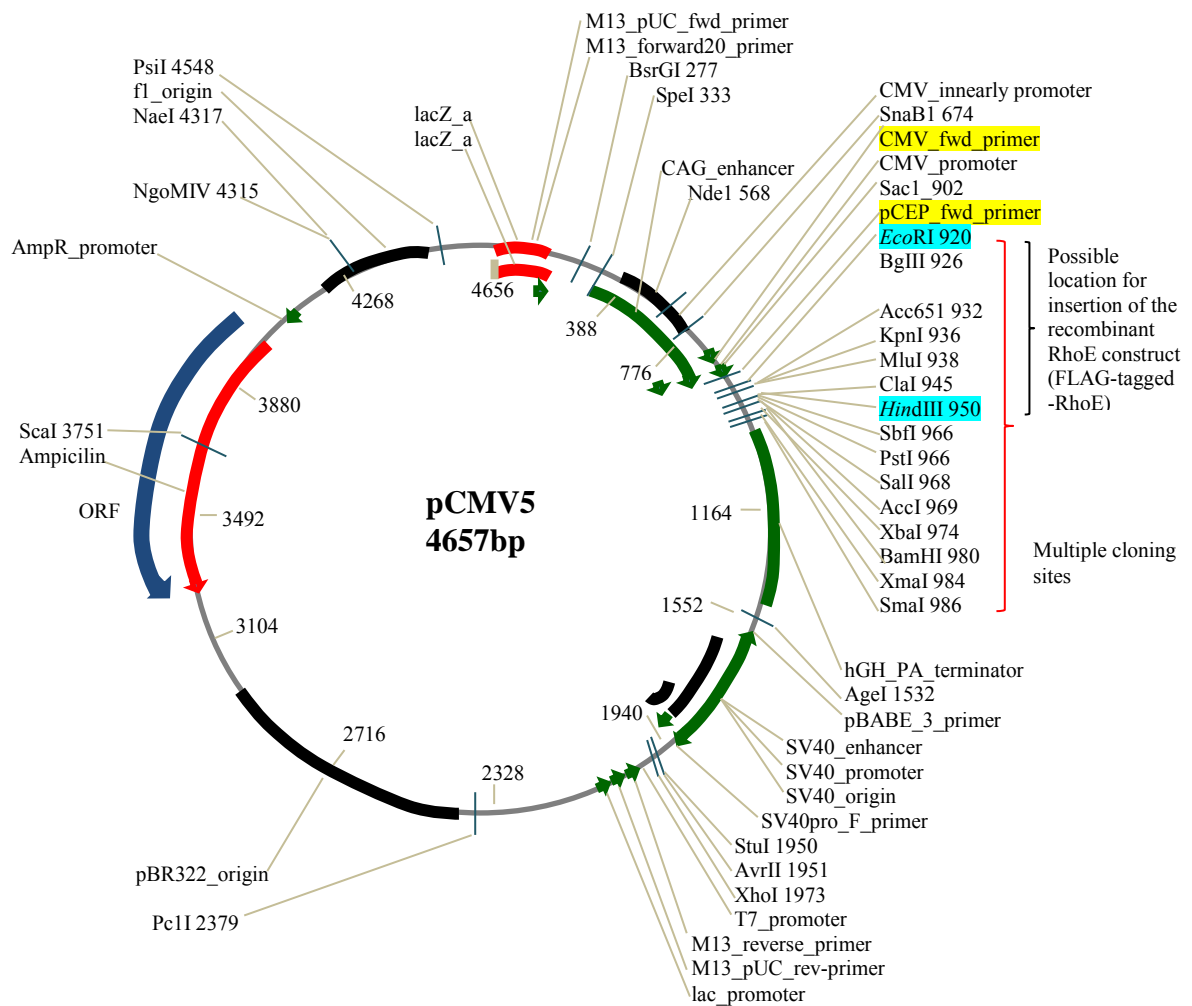


Figure 16: The map of the mammalian expression vector-pCMV5 that was predicted to have RhoE construct in between *EcoRI* and *HindIII* (highlighted in blue). The position of the nearest primers namely *CMV_fwd_primer* and *pCEP_fwd_primer* are highlighted in yellow. These primers are mapped adjacent to the multiple cloning sites (MCS) (Adapted from Brewer 2011; Chubet and Brizzard 1996; Riento et al. 2003).

Table 5: Primers for RT-PCR of RhoE Sequence

Primer	Sequence	T_m (°C)
pCMV	pCMV Forward: 5'd[CGCAAATGGGCGGTAGGCGTG]3'	72.2
pCEP	pCEP Forward: 5'd[AGAGCTCGTTTAGTGAACCG]3'	54.8

2.1.5 Antibodies

Antibodies used in this study are listed in Table 6.

Table 6: List of antibodies used in immunoblotting (IB) and immunocytochemistry (ICC)

Type of antibody	Titre of antibody		Species	Company provider	Storage
	IB	ICC			
a) <u>Primary antibody</u>					
RhoE	500	100	Mouse	Upstate, Millipore	-20°C
ROCK1	1000	100	Rabbit	Santa Cruz Biotechnology	4°C
Full Length Caspase 3	1000	N/A	Rabbit	Cell Signalling	-20°C
Cleaved Caspase 3	1000	N/A	Rabbit	Cell Signalling	-20°C
Full Length Caspase 9	1000	N/A	Rabbit	Cell Signalling	-20°C
Cleaved Caspase 9	1000	N/A	Rabbit	Cell Signalling	-20°C
α -Tubulin	5000	N/A	Mouse	Sigma (T6199)	-20°C
Actin Alexa-594-conjugated Phalloidin	N/A	1000	Fungi	Molecular Probes	-20°C
GAPDH	1000	N/A	Rabbit	Santa Cruz Biotechnology	4°C
Lamin	1000	N/A	Mouse	Santa Cruz Biotechnology	4°C
SSRPI	500	100	Mouse	Abcam	4°C
MCM3	1000	100	Rabbit	Abcam	4°C
MCM5	1000	200	Rabbit	Abcam	4°C
CAF1	1000	100	Mouse	Abcam	4°C
Anti-FLAG	1000	100	Mouse	Sigma Aldrich	-20°C

Type of antibody	Titre of antibody		Species	Company provider	Storage
	IB	ICC			
b) Secondary antibody					
Anti-Mouse – HRP	10 000	N/A	Sheep	Fischer scientific	4°C
Anti-Rabbit – HRP	10 000	N/A	Goat	Fischer scientific	4°C
Anti-Mouse – IgG biotinylated	10 000	N/A	Sheep	Amersham GE Healthcare	4°C
Anti-Rabbit – IgG biotinylated	10 000	N/A	Donkey	Amersham GE Healthcare	4°C
Anti-Mouse – link 680nm	20 000	N/A	Goat	Odyssey	-20°C
Anti-Rabbit – link 800nm	20 000	N/A	Goat	Odyssey	-20°C
Anti-Mouse FITC - Alexa Fluor 488nm	N/A	200	Goat	Molecular Probes	4°C
Anti-Rabbit FITC - Alexa Fluor 488nm	N/A	200	Goat	Molecular Probes	4°C
c) Tertiary (Fluorescence Label)					
Streptavidin, DyLight™ 800	40 000	N/A	N/A	ThermoScientific	4°C
Conjugated ECL	1:1	N/A	N/A	ThermoScientific	4°C

2.2 Methods

2.2.1 General Laboratory Procedure

2.2.1.1 Cell Culture

U87 human glioblastoma cell line was received courtesy of Sarah Durant (Professor Roy Bicknell's Lab, Institute for Biomedical Research (IBR), School of Medicine, College of Medical and Dental Sciences, University of Birmingham) and it was cultured in Dulbecco's Modified Eagles Medium (DMEM) (Gibco Cat. No. 41966) supplemented with 100 units/ml penicillin, 100 µg/ml streptomycin (Gibco) and 10% (v/v) of foetal bovine serum (FBS) (Lonza, BioWhittaker). The dish or flask was pre-coated with 0.1% (v/v) animal gelatine before the culturing process. COS7 and 293T cell lines were received courtesy of Jenson Lim (Professor Robin May's Lab, Biosciences, University of Birmingham) and Sylwia Krawczyk (Professor John Heath's Lab, Biosciences, University of Birmingham), respectively. The cells were cultured in Dulbecco's Modified Eagles Medium in a similar way to the U87 cells but without pre-coated with gelatine. HaCaTs, the immortalised keratinocyte cell lines were grown in Dulbecco's Modified Eagles Medium (DMEM) (Gibco Cat. No. 41966) supplemented with 100 units/ml penicillin, 100 µg/ml streptomycin (Gibco) and 5% (v/v) of FBS. Glioma cell line 11 and cell line 21 were received courtesy from the late Dr Carina Helberg (in memorial of School of Biosciences, University of Birmingham). The cells were cultured in Eagle's Minimum Essential Medium (EMEM) (Lonza) supplemented with 100 units/ml penicillin, 100 µg/ml streptomycin (Gibco) and 10% (v/v) of FBS. All the cell types were maintained at 37°C in a humidified 5% CO₂ atmosphere. The cells were passaged when they reached approximately 5 x 10⁶ cells in 1 ml aliquot and the small passage stocks were

stored in liquid nitrogen with 10% (v/v) dimethylsulphoxide (DMSO) preservative in FBS (Thompson 2009).

2.2.1.2 Cell Lysis

All cells were washed with PBS, and trypsinised and they were harvested in cold PBS. The cells were then pooled in a Falcon tube and centrifuged at 500 g for 5 min at room temperature. After that, the cells were lysed for 5 min in ice using RSB + 0.5% NP40 lysis buffer containing a final concentration of 10 mM Tris base pH 7.4, 5 mM MgCl₂, 10 mM KCl, protease inhibitors mix (Complete Mini, Roche Diagnostics) and phosphatase inhibitors cocktail (ThermoScientific). Both nuclear and cytoplasmic fractions were prepared by centrifugation 500 g for 5 min at 4°C. Whole cell lysates and supernatants (cytoplasmic fraction) were mixed with 6 X SDS sample buffer, whereas pellets (nuclear fraction) were mixed with 2 X SDS sample buffer (100 mM Tris, pH 6.8, 1 % Bromophenol blue, 10 % glycerol, 2 % SDS, 20 mM DTT). All fractions were then sonicated for 15 sec for three times and boiled at 95 °C for 5 min. All samples were stored at -20 °C (Lal et al. 2005).

2.2.1.3 Purification of Plasmid DNA

This study used DNA constructs (see Section 2.1.3) that were purified using QiaFilter Plasmid Maxi Kit (Qiagen Cat.No. 12262). 5 ml of LB (Luria Bertani broth) containing the appropriate selection was inoculated with *E. coli* transformed with the plasmid of interest and grown for 8 h at 37 °C. This culture was then diluted into 500 ml of LB (McMullan 2002), containing the appropriate selection and was grown for another 16-18 h at 37°C. The bacteria

were harvested by centrifugation at 2350 g for 15 min at 4°C and maxipreps were performed according to the manufacturer's instructions. The purified DNA plasmids were stored at -20 °C (McMullan 2002).

2.2.1.4 Quantification of DNA Concentration

The concentration of DNA was purified by maxipreps (see Section 2.2.1.3) and it was determined by measuring the absorbance of the DNA solution diluted in distilled water at 260 nm. An optical density unit represents 50 µg/ml of DNA (McMullan 2002).

2.2.1.5 Western Blotting

Equal amount of protein (20-25 µL) were resolved on 10 – 12.5% (v/v) SDS-PAGE gels for 1 h 20 min at 250V, 25mA, 100W at room temperature. Then, gels were transferred to PVDF (Immobilon-P, Millipore, Billerica, MA, USA) using a mini trans-blot apparatus (MiniProtean II, Bio-Rad) for 1 h 15 min at 100 V, 400 mA, 25 W at 4 °C (Colyer 1999).

2.2.1.6 Immunoblotting

The protocols used for immunoblotting were variable depending on types of protein to be detected and imaging system available during that particular time. Table 7 briefly describes the individual protocol.

Table 7: Immunoblotting protocols

Protocol	X-Ograph	Odyssey	Odyssey (biotinylation)
a) <u>Blocking system</u>			
Blocking Buffer/ Solvent	5% skimmed milk in TBST	Absolute Methanol 2 min followed by air dry	5% skimmed milk in TBST
Total time consumed for blocking	1 h, RT	12 min, RT	1 h, RT
b) <u>Primary antibody</u>			
Buffer used for antibody dilution	5% skimmed milk in TBST	Odyssey blocking buffer diluted (1:1) with cold PBS (1X)	5% skimmed milk in TBST
Incubation time and condition	Overnight, 4°C	Overnight, 4°C	Overnight, 4°C
Washing buffer and washing step	TBST 3 x 10 min each	PBST 4 x 5 min each	TBST 3 x 10 min each
Total time consumed for washing	30 min	20 min	30 min
c) <u>Secondary antibody</u>			
Buffer used for antibody dilution	5% skimmed milk in TBST	Odyssey blocking buffer diluted (1:1) with cold PBS (1X)	5% skimmed milk in TBST
Incubation time and condition	1 h, RT	1 h, RT	1 h, RT
Washing buffer and washing step	TBST 3 x 10 min each	PBST, final wash PBST was replaced with PBS 4 x 5 min each (membrane to be kept in the dark)	TBST (1 st wash) TBS (2 nd and 3 rd wash) 3 x 10 min each
Total time consumed for washing	30 min	20 min	30 min

Protocol	X-Ograph	Odyssey	Odyssey (biotinylation)
d)Tertiary (Fluorescence label)			
Reagent	Super signal ECL/ normal ECL	IRDye	Dylight Streptavidine
Time exposure to fluorescence label	5-30 sec	N/A	30 min – 1 h
Buffer used for fluorescence label dilution	N/A	N/A	TBS
Washing buffer	N/A	N/A	TBS
Washing step	N/A	N/A	3 x 10 min each
Total time consumed for washing	N/A	N/A	30 min

2.2.1.7 Image Scanning

The blots were processed by the exposure of medical X-ray film (Scientific Lab Suppliers Ltd), which was then developed using an X-Ograph (Colyer 1999). Alternatively, the immunodetection of proteins in blots can also be spotted by scanning the PVDF membranes onto an Odyssey infrared imaging system (LI-COR Biosciences) at two different wavelength of 700 nm and 800 nm, with 2.5 gains of exposure under red channel (680 nm) and 5.5 gains of exposure under green channel (800 nm) at 169 μm resolution.

2.2.1.8 Densitometry Analysis

The quantification of density (intensity) of bands on Western blot was carried out using Java-based image processing software, Image J.

2.2.1.9 Preparation of Glass Cover Slips for Cell Culture

The glass coverslips were treated for 5 min in concentrated nitric acid at room temperature. The nitric acid was then diluted with tap water, and the cover slips were washed in overflowing water for 30 min. Next, the coverslips were washed in pure methanol for three times, and they were left to evaporate at room temperature for overnight in a sterile condition. The coverslips were dried by incubation at 140 °C for at least 4 h before being used (Robertson 2004).

2.2.1.10 Fixation of U87 Human Glioblastoma Cell Lines on Coverslips

The cells were cultured on pre-coated coverslips with 0.1 % (*w/v*) gelatine from animal skin for 48 h. The coverslips that were previously prepared (Section 2.2.1.9) were rinsed three times with PBS and fixed with 4 % paraformaldehyde (PFA) pH 7.4 for 10 min at room temperature (Thompson 2009).

2.2.1.11 Permeabilisation

The coverslips were permeabilised using cold 0.1% (*v/v*) Triton X-100 in PBS for 5 min at room temperature after PFA fixation. This step is essential for the accessibility of antibody into the cells in detecting the protein. These include intracellular proteins and transmembrane proteins with epitopes that are located in the cytoplasmic region.

2.2.1.12 Immunofluorescence Staining

Immunofluorescence staining was performed as described previously but with some modifications (Ryan, 2010). The cells were washed three times with PBS, and the coverslips were incubated with primary antibody diluted in PBS, about an hour at room temperature. Next, the coverslips were washed three times in PBS and incubated with the relevant secondary antibodies (Alexa 488nm conjugated antimouse or antirabbit) diluted in PBS, about an hour at room temperature. The coverslips were rinsed with PBS contained 0.1% (*v/v*) Tween-20 for 10 min followed by nuclear staining using Hoechst 33342 or DAPI at 1:10 000 dilution in PBS Tween-20. Later, the coverslips were extensively washed with PBS and

rinsed with distilled water to prevent crystallisation (Ryan, 2010). Finally, the coverslips were mounted using Mowiol (Robertson 2004) and the immunostained cells were visualised using a Nikon Eclipse *Ti* microscope that is equipped with Hamamatsu ORCA-R2 camera model C10600-10B. The images were captured and processed using NIS-Elements BR 3.22.00 (710) software (Nikon, Japan).

2.2.1.13 Immunofluorescence Staining for FLAG and Confocal Microscopy

According to Ryan (2010), immunofluorescence staining for FLAG was modified from Sections 2.2.1.11 and 2.2.1.12 by performing a blocking step to reduce non-specific antibody binding. After fixation (see Section 2.2.1.10) cells were incubated with 50 mM NH_4Cl diluted in PBS for 10 min at room temperature, the process is followed by permeabilisation (see Section 2.2.1.11). Then, the cells were washed three times in PBS, for about 5 min each at room temperature. The coverslips were incubated with 10% (v/v) heat-inactivated normal goat serum (HINGS) and 5 % (w/v) bovine serum albumin (BSA) in PBS for 1 h at 37 °C to prevent non-specific binding (Ryan 2010). The anti-FLAG primary antibody was diluted in blocking buffer at 1:1 000 and the coverslips were incubated for 2 h at 37 °C. Then, the coverslips were rinsed with PBS contained 0.1 % (v/v) Tween-20 for 10 min, followed by nuclear staining of using either Hoechst 33342 or Sytox Red 633 (Molecular Probes, Invitrogen) at 1:10 000 dilution in PBS Tween-20. The rest of the protocol is similar with the descriptions mentioned in Section 2.2.1.12.

2.2.2 Experimental Design

2.2.2.1 RNAi Transfection for Knocking Down RhoE

The method that is used to knockdown RhoE is RNA interference (RNAi) by gene silencing. Transfection via small interfering RNA (siRNA) was conducted in the concentration of 9 pmol oligo per 300 000 cells in 35 mm of p6 well tissue culture dish. Two siRhoE oligos were used to deplete RhoE from U87 cells, which are the oligo A, 5'-TAGTAGAGCTCTCCAATCA-3' and the oligo B, 5'-CAAACAGATTGGAGCAGCT-3'. The sustainability of the knocked down in U87 cell line was investigated after the transfection with siRNA oligos. The protein samples were prepared on a daily basis for four days to determine the effectiveness of RhoE knockdown in U87 cell over time.

Figure 17 (A) and (B) show the knocked down effectiveness when using RhoE oligo A and RhoE oligo B. The non-silencing control was used as a control oligo at the same time. Both figures, show that RhoE was totally depleted on day 1 (24 h), and the depletion was prolonged until day 4 (96 h) in knock down RhoE conditions. The knockdown was consistent for both oligos.

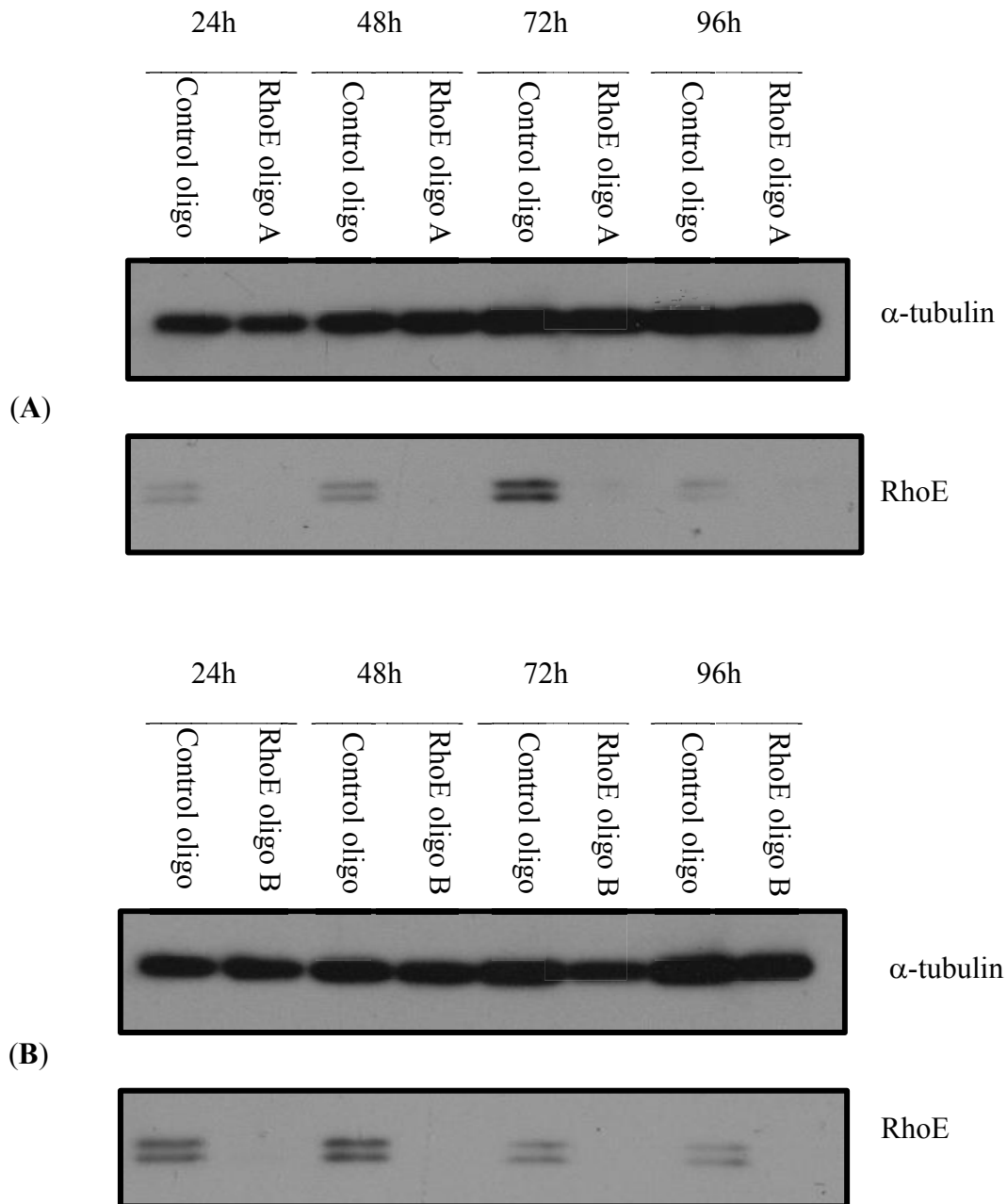


Figure 17: Knock down RhoE of U87 cells using oligo RhoE A (**A**) and oligo RhoE B (**B**) in comparison with control oligo (non-silencing control) over time. The depletion of RhoE was prolonged until at least 96 h.

2.2.2.2 Bromodeoxyuridine (BrdU) Uptake

The entry into S-phase was analysed by the incorporation of BrdU (Bromodeoxyuridine) that uses a BrdU labelling and detection kit from Boehringer Mannheim (Cat. no. 1296732). The cells were grown on glass coverslips for 48 h and they were incubated with BrdU, before being diluted in normal growth medium, for 1 h under normal cell culture conditions. The media was not changed to prevent serum stimulation at the S-phase entry. Cells fixation with 70 % (v/v) ethanol was applied in 50 mM glycine pH 2 for 20 min at -20 °C. BrdU incorporation was assessed by indirect immunofluorescence using a monoclonal antibody against BrdU. DAPI was used to label all nuclei at 1:10 000 dilution. The cells were visualised using a Nikon Eclipse *Ti* microscope that is equipped with a Nikon camera. The microscopic images of both BrdU positive cells and DAPI were taken before being overlapped for each field of view, with seven areas for each condition. For the statistical test, the minimum cells were 250 for each coverslip in triplicate for each set of experiment and conducted in three different batches ($n = 3$). The number of BrdU-positive cells was determined as the percentage (%) of S-phase entry cells for the total number of cells.

2.2.2.3 Optimisation of Apoptosis Assay

This study conducted an apoptosis experiment, using a similar approach by Darenfed et al. (2007). The siRNA RhoE oligos were used to perform the siRNA transfection to get the target gene knockdown for 96 h. The oligo B, 5'-CAAACAGATTGGAGCAGCT-3' was introduced to U87 cells at the beginning of the experiment to enable transient transfection. This study has applied some modifications, particularly to the time frame of the treatment of

ROCK inhibitor (Y27632) to fit the U87 cells condition. In addition, cisplatin was also added within 96 h of RhoE knockdown, and this step was not applied in the previous study.

The ROCK inhibitor (Y27632) was applied 48 h after the knockdown, followed by genotoxic stress that is induced by cisplatin after 78 h post-RhoE-depletion. The U87 cells were also prolonged and incubated with Y27632 by replenishing this compound at every 12 h intervals during cisplatin treatment to conserve ROCK1 inhibited phenotype. The treatment with cisplatin and Y27632 on U87 cells were accomplished at 96 h post-transfection. These cells were then harvested, and cell lysates were prepared for SDS-PAGE, before being transferred to PVDF membrane and subjected to immunoblotting.

Figure 19 shows the experimental design. The flow chart shows the optimised apoptosis experiment and indicates the critical time point for the addition of the apoptotic inducer (cisplatin) and ROCK inhibitor (Y27632).

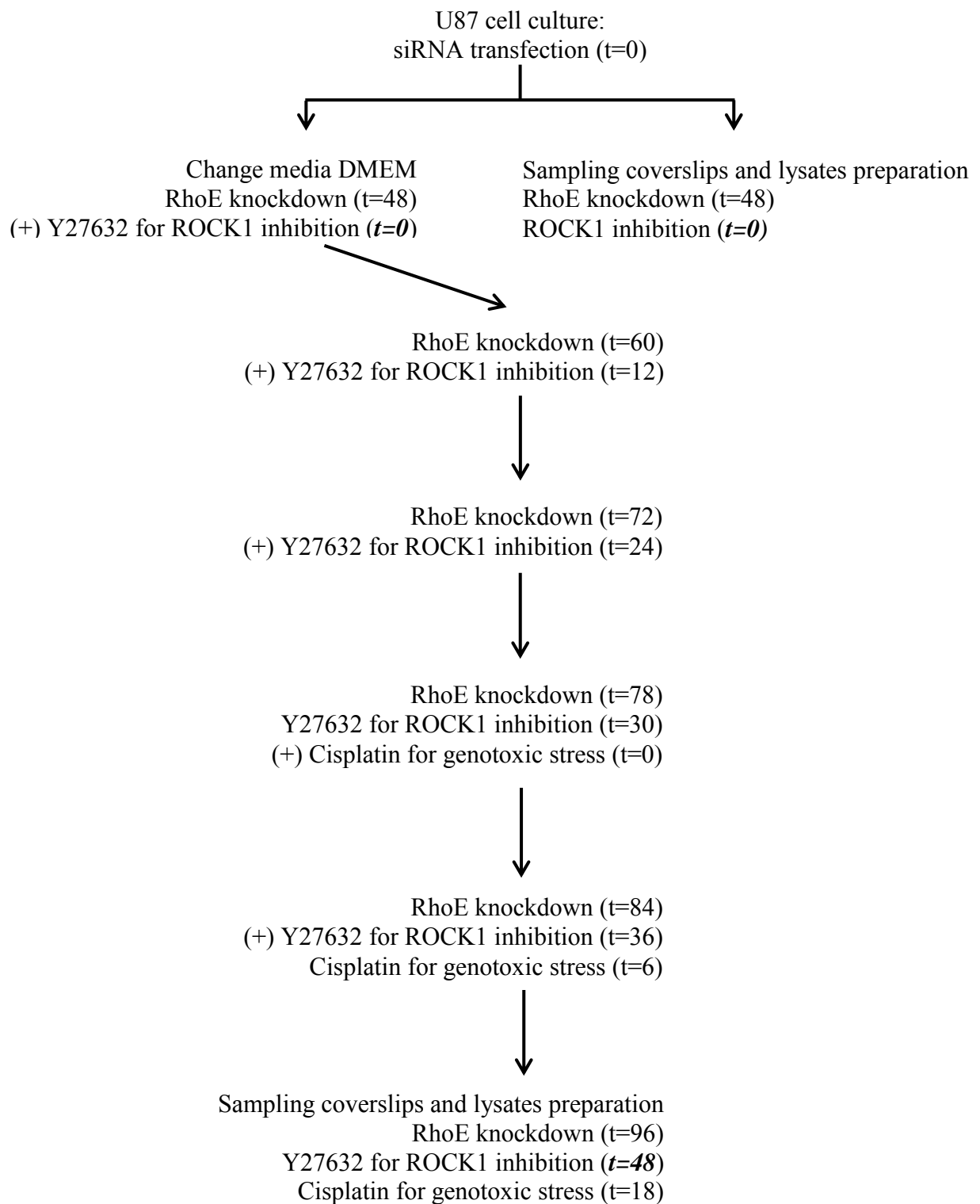


Figure 18: Schematic diagram of optimised apoptosis experiment indicating critical time for the addition (+) of apoptotic inducer (cisplatin) and ROCK inhibitor (Y-27632).

2.2.2.4 Translocation of RhoE to the Nucleus by the Effect of Serine/Threonine Kinase

The U87 cells expressing endogenous RhoE were cultured at 1.0 million units of cells per 100 mm tissue culture dishes for 24 h to obtain 50 % confluence level. Then, these cells were pre-treated with the pharmacological inhibitor of either Y27632 for ROCK1 or/and Gö6976 for PKC α for up to 3 h. For control conditions, the U87 cells were only received the diluents, of either PBS or DMSO. Then, the translocation of RhoE following the inhibition of serine/threonine kinases (ROCK1 and PKC α) was investigated via the activation of novel PKC α by 15 min treatment with phorbol myristate acetate (PMA). Figure 19 shows the schematic diagram for the procedure of this experiment, including detailed descriptions of condition, 1 to 8 for each replicate.

The U87 cells were treated with designated pharmacological compounds before being harvested, and the cell lysates were prepared for SDS-PAGE, transferred to PVDF membrane and subjected to immunoblotting. The semi-quantitative analysis was performed on the PVDF blot to determine RhoE intensity using Image J software. The full set of the experiment, including condition 1 to 8 were conducted in triplicates ($n = 3$). The significant difference between novel activation of PKC α and inhibition of ROCK1 in translocating RhoE between cytoplasm and nucleus was determined with the statistical analysis, which is Student *t*-test (*) ($p < 0.05$).

1	2	3	4
(-) Y27632 (10 μ M) (-) Gö6976 (2.5 μ M)	(+) Y27632 (10 μ M) (-) Gö6976 (2.5 μ M)	(-) Y27632 (10 μ M) (+) Gö6976 (2.5 μ M)	(+) Y27632 (10 μ M) (+) Gö6976 (2.5 μ M)
5	6	7	8
(-) Y27632 (10 μ M) (-) Gö6976 (2.5 μ M)	(+) Y27632 (10 μ M) (-) Gö6976 (2.5 μ M)	(-) Y27632 (10 μ M) (+) Gö6976 (2.5 μ M)	(+) Y27632 (10 μ M) (+) Gö6976 (2.5 μ M)

(Pre-treatment for 3 h)



1	2	3	4
(-) PMA (100 nM)			
5	6	7	8
(+) PMA (100 nM)			

(Treatment for 10 min)

Note:

(-) Y27632 (10 μ M) is replaced by PBS

(-) Gö6976 (2.5 μ M) is replaced by DMSO

(-) PMA (100 nM) is also replaced by DMSO

Figure 19: Schematic diagram for the procedure of investigating the translocation of RhoE to the nucleus using pharmacological compound - ROCK inhibitor (Y27632), PKC inhibitor (Gö6976) and novel PKC activator (PMA). The verification of the experiment was determined by the localisation of endogenous RhoE in U87 cells in the control condition.

2.2.2.5 Localisation of RhoE in U87 Cells via Export-import Mechanism

The preparation for the isolation of the nuclear fraction from cytoplasm is to confirm the hypothesis for the existences of the Nuclear Export Signal (NES) in RhoE. Leptomycin B (LepB) – the NES inhibitor, was introduced into U87 cells for 6 h to allow inhibition of NES, which might lead to RhoE accumulation within the nuclear region. 1.0 million unit cells were cultured in 100 mm diameter of dishes for a series of concentration starting from 0.0 nM up to 15.0 nM. The U87 cell was cultured for 24 h before being treated with LepB. Then, whole cell lysate, nuclear and cytoplasmic fractions of U87 cell were prepared 6 h post-LepB treatment. The samples underwent SDS-PAGE, transferred to PVDF membrane and subjected to immunoblotting.

Besides that, the isolation of the nuclear fraction from cytoplasm was also prepared to investigate the existence of Nuclear Localisation Signal (NLS) in RhoE. Three (3) 150 mm diameter dishes were pre-coated with animal gelatine 0.1 % (w/v) to allow stratified and optimum growth of U87 cells before transfection. Each plate was assigned for the *in vitro* culture of 2.85 million units of U87 cells that were incubated overnight until they reached 60-70% confluence and ready for transfection. RhoE wild-type (RhoE^{WT}) and RhoE double mutants (RhoE^{T173R/V192R}) were transfected into U87 cells with FLAG-tagged RhoE epitope. The overexpression vector that contains empty vector (EV) is also applied for the control of experiment using mammalian expression vector, pCMV5 with FLAG-tagged. The serum-free medium was replaced with complete medium 8 h post transfection (Wallenstein et al. 2010). The nuclear and cytoplasmic fractions of the U87 cell were prepared 42 h post-transfection.

FLAG-RhoE was pulled down from a combination of nuclear and cytoplasmic fractions of the transfected U87 cells. In order to perform this experiment, the cell fractions

from each transfected U87 cells were utilised in co-immunoprecipitation (Co-IP) to pull down RhoE and protein binding partners using FLAG antibody. Then, the Co-IP samples then underwent SDS-PAGE, transferred to PVDF membrane and subjected to immunoblotting.

2.2.2.6 Transient Transfection of RhoE Constructs into U87 Cells

The U87 human glioblastoma cells line were cultured in Dulbecco's modified Eagle medium (GIBCO) containing [+] 4.5g/L D-Glucose and [+] L-Glutamine. This medium is also supplemented with 10 % (v/v) foetal bovine serum (FBS). The cells were left to grow in a humidified incubator with 5 % CO₂ at 37 °C for 24 h before transfection. Lipofectamine PLUS LTX Reagent was utilised according to the manufacturer's instructions (Life Technologies, Invitrogen).

The ratio of plasmid DNA to liposome is 2.5µg DNA: 5µL Lipofectamine LTX: 2.5 µL PLUS Reagent were optimised using FLAG-tagged wild-type RhoE (RhoE^{WT}) before proceeding with the actual experiment using another RhoE mutant plasmid. As a result, 300 000 unit cells were consistently grown on the animal gelatine pre-coated coverslips, as well as in the six wells tissue culture plates (p6 well) at the beginning of the transfection experiment. The serum-free medium was replaced with a complete medium after 8 h post transfection.

After transfection, the cells were harvested for the preparation of whole cell lysate, nuclear and cytoplasmic fractions at 42-44 h post-transfection. The lysates and cell fraction were also prepared in similar manner as described in Section 2.2.1.2, followed by blot analysis (see Section 2.2.1.5 -2.2.1.8). The preparation of coverslips for FLAG staining

(see Section 2.2.1.13) was also conducted at the same time. Later, the quantity of transfected cells for each mutant is calculated for the percentage (%) of FLAG-RhoE expressed by dividing by the total number of cells. The experiment was conducted in triplicates ($n = 3$), where at least 250 cells were counted per coverslips, followed by statistical analysis.

2.2.2.7 Immunoprecipitation Followed by Mass Spectrometry Analysis

RhoE was immunoprecipitated from a nuclear extract of glioblastoma cells. According to Shimwell et al. (2009), the immunoprecipitated proteins can be separated by 1D SDS PAGE and protein bands stained with Coomassie blue. Protein bands can be excised from the gel and the proteins digested into peptides for identification (Newton et al. 2008). Using reverse HPLC coupled to an ion trap mass spectrometer, it is possible to identify peptides belonging to the proteins in an immunoprecipitated sample by comparing the recorded peptide fragmentation pattern with database of peptide in FASTA (Lodge et al. 2007). Novel binding proteins that interact with RhoE are found by BLAST the sequence of peptides to the bioinformatics database.

2.2.2.8 Bioinformatics Analysis on The List of Genes Found from RhoE Pulled-down Assay

This study used Database for Annotation Visualisation and Integrated Discovery (DAVID), as well as Search Tool for the Retrieval of Interacting Genes (STRING) for this analysis. Both databases, DAVID and STRING facilitate the clustering for the abundance of the gene into a more comprehensive set of functional annotation tools. The biological

explanation from a huge genes list was initially interpreted by DAVID (Huang et al. 2008). Then, the biological processes at the cellular level and systematic characterisation were predicted by looking into protein-protein assemblies according to physical and functional interactions using STRING (Szklarczyk et al. 2015).

Later, DAVID is also applied to disclose the list of interacting proteins that are essential in brain tumour development or implicates the diversity of glioma subtype for this research. The analysis of genes signature and profiling in identifying related biomarkers for particular diseases is done using DAVID tools (Huang et al. 2002). This application was also used for the intensive search of individual domain and motif of the specific protein. Besides that, DAVID could also confirm the determination for the functional group of gene by guiding the investigation with appropriate pieces of literature and adapting into the alternative gene description (Huang et al. 2009).

2.3 Statistical analysis

This study repeated all the experiments for at least three times ($n = 3$) except for certain individual experiments. The data were evaluated using appropriate statistical test depending on the variability of the samples and treatment. Welch Two Sample t -test was used for paired samples, ANOVA one-way for multiple samples followed by Tukey Kramer procedure and ANOVA two-factor with replication; whereas multiple comparisons were carried out using Tukey-HSD post-test for variety samples and multiple interactions. The differences were considered statistically significant if the p value is at least below than 0.05 or indicated by the asterisks: (*) $p < 0.05$ or (**) $p < 0.01$ or (***) $p < 0.001$ or (****) $p < 0.0001$ (Crawley 2005).

CHAPTER 3

RHOE REGULATES CELL CYCLE AND APOPTOSIS IN U87 HUMAN GLIOBLASTOMA CELLS

3.1 Introduction

Alteration of Rho GTPase signalling pathway often occurs in malignant growth and cancer development. It is known that the dysregulation of Rho proteins could promote uncontrolled cell proliferation, resistance to apoptotic stimuli, neovascularization or tumour cell motility, invasiveness and metastasis. David et al. (2012) suggested that the inhibition of Rho, Rac and Cdc42 could block cell cycle progression. However, it is important to question whether the restriction occurs during the transition from G₁ to S-phase or G₂ to M-phase on each cell type. The main limitation is the lack of explanation regarding how the cell proliferation in healthy cell lines and literally ill cells are affected by RhoE.

Besides that, Rho proteins also regulate the furrow formation that takes part in the assembly of the actin-myosin network. A model was postulated by Su et al. (2003) that the initial positioning of the cleavage furrow during cytokinesis is partly specified by p190 RhoGAP. They discovered that the overexpression of p190 RhoGAP could alter the cleavage furrow position and split it into unequal daughter cell, followed by uneven furrow contraction and formation of multiple nuclei. Moreover, phosphorylation of p190 RhoGAP is also dependent on the mitotic kinases, and Cdk1 is responsible to down-regulate the GAP activity. RhoE can also antagonise p190 RhoGAP; alternatively, this GAP protein could indirectly

increase the GTPase activity of RhoA. Consequently, the activated RhoA during the absence of RhoE may lead to the activation for the signalling pathway of RhoA/ROCK1/LIMK/Cofilin. As a result, the activated ROCK1 could aid the contraction and membrane blebbing during the late execution phase of apoptosis (Peris et al. 2012).

Previous work by Ryan et al. (2012) discovered that the depletion of RhoE could lead to hyper proliferation of cells, suppress apoptosis and inhibit cell differentiation in keratinocytes. Several researchers also investigated similar case involving RhoE in cell cycle, apoptosis and differentiation. However, the impacts of protein are inconsistent. For instance, Peris et al. (2012) demonstrated the positive role of RhoE in regulating cell differentiation. In contrast, Poch et al. (2007) revealed the negative role of RhoE in regulating cell proliferation and apoptosis. In brief, it is confirmed that the role of RhoE is hugely relevant in cell proliferation and cell death.

This chapter focuses on the role of RhoE in regulating the cell cycle and apoptosis in U87 human glioblastoma. This study is interested in investigating RhoE in the cell cycle and apoptosis using the endogenous RhoE in glioma cell lines *in vitro*, which is advantageous compared to the exogenous system. According to Poch and co-workers (2007), overexpress RhoE by transfecting adenovirus (Ad-RhoE) in U87 human glioblastoma cells can be manipulated for an extrapolation study. The endogenous RhoE might simulate the real condition of brain tumour as it has the ability to mimic the basal level of RhoE in GBM.

3.2 Results

3.2.1 RhoE Regulates the Cell Cycle of U87 Cells

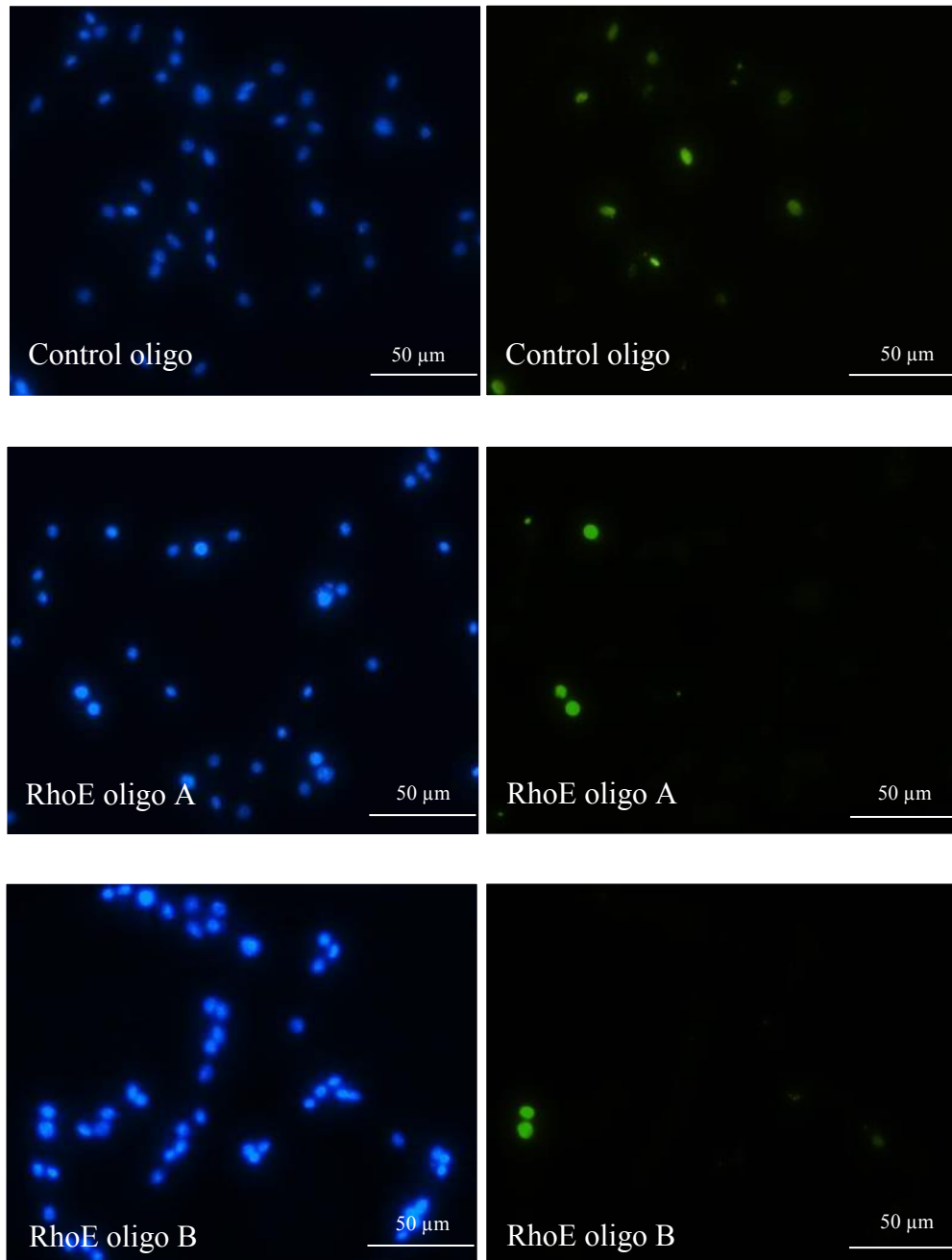
This experiment determined the evaluation of cell cycle by looking at the number of cells entering the synthesis-phase (S-phase). The cells were cultured in gelatine pre-coated coverslips in the 6 well tissue culture plates. 48 h post-RhoE knockdown, the cells were introduced with BrdU (Bromodeoxyuridine) for an hour. The U87 cells, which individually enter the S-phase were identified by the ability of the DNA of this glioma cell incorporating BrdU. The labelling is accurate as BrdU could incorporate into the chromatin of genomic DNA at only the S-phase whilst the cells are proliferating. Then, thymidine is replaced with BrdU and it is incorporated into the DNA of cycling cells during the labelling period.

The U87 cells were stained with an anti-BrdU antibody and a green fluorescence secondary antibody to assess the number of cells in the S-Phase. The BrdU positive cells were detected by FITC under an epifluorescence microscope. The nucleus was stained with DAPI which gives the total number of U87 human glioblastoma cells for each area; whereas individual cell that have BrdU incorporated defined with green fluorescence represents the newly synthesised cellular DNA. Figure 20 shows the results. The presence of RhoE could maintain the number of cells entering the S-phase which is demonstrated by the control oligo using non-silencing control. In contrast, U87 cells with depleted RhoE showed the decrease in the number of cells entering the S-phase.

Further analysis was done to evaluate the number of BrdU positive cells by determining the percentage of cells the entering S-phase (%) out of the total number of cells counted. Figure 21 shows the data regarding the loss of RhoE expression in U87 cells that could lead to the decrease in the number of cells entering the S-phase. Based on the

histogram, the ability of cells entering the S-phase is persistent at 35% in the control condition when RhoE is present. On the other hand, the U87 cells with RNAi-mediated depletion of RhoE; using both oligos, RhoE oligo A and RhoE oligo B, showed less than 20% cells entering the S-phase.

The number of cells entering the S-phase was reduced about half (1/2) in the absence of RhoE. A statistical analysis was done (see Section 2.3) to check the significant difference between the presence of RhoE and RhoE depleted U87 cell. This experiment was conducted in triplicate ($n = 3$), where the minimal total cell numbers counted were 250 and the coverslips were prepared in triplicates for each experiment. The differences between control (Control Oligo) and RhoE knockdown conditions (RhoE oligo A and RhoE oligo B) were statistically significant ($p < 0.05$).



DAPI

BrdU

Figure 20: Less cell number entered S-phase indicated by the green fluorescence of BrdU in RhoE depleted U87 cells (RhoE oligos, A and B) compared to the cells with the presence of RhoE (Control oligo). The cell nuclei were stained with DAPI where the same field is observed for BrdU uptake. The images represent the three separate experiments ($n = 3$).

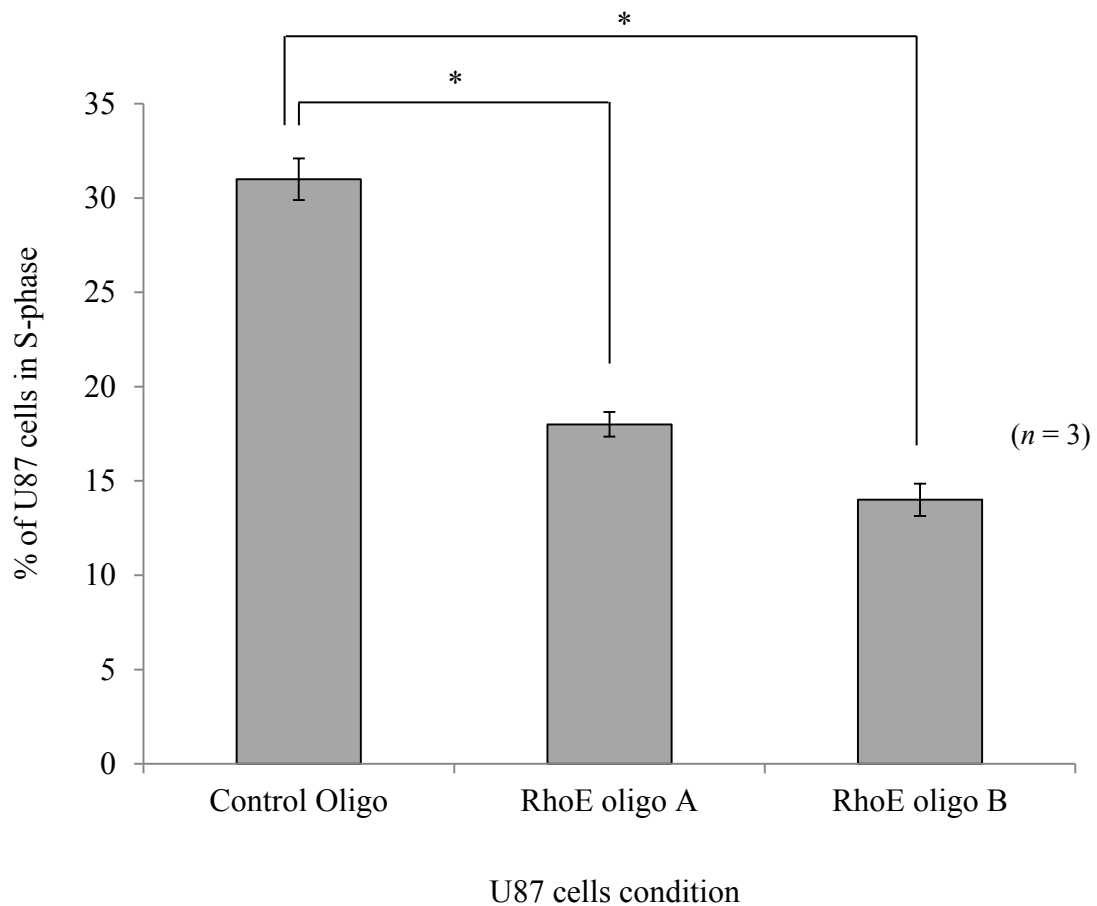


Figure 21: The loss of RhoE expression in U87 cells has resulted in the decreased number of cells entering the S-phase. The percentage of U87 cells in S-phase was analysed and the mean values are presented. The error bars show the standard error of the mean (S.E.M) for each datasets of three separate experiments ($n = 3$), where 250 cells were counted in each of the three coverslips. The differences are significant between the silencing RhoE and control oligo (*) ($p < 0.05$). The statistical analysis was performed using ANOVA single factor.

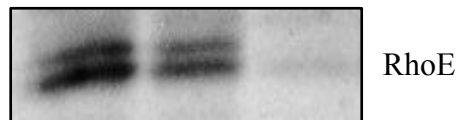
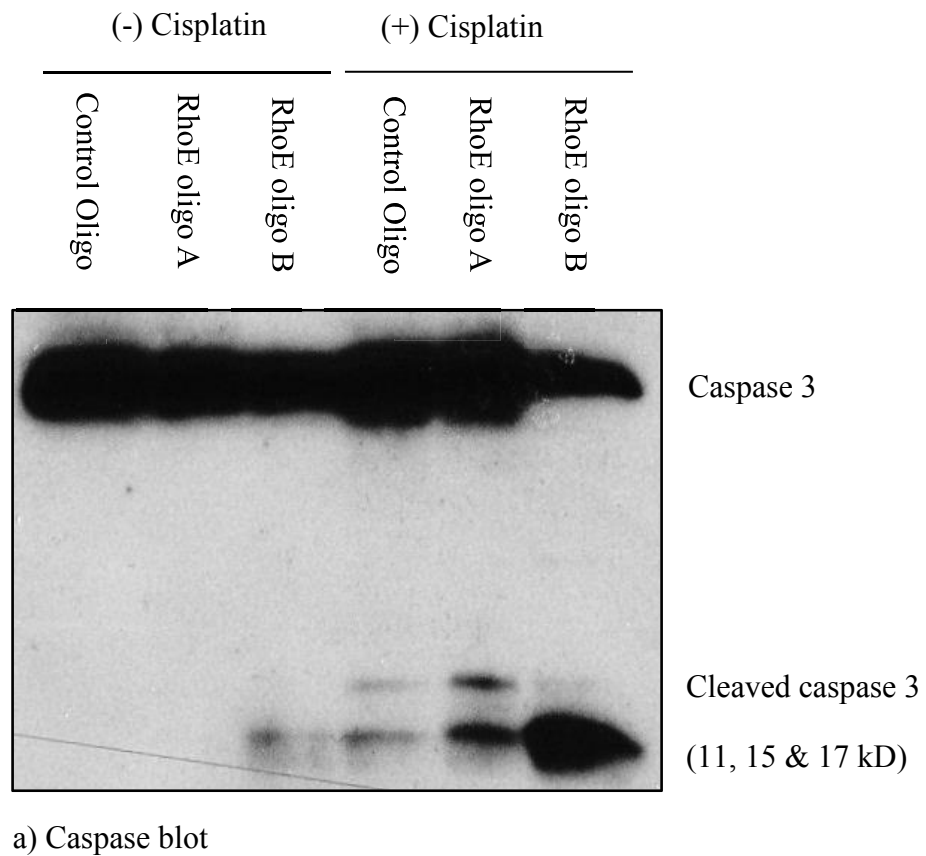
3.2.2 RhoE Regulates Apoptosis in U87 Cells

A study on apoptosis during the depletion of endogenous RhoE was also conducted using U87 human glioblastoma cells. Although, many researchers used different drugs and analysis method, the experimental design in this study was modified and used an alternative apoptotic inducer; Cis-diamminedichloroplatinum (II) or cisplatin. This chemical has been widely used in cancer chemotherapy (Torigoe et al. 2005). This chemical compound was selected due to its potential activity to induce genotoxic stress against solid tumours such as ovary, testis, head, lung and neck (Kartalou and Essigmann 2001).

A preliminary study was done on the effect of cisplatin, in stimulating genotoxic stress in U87 cells with the presence of RhoE, as well as during RhoE depletion. Prior to the treatment with cisplatin, the U87 cells were transiently transfected with siRNA oligos to generate RhoE-depleted U87 cells, and they were cultured for approximately 48 hour. A non-silencing control was transfected into U87 cells as the control of the experiment. The whole cell lysates were prepared 16 hours after being treated with cisplatin at a constant concentration of 50 μ M.

Then, these lysates were separated by SDS-PAGE and immunoblotted with the antibodies against caspase 3, cleaved caspase 3 and RhoE, as well as α -tubulin as a loading control. Figure 22 shows that RhoE depleted U87 cells are more sensitive towards cisplatin compared to U87 cells with the presence of RhoE. The results show that cleaved caspase 3 was elicited at three (3) different molecular weights of 11, 15 and 17 kD in RhoE depleted U87 cells using RhoE oligo B. In contrast, the knockdown RhoE using RhoE oligo A was not successful based on the RhoE blot. This is because, RhoE bands still appear at 27 kD and 29

kD, and similar observation was also found in non-silencing control condition. Relatively, fewer cells died with the presence of RhoE.



b) RhoE blot

Figure 22: Preliminary results on apoptosis show that RhoE depleted U87 cells are more sensitive to cisplatin. There is no result of RhoE blot for the condition without cisplatin due to shortage of sample. For the condition with cisplatin treatment, RhoE was almost entirely depleted using RhoE oligo B whereas RhoE oligo A reached approximately quarter knockdown.

3.2.3 RhoE Regulates Apoptosis but Independent ROCK1

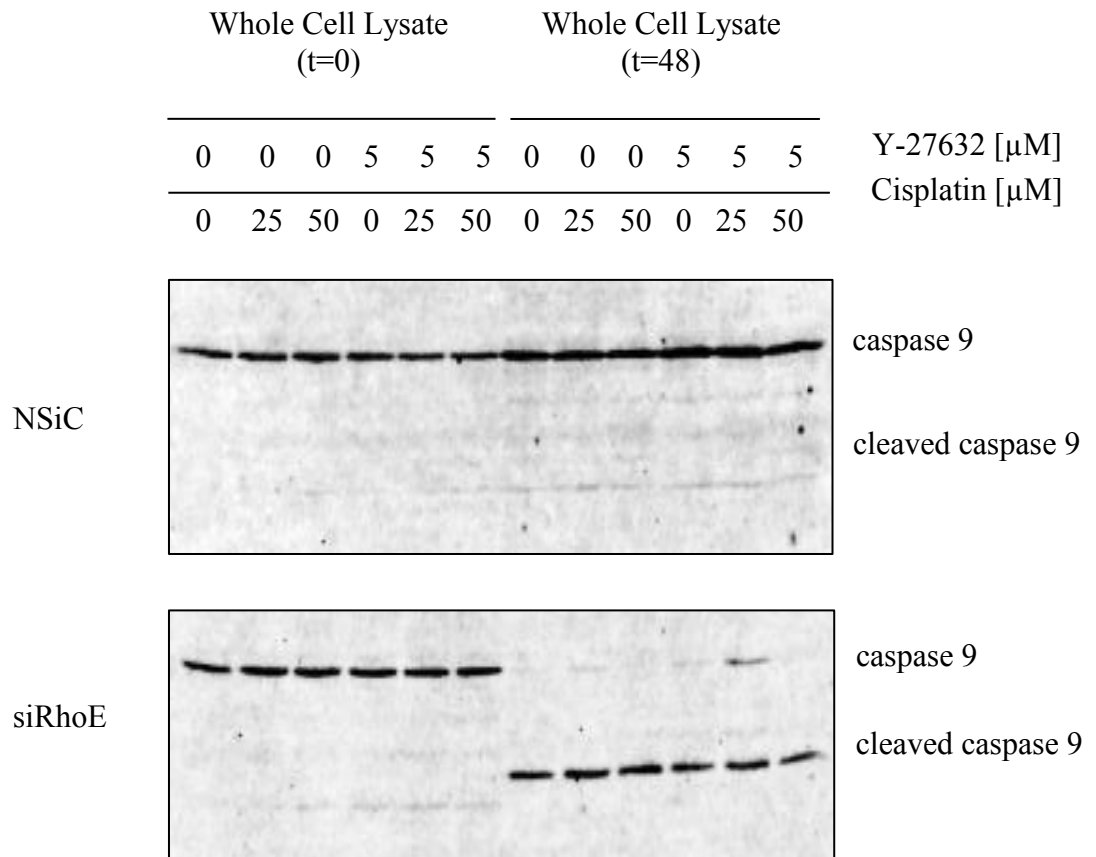
Further investigation was done to determine whether the interaction between RhoE and ROCK1 is crucial during apoptosis. Y27632 [(1)-(R)-*trans*-4-(1-aminoethyl)-N-(4-pyridyl) cyclohexane carboxamide dihydrochloride] is commonly used as a specific inhibitor of Rho-associated coiled-coil forming protein serine/threonine kinase (ROCK) family of protein kinases. This experiment also used Y27632 to investigate whether it inhibits the interaction of RhoE with the kinase domain of ROCK1. In principle, Y27632 inhibits ROCK1 by competing with ATP and binds to the kinase, particularly at the catalytic site (Ishizaki et al. 2000). Then, the Y27632 compound prevents ROCK1 from forming the autoinhibitory loop and disrupts the interaction with p190 RhoGAP. Thus, membrane blebbing is blocked and the cell is prevented from entering the apoptosis pathway.

In this study, the occurrence of apoptosis was detected based on the intrinsic pathway where caspase 9 functions as an initiator for the caspase cascade; and caspase 3 for the execution phase of the caspase cascade. Figure 23 shows the results of immunoblot images for both caspases regarding the detection of apoptotic marker. As shown in Figure 23 (A) and (B), $t=0$ is defined as 48 h post-knockdown and it is the starting point in introducing Y27632; whereas $t=48$ is defined as 96 h post-knockdown and the end point for the treatment of Y27632. Cisplatin was added to the cells 78 h post-knockdown in between the starting point and end point to promote apoptosis. Y27632 compound was fixed at either 0 μM or 5 μM , and a series of cisplatin was used between 0 to 50 μM . The titration of both chemical compounds is labelled horizontally for caspase 9 and caspase 3 blots. Each lane represents the sample of the whole cell lysate that is accordingly loaded to the following titration series: 0Y0C, 0Y25C, 0Y50C, 5Y0C, 5Y25C and 5Y50C. Y is Y27632 and C is cisplatin.

Figure 23 (A) shows the full length of caspase 9 and it was completely intact in both conditions of either NSiC or siRhoE at the beginning of the experiment ($t=0$). However, at the end of the experiment ($t=48$), siRhoE showed the loss of full length caspase 9 at 47 kD for each titration tested, excluding 5Y25C. The cleaved caspase 9 was elicited at 35 kD at every concentration tested in siRhoE. Consequently, the RhoE depleted U87 cells using RhoE oligo B did not show the inhibition effect of ROCK1 in preventing apoptosis, and the cells were dead as indicated by the formation of cleaved caspase 9. It was found that the full-length caspase 9 was intact and expressed more at each titration in NSiC.

Parallel observation was found using caspase 3. Figure 23 (B) shows the full length of caspase 3, as well as cleaved caspase 3 indicating that apoptosis underwent the execution phase in siRhoE. The three different bands of 15, 17 and 19 kD appeared at each titration tested in siRhoE with 15 kD, showing the strongest signal compared to the other two cleaved caspase; which are 17 kD and 19 kD. Moreover, the half part of the full length caspase 3 still remained at 35 kD, showing that the execution pathway is still progressing during the time of sampling. Contrary to siRhoE, the cleaved caspase 3 was not detected in control condition (NSiC). The caspase 3 eventually remain intact even when there is more expression at 35 kD, which is consistent with the increased concentration of cisplatin with or without ROCK inhibitor.

(A) Caspase 9



(B) Caspase 3

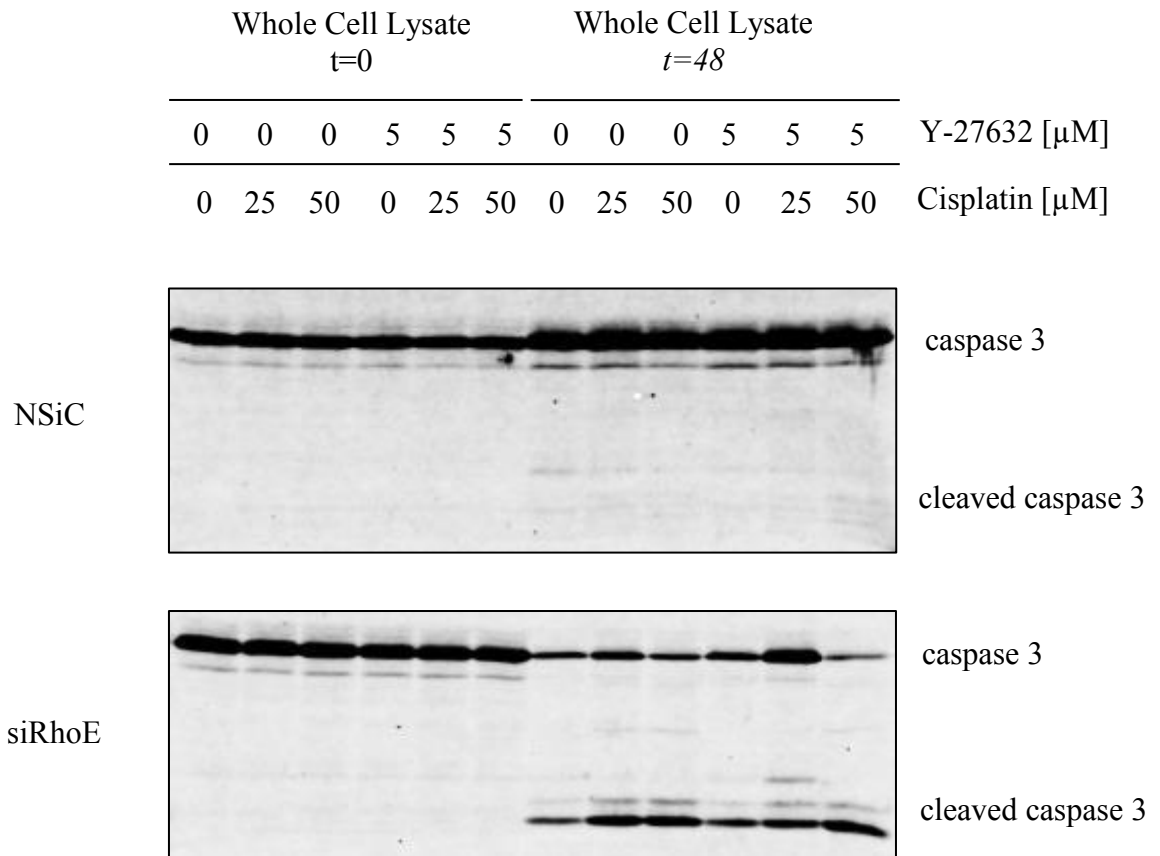


Figure 23: The occurrence of apoptosis was detected based on the intrinsic pathway, where caspase 9 functions as the initiator of caspase cascade; and caspase 3 for the execution phase of caspase cascade.

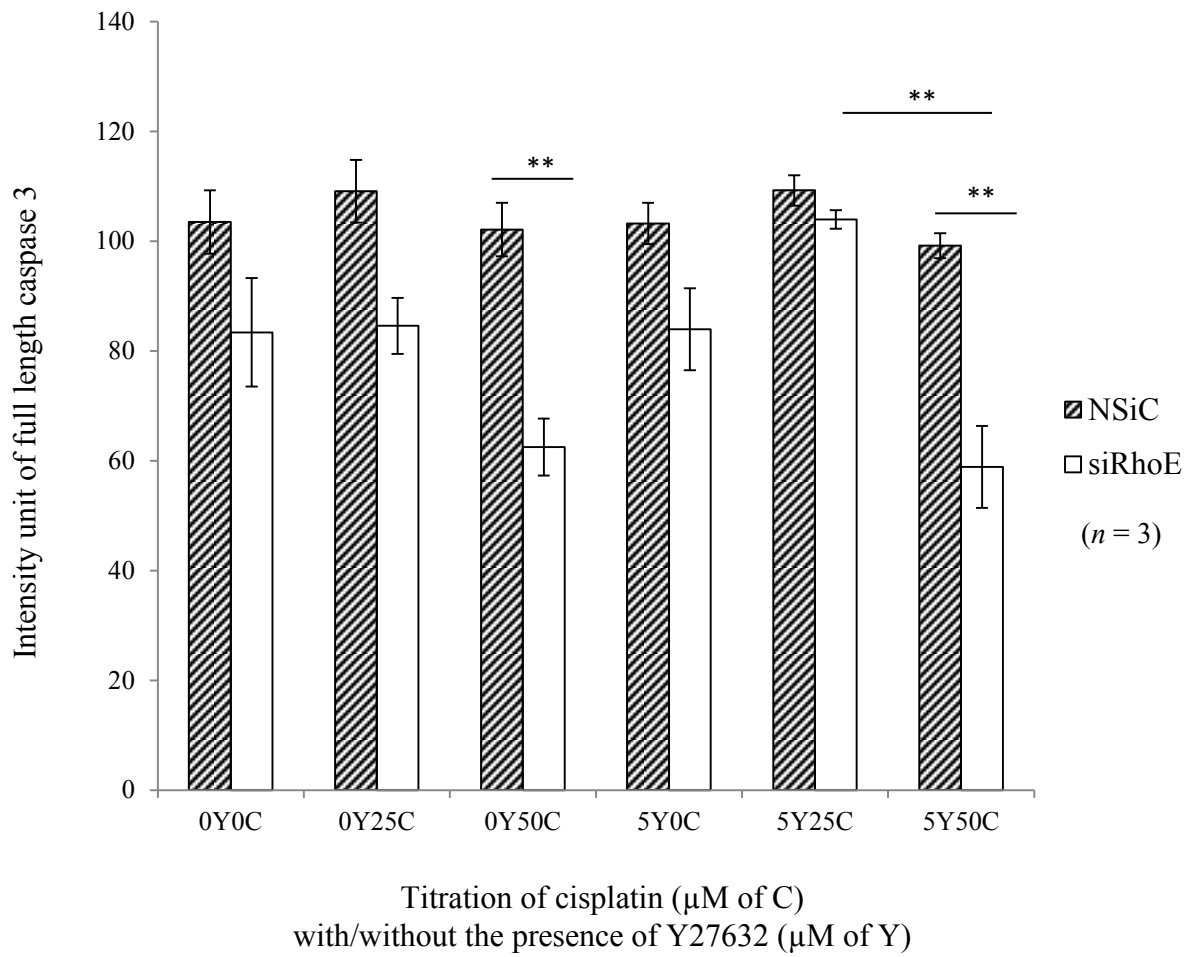
(A): Apoptotic marker detection of the full length caspase 9 that remains intact at 47 kD in Control Oligo (NSiC), but entirely lost in RhoE depleted U87 cells (siRhoE) (except at 5 μ M Y27632/ 25 μ M Cisplatin) and it was replaced with cleaved caspase 9 that was elicited at 35 kD. This blot is a representative for this single experiment ($n = 1$).

(B): Apoptotic marker detection of the full length caspase 3 that remains intact at 35 kD in NSiC, but partially degraded in siRhoE with the formation of cleaved caspase 3 that was elicited at 15 kD. However, there is an exception for siRhoE at 5 μ M Y27632/ 25 μ M Cisplatin, and the full length caspase 3 was quarter degraded with the formation of cleaved caspase 3 at three different molecular weight; which are 15, 17 and 19 kD. This blot is a representative for three separate experiments ($n = 3$).

Further analysis was conducted via densitometry using image J to quantify the loss of full length, as well as the formation of cleaved caspase 3. This study has also made a comparison between control (NSiC) and Rho depleted U87 cells (siRhoE). The semi-quantitative analysis is essential to validate the presence of apoptotic marker, particularly caspase 3 as this is an indicator that the cells underwent late stage of apoptosis. Figure 24 (A) and (B) show the densitometry of full length and cleaved caspase 3 respectively, to observe the effect of RhoE in regulating apoptosis.

The differences between control (NSiC) and RhoE knockdown conditions (siRhoE) were not statistically significant for the full length caspase 3 (ns) ($p > 0.05$); except during the titration of 0Y50C and 5Y50C (**) ($0.001 < p < 0.01$). RhoE depleted U87 cells was severely affected by cisplatin though in the presence of Y27632 for the titration 5Y50C if compared to 5Y25C (**) ($0.001 < p < 0.01$). In contrast, the cleaved caspase 3, siRhoE was significantly different from NSiC. ANOVA two factors with replication were performed in both datasets (NSiC and siRhoE). Then, multiple comparisons were carried out using Tukey-HSD post-test for increasing concentration of cisplatin in the U87 cell's system. The effect of cisplatin was significant in siRhoE to induce apoptosis as indicated by the asterisks (****) $p < 0.0001$ (see the histogram in Figure 24 B). Nevertheless, there were no significant differences between the conditions without or with Y27632 treatment in both the presence of RhoE or RhoE knockdown conditions (ns) ($p > 0.05$).

(A) Full-length caspase 3



(B) Cleaved caspase 3

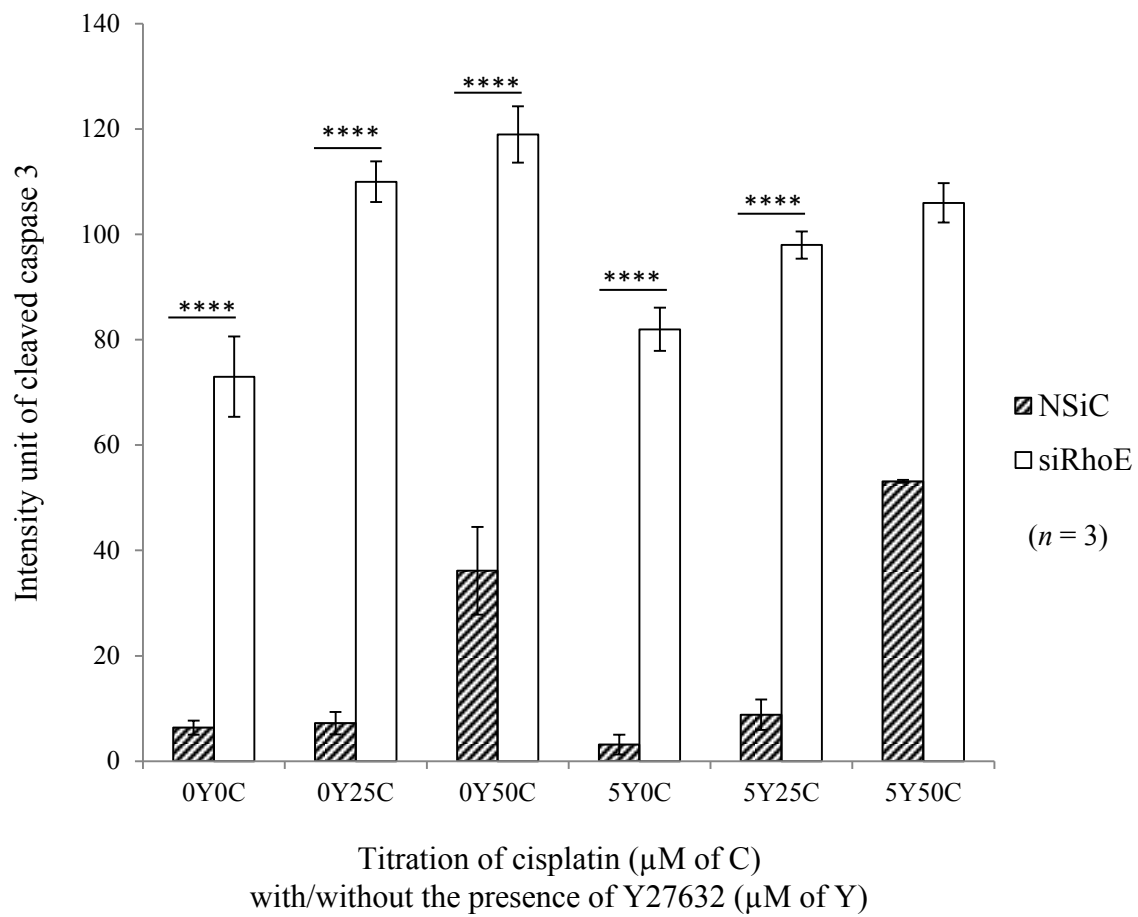


Figure 24: The densitometry analysis of late-stage apoptotic marker (execution pathway); the caspase 3 using Image J. **(A)** Semi-quantitative analysis to compare full-length caspase 3 between siRhoE and NSiC when increasing the concentration of cisplatin with and without the presence of ROCK inhibitor, Y27632. There were no significant different for the full length caspase 3 (ns) ($p > 0.05$); except during the titration of 0Y50C and 5Y50C (**) ($0.001 < p < 0.01$). The siRhoE was severely affected by cisplatin though in the presence of Y27632 for the titration 5Y50C if compared to 5Y25C (**) ($0.001 < p < 0.01$). **(B)** Semi-quantitative analysis to compare cleaved caspase 3 between siRhoE and the NSiC when increasing the concentration of cisplatin with and without the presence of ROCK inhibitor, Y27632. The difference between NSiC and siRhoE as well as the increased concentration of cisplatin compared to without cisplatin were considered statistically significant for cleaved caspase 3 with (****) $p < 0.0001$. These data are representatives for three separate experiments ($n = 3$).

3.2.4 RhoE is Essential in Attenuating Genotoxic Stress in Glioma

The previous section describes the end of apoptosis, which is manifested by the execution phase based on the detection of the apoptotic marker, including the loss of full-length caspase 3 and formation of cleaved caspase 3. The previous experiment (see Section 3.2.3) investigated apoptosis by using pharmacological approach that targeting either metabolite or intermediate compound during caspase cascades. However, the investigation was limited and only focused on the implication of signalling pathway at the intracellular level. Previous research did not explore the mechanisms that inhibit apoptotic machinery at the gene level. Hence, this section intended to understand the resistance mechanisms that prevent chromatin condensation. It is hoped that this experiment could explain how RhoE is relevant in regulating apoptosis at the molecular level, particularly in preventing DNA damage in glioma.

Ryan (2010) reported that RhoE expression is induced by a number of apoptosis-inducing stimuli, including camptothecin, cisplatin and UVB irradiation. In addition, the researcher also emphasised that RhoE is also a transcriptional target of tumour suppressor protein p53, which supposed to promote apoptosis, and induces RhoE transcription in response to DNA damage. This study also obtained a similar observation when the treatment of cisplatin led to enhance RhoE expression in U87 cells. However, increasing RhoE expression did not elevate apoptosis but a contrary result revealed when genotoxic stress was attenuated in control condition using non-silencing control oligo.

Figure 25 showed that relatively cisplatin encourages more expression of RhoE but maintain cell survival in control condition. The siRhoE has relatively capable underwent apoptosis with or without cisplatin. The result exhibited in Figure 25 also suggested that

increased cisplatin concentration activates the caspase 3 cascade activity in knockdown RhoE condition; particularly at the concentration of 25 μ M (the fifth lane). Consequently, the caspase 3 encourages cleaved of 160 kD endogenous ROCK1 protein into a 130 kD ROCK1 fragment. The previous study by Jie et al. (2015) observed similar findings with this experiment by which they used gene knockout mouse as a model. They demonstrated that depletion of RhoE increased the activity of ROCK1 and its downstream effectors in mouse hearts. As a result, the mouse suffered from apoptotic cardiomyopathy and heart failure.

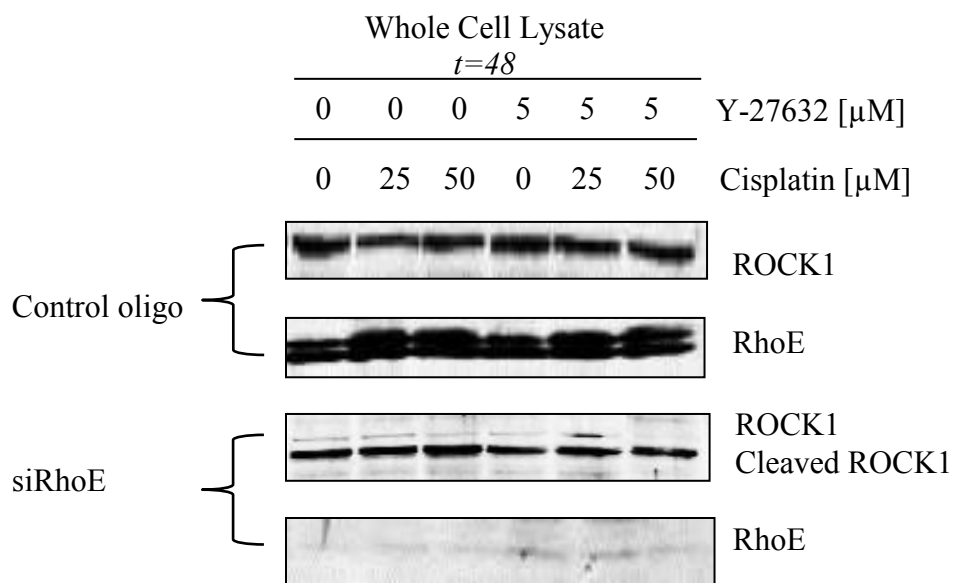


Figure 25: RhoE is essential in attenuating genotoxic stress in glioma. RhoE also reflects the stability of ROCK1 expression at 160 kD in control condition. Cisplatin could induce the expression of RhoE in U87 cells but it did not happen in RhoE knockdown condition. The ROCK1 blot in RhoE knockdown condition presented with smaller molecular weight at approximately 130 kD that represents the caspase-cleaved form of ROCK1.

Coleman and Olson (2002) characterised the apoptotic phenotype cells by the alteration cell morphologies, including shrinking cell, condensed chromatin, membrane blebbing and formation of apoptotic bodies. This section is about evaluation of chromatin condensation to confirm that RhoE depleted U87 cells underwent apoptosis. The condensed chromatin was visualised via microscope under DAPI fluorescence. The data was assessed by using colony counter application, which is a plug in software in Image J. The evaluation of cell damage is based on the percentage (%) of apoptotic cells over the total cell number. Figure 26 shows the percentage (%) of nuclear condensation over the total cell number based on the titration of both chemical compounds, Y27632 (Y) that was fixed at either 0 μ M or 5 μ M, and a series of the cisplatin (C) used between 0, 25 and 50 μ M.

The basal level of apoptosis in the control experiment, which is (0Y0C), showed that RhoE depleted U87 cells (siRhoE) underwent apoptosis and could reach up to 56 % compared to the control U87 cell (NSiC) with the result of 11 %. Therefore, the apoptosis in siRhoE is five (5) fold more than NSiC for this titration. In comparison, the mean percentage of cells undergoing apoptosis without cisplatin with the presence of Y27632 (5Y0C) showed a decreasing trend where 46 % of the cells were apoptotic in the siRhoE condition and 2 % were apoptotic in NSiC. Thus, apoptosis in siRhoE is approximately 20 fold more than NSiC for this titration.

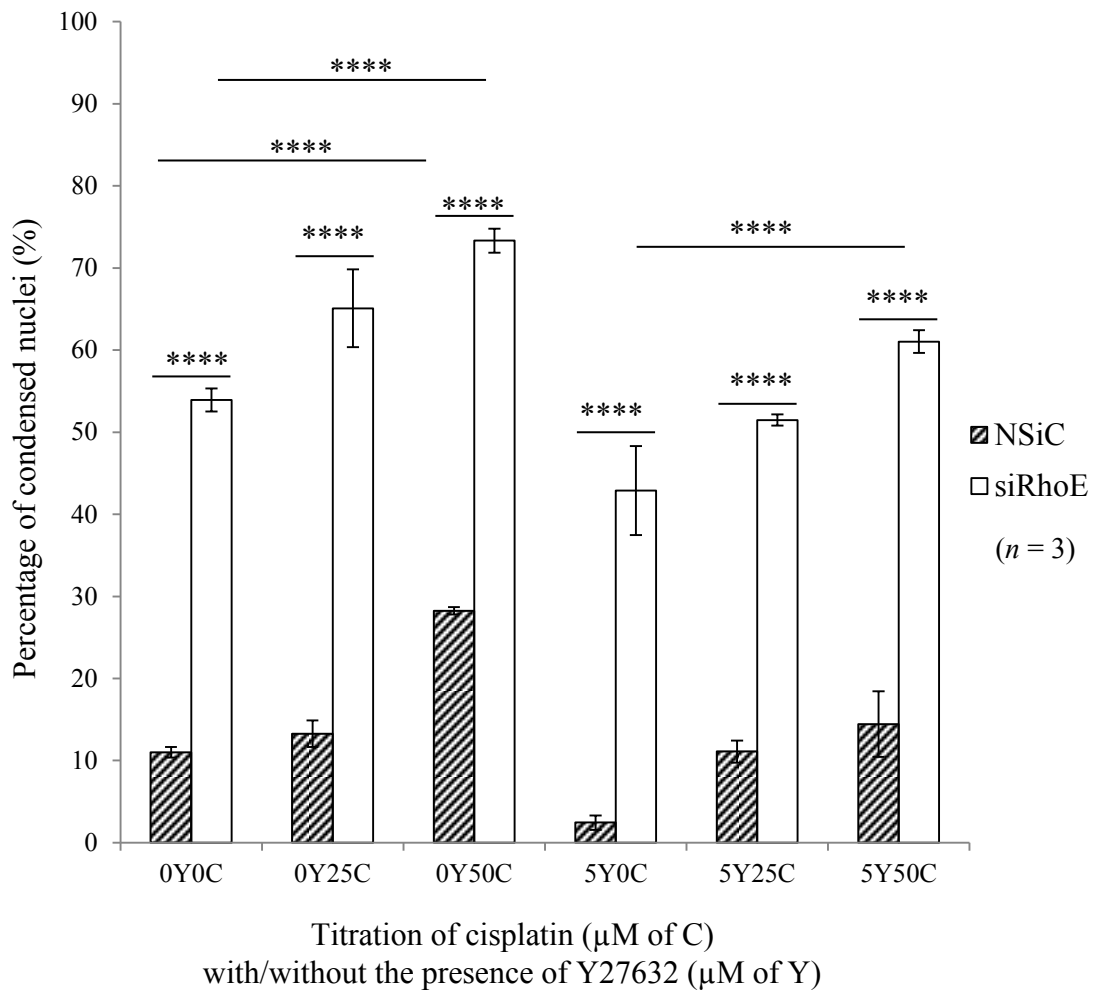


Figure 26: The evaluation of nuclear condensation in U87 cells with the presence of RhoE (NSiC) and in RhoE depleted U87 cells (siRhoE). The U87 cells were observed under DAPI fluorescence and the percentage (%) of condensed nuclei was calculated by counting the number of cells that appeared condensed at the nucleus, which is then divided by the total number of cells grown on coverslips. The difference between NSiC and siRhoE were considered statistically significant for condensed nuclei, since (****) $p < 0.0001$. This data is representatives for three separate experiments ($n = 3$).

The next level of titration was 0Y25C. The cells in siRhoE condition achieved 65 % of apoptosis, compared to NSiC with the result of 13%. The apoptosis in siRhoE with the presence of ROCK inhibitor (5Y25C) was maintained at five (5) fold more than NSiC. However, there is a decreasing trend for the number of percentage, which is 50% in siRhoE compared to 10% in the NSiC.

The final titration was 0Y50C, with the highest apoptosis percentage of 75 % in siRhoE condition, and there is a drastic increase until up to 30 % in NSiC. The percentage of apoptosis in siRhoE is 2.5 fold more than NSiC. However, the addition of ROCK inhibitor, (5Y50C), has reduced the apoptosis percentage to 60 % whilst NSiC also decreases to 13 %.

The results in this experiment supported the preliminary findings that were discussed in Section 3.2.2. The data from this experiment showed that RhoE plays a positive role in tumour development and becomes potential tumour enhancer. Apoptosis could occur with the absence of cisplatin when RhoE was depleted (siRhoE). In contrast to the observation in Section 3.2.3, the interaction between RhoE and the kinase domain of ROCK1 is important as indicated by the decreased percentage of condensed chromatin in the control cell (NSiC) (5Y25C, 5Y50C). However, the apoptotic cells were easily detached from the coverslips and increase the risk of cells being washed out during sampling and immunostaining. Overall, the importance of RhoE interaction with the kinase domain of ROCK1 during apoptosis is still ambiguous.

3.3 Discussion

The results have proven that RhoE could regulate the cell cycle progression, as well as interfering with the regulation of apoptosis. However, this effect is not exclusive for the U87 cell line. This effect can be seen in other cell types, including keratinocytes that is a typical healthy cell as well as other abnormal cell, such as human tumour-derived cell lines. Poch et al. (2007) found that overexpressed RhoE in U87 human glioblastoma cells showed the disorganisation of actin cytoskeleton, rounding of the cell body, and formation of long branches between adhered cells. Besides that, the role of RhoE in glioblastoma was found to be consistent with earlier studies by Bohmer et al. (1996). These researchers primarily disclosed that a proper assembly of actin cytoskeleton is essential to proceed beyond the G₁ to S-phase checkpoint of the cell cycle (Bohmer et al. 1996).

Then, Poch et al. (2007) evaluated the effect on cell cycle progression via depletion of endogenous RhoE from the U87 cell system. The previous work particularly assessed the overexpression of RhoE via the manipulation of the adenoviral system to transfect RhoE in U87 cells, and this methodology might resulted in altered gene expression. Besides that, the alteration might implicate numerous genes that regulate the signalling pathways during cell proliferation. The limitations of the previous system by RhoE overexpression are modified. Alternatively, the gene depletion methodology was used in this study as a different tool. As a result, this approach reduced the interference by other genes in regulating signalling pathway during cell cycle progression.

Poch et al. (2007) also found that RhoE expression induces the decrease in phosphorylation of Rb and the expression of cyclin D1. It is assumed that other genes (Cdk1 in association with of CDK4 or CDK6) might also be affected by RhoE overexpression during

the transfection, as well as altering the progression of the cell cycle. Coleman et al. (2004) also observed the effect of Cdk in cell proliferation. They suggested that cell cycle progression is controlled by the complexes formation of cyclins and cyclin-dependent kinases (Cdks). The association of cyclins to Cdks has led to phosphorylation of retinoblastoma (pRb) pocket proteins. As a consequence, the assembly of all these regulatory proteins promotes the advancement of the cell cycle and switches on the cell proliferation (Coleman et al. 2004).

Lonjedo et al. (2013) had identified the potential involvement of RhoE in cell cycle regulation, in which RhoE and p27 levels decrease after the overexpression of F-box protein Skp2. They found that there is a region between amino acids 231 and 240 of RhoE that facilitates the cells when entering the S-phase, which are Skp2 and Skp2-interacting domain. Section 1.4.2.2 describes this phenomenon in detail. According to this finding, they proposed a mechanism in which Skp2 regulates its protein levels via proteasomal degradation of RhoE to control cellular proliferation (Lonjedo et al. 2013).

Poch et al. (2007) found that RhoE plays a significant role in the apoptosis of U87 human glioblastoma cells. They isolated the live and dead cell populations using flow cytometry method. The extracellular surface of apoptotic cells were tagged by fluorescence label using Annexin-V (A5), which is a protein that specifically interacts with lipid phosphatidylserine (PS) in the cell membrane. During cell sorting, the membrane integrity was measured and segregated by either A5 or propidium iodide (PI); or A5 and 7-Amino-actinomycin D (7AAD) to differentiate between late apoptotic and necrotic cells.

A5 alone could only recognise early apoptotic cells. This approach was used to monitor whether RhoE-expressing U87 cells were dying by as a cause of apoptosis or necrosis. Besides that, investigations on other tumour cell lines were also conducted, and they

consistently observed apoptosis in the presence of RhoE (Poch et al. 2007). Nevertheless, the results in this study contradicted with Poch and coworkers (2007). The results in this study are similar with Ongusaha et al. (2006) and Boswell et al. (2007). Both studies also used siRNA to inhibit RhoE expression. Following the silencing of RhoE, they introduced apoptotic stimuli, and found RhoE depletion could increase the level of apoptosis (Boswell et al. 2007).

In principle, cisplatin enters the cells and its chloride ligands are replaced by water molecules which in turn form a positively charged aqueous species that can react with nucleophilic sites on the intracellular macromolecules to form protein, RNA and DNA adducts (Torigoe et al. 2005). Due to the cytotoxic mode of action that formed these intermediates, these would activate several signal transduction pathways, including ATR, p53, p73 and MAPK (Siddik 2003).

The presence of endogenous RhoE in U87 cells might accelerate the crosslink between adducts intermediate and intra strand. Subsequently, the communication or response for apoptosis activation is terminated. Some information on how RhoE regulates and which pathway involved remain unclear but the possible effect from the crosslinking could promote DNA replication and RNA transcription. As a result, the stimulation of S-phase entry of the cell cycle is activated. Thus, cell proliferation is prolonged in glioma cells, at the same time block the apoptosis.

Another important aspect in monitoring apoptosis is to consider the p190 RhoGAP levels. This GTPase activating protein can regulate the apoptotic response in cancer cell line through its regulation of ROCK1 (Ludwig and Parsons 2011). The multinucleation and dendritic formation are two phenotypes that commonly appear within cells that are

undergoing apoptosis. They also confirmed that p190 RhoGAP could affect the downstream effectors of Rho, including caspases that have important role in mediating cell death.

CHAPTER 4

LOCALISATION OF RHOE TO THE NUCLEUS OF U87 CELLS IS INDEPENDENT ROCK1

4.1 Introduction

RhoE is predominantly a membrane-associated protein and in particular this signalling protein localised to the Golgi membrane. In principle, intracellular localisation of RhoE requires a post-translational modification including farnesylation and prenylation activity. As described in Section 1.4.3.4, the process of geranylgeranylation (GG) is involved during farnesylation for shifting the localisation of RhoE between cytoplasm and plasma membrane. Previous work by Madigan (2008) has affirmed this principle and demonstrated that the stimulation of protein kinase C (PKC) enables the activation of electrophoretic mobility shift of RhoE to enable the enrichment at the internal membranes.

Phosphorylation of RhoE is important in regulating either its localisation or stability. PKC α and ROCK1 are two types of kinases that are well known in interacting with RhoE, and this was described in detail in Section 1.4.3.4. For instance, Riento et al. (2005) found seven sites of ROCK1 phosphorylation of RhoE were identified *in vitro*, and from that finding Ser¹¹ was phosphorylated in response to the extracellular stimuli. An extended study by Riou et al. (2013) found that both of these kinases shared similar phosphorylation site at Ser¹¹ and Ser²⁴⁰ of the amino acids sequence of RhoE.

One of the limitations with the available literature is that it does not explain the reason RhoE was found in the nucleus. Although all previous works indicated a specific interaction

between RhoE and both kinases; ROCK1 and PKC α , but none of the literature revealed if these interactions are involved during the translocation RhoE to the nucleus. Therefore, this experiment is crucial to reveal new insight and determine the mechanism involved during the localisation of RhoE to the nucleus of U87 cells.

The inadequate information about nuclear RhoE localisation was the main loophole in this study. The mechanism is essential to explain the preliminary finding (Ryan, 2010) as of the reason RhoE interacts with several proteins in nuclear processes such as MCM3, MCM5, SSRPI, CAF1 and ORC3L (Section 1.5). The mechanism by which RhoE shuttles across nuclear pore complex (NPC) of U87 cells is one of the main concerns in this study. The idea is to manipulate the knowledge on RhoE post-translational modification. For example, the process of phosphorylation that accompanied farnesylation via prenylation could possibly modulate the translocation of RhoE between nucleus and cytoplasm.

RhoE is a small molecular weight protein that is either 27 or 29 kD. Therefore, in canonical situation, the interaction of RhoE with importin or exportin is speculated as none essential as it should be able to traverse alone between cytoplasm and nucleus across the NPC via passive diffusion. However, the engagement of integrin may regulate downstream signalling of RhoE by inducing the PKC α -mediated phosphorylation and enlarging the protein size. Although the size of RhoE is less than 45 kD, the complex formation with other protein partners can possibly increase the size. Thus, it is possible to have an interaction with specific nucleocytoplasmic machinery. This chapter also includes the discussion on probability for the existence of either nuclear export signal (NES) or nuclear localisation signal (NLS) in RhoE.

4.2 Results

4.2.1 The Localisation of Endogenous RhoE to the Nucleus of Glioblastoma

Section 2.2.1.2 describes the cytoplasmic and nuclear fractions that were prepared and blotted for RhoE expression to analyse the localisation of RhoE. Figure 27 shows the results in which a clean separation of nuclear and cytoplasm based on expression of the nuclear lamin A/C and the absence of α -tubulin in the nuclear fraction. RhoE was observed in every fraction including whole cell lysate, nuclear fraction and cytoplasm. This experiment revealed that RhoE is expressed in the nucleus and cytoplasm. Figure 27 shows the blots that represent the immunoblots of three ($n = 3$) separate experiments, in which the results of each replicate are identical.

Following the western blotting, densitometry analysis was carried out using Image J software to evaluate the distribution of RhoE between nucleus and cytoplasm in U87 cell. Figure 28 shows the results. It was found that RhoE antibodies could recognise two distinct forms of RhoE at 27 kD and 29 kD. The higher molecular weight band is believed to represent the phosphorylated form of RhoE (Madigan et al. 2009). Therefore, the RhoE that is in the nucleus is probably predominantly phosphorylated.

Riento et al. (2003) suggested the use of RNAi to knockdown the expression of RhoE to confirm both bands are indeed RhoE and no other members of the Rnd family. In agreement with this finding, RNAi knockdown of Rnd1 has no effect on the expression of these two bands (Ryan and Hotchin, unpublished). Figure 30 (Section 4.2.2) shows the loss of both bands, suggesting that both forms are RhoE. A higher molecular weight RhoE (29 kD) was equally distributed in both nuclear and cytoplasmic fractions. However, the lower molecular weight RhoE (27 kD) was mainly localised to the cytoplasm ($p < 0.05$).

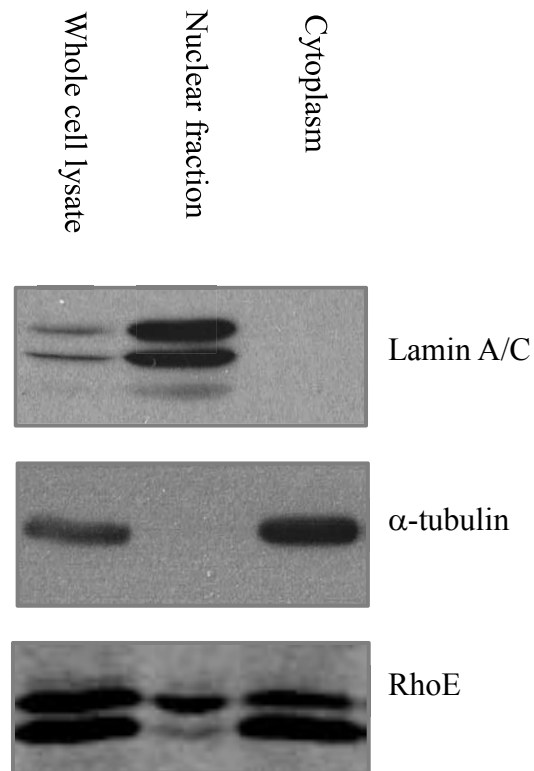


Figure 27: Localisation of endogenous RhoE in U87 cells. U87 cells were lysed in a buffer containing Nonidet P-40. Nuclear and cytoplasmic fractions were prepared, separated by SDS-PAGE and immunoblotted with an antibody against RhoE. The effective isolation of nuclear and cytoplasmic fractions was confirmed using antibodies against Lamin A/C and α -tubulin respectively. These blots represent the results of three separate experiments ($n = 3$).

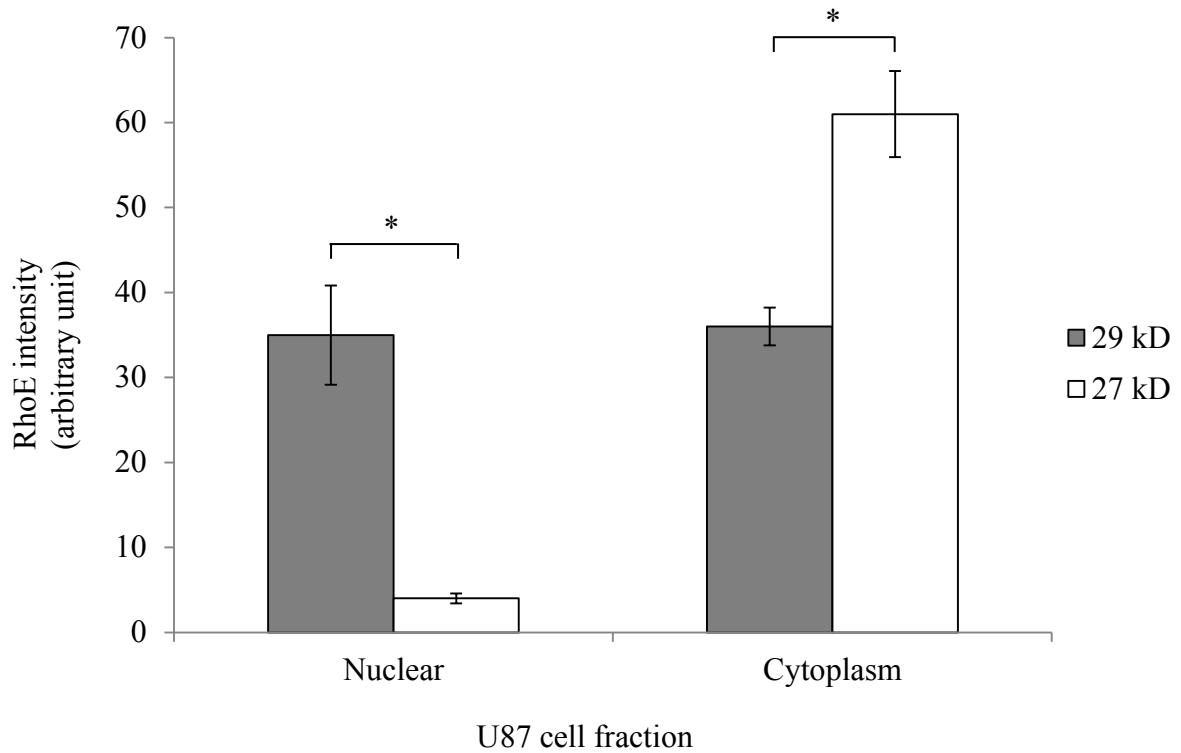


Figure 28: The relative distribution of endogenous RhoE in U87 cells. A semi-quantitative analysis was conducted using Image J to quantify the RhoE intensity for the blot in Figure 4.1. It was also used to determine the distribution of the different forms of RhoE (27 kD and 29 kD). A statistical analysis was done on paired datasets (29kD and 27 kD) of each fraction using Welch Two Sample *t*-test. These data represent results for the three separate experiments ($n = 3$), and the difference are significant with the p value is below than 0.05 (*) ($p < 0.05$). Error bars indicate the standard error of the mean (S.E.M) and they are shown alongside the histogram of each mean value.

Next, the localisation of RhoE in other cell lines was also investigated. This study used two different cell lines derived from gliomas, which are cell line 11 and cell line 21 (Hångerstrand et al. 2011) and a normal human keratinocyte cell line (HaCaT). Figure 29 shows the results of the study. In HaCaT, RhoE is mainly located in the cytoplasm, consistent with the data from other normal mammalian cell lines. However, RhoE was highly expressed in the nuclear fractions of U87 cells and cell line 11 suggesting a nuclear localisation of RhoE may be important in glioma. Interestingly, RhoE was not expressed in glioma cell line 21. A parallel study in the Hotchin lab observed differential expression of Rho GTPases (including RhoE) during progression of glioma (Clarke et al. 2015). Thus, it is possible that a difference in expression of RhoE is a reflection of tumour subtype (Hångerstrand et al. 2011).

The localisation of RhoE in the nucleus of U87 and glioma Type 11 cells suggests that RhoE may have a nuclear function during brain tumour progression. The nuclear functions may include regulating gene transcription, the replication of DNA and protein trafficking but further investigation is required to validate the presumption. Madigan et al. (2008) reported that other Rho subtypes are localised mainly to the cytoplasm. For instance, RhoA and RhoC are shown localised to the plasma membrane and the cytoplasm whereas RhoB is primarily found in the early endosomes. However, none of these cited literature emphasised on the fact that RhoE was found in the nucleus.

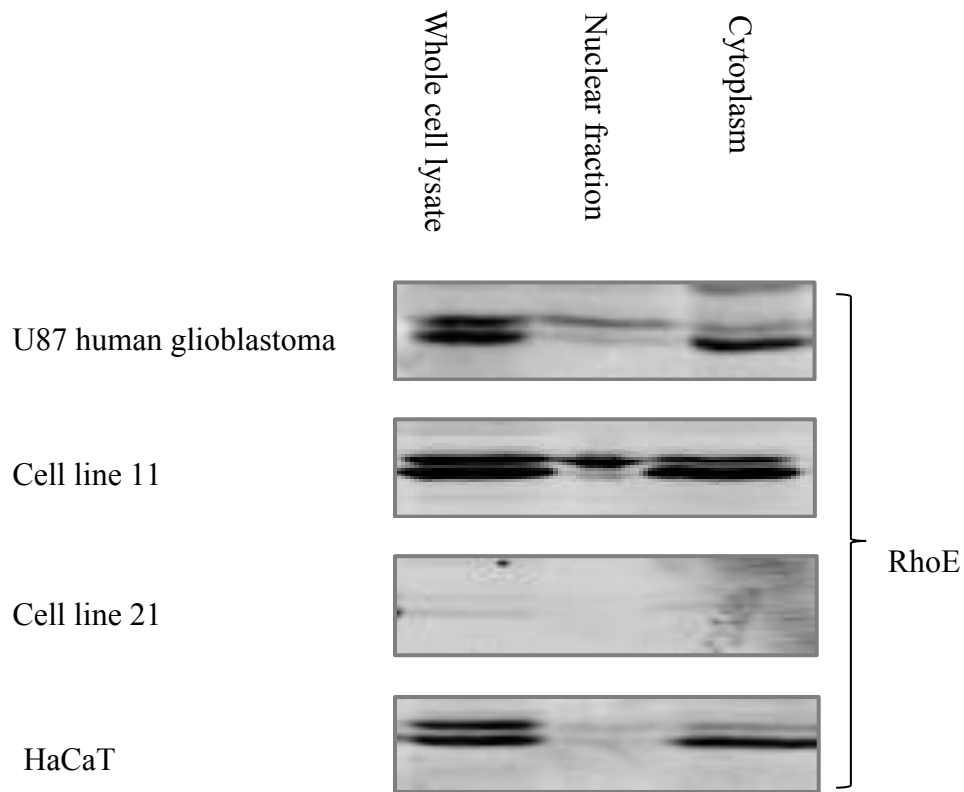


Figure 29: Localisation of RhoE in multiple types of cell lines. Each cell lines were lysed in a buffer containing Nonidet P-40. Then, nuclear and cytoplasmic fractions were prepared, separated by SDS-PAGE and immunoblotted with an antibody against RhoE. An effective isolation of nuclear and cytoplasmic fractions was confirmed using antibodies against Lamin A/C and α -tubulin respectively. Glioma Type 11 and 21 are cell lines that represent brain tumour at Stage IV, whereas HaCaT represents normal cell type.

4.2.2 Confirmation of Endogenous RhoE Localisation to the Nucleus of U87 Cells

The RNAi technique that specifically knockdown the expression of RhoE has used two different oligos; RhoE oligo A and RhoE oligo B. Prior to further used, each vial of oligo purchased was first validated as described in Section 2.2.2.1. The application of RNAi is convenient to confirm the expression of endogenous RhoE in the nucleus of U87 cells. Figure 30 shows that RhoE was expressed in the nucleus. The knockdown of RhoE using both oligos has led to the loss of RhoE in either the nucleus or cytoplasm.

Subsequently, the localisation of RhoE to the nucleus was confirmed using epifluorescence microscopy via staining cells with an anti-RhoE/Rnd3 antibody. As seen in Figure 31 (A), panel (c), shows that RhoE was localised to both nucleus and cytoplasm of NSiC of the U87 cells. The microscopy images proving that RhoE's appearance in both cell compartments were consistent with the western blot data.

Panel (c) in Figure 31(B) and Figure 31 (C) demonstrate that the fluorescence of RhoE was not found in both compartments of U87 cells, in either nuclear or cytoplasmic region. The microscopy images that show RhoE's disappearance using siRhoE found that U87 cells were successfully knocked down using both oligos, RhoE oligo A and RhoE oligo B.

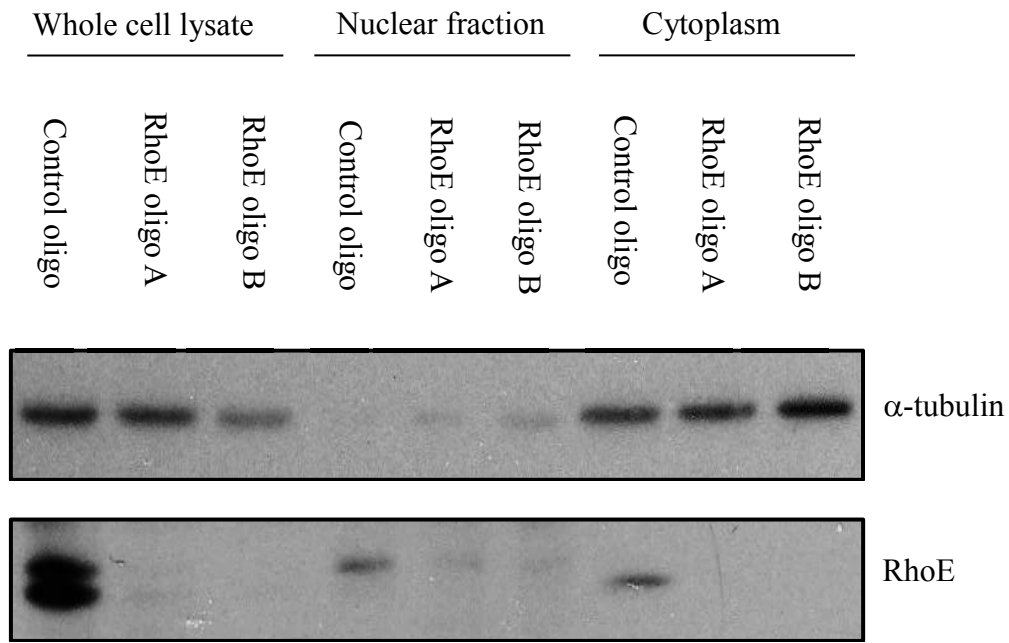
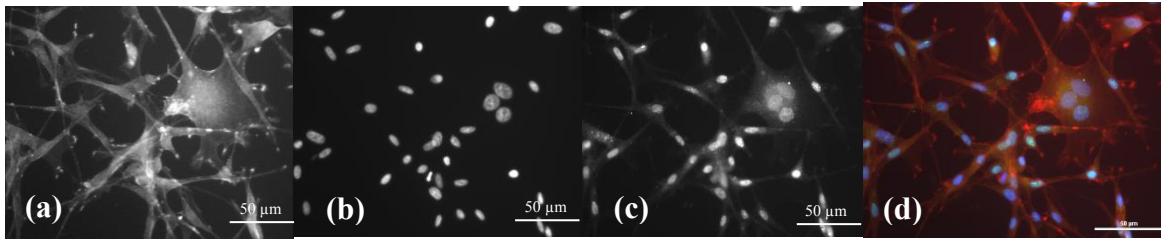
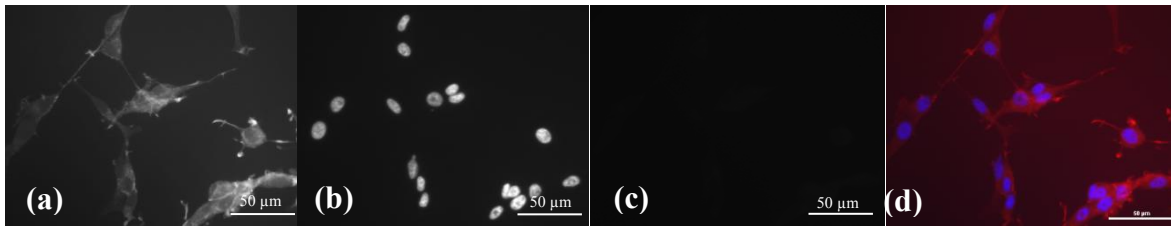


Figure 30: The localisation of endogenous RhoE to the nucleus of U87 cells was confirmed using RNAi. U87 cells were knockdown for 48 h and cells were harvested from the 6 wells plate. U87 cells were lysed in buffer containing Nonidet P-40. Next, nuclear and cytoplasmic fractions were prepared, separated by SDS-PAGE and immunoblotted with an antibody against RhoE. An effective isolation of nuclear and cytoplasmic fractions was confirmed using antibodies against α -tubulin. These blots represent the results of three (3) separate experiments ($n = 3$).

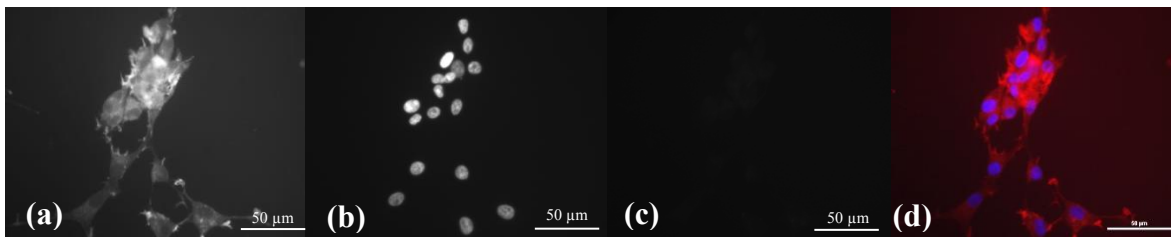
(A) Control oligo



(B) RhoE oligo A



(C) RhoE oligo B



Note:

(a) Actin staining (b) Nuclear staining (c) Rnd3/RhoE staining (d) Merged images

Figure 31: Immunostaining of U87 cells (A) U87 cell of non-silencing control using control oligo, (B) RhoE depleted U87 cells using RhoE oligo A (C) RhoE depleted U87 cells using RhoE oligo B. U87 cells were cultured for 24h on coverslips and observed under epifluorescence microscope at 40 x magnification. (a) U87 cells staining for F-actin observed at 900 ms exposure under Texas Red isothiocyanate (TRITC) filter (b) U87 cells staining for nuclear observed at 100 ms exposure under DAPI filter (c) U87 cells staining for Rnd3/RhoE observed at 400 ms exposure under FITC filter (d) U87 cells' merged image of three (3) different fluorescence filters (TRITC/DAPI/FITC).

4.2.3 The Expression of RhoE in the Nucleus of U87 cells is ROCK1 Independent

The knockdown of ROCK1 via RNA interference (RNAi) was applied using ROCK1 oligo 6 (ROCK1 6) and ROCK1 oligo 7 (ROCK1 7) for 48 h to investigate the interaction of ROCK1 and RhoE in brain tumour development. At the same time, Control oligo (NSiC) was used as the control condition for U87 cell.

After 48 h of incubation, the whole cell lysates were prepared for nuclear and cytoplasmic fractions (see Section 2.2.12). Following this, lysates were immunoblotted for ROCK1 to confirm knockdown and RhoE for identifying the effect on expression and localisation after disruption of ROCK1: RhoE interaction. The lysates were also immunoblotted for α -tubulin as a loading control. Figure 32 shows the results. These blots represent four separate experiments ($n = 4$) in which the result for every replicate was consistent.

As shown in Figure 32, the first three lanes on the left are for the whole cell lysates. Control oligo shows less expression of RhoE in the first lane when compared to ROCK1 depleted U87 cell that is located in the second and third lanes. This observation is consistent with the other three lanes at the right side (cytoplasmic fraction), where more RhoE are expressed after ROCK1 is knocked down. However, nuclear RhoE appeared to be evenly expressed either when ROCK1 is present or depleted from U87 cell. The individual expression of nuclear RhoE in ROCK1 depleted U87 cell and in the presence of ROCK1 are represented using three lanes in the middle, in which this observation is true for both oligos.

A semi-quantitative analysis on the expression level of RhoE after ROCK1 knockdown was carried out using Image J from four replicated experiments ($n = 4$). The results on densitometry analysis using image J for RhoE intensity after ROCK1 knockdown in

U87 cell are shown in Figure 33, where the intensity of RhoE for each fractions of nuclear (29 kD) and cytoplasm (29kD and 27 kD) was determined.

ROCK1 in U87 cell was depleted using oligos, ROCK1 oligo 6 and ROCK1 oligo 7 for 48 h. The statistical analysis using Tukey Kramer procedure to one factor ANOVA showed that RhoE intensity in nuclear consistently increased when compared to the cytoplasm for the higher band. The differences between ROCK1 depleted U87 cells and the control oligo are statistically significant ($p < 0.0001$).

The RhoE intensity was increased nearly to 2/3 fold (from 40 unit to 60 unit) in ROCK1 depleted U87 cell when compared to the control condition. Although more RhoE expression were observed in the U87 cell after ROCK1 depletion, more 29 kD form of RhoE was translocated to the nucleus, whereby increased the accumulation of 27 kD form of RhoE in the cytoplasm. Thus, the RhoE translocation from cytoplasm to the nucleus is not hindered even in the absence of ROCK1, indicating that the RhoE function is independent of ROCK1. Table 8 shows the exact ratio of each U87 cells condition.

The proportion of nuclear RhoE (29 kD) to cytoplasm (29 kD) in ROCK1 depleted U87 cells shows a value of more than 2.00, which indicates the upper band of RhoE (29 kD) was mainly translocated to the nucleus. In contrast, the ratio of upper band nuclear RhoE (29 kD) over lower band of cytoplasmic RhoE (27 kD) is less than 0.7; this indicates that the lower band of RhoE (27 kD) was accumulated in cytoplasm of ROCK1 depleted U87 cells. The distribution of RhoE for both bands (29 kD and 27 kD) in control oligo was relatively equal by ratio ~ 1.00 .

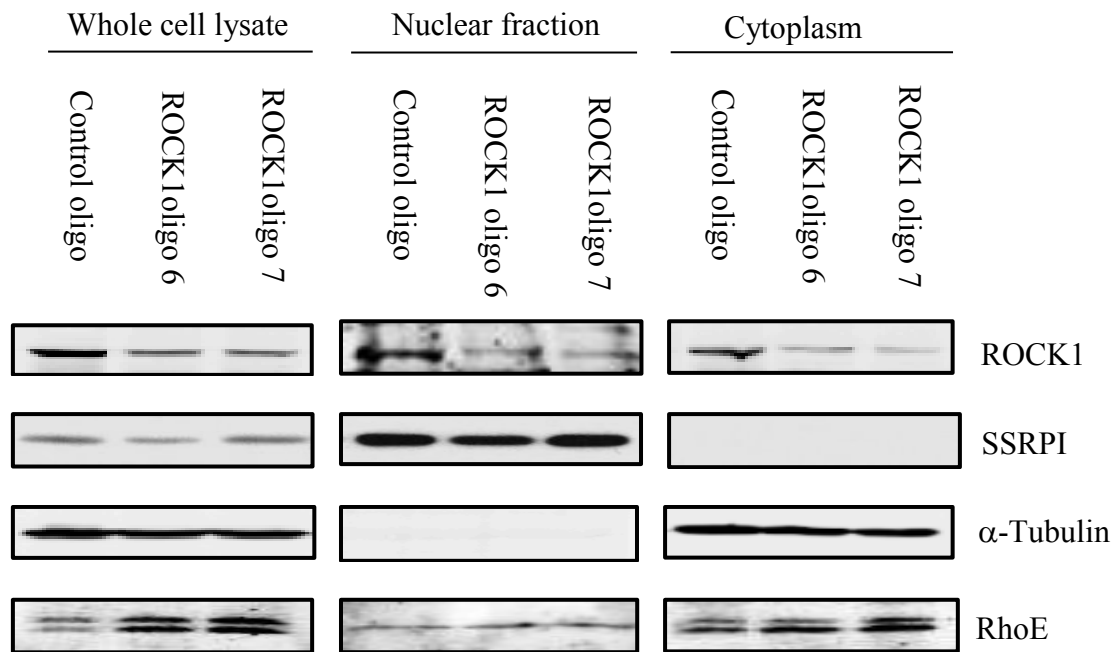


Figure 32: The localisation of RhoE to the nucleus is not regulated by ROCK1. U87 cells were lysed in a buffer containing Nonidet P-40. Next, nuclear and cytoplasmic fractions were prepared, separated by SDS-PAGE, and immunoblotted with an antibody against RhoE. The effective isolation of nuclear and cytoplasmic fractions was confirmed using antibodies against SSRPI and α -tubulin, respectively.

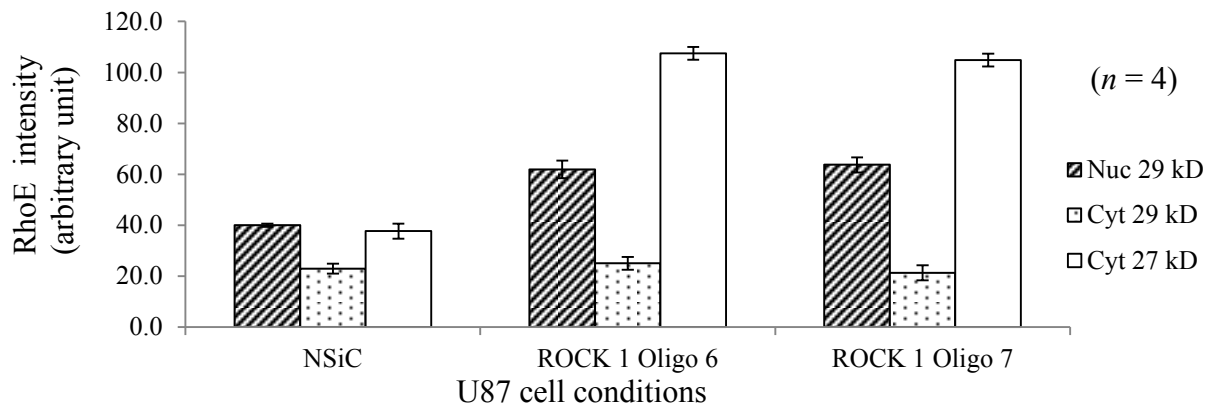


Figure 33: The acceleration of 29 kD RhoE in the nuclear proportionate to 27 kD of RhoE in cytoplasm were observed in ROCK1 depleted U87 cells. The densitometry of RhoE using Image J in ROCK1 depleted U87 cells using both oligos were compared to the control condition. The intensity unit for nuclear and cytoplasmic RhoE from each condition is arbitrary and it was respectively normalised either to SSRPI or to α -tubulin as the loading control. Error bars indicate standard error of the mean (S.E.M) of each data set according to U87 cells conditions. This study employed statistical analysis using Tukey Kramer procedure on one factor ANOVA for the whole dataset from four replicated independent experiments ($n = 4$) ($p < 0.01$).

Table 8: The data are the mean ratio that listed along with standard error of the mean (S.E.M) from four replicated independent experiment ($n = 4$).

U87 cells condition	Nuclear RhoE (29 kD) over cytoplasm (27 kD)	Nuclear RhoE (29 kD) over cytoplasm (29 kD)
Control oligo	1.076 ± 0.075	1.412 ± 0.081
ROCK1 oligo 6	0.575 ± 0.029	2.01 ± 0.207
ROCK1 oligo 7	0.623 ± 0.068	2.468 ± 0.306

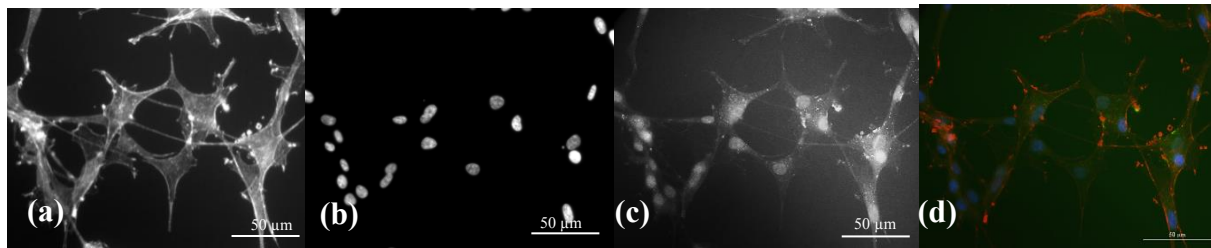
4.2.4 ROCK1 Interaction is Not Solely Required for Nuclear Localisation of RhoE

Other than immunoblot analysis, the RhoE protein localisation in U87 cell was also visualised under epifluorescence microscopy after applying immunofluorescence staining, which was previously described in Section 2.2.1.12. RhoE in the control condition (NSiC) and ROCK1 depleted U87 cell using ROCK1 oligo 7 (siROCK1) were stained using anti-Rnd3/RhoE antibody. Figure 34 shows the results on microscopic images. The RhoE expression was represented using a green fluorescence of FITC in Figure 34 (A) and 34 (B) - panel (c).

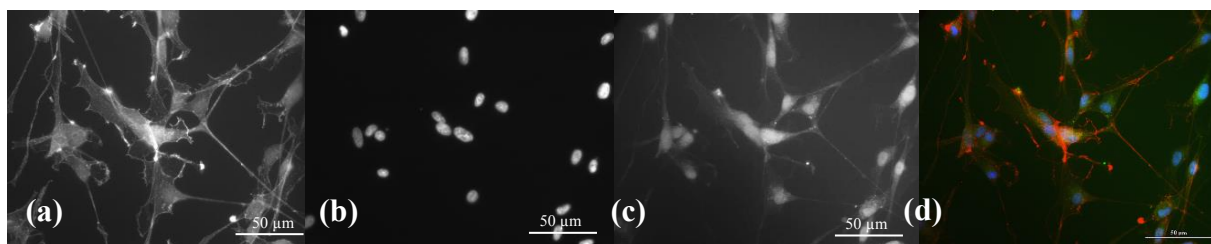
The microscopic image of U87 cells in siROCK1 shows that RhoE was expressed in both regions, which are nucleus and cytoplasm, and it was slightly more intense than the NSiC. Microscopic images only display a qualitative observation but comparison to the previous observation is still done (refer to Section 4.2.3; Figure 32) particularly on the RhoE blot of whole cell lysate and cytoplasm. Results on immunoblotting and immunostaining are consistent in terms of more RhoE is expressed in siROCK1 compared to NSiC. More expression of RhoE indicates that the absence of ROCK1 affected the stabilisation of RhoE in glioblastoma. However, the mechanism of RhoE stabilisation in siROCK1 is still unclear.

This experiment also investigated the stress fibre formation demonstrated by F-actin staining. The depletion of ROCK1 has led to the loss of actin and stress fibre as shown in panel (a) of Figure 34 (B). In contrast, actin cytoskeleton was maintained in NSiC, as shown in panel (a) of Figure 34 (A). ROCK1 is antagonising the function of RhoE by inducing the loss of stress fibre from U87 cells. Data on stress fibre phenotype also demonstrated that ROCK1 was successfully depleted using siRNA oligo 7 via RNAi technique.

(A) NSiC



(B) siROCK1



Note:

- (b) Actin staining
- (c) Nuclear staining
- (d) Rnd3/RhoE staining
- (e) Merged images

Figure 34: Immunostaining of U87 cells show the interaction of ROCK1 is not solely required for the RhoE localisation to the nucleus. (A) U87 cell of non-silencing control (NSiC) using control oligo, (B) ROCK1 depleted U87 cells (siROCK1) using ROCK1 oligo 7. U87 cells were cultured for 48h on coverslips and observed under epifluorescence microscope at 40 x magnification. (a) U87 cells staining for F-actin observed at 900 ms exposure under Texas Red iso-thiocyanate (TRITC) filter (b) U87 cells staining for nuclear observed at 100 ms exposure under DAPI filter (c) U87 cells staining for RhoE observed at 400 ms exposure under FITC filter (d) Merged image of U87 cells at three different fluorescence filters (TRITC/DAPI/FITC).

4.2.5 Localisation of RhoE to the Nucleus is Alternatively Dependent on PKC α

A previous study by Riento et al. (2003) observed that only ROCK1 binds to and phosphorylates RhoE efficiently, and that was the first evidence that showed ROCK1 has a specific target for RhoE. However, Chardin (2006) stated that inhibition of ROCK1 did not completely block RhoE phosphorylation. Instead, other kinases such as protein kinase C alpha (PKC α) might be involved in this process particularly in phosphorylating Ser¹¹.

In agreement to Chardin (2006), the phosphorylation sites that were predicted in RhoE were conducted via NetPhos 2.0 Server (Technical University of Denmark, 2012). Results retrieved from this server indicate that RhoE is highly specific as a substrate of kinases. Based on the sequence position, more than twenty (> 20) phosphorylation sites were predicted in RhoE, in which fifteen sites for serine (Ser), and four sites each for both threonine (Thr) and tyrosine (Tyr), respectively. Appendix 3 shows the details on phosphorylated peptide sequences for each residue of amino acid (Ser, Thr and Tyr).

Phosphorylation of RhoE by ROCK1 is primarily required in enabling the translocation of protein complexes, from cytosol to the plasma membrane (Madigan 2008). The similar hypothesis was presumed essential in translocating RhoE to other regions intracellularly, including to the nucleus. The treatment of U87 cells with selective serine/threonine inhibitors was probably relevant to validate this hypothesis. Therefore, Y27632 and Gö6976 were used in this experiment to inhibit ROCK1 and PKC α in the U87 cells, respectively.

Y27632 is an ATP competitive inhibitor for ROCK1 and ROCK2 *in vitro* and the inhibition is specific for the catalytic site of both kinases (Yu et al. 2012). Meanwhile,

Gö6976 is an ATP competitive PKC inhibitor that is specific for Ca²⁺-dependent PKC α and PKC β 1 isozymes (Madigan et al. 2009). Post 24 h culture of U87 cells lines, they were treated with pharmacological inhibitors of either ROCK1 or/and PKC α using Y27632 (10 μ M) and Gö6976 (2.5 μ M), respectively for 3 h. Following the 3 h inhibition of conventional ROCK1 and PKC α , the translocation of RhoE was investigated during the activation of PKC α using PMA (100 nM) for 15 min. After the designated treatment was completed, U87 cells were lysed in a buffer containing Nonidet P-40. Then, nuclear and cytoplasmic fractions were prepared, separated by SDS-PAGE, and immunoblotted with an antibody against Rnd3/RhoE.

The localisation of RhoE to the nucleus of U87 cells is shown in Figure 35. Accordingly, RhoE intensity was measured and the arbitrary result is shown in Figure 36. In Figure 35, the SSRPI blot was also detected at 92 kD, which is a loading control for nuclear RhoE. It represents the equal protein loaded for each sample from the nuclei. Meanwhile, α -tubulin was not found in any sample tested for nuclear fraction and this finding has proven that the separation of nuclei from cytoplasm was successful.

The localisation of RhoE to the cytoplasm is shown in Figure 37. Again, RhoE intensity was measured and the arbitrary result is shown in Figure 38 (A) for 29 kD form of RhoE and Figure 38 (B) for 27 kD form of RhoE. There was also a clean separation of nuclear from cytoplasm, as SSRPI disappeared in cytoplasm. Then, α -tubulin was also applied to cytoplasmic fraction where bands appeared vice-versa to the nuclei.

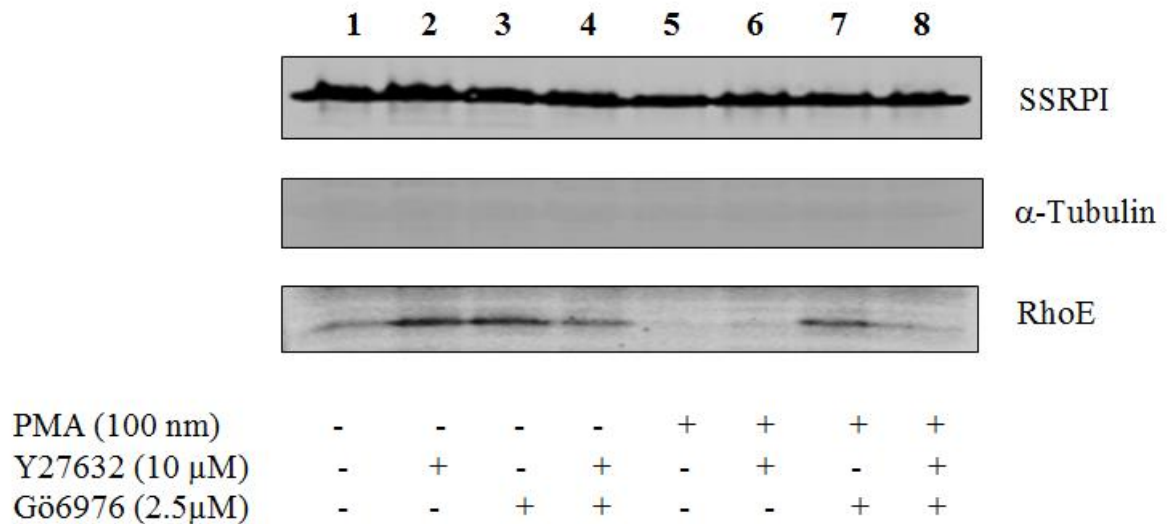
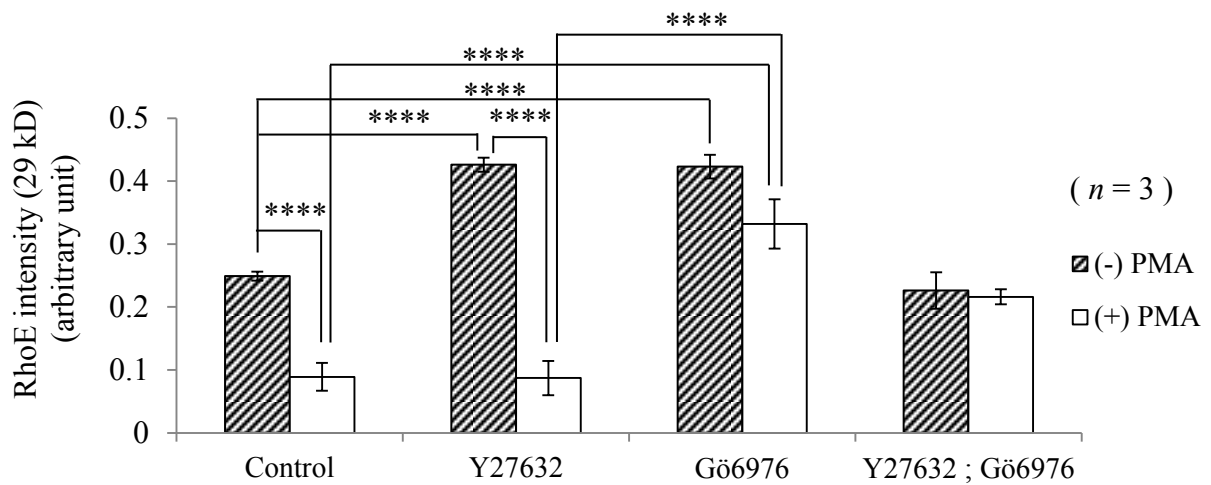


Figure 35: Localisation RhoE to the nucleus is alternatively dependent on PKC α without the assistance of ROCK1. RhoE (29kD) almost completely lost from the nucleus by the stimulation of conventional PKC α with or without RhoE interaction to ROCK1. A clean separation of the nuclear RhoE from the cytoplasm was confirmed based on the empty α -tubulin blot and the appearance of each individual band at the SSRPI blot. Y27632 used to inhibit the interaction of ROCK1 to RhoE, enabled individual interaction with PKC α . Gö6976 prevented the interaction of PKC α to RhoE, allowed a sole interaction with ROCK1.



Treatment of pharmacological inhibitor in the nuclear of U87 cells

Figure 36: Histogram of nuclear RhoE intensity according to the treatment of pharmacological inhibitor in U87 cells. RhoE almost completely lost from the nucleus by the stimulation of conventional PKC α with or without RhoE interaction to ROCK1. The activation of novel PKC α by PMA exhibit an increased the upper band of RhoE (29kD) and it remains more in the nucleus consistent with the active conventional PKC during ROCK1 inhibition. The intensity unit for nuclear RhoE (29 kD) from each condition was normalised to SSRPI as the nuclear loading control. The RhoE intensity was compared between U87 cells treated with pharmacological inhibitors, (+) Y27632 or/and (+) Gö6976 for 3 h () and the activation of PKC with the addition of PMA in U87 cells (). The statistical analysis for two factor ANOVA with replication involving multiple comparisons uses Tukey's HSD procedure to identify the difference within the whole datasets of three independent experiment ($n = 3$) (****) ($p < 0.0001$).

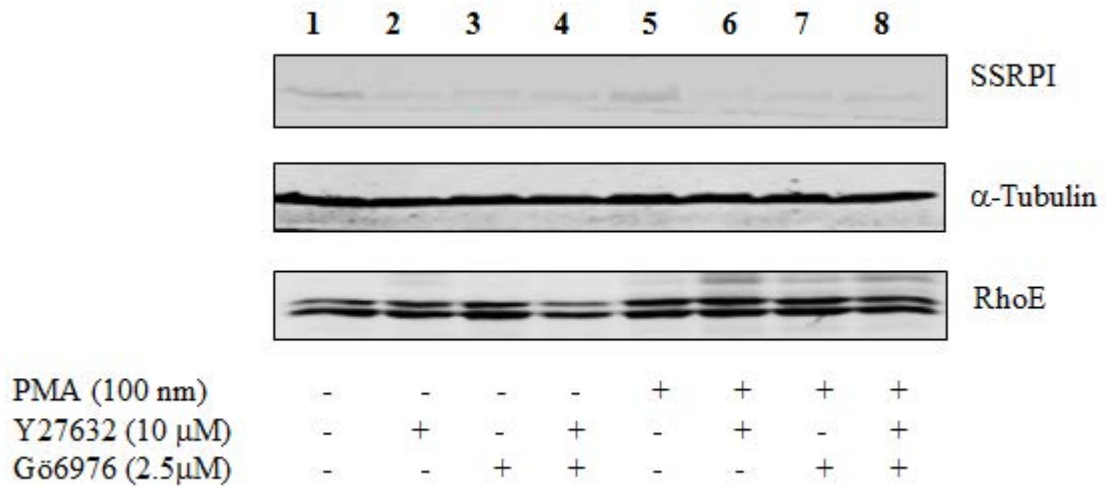
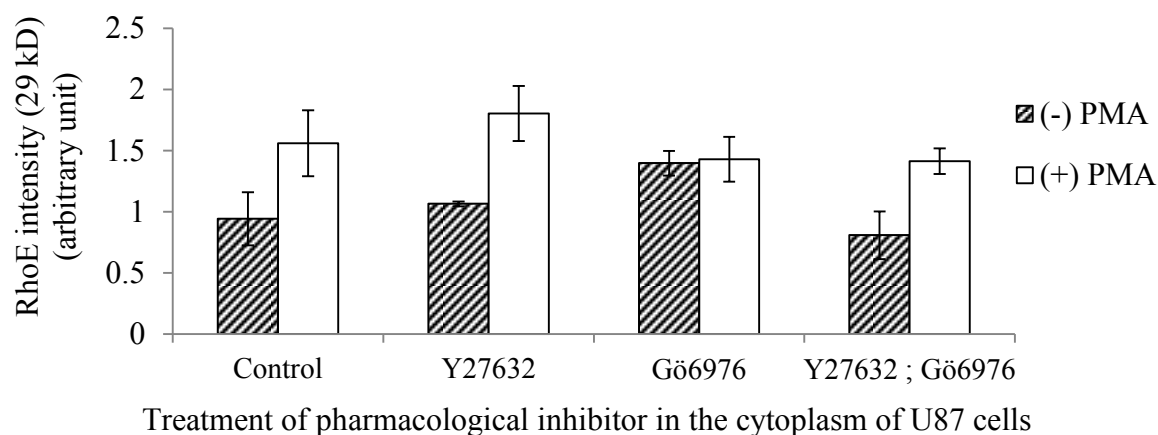
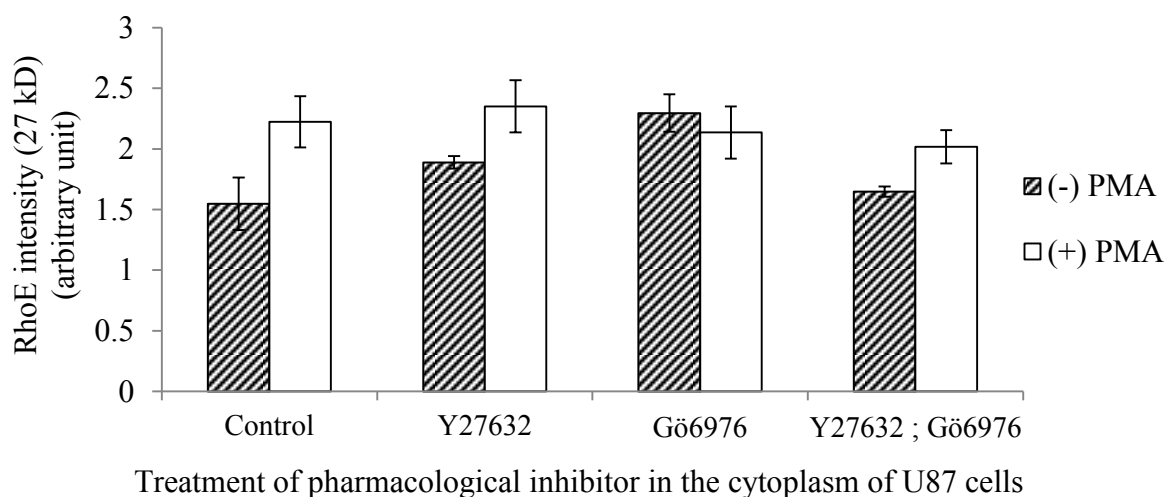


Figure 37: Immunoblot of cytoplasmic fraction of U87 cells post 24 h culture. Cells were treated with pharmacological inhibitors either ROCK1 or/and PKC α using Y27632 (10 μ M) and Gö6976 (2.5 μ M) for 3 h. Then, the activation of PKC was applied using PMA (100 nM) for 15 min. U87 cells were lysed in a buffer containing Nonidet P-40. Then, nuclear and cytoplasmic fractions were prepared, separated by SDS-PAGE and immunoblotted with an antibody against Rnd3/RhoE. α -tubulin blot detected at 55 kD is a loading control for cytoplasm that represents equal protein loaded for each sample from the cytoplasmic fraction. A clean separation of the cytoplasm is shown from the empty SSRPI blot.



(A)



(B)

Figure 38: (A) Data presents the mean of cytoplasmic RhoE intensity as determined from triplicate experiment ($n = 3$) of western blotting of the cytoplasm. The intensity unit of cytoplasmic RhoE (29 and 27 kD) was normalised to α -tubulin as the loading control. The RhoE intensity was compared between U87 cells treated with pharmacological inhibitors, (+) Y27632 or/and (+) Gö6976 for 3 h (▨) and the activation PKC with the addition of PMA in U87 cells (□). A statistical analysis using two factor ANOVA with replication involving multiple comparisons uses Tukey's HSD procedure to identify the difference within the whole datasets of three independent experiment ($n = 3$).

A semi-quantitative analysis was conducted to evaluate the distribution of RhoE intracellularly. The statistical difference was to determine whether the treatment of ROCK and PKC inhibitor could affect the RhoE translocation. Figure 36 and Figure 38 (A) and (B), show the results on densitometry analysis for nuclear and cytoplasm. The intensity of RhoE upper band (29 kD) in the nuclei in Figure 36 was calculated by normalising the value of RhoE intensity from each condition (1 to 8, Section 2.2.2.4) to SSRPI. A similar method was used to determine the intensity of RhoE upper band (29 kD) and lower band (27kD) in the cytoplasm that are shown in Figure 38 (A) and (B). The cytoplasmic RhoE intensity from each condition (1 to 8, Section 2.2.2.4) was calculated by normalising the value to α -tubulin.

Figure 36 is implied to nuclear RhoE (29 kD), in which the differences for activation of novel PKC was found crucial to translocate RhoE out from the nucleus for the control and (+) Y27632. The difference is statistically significant (****) ($p < 0.0001$) ($n = 3$). Next, Figure 38 (A) shows the upper band of RhoE (29 kD) in the cytoplasm. The difference for the activation of novel PKC was found unnecessary to translocate RhoE into the cytoplasm. The difference is not significant. Finally, Figure 38 (B) indicates the lower band of RhoE (27 kD) in the cytoplasm, and the activation of novel PKC was found not significant to translocate RhoE into the cytoplasm for the control and (+) Y27632; (+) Gö6976. The differences are not statistically significant for the control, and (+) Y27632; (+) Gö6976, respectively. Overall observation for this experiment (Figure 35-38) is to describe the details on the localisation of RhoE to the nucleus that is alternatively dependent on PKC α instead of ROCK1.

The first lane of the blot in Figure 35 had shown that endogenous RhoE localises to the nucleus of the U87 cell. Introducing 100 nM PMA to the cells activate the conventional PKC α and promote loss of RhoE from the nucleus. Although the fifth lane of the same blot

showed that RhoE was invisible in the nuclear fraction, in Figure 37, the fifth lane has revealed more expression of RhoE in cytoplasms compared to the first lane of the same blot. Prior to the experiment, the phosphorylation status of RhoE was speculated due to interaction with either ROCK1 or PKC α to alter the localisation of RhoE.

Next, the second lane of the blot in Figure 35 indicated that the inhibition of ROCK1 by adding 10 μ M of Y27632 causes more expression of endogenous RhoE in the nucleus. However, the observation in the sixth lane of the same blot was against the second lane by which inhibition of ROCK1 followed by the activation of conventional PKC α has led to a loss of RhoE from the nucleus. As compared to the sixth lane in Figure 37, more expression of RhoE was observed in cytoplasms. This result confirmed that PKC α interaction with RhoE is essential to translocate RhoE between nucleus and cytoplasm even though without the assistance of ROCK1.

Later, 2.5 μ M Gö6976 was used to inhibit PKC α in order to block its interaction with RhoE. The result shown in the third lane of the blot in Figure 35 has demonstrated that more expression of RhoE in the nucleus. In parallel, the seventh lane of the same blot also disclosed that the inhibition of conventional PKC α followed by the activation of novel PKC α in the presence of ROCK1 causes RhoE to accumulate in the nucleus. Consistently, the third and the seventh lane of the blot in Figure 37; both showed relatively similar expression of RhoE in cytoplasms. The effect of either conventional or novel PKC α in regulating the localisation of RhoE in U87 cells demonstrated a consistent potential in both fractions, either nuclei or cytoplasm.

Finally, the inhibition of ROCK1 and conventional PKC α led to the accumulation of endogenous RhoE in the nucleus. The result is shown in the fourth lane of the blot in Figure

35. In contrast, result in the eighth lane of the same blot exhibited much loss of RhoE from the nucleus. The inhibition of ROCK1 and conventional PKC α , followed by the activation of novel PKC α enable the partial loss of RhoE from the nucleus. In parallel, the fourth lane of the blot in Figure 37 showed less 29 kD RhoE whereas the eighth lane of the same blot relatively showed more expression of both 29 kD and 27 kD RhoE in cytoplasms. In summary, this experiment confirmed that the localisation of RhoE to the nucleus is alternatively dependent on PKC α without the assistance of ROCK1.

4.2.6 Nucleocytoplasmic Transport is Essential for the Localisation of RhoE

Nucleocytoplasmic shuttling process is a possible mechanism for the RhoE localisation to the nucleus. This transportation machinery is triggered by either the recognition of nuclear export signal (NES) or the nuclear localisation signal (NLS) by the exportin or importin, which was described Section 1.3.3. This hypothesis was presumed after considering that some of the translated proteins in the cytoplasm were assigned as the transcription factors and transported back to the nucleus. Both signals, either NES or NLS, are possibly important to enable the communication of RhoE with other interacting proteins partners. The communication is particularly important to enable the recognition of RhoE by the intermediary - nucleocytoplasmic transport receptor (NTR/KPN) for the localisation of RhoE intracellularly. However, the RhoE localisation to the nucleus that relies on the existence of NES and NLS has been poorly studied and needs validation.

Prediction analysis on RhoE amino acids sequence was conducted to determine whether this protein consists of NES. An established FASTA format of RhoE protein

sequence was searched and copied from UniProtKB (see Section 1.4.1), then BLAST to the NetNES 1.1 server prediction programme: (<http://www.cbs.dtu.dk/services/NetNES/>). As a result, this prediction revealed a leucine rich region within point 68 to 75. There are eight amino acids in a sequence with the following prediction: TQRIEL⁷³SL⁷⁵. Appendix 4 shows further details on the NES prediction analysis. The molecular structure of RhoE was visualised as three dimensional individual proteins using PyMOL Molecular Visualisation and Figure 39 shows a clear visualisation of NES sequence of RhoE in 3D form.

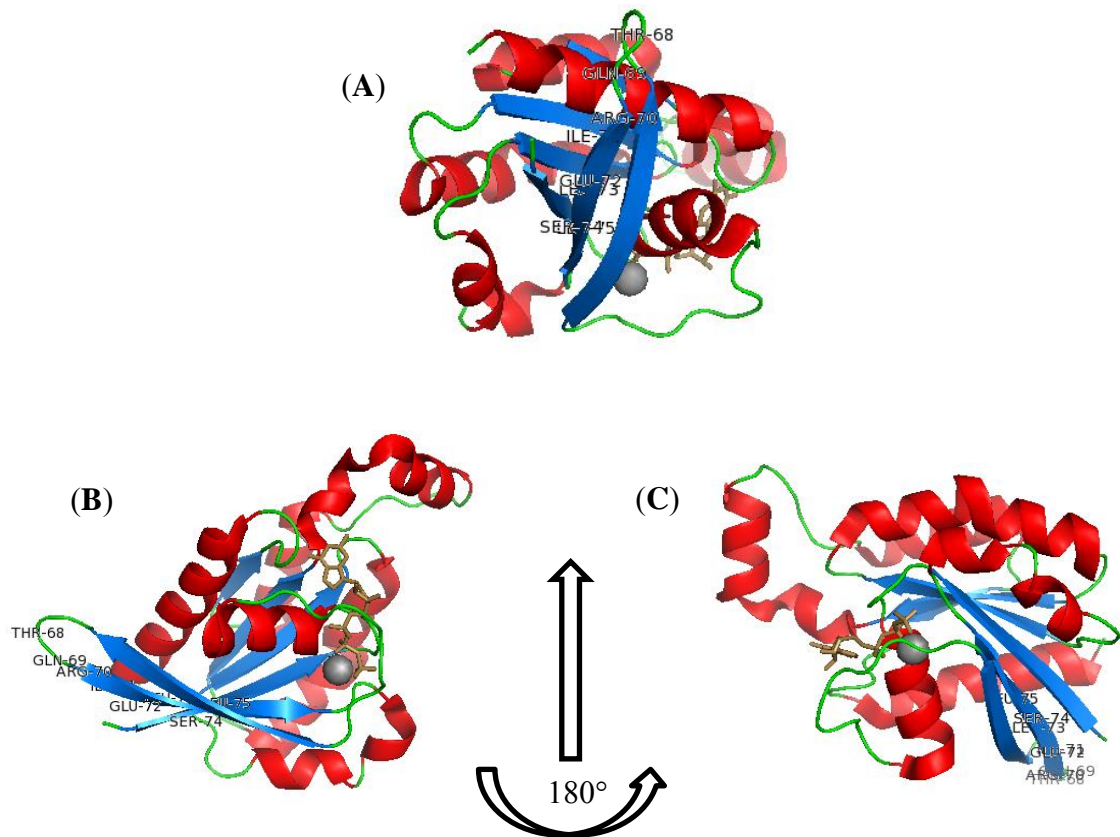
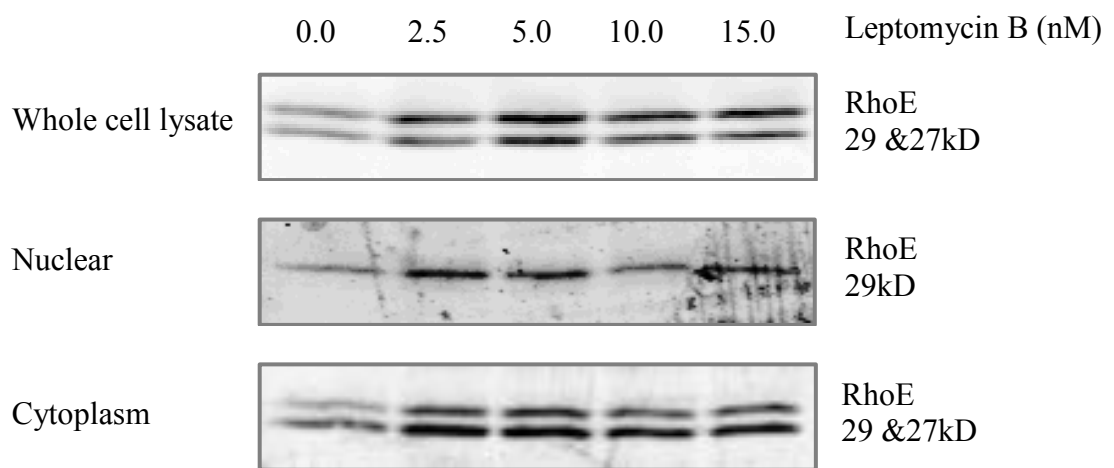


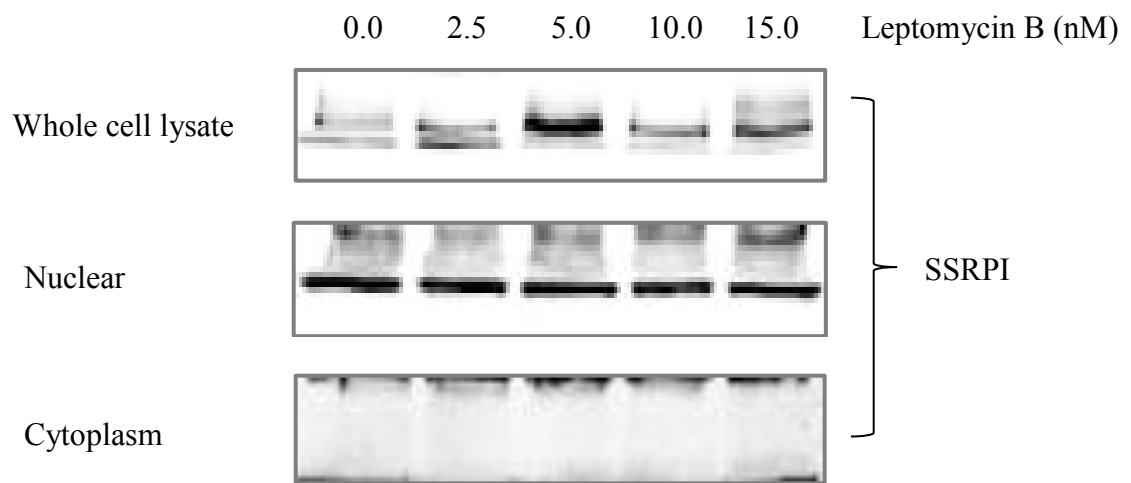
Figure 39: NES predicted in human RhoE (pdb: 1M7B) is visualised at different orientations. The high resolution structure of RhoE that appears with the NES was visualised in PyMOL Molecular Visualisation and retrieved in PNG file format. The predicted NES (TQRIEL⁷³SL⁷⁵) in RhoE was indicated with labelled of amino acids, and the position in 3D is visualised at different directions. (A) NES sequence view at vertical axis (B) NES sequence view at diagonal direction (C) NES sequence view at skew position.

Figure 39 (A), (B) and (C) are the visualisation of NES at different directions. It is clear that NES is located at the periphery of RhoE protein folding structure. The existence of NES at peripheral position has made RhoE visible and enables the recognition by exportin. In addition, the leucine rich region of NES enhances exportin affinity to RhoE and it can accelerate the anchoring ability between these proteins complexes. Thus, this interaction is likely to be important for subcellular localisation of RhoE to exit the nucleus. The existence of NES in RhoE could possibly create a specific docking site for protein-protein interactions with the exportin.

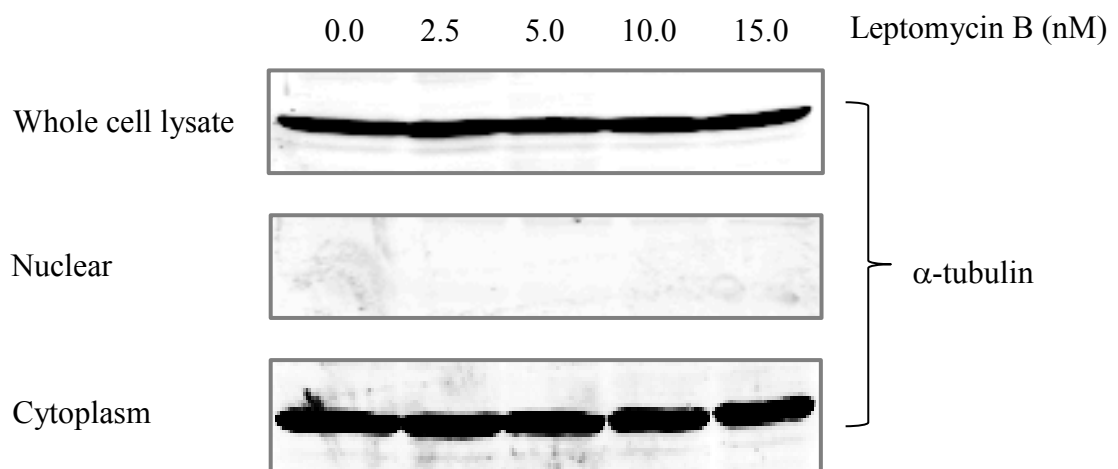
This experiment was conducted to look at the RhoE expression, and to determine whether the treatment with NES inhibitor could block this dynamic process. Nuclear and cytoplasmic fraction was prepared to confirm the hypothesis. In the beginning, 1.0 million units of U87 cells were cultured in 100 mm diameter of tissue culture dishes for a series of concentration, starting from 0.0 nM and up to 15.0 nM. U87 cell was grown for 24 h before it was treated with the NES inhibitor, Leptomycin B (LepB). The whole cell lysate, nuclear and cytoplasmic fraction of U87 cell were prepared for 6 h post LepB treatment (see Section 2.2.1.2). The samples then underwent SDS-PAGE, transferred to PVDF membrane, and subjected for immunoblotting. Figure 40 (A) shows the scanned images of RhoE blots for whole cell lysate as well as individual subcellular fractions, nuclei and cytoplasm. Figure 40 (B) and 40 (C) are loading control for this experiment.



(A) RhoE blots



(B) SSRPI blots



(C) α -tubulin blots

Figure 40: The RhoE expression in U87 cells is unaffected by the inhibition of NES. After 6 h treatment with the increased concentration of Leptomycin B (LepB) (0.0-15.0 nM), U87 cells were lysed in a buffer containing Nonidet P-40. Nuclear and cytoplasmic fractions were prepared, separated by SDS-PAGE and immunoblotted with an antibody against Rnd3/RhoE. The effective isolation of nuclear and cytoplasmic fractions was confirmed using antibodies against SSRPI and α -tubulin respectively. These blots represent the result of only a single experiments ($n = 1$).

(A) RhoE blots of the whole cell lysate, nuclear fraction and cytoplasm of U87 cells.

(B) Nuclear loading marker; SSRPI blot detected at 92 kD is a loading control for nuclei representing equal protein loaded for each sample from the nuclear fraction.

(C) Cytoplasm loading marker; α -tubulin detected at 55 kD is a loading control for cytoplasm representing equal protein loaded for each sample from the cytoplasmic fraction. A similar loading maker was used for the whole cell lysate.

As shown in Figure 40 (A), there is relatively more expression of RhoE in the nuclear of U87 cells for 2.5 nM, 5.0 nM and 15.0 nM of LepB relatively than the control, 0 nM. In contrast, U87 cells that were treated with 10.0 nM of LepB showed a similar expression with U87 cells without LepB treatment, 0 nM. The RhoE expression level fluctuated when increasing the dosage of LepB. SSRPI blots in Figure 40 (B) confirmed that each sample tested for nuclear fraction has been loaded equally in the Western blot. The whole cell lysate and cytoplasmic fractions also have similar findings. α -tubulin blots in Figure 40 (C) was used as the loading marker for both fractions.

The result in this experiment was contrary to the earlier speculation that NES is essential for the localisation of RhoE to the nucleus of glioblastoma. The expression was not affected by LepB as showed in Figure 40 (A) that the RhoE expression was inconsistently increased in U87 cells. The technical incompetence was not the reason for fluctuated expression of RhoE at 5.0 to 10.0 nM, and it was confirmed by loading markers, SSRPI in Figure 40 (B) for nuclei and α -tubulin in Figure 40 (C) for the whole cell lysate and cytoplasm. The increased of LepB treatment did not affect the retention of this protein in the nucleus. The RhoE expression was independent of NES and low affinity to exportin, but it was possibly regulated at the gene level.

In principle, one or two clusters of basic residues of NLS are recognised by the import receptor, importin. The RhoE destined for the nucleus possibly contains targeting sequences termed nuclear localisation signal (NLS). In principle, NLS is recognised by the adaptor molecule which is importin alpha ($\text{Imp}\alpha$). Then, this cargo then links to the carrier molecule or intermediate that is called importin beta ($\text{Imp}\beta$). The complex of cargo protein

(RhoE-Imp α -Imp β) translocates into the nucleus crossing the nuclear pore within the nuclear envelope.

Basically, the process of DNA delivery is internalised to the nucleus to allow RhoE overexpression. To understand the mechanism of nuclear-cytoplasmic machinery, this study used a number of FLAG-tagged RhoE cDNA constructs that have been generated by Komander et al. (2008). In brief, they constructed a variety of mutants that prevent RhoE from interacting with its potential protein binding partners including the importin. Manipulating these constructs in this study was beneficial in order to identify novel RhoE interacting partners in U87 cells. Identification and characterisation of gene modifications for individual mutants were described further in Chapter 5. One of the mutants generated allied with disruption of ROCK1: RhoE interface which is RhoE double mutants (RhoE^{T173R/V192R}) and these constructs were applied to U87 cells to investigate if localisation of RhoE to the nucleus was related to the interaction with either Imp α or Imp β .

RhoE wild-type (RhoE^{WT}) and RhoE double mutants (RhoE^{T173R/V192R}), both with FLAG-tagged RhoE epitope were transfected into U87 cells. Overexpression vectors containing empty vector (EV) were also applied for the control of the experiment using construct plasmid pCMV5 EV FLAG. As recommended by Wallenstein et al. (2010), a serum free medium was used at the beginning of the transfection to reduce the interference of growth factor by the presence of foetal bovine serum (FBS). Then, the serum free medium was replaced with a complete medium, 8 hours post transfection. The nuclear and cytoplasmic fractions of U87 cells were prepared for 42 hours post-transfection.

Nuclear and cytoplasmic fractions were prepared for FLAG-RhoE pulled down assay. Co-Immunoprecipitation (Co-IP) technique was used to pull-down RhoE from a combination

of nuclear and cytoplasmic fractions of the transfected U87 cells. Three (3) tissue culture dishes with 150 mm diameter were pre-coated with animal gelatine 0.1 % (w/v) to allow stratified and optimum growth for U87 cells before the transfection process. Each plate was assigned for *in vitro* culture of 2.85 million units of U87 cells overnight until they reached 60 % to 70 % confluent and ready for transfection.

Further, these cell fractions were utilised for Co-IP to pull down the RhoE and interacting binding partners using FLAG antibody. At the same time, negative control for the Co-IP experiment was also conducted using the reagent blank without candidate protein sample. Then, yields from Co-IP samples underwent SDS-PAGE, transferred to PVDF membrane, and subjected for immunoblotting. Figure 41 shows scanned images of immunoblot for the cargo carrier, the Importin-7 (Imp β), the FLAG-RhoE and RhoE blots for individual constructs.

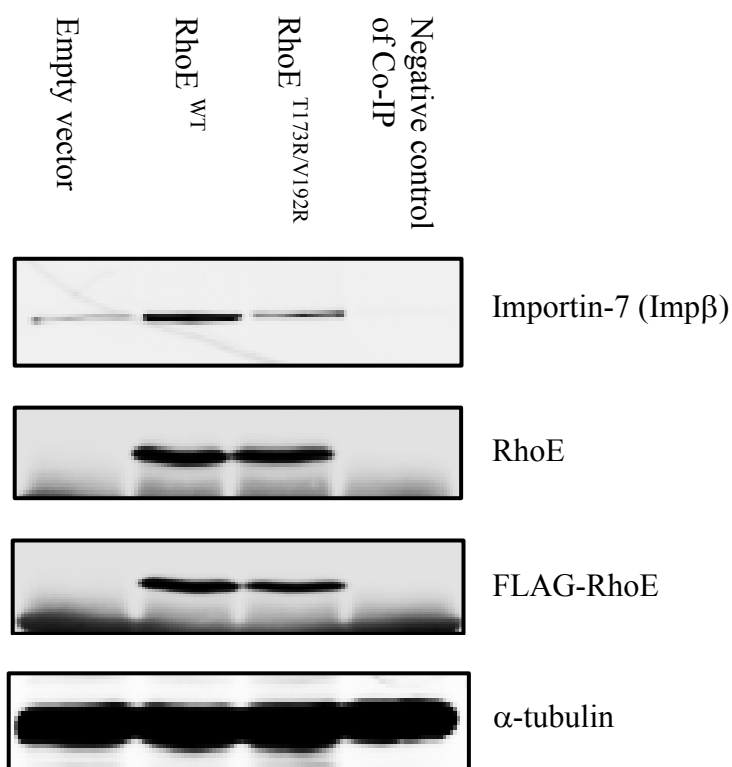


Figure 41: Overexpressed RhoE in U87 cells (RhoE^{WT}) shows high affinity to $\text{Imp}\beta$, indicating that the nuclear localisation signal (NLS) existed in RhoE. RhoE wild-type (RhoE^{WT}) and RhoE double mutants ($\text{RhoE}^{\text{T173R/V192R}}$) with FLAG-tagged RhoE epitope were transfected into U87 cells. Overexpression vectors containing empty vector (EV) were also applied for the control of the experiment using construct plasmid pCMV5 EV FLAG. Co-Immunoprecipitation (Co-IP) technique was used to pull-down RhoE from a combination of nuclear and cytoplasmic fractions of the transfected U87 cells. At the same time, negative control for the Co-IP experiment was also conducted using the reagent blank without candidate protein sample. Then, yields from Co-IP pulled down assay went through SDS-PAGE and immunoblotted with antibodies against $\text{Imp}\beta$, Rnd3/RhoE, FLAG-RhoE and α -tubulin. These blots represent the results of a single experiment ($n = 1$).

From left, each lane in Figure 41 respectively represents the empty vector, which are RhoE wild-type (RhoE^{WT}), RhoE double mutants (RhoE^{T173R/V192R}), and the negative control for the Co-IP. The first row shows the immunoblot of Importin-7 (Imp β) and more expression was found in RhoE^{WT} as compared to the empty vector. Although there was less expression of Imp β in RhoE^{T173R/V192R}, it was not totally depleted in the double mutants RhoE. The negative control for the Co-IP experiment shows a clear lane.

Regarding transfection efficiency, both constructs performed the same level expression of RhoE. However, when looking at the FLAG-RhoE blot, there is a slight decrease for the FLAG-RhoE pull down by RhoE double mutants compared to the wild-type. α -tubulin was used as the loading marker for each sample which shows that total protein was equally loaded. However, a cross reaction with IgG hyper-variable chain as indicated by the band that appeared at the negative control of Co-IP lane was ambiguous.

4.3 Discussion

Foster et al. (1996) had initially reported that the localisation of RhoE was to the plasma membrane of the post transfected COS7 cell. In agreement, Guasch et al. (1998) has supported this finding by demonstrating that RhoE was localised subcellular to the lateral membranes of the MDCK cells, and manifested the role of RhoE in cell-cell adhesion. Later, Riento et al. (2003) also investigated the intracellular localisation of RhoE. They extended the research by manipulating the interaction of RhoE with ROCK1 and suggested that subcellular localisation of RhoE was not limited to the plasma membrane. Instead, they recommended that RhoE was also localised to the trans-Golgi network. They used COS7 cell to overexpress

RhoE and found that this protein was scattered on intracellular membrane such as in the perinuclear region, vesicular structure of Golgi complex and cytoplasm, despite the fact that it was primarily localised to the plasma membrane.

A subsequent study was carried out by a similar working group led by Anne Ridley and they demonstrated that ROCK1 binds to and phosphorylates RhoE on seven sites (see Section 1.4.3.2). Overexpressed RhoE in COS7 cells showed that the phosphorylated form of RhoE was found only in the cytoplasm (Riento et al. 2005a). Further, Riento and the co-workers found that non-phosphorylated RhoE was associated mostly with membranes in Swiss 3T3 fibroblasts, where it sequestered ROCK1 that was associated with myosin (Riento et al. 2005b). Moreover, they also studied endogenous RhoE in PDGF starved Swiss 3T3 as well as NIH 3T3 cells, induced RhoE phosphorylation at the specific site, Ser¹¹. However, the localisation of RhoE in these cells after phosphorylation was unsuccessful due to the low expression level of RhoE (Riento et al. 2005b).

After that, they used HeLa cells and carried out a similar PDGF starved stimulation to increase the phosphorylation of RhoE. As a result, they observed that RhoE was localised to a perinuclear region at the beginning of the stimulation but diffused to the cytoplasm after the phosphorylation (Riento et al. 2005b). A parallel observation was also demonstrated by Komander et al. (2008), in which they found that the cellular localisation of RhoE also altered as the phosphorylation was affected by ROCK1. Komander et al. (2008) suggested that ROCK1 promotes phosphorylation event to stabilise RhoE and prevent stress fibre assembly. Most recently Gomez et al. (2014) demonstrated that RhoE was found at the atypical part of the cytoplasm, between the nucleus and the ductal lumen of Leydig cells in testicular tissue. Nevertheless, neither of these studies mentioned that RhoE was found exactly in the nucleus.

Thus, the localisation of RhoE to the nucleus that was demonstrated in Section 4.2.1 and Section 4.2.2 is novel, and the finding is expected to bring a huge impact to the development of glioblastoma.

ROCK1 is a well characterised serine/threonine kinase that functions downstream of RhoA to regulate the myosin light chain (MLC) by phosphorylating and blocking the activity of MLC phosphatase (Chardin 2006). ROCK1 also interacts with and phosphorylates RhoE as previously described in Section 1.4.3.2. Results in Section 4.2.3 and 4.2.4 show that ROCK1 affected the stabilisation of RhoE in glioblastoma. However, the mechanism to stabilise RhoE in ROCK1 depleted U87 cells is poorly understood. A slightly similar research was conducted by Riento et al. (2005b) to verify whether RhoE protein stability is regulated by ROCK1 phosphorylation. Riento et al. (2005b) tried to overexpress FLAG-tagged wild-type RhoE (RhoE^{WT}) in COS7 cells with or without myc-D1 ROCK1. They consistently observed that the expression of ROCK1 could increase the amount of RhoE protein. Therefore, they concluded that ROCK1 phosphorylation increases the stability of RhoE.

U87 cells treated with the ROCK inhibitor, Y27632 suggested that kinase activity of ROCK1 was not solely required for RhoE localisation to the nucleus as described in Section 4.2.5. In principle, RhoE binds to the kinase domain of ROCK1 that is localised at the N-terminal region, besides blocking the kinase activity of ROCK1. The region of 76 to 375 in ROCK1 was not sufficient for RhoE binding as it also required extended residues, starting from 1 to 375 of amino acids within the N-terminal region of ROCK1. Consequently, the Rho binding domain (RBD) was hindered from RhoA binding due to the formation of an auto-inhibition loop. As a result, RhoA was prevented from binding to ROCK1 when RhoE was bound to ROCK1. Loirand and co-workers (2006) also disclosed that the phosphorylation

state of RhoE did not affect the binding to ROCK1. Considering that U87 cells were treated with Y27632 to inhibit ROCK1 for 3h, followed by PMA to activate conventional PKC α for 15 min, these applications enabled translocation of RhoE to exit the nucleus and enter the cytoplasm. Thus, the result consistently showed that RhoE can also be phosphorylated by other kinases.

Results in Section 4.2.5 and literature review clearly show that RhoE is a substrate of both kinases, ROCK1 and PKC α . However, ROCK1's effect is antagonistic to PKC α in terms of translocating RhoE in and out of the nucleus and the cytoplasm of U87 cells. As described in Section 1.4.3.4, ROCK1 and PKC α are well known to share a common phosphorylation recognition sequence in RhoE; particularly at Ser¹¹ and Ser²⁴⁰. The inhibition of either one of the kinases, PKC α and ROCK1 with Gö6976 and Y27632 respectively, encouraged the localisation of RhoE to the nucleus. This is consistent with the treatment of both inhibitors that prevented RhoE from exiting this region. In contrast, the activation of conventional PKC α which was not novel triggered the localisation of RhoE to the cytoplasm.

On the other hand, the shuttling process of RhoE and subcellular localisation of either to the cytoplasm or the nucleus persistently occurred depending on the substrates availability or diverted to the downstream pathway that requires ROCK1: RhoE complexes. The accumulation of RhoE in the nucleus potentially indicates that this protein has NES at the particular region of its amino acids sequence. This study used Leptomycin B (LepB) as a specific inhibitor of NES and the results are shown in Section 4.2.6. This pharmacological inhibitor specifically targets at the chromosome region maintenance which is Crm-1-dependent nuclear export (Mihlan et al. 2013).

Ideally, 24 h prior to the treatment of Leptomycin B, RhoE was synthesised in the nucleus, translated in the cytoplasm and transported back to the nucleus after phosphorylated by the kinases such as ROCK1. The introduction of LepB for 6 h into U87 cells might have inhibited NES and led to the RhoE accumulation within the nuclear region. Surprisingly, the increased LepB treatment did not affect the accumulation of this protein in the nucleus. RhoE expression was found independent to NES, but possibly regulated at the gene level, and RhoE possibly has low affinity to exportin.

This chapter also revealed the preliminary evidence that transportation machinery with NLS is essential in translocating RhoE to the nucleus. After the failure to prove the existence NES in RhoE, another prediction analysis on RhoE amino acids sequence was conducted with the speculation that NLS exists in this protein. Simultaneously, an established FASTA format of RhoE protein sequence was searched and copied from UniProtKB (see Section 1.4.1), then BLAST to the cNLS mapper prediction programme: (http://nls-mapper.iab.keio.ac.jp/cgi-bin/NLS_Mapper_form.cgi). This server predicted nuclear localisation signals (NLS) specific to the Imp α and Imp β pathways by calculating the level of NLS activity (NLS score).

As a result, this prediction revealed a lysine (K) and arginine (R) rich region within point 207 to 242. There are thirty-six (36) amino acids in a sequence and the following is the prediction:

R²⁰⁷NK²⁰⁹SQR²¹²ATK²¹⁵R²¹⁶ISHMPSR²²³PELSAVATDLR²³⁴K²³⁵DK²³⁷A²³⁸K²³⁹SCT

Appendix 5A has a detailed description on NLS prediction analysis. However, the visualisation of the NLS position in 3D form of RhoE using PyMol Molecular Visualisation software is unavailable. Although the predicted NLS residues were possibly truncated upon

crystallisation, it is important to obtain the verification of the hypothesis that NLS exists in RhoE.

Results in Section 4.2.6 demonstrated that the overexpressed RhoE using wild-type construct in U87 cells required more carrier molecule or intermediates (Imp β) to translocate RhoE when more RhoE was available due to overexpression in the cytoplasm. RhoE would be transported to the nucleus through nuclear pore complex (NPC) that immediately bound Imp α , to the cargo carrier, Imp β . In contrast, when interaction of RhoE to ROCK1 is disrupted, as indicated by U87 cells transfected with RhoE double mutants, there is less requirement for the binding to Imp β .

CHAPTER 5

IDENTIFICATION OF NOVEL RHOE INTERACTING PROTEINS

5.1 Introduction

In the previous chapter, RhoE has been identified to localise in the nucleus of U87 cells and the translocation is independent ROCK1. In contrast, RhoE is rather dependent on either PKC α or Imp β to translocate between the cytoplasm and the nuclei. U87 cells expressing endogenous RhoE at constant level is contrary to the report by Poch et al. (2007) that demonstrated low levels of RhoE expression in U87 cells. Due to this contradiction, the expression of RhoE needs to be increased; thus the U87 cells were transfected, starved for 8 hours and then the cultures were serum stimulated for another 34 hours. In order to analyse the protein-protein interaction, the U87 cells were transfected with a number of different FLAG-tagged RhoE cDNA expression constructs.

Apart from the interaction with ROCK1, PKC α and Imp β , the overexpression RhoE is also applied in an attempt to identify any potential novel interactions with nuclear proteins. This effort is based on preliminary finding by Ryan (2010) where RhoE interacts with several proteins that are involved in the nuclear processes which have been previously described in Section 1.5. For instance, she identified MCM3 and MCM5 as a part of hexamers subunit from the replicative helicase MCM2-7, which are essential for DNA loading. Moreover, she also identified ORC3L as a component of 6-subunit origin-recognition complex (ORC) that binds to the origin of replication and it is required in assembling pre-replication complex.

These nuclear proteins were essential during DNA replication that occurs at G₁-phase as well as early S-phase of the cell cycle (Riera et al. 2013).

The preliminary result on the existence of NLS in RhoE and interaction with Imp β as previously described in Section 4.2.6 also requires further explanation. Instead of utilising Co-IP, the immunoprecipitation technique was applied to pull down the overexpressed RhoE from the transfected U87 cells. Following this, the mass spectrometry analysis was carried out on the digested proteins, which have been isolated from RhoE pull-down assay. Liposomes reagent was used purposely for delivering the gene of interest to incorporate the genome of the host. Wong et al. (2007) mentioned that transfection efficiency is dependent on the transport system of gene delivery to the host cells. The mechanism by which cationic liposome - DNA forming complexes that are internalised and delivered to the nucleus have to be determined prior to transfection (Wong et al. 2007). For example, previous researchers found several forms of endocytosis that are involved in DNA uptake such as clathrin-mediated, caveolae-mediated and macropinocytosis. Thus, endocytosis became the most preferred route for cell entry (Rejman et al. 2005).

In addition, the previous chapter has briefly mentioned about a number of FLAG-tagged RhoE cDNA constructs that have been generated by Komander et al. (2008). They constructed a variety of mutants that prevent RhoE from interacting with its potential protein binding partners. Modifications of individual mutants were listed in Table 9. Amongst all, one of the mutants generated allied with disruption of ROCK1: RhoE interface which is RhoE double mutants (RhoE^{T173R/V192R}) and needs further investigation. The most exciting about the double mutant is their inability to pull down ROCK1. Besides, the construct also sustains a loss of stress fibre similar to the wild-type phenotype indicated by cell become round up when expressed.

Table 9: Mutagenesis of ROCK1: RhoE Interface (Adapted from Komander et al. 2008)

Types of mutants	Amino acids mutated	Effect on interaction between RhoE and ROCK1
RhoE ^{WT}	Nil	Enable interact with ROCK1 Loss of stress fibres when highly expressed
RhoE ^{V56Y}	Valine 56 to Tyrosine	Mutation of effector site residues Maintain stress fibres (dominant negative RhoE mutants) No inhibition on binding to ROCK1
RhoE ^{T173R/V192R}	Threonine 173 (β 6 strand) and Valine 192 (α 5 helix) to Arginine	Unable to pull down ROCK1 No difference in actin organisation compared to the wild-type Induced strong reduction of stress fibres (cell become round up)
RhoE ^{V57Y}	Phenylalanine 57 to Tyrosine	Mutation of effector site residues Maintain stress fibre (dominant negative RhoE mutants)
RhoE ^{Y60A}	Tyrosine 60 to Alanine	Mutation of effector site residues No difference in actin organisation compared to the wild-type Induced strong reduction of stress fibres (cell become round up)
RhoE ^{V192R}	Valine 192 (α 5 helix) to Arginines	Unable to interact with ROCK1 (normal interaction occurred in the absence of additional AMP-PNP) No difference in actin organisation compared to the wild-type Induced strong reduction of stress fibres (cell become round up)

5.2 Results

5.2.1 Overexpressed RhoE in the U87 Cells

The experiment used overexpression vectors that contain wild-type (wt) mouse RhoE (pCMV5 FLAG RhoE^{WT}), empty vector (EV) as a control (pCMV5 EV FLAG) and double mutant constructs (pCMV5 FLAG RhoE^{T173R/V192R}). The immunofluorescence staining for FLAG-tagged RhoE of transfected U87 cells with each construct was conducted in the experiment as previously described in Section 2.2.1.13. Figure 42 (A), (B) and (C) shows the results of the observation under the epifluorescence microscope for each of RhoE mutant, allied with the wild-type and empty vector.

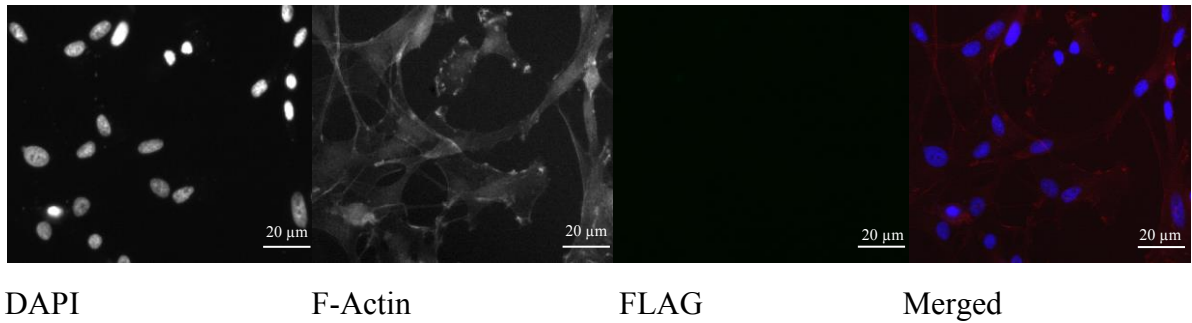
Figure 42 (A) shows that the U87 cells were transfected with empty vector (plasmid pCMV5 EV FLAG) which is the result of the empty fluorescence in FLAG staining. This is the control for the experiment to ensure that the results on other mutants are not false positive. Thus, it means that the primary and secondary antibody conjugated-fluorophore (goat anti mouse conjugated FITC) are bound to be very specific to the FLAG-tagged RhoE fusion protein.

Figure 42 (B) shows that the U87 cells were transfected with wild-type (wt) mouse RhoE (pCMV5 FLAG RhoE^{WT}) and demonstrated a bright green fluorescent in FLAG staining. Both cell compartments were well stained with FLAG-RhoE in either nuclear region and/or cytoplasmic region. Based on the observation on actin staining, it is showed that overexpressed RhoE has induced the loss of stress fibres as most of the cells became round shaped rather than flattened morphology with tentacle-like projections that scatter in the marginal area of cells as it was commonly found in non-transfected U87 cells.

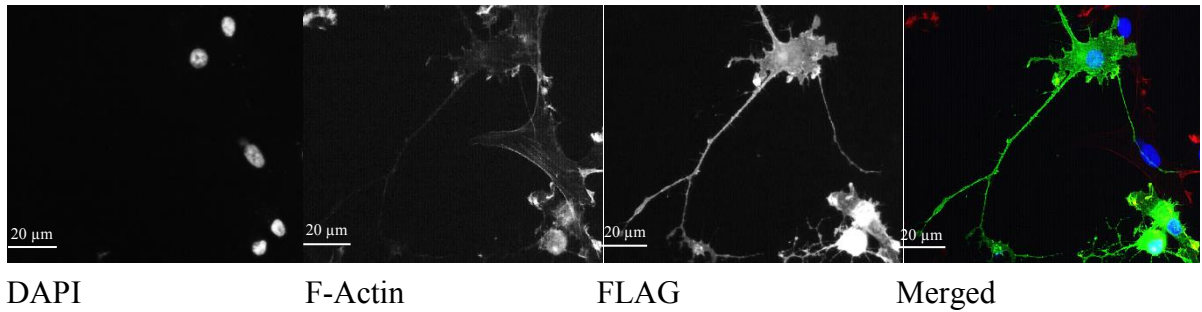
Figure 42 (C) shows the observation of U87 cells that are transfected with double mutants RhoE which is consistent with the result in Chapter 4 (see Section 4.2.5). Accordingly, a strong green fluorescence of FITC mainly appeared in the nucleus. This observation shows that the interface disruption between RhoE: ROCK1 has led to RhoE localisation to the nucleus.

As shown in Figure 42, principle method used to recognize successful transfection of RhoE wild-type (RhoE^{WT}) and RhoE double mutants constructs (RhoE^{T173R/V192R}) into the U87 cells are by the appearance of the FLAG-tagged RhoE epitope. The overexpression vectors containing empty vector (EV) were also applied as a control of the experiment using construct plasmid pCMV5 EV FLAG showing disappearance of FLAG-tagged RhoE. The FLAG-RhoE was visualised using FITC at 400 ms exposure whereas The F-Actin was visualised using TRITC at 900 ms exposure. The nuclear visualisation of each coverslip used DAPI at 100 ms exposure. Each of the immunofluorescence stainings of the transfected U87 cells was observed under an epifluorescence microscope visualised at 40 x magnifications.

(A) Empty vector



(B) RhoE^{WT}



(C) RhoE^{T173R/V192R}

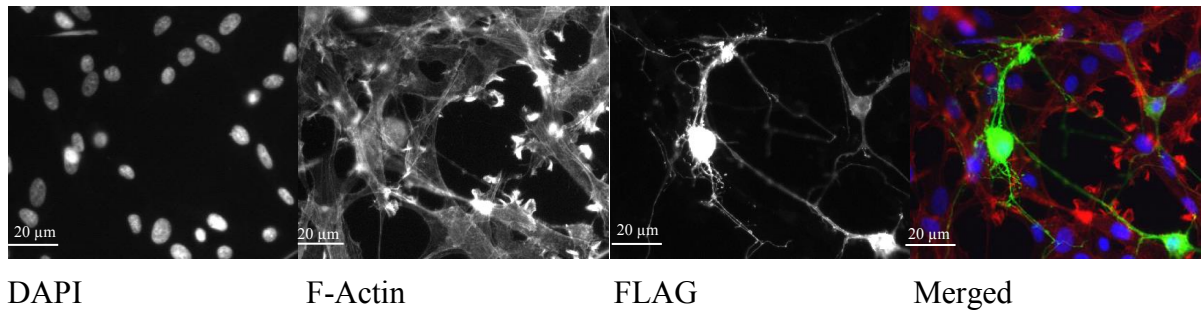


Figure 42: The overexpressed RhoE in U87 cells shows that RhoE was localised to the nucleus and cytoplasm in double mutants RhoE. (A) U87 cells transfected with pCMV Empty Vector. (B) U87 cells transfected with pCMV5 FLAG-RhoE^{WT} (C) U87 cells transfected with pCMV5 FLAG-RhoE^{T173R/V192R}.

Following the immunostaining, western blot analysis was carried out. A similar overexpression technique to the immunostaining experiment was applied where the U87 cells were transfected, starved for 8 hours and then culture was serum stimulated for another 34 hours. The transfected U87 cells were lysed in buffer containing Nonidet P-40 at 42 hours post-transfection. Nuclear and cytoplasmic fractions were prepared, separated by SDS-PAGE and immunoblotted with antibodies against anti-FLAG antibody to detect RhoE (29 kD). Figure 43 (A) shows the results of immunoblot on overexpressed RhoE. In accordance with RhoE expression, an equivalent amount of total protein loaded to each well is verified via immunoblotted with antibodies against SSRPI and α -tubulin to identify nuclear and cytoplasmic marker respectively at (92 kD) and (55 kD) as shown in Figure 43 (B).

Figure 43 (A) showed the selected of the RhoE constructs that allied with the wild-type and were successfully transfected into the U87 cells. This observation described the blot of FLAG-tagged RhoE at 29 kD for the whole cell lysate, nuclear fraction and cytoplasm. The double mutants RhoE (RhoE^{T173R/V192R}) appeared to be strongly expressed in the nucleus as shown in the fourth lane of the nuclear fraction blot. In parallel, the localisation of RhoE to the nucleus in this experiment is not correlated with disruption of residual site in RhoE interfacing ROCK1. On the other hand, the localisation of RhoE to the cytoplasm in previous result that showed in Figure 42 (B) by RhoE^{WT} construct indicated that the binding at effector region by RhoE to ROCK1 is essential in maintaining the stress fibre formation and this process commonly occurs in the cytoplasm.

(A) RhoE blots

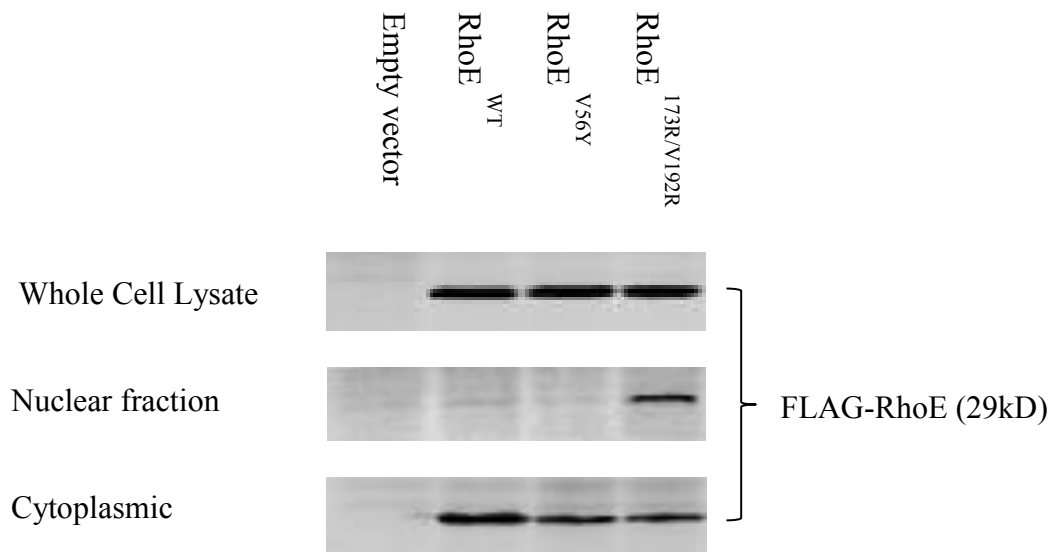


Figure 43: The immunoblot of FLAG confirmed that the double mutants RhoE (RhoE^{T173R/V192R}) overexpressed in the U87 cells and localised to the nucleus and cytoplasm.

(A) The localisation of FLAG-RhoE expressed after transfection with RhoE mutant plasmids into the U87 cells in whole cell lysate, nuclear and/or cytoplasmic fractions. RhoE wild-type (RhoE^{WT}) and other selected RhoE mutant constructs (RhoE^{V56Y} and RhoE^{T173R/V192R}) transfected into the U87 cells and recognised by FLAG-tagged RhoE epitope. The overexpression vectors containing empty vector (EV) were also applied as a control of the experiment using construct plasmid pCMV5 EV FLAG. In addition, lane three indicates another RhoE mutant construct pCMV5 RhoE^{V56Y} that is a mutation of effector side residues. This mutant successfully maintained stress fibres (result not shown) and known as a dominant negative RhoE mutant. U87 cells transfected with pCMV5 RhoE^{V56Y} also allow binding to ROCK1 and not essential in this study.

(B) Loading marker blots

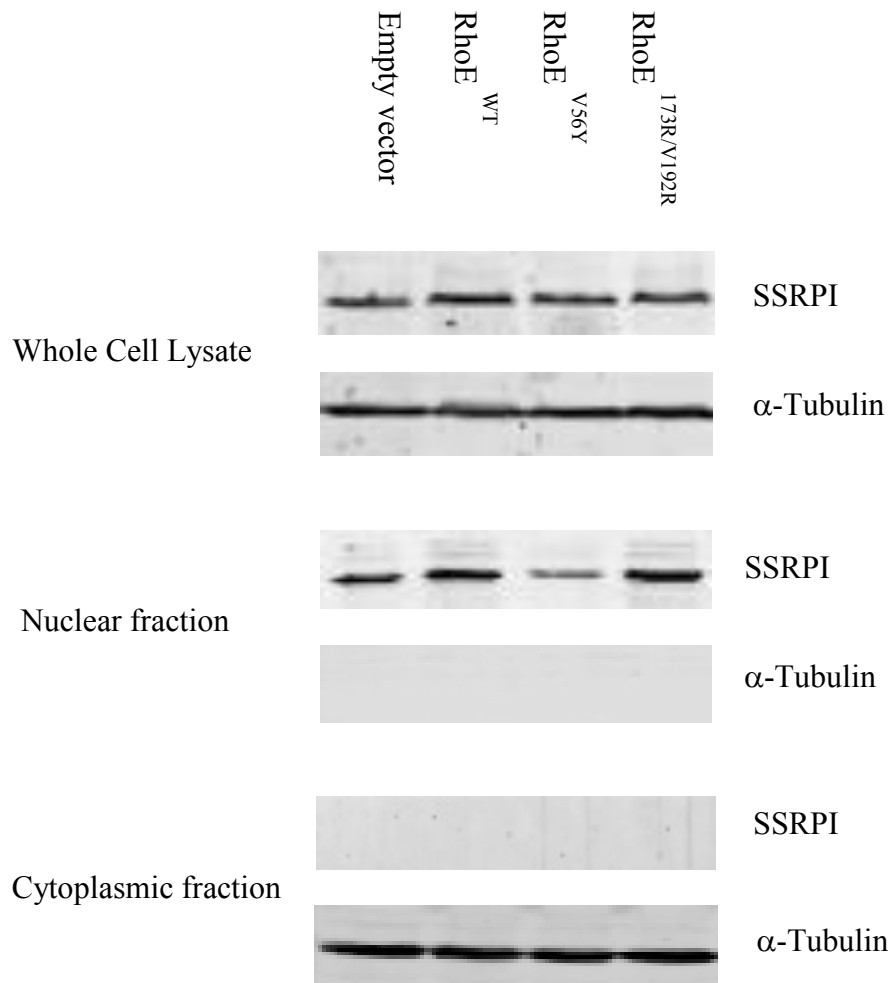


Figure 43: **(B)** The loading control using SSRPI (81 kD) for nuclear and α -tubulin (55 kD) for cytoplasmic markers. The U87 cells were transfected, starved for 8 hours, and the culture were then serum stimulated for another 34 hours. The transfected U87 cells were lysed in buffer containing Nonidet P-40 at 42 hours post transfection. The nuclear and cytoplasmic fractions were prepared, separated by SDS-PAGE, and immunoblotted with antibodies against SSRPI and α -tubulin. These blots are representative of triplicate experiment ($n = 3$).

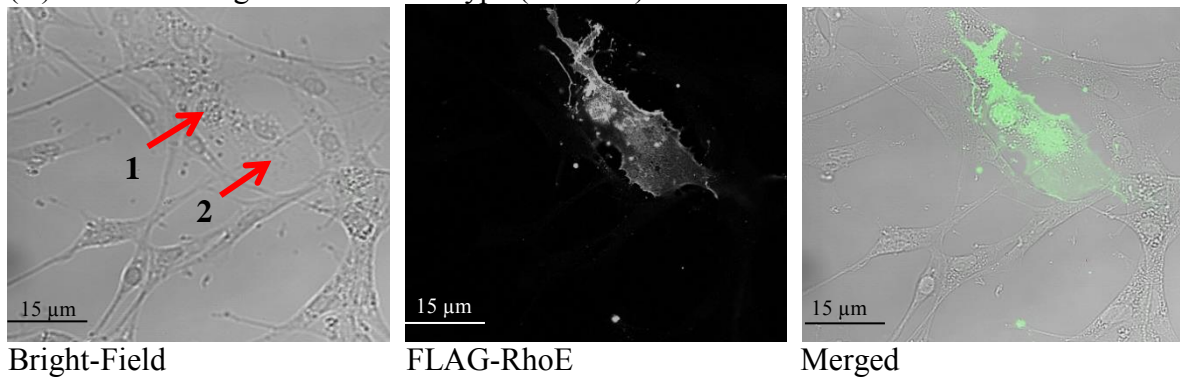
5.2.2 Confocal Analysis Confirmed RhoE Localised to the Nucleus of U87 Cells

Further observation on the transfected U87 cells was conducted under confocal laser scanning microscopy (CLSM) to confirm the localisation of RhoE to the nucleus. The U87 cells were fixed with PFA 4 % (w/v) and immunostained with a mouse monoclonal antibody, which raised against the FLAG-tagged RhoE epitope, followed by the secondary antibody antimouse conjugated Alexa Fluor 488 nm to visualise the localisation of FLAG-tagged RhoE in an individual transfected cell. Figure 44 shows the results; panel (A) for U87 cells transfected with pCMV5 FLAG-RhoE^{WT} and panel (B) for U87 cells transfected with pCMV5 FLAG-RhoE^{T173R/V192R}.

The localisation of RhoE is widely scattered within both regions, which are nuclear and cytoplasmic regions of U87 cells transfected with RhoE wild-type construct (pCMV5 FLAG-RhoE^{WT}) is shown in Figure 44 (A). In contrast, Figure 44 (B) of RhoE double mutants (pCMV5 FLAG-RhoE^{T173R/V192R}) indicates discrepancy by most expression of FLAG-RhoE in the nuclei. In addition, the dysfunctional RhoE double mutants by the replacement of threonine 173 and valine 192 both with arginine, prevent RhoE to bind ROCK1.

More expression of 29 kD RhoE observed in the nucleus of U87 cells as shown in Figure 45 is found consistent with the result of the acceleration of nuclear localisation of RhoE in ROCK1 depleted U87 cells by the siROCK1 (Figure 33, Chapter 4). The possible reason was due to phosphorylation by other kinases and ROCK1 independent. It is clear evidence that ROCK1 does not regulate the nuclear localisation of RhoE. Another observation is the Imp β required for RhoE localisation to the nucleus which is parallel with the NLS prediction. Thus, the role of ROCK1 is inessential for the function of RhoE in the nucleus.

(A) Confocal image of RhoE wild-type (RhoE^{WT})



(B) Confocal image of RhoE double mutants (RhoE^{T173R/V192R})

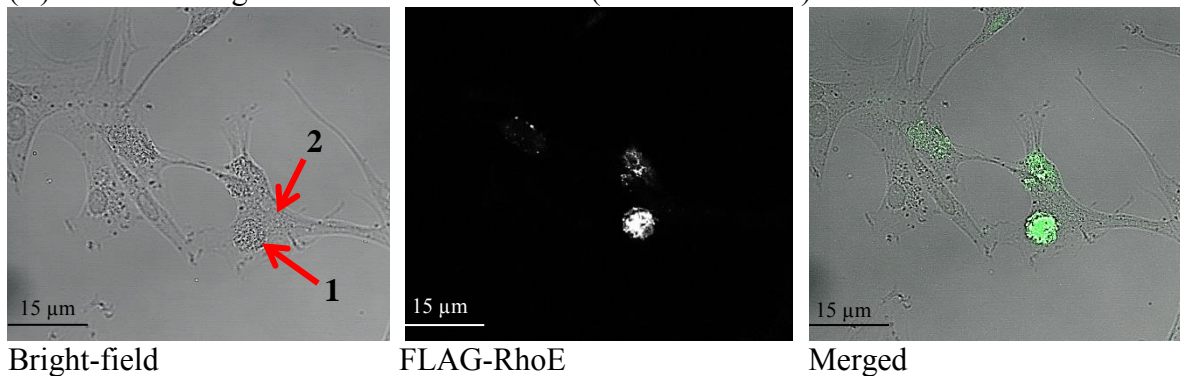
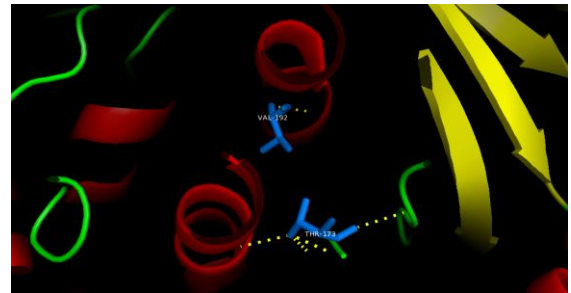
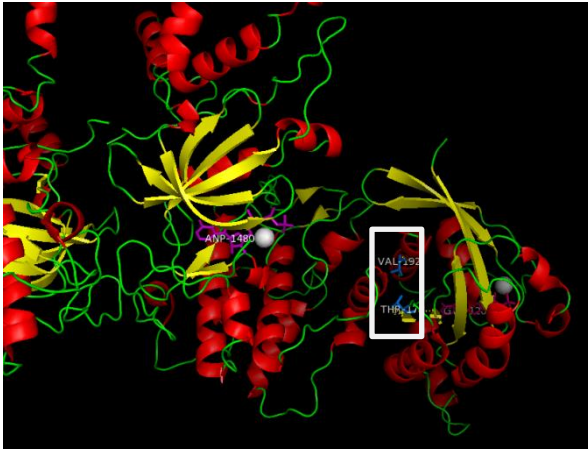
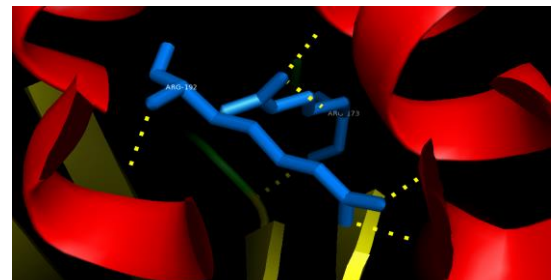
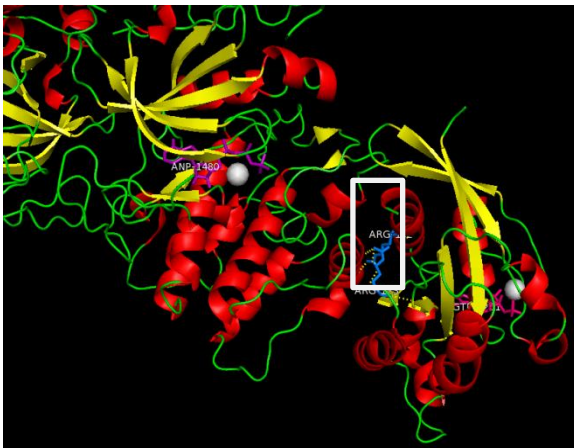


Figure 44: The localisation of RhoE to the nucleus of U87 cells at 42 hours post-transfection. The immunostaining of U87 cells was conducted for FLAG to detect RhoE. The primary antibody used an anti-FLAG which was raised in a mouse to detect RhoE. On the other hand, the secondary antibody used an anti-mouse with conjugated Alexa Fluor 488nm, which was raised in a goat that has green fluorescence. Laser acquisition and vertical sectioning were applied within multiple layers of U87 cells towards a region of interest (ROI) on the coverslips until up to 100 layers via Z-Stack experiment. The thickness of the layers on each selected ROI is fixed to create an accurate overlapping between channels (bright field and 488 nm laser). (A) Confocal image of RhoE wild-type (RhoE^{WT}) and (B) Confocal image of RhoE double mutants (RhoE^{T173R/V192R}). (1) Arrow indicates nuclei of U87 cells; (2) Arrow indicates cytoplasm of U87 cells.



Enlarged

Original sequence: RhoE (V192) or RhoE (T173/V192)



Enlarged

Mutated sequence of double mutant RhoE (R173/R192)

Figure 45: The high-resolution structure of RhoE interacts with ROCK1 (pdb: 2V55) - heterodimer was visualised in PyMOL Molecular Visualisation and retrieved in PNG file format. Localisation of single mutant or double mutant RhoE interfacing ROCK1 lead to disruption of RhoE: ROCK1 interaction. Each mutated residue is shown in blue stick within folding protein structure.

5.2.3 Bioinformatics Analysis on RhoE Pull-Down Assay

5.2.3.1 Immunoprecipitation Followed by Mass-Spectrometry Analysis

The identification of the genes that encode the regulatory proteins involved in most of the nuclear processes in U87 human glioblastoma cells was necessary in this study. The nuclear processes include protein biosyntheses such as the transcription and translation of the genes, DNA replication, cell cycle, mitosis, and telomere maintenance. Notably, the regulatory proteins were speculated to be more likely found in the nuclei. In addition, cytosolic protein is also a major interest as it is related to a GTPase activity, active transport, metabolic processes, as well as the protein stabilisation for post-translational modification of RhoE. Thus, obtaining the list of genes from RhoE pull-down assay is a basic requirement in further analysis using bioinformatics applications.

The source of large gene lists was obtained from the mass spectrometry data of RhoE pull-down assay. This assay was prepared via the immunoprecipitation of RhoE wild-type (RhoE^{WT}) and RhoE double mutants (RhoE^{T173R/V192R}) that were transfected into the U87 cells with FLAG-tagged RhoE epitope. Pertaining to this hypothesis, the RhoE was immunoprecipitated from a combination of nuclear and cytoplasmic extracts of the transfected U87 cells. Next, the immunoprecipitated proteins were separated by SDS PAGE and the protein bands were stained with Coomassie blue. Figure 46 shows the result for the immunoprecipitation of RhoE^{WT} and RhoE^{T173R/V192R} aligned with the empty vector (EV) as the control of the experiment.

Next, these protein bands were excised from the gel and the proteins were digested into the peptides for identification (Newton et al. 2008). Using reverse HPLC coupled to an ion trap mass spectrometer, the peptides belonging to the proteins in the immunoprecipitated

sample were identified by comparing the recorded peptide fragmentation pattern with the database of the peptide sequences (FASTA) (Lodge et al. 2007).

The novel binding proteins that interacted with RhoE were found by BLAST in the sequence of peptides. The description of the RhoE-interacting protein partners were encoded by their accession numbers. Then, the individual accession numbers were renamed via Gene Cards: the common gene identifiers that provide genomic, proteomic, transcriptomic, genetic, and functional information of all known and predicted human genes. In addition, the Gene Cards coding system is acknowledged by majority of genes uploader in the bioinformatics application system.

In recent years, the high throughput enrichment tools for analysing the list of genes include DAVID (2008), BioVenn (2008), BioProfiling (2011) and STRING (2013). However, none of these analysing tools could be considered as a “gold” standard procedure due to their own limitations (Huang et al. 2009). Thus, this research decided to exploit DAVID in its first attempt of analysing the genes. As a result, there are 195 genes discovered from RhoE^{T173R/V192R}, which are less than 229 genes found in. Table 10 and Table 11 list the specific genes obtained for the experiment. The U87 cells transfected with both constructs; RhoE^{WT} and RhoE^{T173R/V192R}.

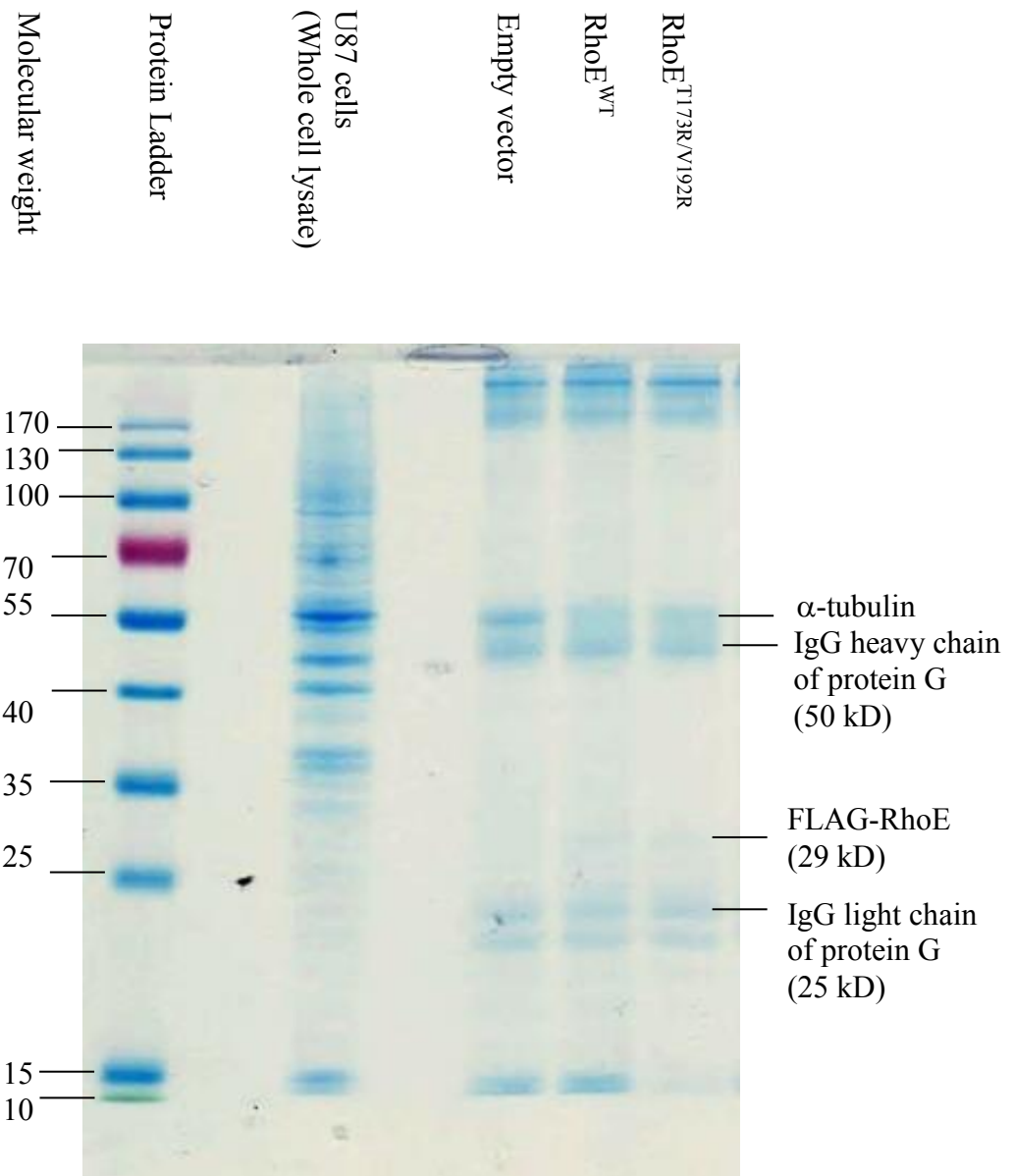


Figure 46: The immunoprecipitation of RhoE wild-type (RhoE^{WT}) and RhoE double mutants (RhoE^{T173R/V192R}) that are compared to the Empty Vector. The individual lane shows distribution of monomeric protein after 2-D separation via electrophoresis through SDS-PAGE followed by staining with Coomassie blue. The faint FLAG-RhoE band was only found in RhoE^{WT} and RhoE^{T173R/V192R} but none could be found in Empty Vector.

5.2.3.2 Manipulating Bioinformatics Tools to Identify Novel RhoE Binding Partners

The Database for Annotation Visualisation and Integrated Discovery (DAVID) is the bioinformatics software that analyses highly complex and massive volume datasets. This bioinformatics application modulates the extraction of structural features in the gene list into a more understandable biological explanation for the output gene list. DAVID was used to identify novel RhoE binding partners. It is essential to analyse of data from a huge list of genes in determining a subsequent effort in revealing high-throughput proteomic data. Moreover, bioinformatics analysis of the abundance of genomics and proteomics data offers precise values for further investigation of diverse biological mechanisms that are linked to cancer as well as other diseases (Huang et al. 2008).

On the other hand, Huang et al. (2008) suggested several characters to demonstrate a satisfactory gene list. First, a definitive value from a massive gene list is represented by functional genes or essential markers that are correlated to the investigation. For example, most of the pulled down genes during RhoE overexpression for this study were involved in diverse biological processes as listed in Table (A) and Table (B) (see Appendix 6). Second, an appropriate amount of genes appeared moderate, above hundred and below a few thousands. For instance, this study discovered 229 genes for RhoE^{WT} and 195 for RhoE^{T173R/V192R}. Third, the selection of genes typically met the statistical limit. The difference relies on the statistic comparison using *t*-test analysis, for genes expressed in the control of the experiment against the subjected cells ($p < 0.05$). In this study, the comparison was made particularly between glioma transfected with empty vector against glioma transfected with either RhoE^{WT} or RhoE^{T173R/V192R}.

In agreement, the additional characters to indicate satisfactory gene list also include the trend of overexpression or underexpression of the genes. A particular set of genes is frequently up-regulated when it takes part in the specific cellular functions. Otherwise, every functional gene should not arbitrarily appear in any available mechanism intracellularly (Huang et al. 2008). Moreover, the significant list of genes should maintain advancement and offer systematic biological input rather than vague information although the arbitrary gene list has similar extent while performing DAVID analysis (Huang et al. 2008).

A similar working group also emphasised that the lists of genes are much more valuable if several replication could be done and it must be repeatable in different batches of the experiment. By limiting the variables, an individual set of gene list will be statistically tested to create an identical gene list under the similar setting. Finally, the most important character of a satisfactory gene list should exhibit a discrete feature of a high-throughput data that can be validated. For instance, performing similar bench-work in the laboratory might be able to verify the validity of the existing data (Huang et al. 2008).

Therefore, a functional annotation chart in DAVID was used to provide the enrichment of typical gene ontology terms in this study. This tool has enabled the identification of the most relevant biological terminology associated with the gene list obtained from mass spectrometry. Then, the results of the appropriate gene cluster were functionally classified into similar biological processes or molecular functions. Table 10 and Table 11 show the satisfactory gene lists for the U87 cells transfected with RhoE^{WT} and RhoE^{T173R/V192R}.

Table 10: Functional annotation chart showing RhoE (Rnd3) and its binding partners that are clustered into molecular function (MF) and biological processes (BP) in the U87 cells transfected with pCMV5 FLAG-RhoE^{WT}

CATEGORY	SCORE	FUNCTIONAL ANNOTATION CHART
SP_PIR_KEYWORDS	50/229 (21.6%) <i>p</i> value 1.8 x10 ⁻⁹	<u>Nucleotide Binding</u> (ATP1A1, DX3Y, DDX47, GNAS, GTPBP4, NAT10, RND3, RUVBL1, RUVBL2, SMARCA5, TXK, XRCC5, XRCC6, ACTBL2, ALDH18A1, RARS, ATR, CSNK2A2, CCT3, EEF1A1, EIF5B, QARS, EPRS, HSP90AA1, HSP90B1, HNRNPU, HK1, TUBA1B, LARS, MARS, MCM5, MYO1C, NMNAT1, FARSA, PIK3CG, PRKCD, SEPT7, SEPT9, SRPR, SRPRB, ATAD3B, SNRNP200, RECQL, EIF4A, SMC1A, SMC2, SMC4, TUBB2B, VARS, VDAC2)
	16/229 (6.9%) <i>p</i> value 1.8 x10 ⁻⁷	<u>Methylation</u> (RND3, EEF1A1, FAM120A, FBL, FMR1, GAPDH, HNRNPK, HNRNPU, HIST1H2BC, HIST4H4, HIST3H3, TUBA1B, ILF3, MYO1C, NCL, SNRPD3)
	11/229 (4.8%) <i>p</i> value 5.6 x10 ⁻³	<u>GTP Binding</u> (GNAS, GTPBP4, RND3, EEF1A1, EIF5B, TUBA1B, SEPT7, SEPT9, SRPR, SRPRB, TUBB2B)
UP_SEQ_FEATURE	11/229 (4.8%) <i>p</i> value 2.6 x10 ⁻³	<u>Nucleotide phosphate-binding region: GTP</u> (GNAS, GTPBP4, RND3, EEF1A1, EIF5B, TUBA1B, SEPT7, SEPT9, SRPR, SRPRB, TUBB2B)
	4/229 (1.7%) <i>p</i> value 2.2 x10 ⁻³	<u>Lipid moiety-binding region: S-farnesyl cysteine:</u> (RND3, LMNA, LMNB, NAP1L1)
GOTERM_BP_FAT	14/229 (6.1%) <i>p</i> value 1.2x10 ⁻²	<u>Cytoskeleton organisation:</u> (RND3, CAV1, CFL1, FLNA, FMNL2, TUBA1B, EZR, KRT4, KRT6C, KRT9, MACF1, SMC1A, SDCBP, TCHH)

CATEGORY	SCORE	FUNCTIONAL ANNOTATION CHART
GOTERM_MF_FAT	59/229 (25.5%) <i>p</i> value 3.9×10^{-6}	<u>Nucleotide binding:</u> (ATP1A1, DDX3Y, DDX47, GNAS, GTPBP4, NAT10, RND3, ARHGEF5, RUVBL1, RUVBL2, SMARCA5, TXK, XRCC5, XRCC6, ACTBL2, ALDH18A1, RARS, ATR, CSNK2A2, CCT3, EEFF1A1, EIF3G, EIF5B, QARS, EPRS, GAPDH, HSP90AA1, HSP90B1, HNRNPM, HNRNPR, HNRNPU, HK1, HADHA, TUBA1B, LARS, MATR3, MARS, MCM5, MYO1C, NMNAT1, NCL, FARSA, PIK3CG, PRKCD, SEPT7, SEPT9, SRPR, SRPRB, ATAD3B, SNRNP200, RECQL, EIF4A1, SNRNP70, SMC1A, SMC2, SMC4, TUBB2B, VARS, VDAC)
	50/229 (21.6%) <i>p</i> value 1.2×10^{-5}	<u>Purine ribonucleotide binding:</u> (ATP1A1, DDX3Y, DDX47, GNAS, GTPBP4, NAT10, RND3, ARHGEF5, RUVBL1, RUVBL2, SMARCA5, TXK, XRCC5, XRCC6, ACTBL2, ALDH18A1, RARS, ATR, CSNK2A2, CCT3, EEFF1A1, EIF5B, QARS, EPRS, HSP90AA1, HSP90B1, HNRNPU, HK1, TUBA1B, LARS, MARS, MCM5, MYO1C, NMNAT1, FARSA, PIK3CG, PRKCD, SEPT7, SEPT9, SRPR, SRPRB, ATAD3B, SNRNP200, SMARCA5, EIF4A1, SMC1A, SMC2, SMC4, TUBB2B, VARS)
	50/229 (21.6%) <i>p</i> value 1.2×10^{-5}	<u>Ribonucleotide binding:</u> (ATP1A1, DDX3Y, DDX47, GNAS, GTPBP4, NAT10, RND3, ARHGEF5, RUVBL1, RUVBL2, SMARCA5, TXK, XRCC5, XRCC6, ACTBL2, ALDH18A1, RARS, ATR, CSNK2A2, CCT3, EEFF1A1, EIF5B, QARS, EPRS, HSP90AA1, HSP90B1, HNRNPU, HK1, TUBA1B, LARS, MARS, MCM5, MYO1C, NMNAT1, FARSA, PIK3CG, PRKCD, SEPT7, SEPT9, SRPR, SRPRB, ATAD3B, SNRNP200, SMARCA5, EIF4A1, SMC1A, SMC2, SMC4, TUBB2B, VARS)

CATEGORY	SCORE	FUNCTIONAL ANNOTATION CHART
GOTERM_MF_FAT	9/229 (3.9%) <i>p</i> value 1.2×10^{-2}	<u>GTPase activity:</u> (GNAS, GTPBP4, RND3, EEF1A1, EIF5B, TUBA1B, SEP9, SRPR, TUBB2B)
	12/229 (5.2%) <i>p</i> value 2×10^{-2}	<u>GTP binding:</u> (GNAS, GTPBP4, RND3, ARHGEF5, EEF1A1, EIF5B, TUBA1A, SEPT7, SEPT9, SRPR, SRPRB, TUBB2B)
	12/229 (5.2%) <i>p</i> value 2.4×10^{-2}	<u>Guanyl ribonucleotide binding:</u> (GNAS, GTPBP4, RND3, ARHGEF5, EEF1A1, EIF5B, TUBA1B, SEPT7, SEPT9, SRPR, SRPRB, TUBB2B)
	12/229 (5.2%) <i>p</i> value 2.4×10^{-2}	<u>Guanyl nucleotide binding:</u> (GNAS, GTPBP4, RND3, ARHGEF5, EEF1A1, EIF5B, TUBA1B, SEPT7, SEPT9, SRPR, SRPRB, TUBB2B)

Note:

Thirteen (13) functional annotation clusters of gene that closely interacted with RhoE by U87 cells transfected with RhoE^{WT}

Table 11: Functional annotation chart showing RhoE (Rnd3) and its binding partners that are clustered into molecular function (MF) and biological processes (BP) in U87 cells transfected with pCMV5 FLAG-RhoE^{T173R/V192R}

CATEGORY	SCORE	FUNCTIONAL ANNOTATION CHART
SP_PIR_KEYWORDS	44/195 (22.6%) <i>p</i> value 6.2×10^{-9}	<u>Nucleotide binding</u> (SNRNP35, ATAD3A, DDX1, DDX18, DDX27, DDX3Y, RECQL, RND3, ACTG2, DARS, BAZ1B, CSNK2A2, CLCN3, DCTPP1, QARS, EPRS, GBP1, HSPA1A, HSP90AA1, HNRNPU, LARS2, KARS, MARS, MTHFD1, MAST2, MCM3, MCM5, MLL, PKLR, CCT8, EIF4A1, PRKDC, SRP72, SMC1A, SMC2, SMC3, SMC4, TTN, TOP2B, TUBA1A, TUBB2C, UBE2B, VARS, VDAC2)
	8/195 (4.1%) <i>p</i> value 1.1×10^{-2}	<u>Methylation</u> (RND3, FBL, HNRNPK, HNRNPU, HIST1H2BH, HIST1H4C, NCL, PABPC1)
GOTERM_BP_FAT	16/195 (8.2%) <i>p</i> value 5.1×10^{-4}	<u>Cytoskeleton organisation</u> (RND3, CDSN, CAV1, CFL1, FLNA, FMNL2, EZR, KRT16, KRT4, KRT9, MAP1B, NOP2, SMC1A, SMC3, TTN, UBE2B)
	7/195 (3.6%) <i>p</i> value 7.3×10^{-2}	<u>Actin cytoskeleton organisation</u> (RND3, CALD1, CFL1, FLNA, FMNL2, EZR, TTN)
	7/195 (3.6%) <i>p</i> value 9.1×10^{-2}	<u>Actin filament-based process</u> (RND3, CALD1, CFL1, FLNA, FMNL2, EZR, TTN)

CATEGORY	SCORE	FUNCTIONAL ANNOTATION CHART
GOTERM_MF_FAT	55/195 (28.2%) <i>p</i> value 1.2×10^{-5}	<u>Nucleotide binding</u> (SNRNP35, ATAD3A, DDX1, DDX18, DDX27, DDX3Y, RECQL, RND3, STEAP3, ACTG2, DARS, BAZ1B, CSNK2A2, CLCN3, DCTPP1, EIF3G, QARS, EPRS, GBP1, HSPA1A, HSP90AA1, HNRNPM, HNRNPU, HADHA, LARS2, KARS, MARS, MTHFD1, MAST2, MCM3, MCM5, MLL, NCL, PARP1, PABPC1, PKLR, RPS24, CCT8, EIF4A1, PRKDC, SRP54, SFRS2B, SART3, SMC1A, SMC2, SMC3, SMC4, SYNCRIP, TTN, TOP2B, TUBA1A, TUBB2C, UBE2B, VARS, VDAC2)
	42/195 (21.5%) <i>p</i> value 9.0×10^{-4}	<u>Ribonucleotide binding</u> (SNRNP35, ATAD3A, DDX1, DDX18, DDX27, DDX3Y, RECQL, RND3, ACTG2, DARS, BAZ1B, CSNK2A2, CLCN3, QARS, EPRS, GBP1, HSPA1A, HSP90AA1, HNRNPU, LARS, KARS, MARS, MTHFD1, MAST2, MCM3, MCM5, MLL, PKLR, CCT8, EIF4A1, PRKDC, SRP54, SMC1A, SMC2, SMC3, SMC4, TTN, TOP2B, TUBA1A, TUBB2C, UBE2B, VARS)
	42/195 (21.5%) <i>p</i> value 9.0×10^{-4}	<u>Purine ribonucleotide binding</u> (SNRNP35, ATAD3A, DDX1, DDX18, DDX27, DDX3Y, RECQL, RND3, ACTG2, DARS, BAZ1B, CSNK2A2, CLCN3, QARS, EPRS, GBP1, HSPA1A, HSP90AA1, HNRNPU, LARS2, KARS, MARS, MTHFD1, MAST2, MCM3, MCM5, MLL, PKLR, CCT8, EIF4A1, PRKDC, SRP54, SMC1A, SMC2, SMC3, SMC4, TTN, TOP2B, TUBA1A, TUBB2C, UBE2B, VARS)
	43/195 (22.1%) <i>p</i> value 1.1×10^{-3}	<u>Purine nucleotide binding</u> (SNRNP35, ATAD3A, DDX1, DDX18, DDX27, DDX3Y, RECQL, RND3, STEAP3, ACTG2, DARS, BAZ1B, CSNK2A2, CLCN3, QARS, EPRS, GBP1, HSPA1A, HSP90AA1, HNRNPU, LARS2, KARS, MARS, MTHFD1, MAST2, MCM3, MCM5, MLL, PKLR, CCT8, EIF4A1, PRKDC, SRP54, SMC1A, SMC2, SMC3, SMC4, TTN, TOP2B, TUBA1A, TUBB2C, UBE2B, VARS)

Note:

Nine (9) functional annotation clusters of gene that interacted with RhoE (Rnd3) by U87 cells transfected with RhoE^{T173R/V192R}

As shown in DAVID analysis on RhoE^{WT} - Table 10 and RhoE^{T173R/V192R} - Table 11 using a functional annotation chart, it was discovered that RhoE binding partners of both constructs are clustered into several similar functions including nucleotide binding, methylation and cytoskeleton organisation. Interestingly, the genes that are clustered into nucleotide binding such as purine nucleotide or ribonucleotide are statistically enriched ($p < 0.05$). Moreover, the novel interaction of RhoE with mini-chromosomal maintenance (MCM) proteins (MCM3 and MCM5) is strong evidence that RhoE is involved in regulating the nuclear process of U87 human glioblastoma. MCM proteins are well-known as the replicative helicase that is commonly loaded onto the double stranded DNA at the replication origins.

I tried BioVenn to evaluate the overlapping genes expressed in the U87 cells transfected with RhoE^{WT} over RhoE^{T173R/V192R}. For this procedure, the large gene lists have to be classified into similar molecular functions. Manipulating the BioProfiling.de online software helps to cluster of the identical gene ontology terms into individual molecular functional profiling with the statistically enrichment scheme. This tool enables me to narrow down the selection of individual genes rather than randomly choosing the gene of interest. Figure 47 shows the result for the overlapping genes between the U87 cells transfected with RhoE^{WT} over RhoE^{T173R/V192R}. There is about 68% similarity for the functional genes in RhoE^{T173R/V192R} with the function of genes in RhoE^{WT}.

Finally, DAVID was also used in conjunction with Search Tool for Retrieval of Interacting Genes/Proteins (STRING) for this research. STRING is able to demonstrate high significant network connectivity between protein rather than setting it in random. Nevertheless, according to the data in Table 10 and 11, STRING showed unreliable

interaction between RhoE with other potential protein partners observed by DAVID, where RhoE has a frequent interaction with ROCK1 as an intermediate whilst expanding the network (results not shown). Although ROCK1 is known to have an interaction with RhoE, it was not successfully pulled down by immunoprecipitation technique. Thus, more advance research on interaction of RhoE with PKC should be done in the future as it consistently existed in the mass spectrometry data.

BioVenn
(C) 2007 - 2013 Tim Hulsen

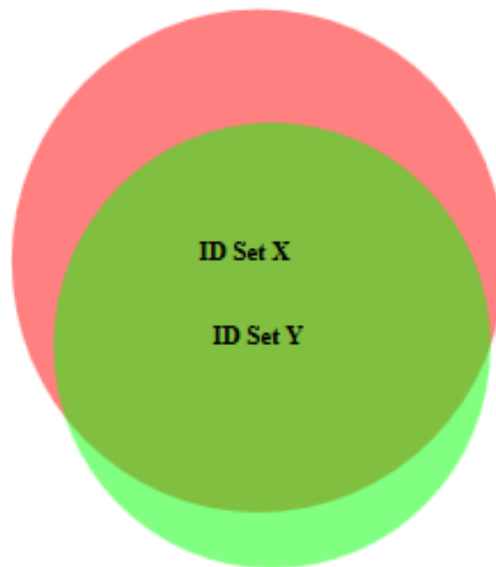


Figure 47: Bio-Ven – a web application for the comparison and visualisation of biological list using area-proportional Venn diagrams. ID Set X represents a total of 65 GO term list found in U87 cells transfected with RhoE^{WT} whereas ID Set Y represents a total of 51 GO term list found in U87 cells transfected with RhoE^{T173R/V192R}. The total overlapping between ID Set Y with ID set X is 44 GO term list. This is equals to 68% similarity shared between RhoE double mutants with the wild-type.

5.2.4 RhoE Involves in DNA Replication of U87 Glioblastoma Cells

Section 5.2.4.2 showed that RhoE interacts with nucleotide binding protein, particularly in the purine base. This result is consistent between RhoE wild-type and RhoE double mutants. Interestingly, minichromosomal maintenance proteins (MCMs) that are involved in DNA replication was found to be RhoE interacting binding partner (result was not shown). Similarly, MCMs play a critical role in the initiation of DNA synthesis and the expressions are correlated with cell proliferation as DNA replication precedes each cell division as previously described in Section 5.1.

Interestingly, MCM3 represents a glioma-associated antigen and therefore becomes a potential tumour marker for brain tumour. Söling et al. (2005) demonstrated that MCM3 is overexpressed in human with brain malignancies but it does not occur in healthy people. They have examined the immunoreaction of MCM3 via a serological test using the serum specimens from the patients with brain tumour and metastasis and comparing the specimens with the control of serum specimen from healthy people (Soling et al. 2005). Therefore, an investigation on the interaction between RhoE and MCM3 is relevant to reveal the function of RhoE in glioblastoma during DNA replication

A RhoE knockdown experiment was conducted using RNA interference approach and it used RhoE oligo A and RhoE oligo B for 48 hours. This method was previously explained in section 2.2.2.1. At the same time, a non-silencing control was used as the control of the experiment. The U87 cells were lysed in a buffer containing Nonidet P-40, and nuclear cytoplasmic fractions were prepared, separated by SDS-PAGE, and immunoblotted with the antibodies against RhoE, MCM3, and α -tubulin. Result for this experiment is shown in Figure 48, which particularly displayed only MCM3 blot.

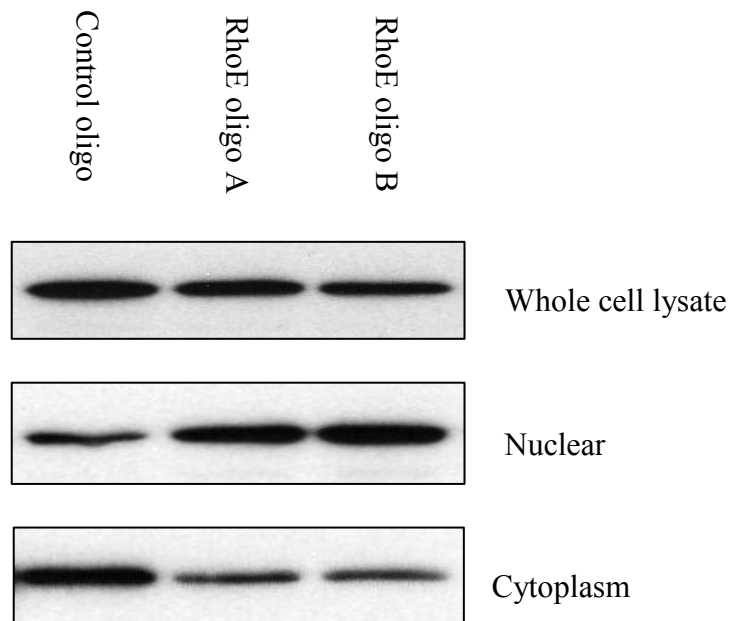
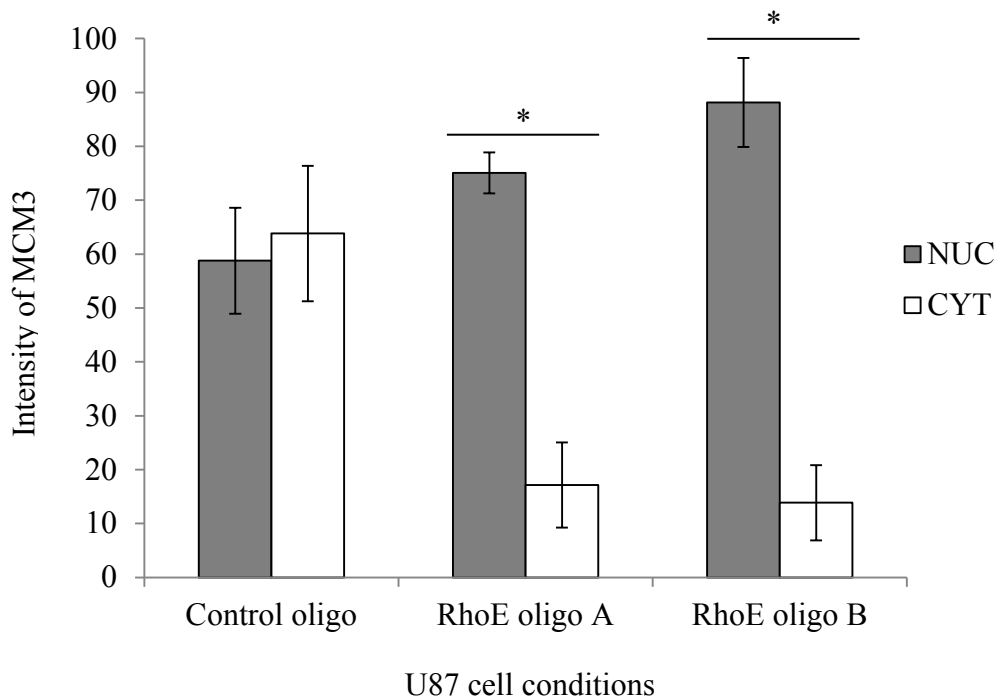


Figure 48: The immunoblots of MCM3 accumulation in U87 cells with and without the presence of RhoE. U87 cells were lysed in a buffer containing Nonidet-P 40 and nuclear. Cytoplasmic fractions were prepared, separated by SDS-PAGE, and immunoblotted with an antibody against MCM3. An effective isolation of nuclear and cytoplasmic fractions was confirmed using antibodies against Lamin A/C and α -tubulin, respectively (result not shown). These data are representative of three separate experiments ($n = 3$).

Figure 48 shows relatively more MCM3 were accumulated in the nuclear after the RhoE knockdown. The amount of MCM3 protein was decreased in cytoplasm and this was due to protein accumulation in the nucleus. Following western blot, a densitometry analysis was carried out using Image J on the MCM3 blot to evaluate the distribution of this protein between nucleus and cytoplasm with and without the presence of RhoE in the U87 cells. Figure 49 shows result on densitometry analysis of MCM3.

The intensity of MCM3 in the nuclear reached about four to six fold than in the cytoplasm in the RhoE-depleted U87 cells. The difference of intensity between nuclear and cytoplasmic MCM3 in this condition was found statistically significant ($p < 0.05$) and this is true for both oligos (RhoE oligo A and RhoE oligo B). In contrast, the MCM3 intensity between nuclear and cytoplasm in control condition (Control oligo) was not significantly different and the MCM3 proportion between both fractions (almost equal to 1.0).

MCM3 localisation was further investigated via immunostaining followed by observation under epifluorescence microscope. Figure 49 shows the result. The depletion of RhoE promotes localisation of MCM3 to the nucleus indicated by strong green fluorescence (image represented in black and white) in the nuclei of U87 cells with siRhoE using both oligoes, A and B. This observation was contradicted to the control condition when MCM3 was evenly distributed between nuclear and cytoplasm.



(*) ($p < 0.05$) ($n = 3$)

Figure 49: Densitometry analysis using Image J for the semi-quantification of the MCM3 intensity in U87 cells with and without the presence of RhoE from three separate experiments ($n = 3$). Data were statistically evaluated using Welch Two Sample t -test used for paired samples, (*) (p value < 0.05). The error bars show the standard error of the mean (S.E.M) for each datasets of three separate experiments ($n = 3$).

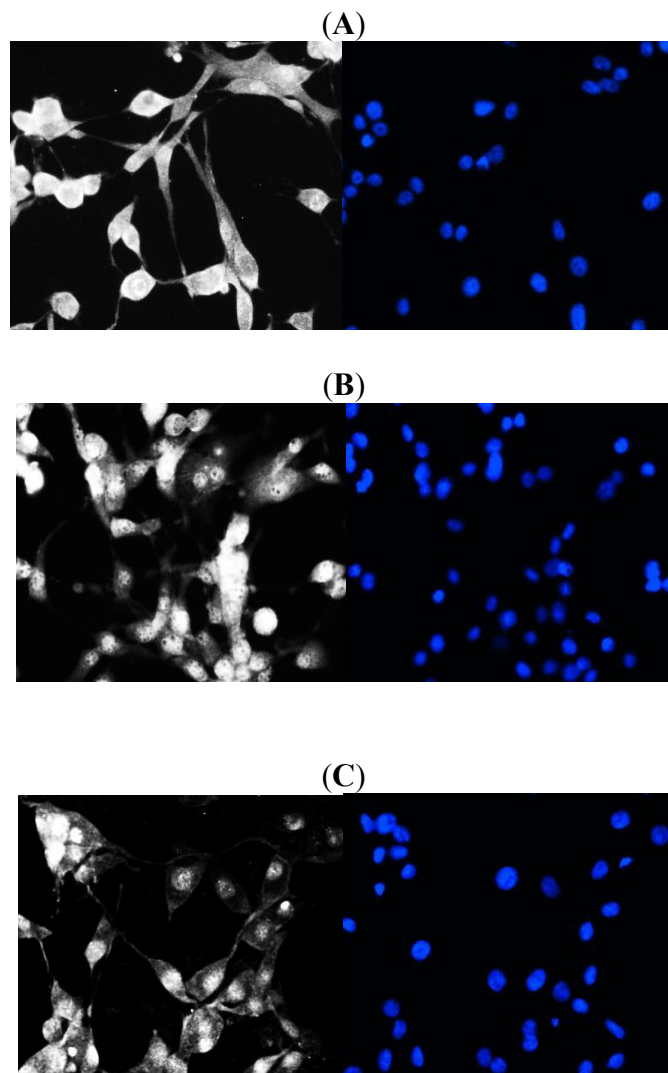


Figure 50: MCM3 is a novel interacting partner for RhoE. Depletion of RhoE promotes the localisation of MCM3 to the nucleus. (A) MCM3 in control condition; (B) MCM3 in siRhoE using RhoE oligo A; (C) MCM3 in siRhoE using oligo B. Right: Nuclear visualisation using DAPI at 300ms exposure, 40 x magnification. Left: Black and white image of MCM3 showing exact localisation of MCM3 using MCM3 antibody at 900ms exposure, 40 x magnification.

5.3 Discussion

RhoE is known to interact with ROCK1 via phosphorylation to increase its stability through its binding to the kinase domain (Sebti and Der 2003). Referring to the previous work by Komander et al. (2008), they confirmed that a high-resolution structure of RhoE in complex with the ROCK1 kinase domain was substantially found as a diverse phosphorylation site. A crystal diffraction analysis by the same working group also demonstrated that RhoE binds to ROCK1 specifically at the C-lobe of α -G helix domains. In particular, this area is adjacent to the catalytic site of ROCK1 that is located at N and C termini, but at a far distance from RhoE effector region.

Important aspect in this study was manipulating the interaction RhoE to ROCK1 in investigating the localisation of RhoE to the nucleus. Mutations of RhoE construct carried by the mammalian expression vector plasmid; pCMV5 contains the substitution of threonine 173 at β 5 strand and valine 192 at α 5 helix; both into arginine. Although, this mutant is unable to pull down ROCK1, it has maintained its ability to reorganise actin similar to the wild-type. This mutant induced substantial reduction of stress fibres thus making the cells to appear with round up phenotype. In parallel, results on F-actin staining in U87 cells demonstrated that RhoE double mutants (RhoE^{T173R/V192R}) are vulnerable to lose stress fibre. This phenotype consistently showed that ROCK1: RhoE interaction is crucial in maintaining stress fibre.

The validation of F-actin staining was made using a mutant construct, RhoE^{V56Y}. This RhoE construct has the mutation at effector site residues. There is an impact of having the

mutation in the effector region as it would possibly attenuate RhoE-mediated disorganisation of the actin cytoskeleton. However, this mutant successfully maintained stress fibres (result not shown) and known as dominant negative RhoE mutant. U87 cells transfected with pCMV5 RhoE^{V56Y} still allows interaction to ROCK1. Thus, this mutant has proven that ROCK1 is functional. ROCK1 dysfunctional by specific RhoE cascade only occur by blocking the interaction to its effector region (Komander et al. 2008).

In this study, Lipofectamine LTX Plus (Invitrogen) was used for optimal transfection of U87 cells. The manufacturer provides improved protocols with the liposome. LTX-transfected DNA enters the cell via clathrin-mediated endocytosis with both pathways assembling at the late endosome or lysosome during lipid delivery (Rejman et al. 2005). As a result, challenging cell types such as U87 cells that have morphologies quite similar to primary neural progenitor cells as well as primary fibroblasts cells have successfully gone through plasmid transfection. Moreover, this reagent offers a balance of potency and gentleness for the U87 cells, resulting in high transfection efficiencies and viabilities.

The viable count of U87 cell was determined using disposable cell counter with a tiny 16 grids that represent cell number times 10 000 per mL of the newly-split U87 cells. 10 µL out of 10 mL cell suspension pipetted onto the grid and it was observed under the light microscope. It is good to maintain the counted cell number at 300 000 cells at the beginning of the experiment. Theoretically, the consistency in applying an equal number of cells preserved potency in expressing FLAG-tagged RhoE fusion protein carried by the vector, and in this case, plasmid pCMV5 at the same expression level because the cells are sufficient. The equivalent number of the U87 cell was most likely to be adequate for the vector to incorporate the DNA of interest into the genome of the host during the transfection.

DAVID application is used to cluster the abundance of gene into a more comprehensive set of functional classification to understand the biological meaning behind the huge gene list. For instance, the high-throughput data can be collectively translated into a sophisticated biological data which are more precise into a designated gene ontology (GO) term. Then, these gene clusters are classified into excessive glossary and terminologies that demonstrate a link between “many-genes-to-many-terms” on two-dimensional (2-D) graphical perspective. As a result, any gene that is out of the list, but closely linked to the marker genes could also be retrieved.

Moreover, DAVID would make it possible to determine the potential interacting protein partners for RhoE (RND3) in regulating multiple nuclear processes in glioblastoma. DAVID tools offer analysis of the gene signature and profiling as well as related biomarkers for particular diseases. This application is also utilised for intensive search on individual domain and motif of the specific protein. Besides that, DAVID is also applied to confirm the determination for the functional group of the gene as it serves as a guide for the literature as well as adapting into the alternative gene description.

Although the protein-protein interactions analysis by DAVID was widely discussed in this section but bioinformatics analysis was also carried out using other applications such as BioProfiling and BioVenn (Antonov 2011;Hulsen et al. 2008) as well as STRING (Franceschini et al. 2013) simultaneously. Besides, this study aimed to find the potential interacting binding partners of RhoE and determining whether the interaction is either direct or indirect using DAVID, which are still uncertain at this stage. The purpose of performing

bioinformatics analysis using different application is to confirm that the results demonstrated on protein-protein interactions by DAVID is neither artefact nor retrieved by chance. On the other hand, the coverage of annotation is extended from the only GOTERM (Gene Ontology) to another annotation category including protein-protein interactions, protein functional domains, disease associations, bio-pathways, sequence features, homology, gene functional summaries and gene expression (Antonov 2011; Franceshini et al. 2013).

RhoE also involves in DNA replication of U87 cells. In this study, the investigation on the participation of MCM3 as part of replicative helicase (MCM2-7 double hexamer) is clear evidence that RhoE interaction to this nuclear protein has triggered the localisation of RhoE to the nucleus. MCM3 has important role in replication of DNA and interaction of RhoE to this protein during nucleotide binding is novel. Thus, this discovery is important because overexpression of protein complex in DNA replication can be manipulated to regulate cancer.

CHAPTER 6

CONCLUDING REMARKS AND FUTURE DIRECTIONS

6.1 Conclusion

The loss of RhoE expression in U87 human glioblastoma has decreased the number of cells entering the S-phase. On the other hand, the progression into the S-phase is promoted by the presence of RhoE. The siRhoE U87 cells were unable to incorporate BrdU, in the place of thymidine in the DNA of cycling cells during the labelling period as the S-phase entry is restricted for RhoE depleted U87 cells.

The effect of RhoE on apoptosis in U87 human glioblastoma cells was the dissociation from its cytoskeletal functions. ROCK inhibition using Y27632 could promote cell survival in U87 cells after increasing the concentration of cisplatin treatment by the indication that RhoE interacts with another protein, such as Rac1 and not exclusively ROCK1. The depletion of RhoE in U87 cells in increasing apoptosis is confirmed by the formation of cleaved caspase 3 and condensed nuclei with and without cisplatin treatment. Although Y27632 was introduced to inhibit ROCK1, the apoptosis in siRhoE U87 cells still occurred, but the cell death was independent ROCK1.

In summary, the loss of RhoE in glioma did not protect cell from apoptosis. This data contradicted the findings by Poch et al. (2007) when they repeatedly observed apoptosis in the presence of RhoE. Ryan (2010) found contrary finding when she discovered the presence of

RhoE in promoting cell death in keratinocytes. Thus, the molecular signature defines the resistant phenotype that varies between tumours and glioma responded with cisplatin resistance.

The phosphorylation sites prediction encourages earlier speculation of that higher molecular weight RhoE (29kD) in U87 cells is potentially phosphorylated which is shown in Section 4.2.1. It was discovered that more expression of RhoE in the nucleus of U87 cells in either the inhibition of ROCK1 or PKC α . This finding suggested that ROCK1 is not solely required in translocating RhoE into the nucleus. The introduction of PMA for a short duration (15 min) to the U87 cells has led to the loss of RhoE in the nucleus. The inhibition of ROCK1 prevents the loss of RhoE from the nucleus. The experiment discovered that the activation of novel PKC α by PMA has increased the upper band of RhoE (29kD) and it remains more in the nucleus compared to the active conventional PKC (Figure 36).

Although RhoE can intracellularly traverse on its own by passive diffusion due to its low molecular weight (27-29 kD), but the complex formation to the kinases might increase the size. Higher molecular weight protein is formed when RhoE complexes with the serine and threonine kinases, be either ROCK1 with 160 kD or PKC with 80 kD. Therefore, the translocation of RhoE between nucleus and cytoplasm has to be facilitated by nucleocytoplasmic transport and the available mechanism to date, which is the KPN (importin and exportin) (Tran et al. 2014). Ideally, the attempt in using Co-IP should be able to pull down the cargo proteins – Imp α , RhoE and the cargo carrier, which is Imp β . Imp α is an adaptor molecule whereas RhoE provides NLS. Then, the cargo translocated from cytoplasm to the nuclear and is assisted by carrier protein, Imp β .

Figure 41 shows the preliminary result (see Section 4.2.6) and found that U87 cells transfected with RhoE^{WT} show high affinity to Imp β . In parallel, the mass spectrometry analysis also discovered that RhoE interacts with KPNA2 – the Imp α (see Appendix 6 A). The protein-protein interaction between RhoE with Imp β is presumed to be indirect as Imp α functions as an adaptor that recognises NLS and this signal potentially exists in RhoE protein. In conclusion, KPN influences the mechanisms of nucleocytoplasmic transport of RhoE in complex with the kinases of either ROCK1 or PKC α in glioblastoma cells, via recognition of NLS.

The MCM protein is also known as the replicative helicase, which is essential during the replication of DNA and novel interaction with RhoE during nucleotide binding. This protein is believed to bring salt-stabilise complex in DNA (Samson and Bell 2013). The overexpression of protein complex involved in DNA replication origin licensing factors is known to regulate cancer (Champeris Tsaniras et al. 2014). For example, the participation of MCM proteins have been shown to efficiently deregulate the cell cycle, particularly during cancer cells development. In agreement to the statement, Riera et al. (2014) claimed that the replicative helicase (MCM2-7 double-hexamers) needs to be activated in the S-phase for the active Cdc45-MCM-GINS (CMG) helicase that surrounds the newly formed single-stranded DNA. The formation of CMG component is required to unwind the DNA to let the double helix DNA, synthesises the new DNA strands that are complementary to the two parental strands (Riera and Speck 2014).

6.2 Model Postulation on the Role of RhoE in Glioblastoma

This research aimed to analyse the role of RhoE in the nucleus as well as understanding the mechanism on how RhoE translocates into the nucleus. The manipulation of glioblastoma as a model of an abnormal living cell system has brought huge advantage as it is very difficult to treat glioblastoma (see Section 1.2). It is important to find the molecular insight through the study on protein-protein interaction in U87 cells since the preliminary experiment found that RhoE is highly expressed in the nucleus of glioma than healthy cells. The ability to tackle the abnormality of cell behaviour like glioblastoma could provide a magnitude for any deformity that is caused by other cancer cell type.

The analyses on cell cycle and apoptosis in U87 cells discovered that RhoE is a positive regulator and a tumour enhancer. The RNAi technique was used to knockdown RhoE and siRhoE has led the decrease in the number of cells entering the S-phase. It is possible to fail assembling a proper pre-replication complex as siRhoE could lead to the accumulation of MCM3 in the nucleus of U87 cells. As previously mentioned in Section 5.1, the assembly of MCM protein is essential during the DNA replication that occurs at the G₁-phase as well as at the early S-phase of cell cycle. Therefore, the deformity of MCM protein complex formation could promote the initiation of DNA replication when inappropriate multiple MCM2-7 double-hexamers are loaded in the DNA. In agreement, the inhibition of helicase loading is inspected by a licensing checkpoint. Thus, the uncontrolled proliferation in U87 human glioblastoma by control oligo might occur when lose this checkpoint, making the cell vulnerable to helicase loading (Riera et al. 2014).

In summary, this study has proposed a model of localisation of RhoE to the nucleus which is shown in Figure 51. The endogenous RhoE primarily localises to the nucleus of U87

cells. The inhibition of ROCK1 causes endogenous RhoE to accumulate in the nucleus whereas the inhibition of conventional PKC α prevents the translocation of RhoE to exit the nucleus. The inhibition of ROCK1 and PKC α block endogenous RhoE from exiting the nucleus. The activation of conventional PKC α promotes RhoE to exit the nucleus and translocates into the cytoplasm. Furthermore, the inhibition of ROCK1 followed by the activation of conventional PKC could promote RhoE to enter the cytoplasm, allowing the interaction with 14-3-3 and sequestering into the plasma membrane.

The most exciting observation in this experiment was the activation of novel PKC α by PMA exhibit an increased the upper band of RhoE (29kD) and it remains more in the nucleus consistent with the active conventional PKC during ROCK1 inhibition (Figure 36, Chapter 4). The presence of NLS in RhoE promotes the recognition by the nucleocytoplasmic transporter (Importin, Imp α/β) and directs RhoE: PKC α complex to enter the nucleus. Then, interacts with helicase loading and regulates the cell cycle. Figure 51 shows a model proposed for the localisation of RhoE to the nucleus.

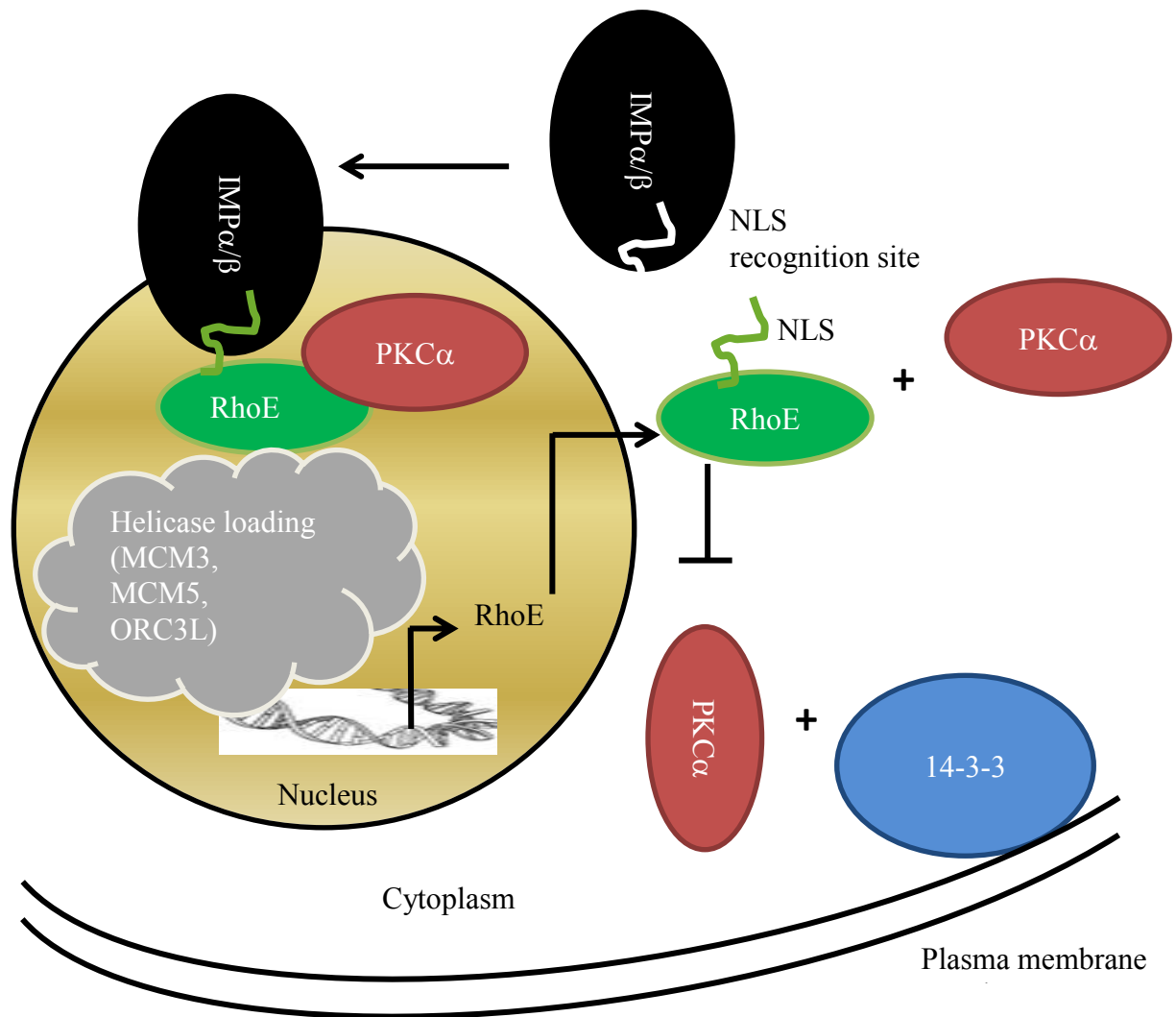


Figure 51: Model of the localisation of RhoE to the nucleus. The activation of PKC α led to increasing the upper band of RhoE (29kD) and triggered translocation of RhoE to the nucleus even though without the assistance of ROCK1. The presence of nuclear localisation signal (NLS) in RhoE promotes the recognition by the nucleocytoplasmic transporter (Importin, Imp α/β) and directs RhoE: PKC α complex to enter the nucleus, interacts with helicase loading (MCM3 and MCM5 as well as ORC3L), and regulates the cell cycle.

6.3 Suggestions for Future Work

6.3.1 Microarray Analysis of RhoE Function in U87 Human Glioblastoma Cell Line

A sophisticated genomic tool like “transcriptomic profiling” can be used to understand the relevant signalling cascade of regulatory protein at the gene level by linking the cell differentiation in the development of tissue. Besides that, Soulet et al. (2010) discovered the related molecular processes using the chicken chorioallantoic membrane (CAM) model. They implanted the tumour tissue in the CAM and successfully revealed a significant number of advanced biomarkers that were up-regulated at different time intervals as compared to the control of the experiment. Furthermore, the signalling cascades of the particular regulatory protein are also consistent with several biomarkers that were accelerated in the chick embryo model. Then, they extended the transcriptome analysis in the “wound model” using CAM, which is an alternative model for cell differentiation during tissue development.

In collaboration with Professor Falciani and S. Durant, an investigation was done on the U87 human glioblastoma cell line, which was implanted into the Chick Chorioallantoic Membrane, (CAM) to investigate tumour cell progression. The implantation of the tumour cells was done by either in control condition or after RhoE knock down that has a high potential in revealing the progression of tumour phenotypic expression in vivo by distinguishing the difference with or without the presence of RhoE. This study has prepared the mRNA samples from the implanted tumour and checked the samples over the period of time after the implantation to discover any possible signalling protein that directly or indirectly interacted with RhoE when RhoE expression is either upregulated or downregulated.

In addition, the identification of RhoE protein partners and the pathways that are involved in tissue granulation and neoangiogenesis ensured that the simulation of study for *in vitro* is consistent with the study for *in vivo*. The microarray analysis of the genes is up-regulated and down-regulated in U87 cells lines after the knock down of RhoE. The chick chorioallantoic wound model might be able to produce evidence if RhoE is one of the gene signatures for tumour markers.

6.3.2 Phosphorylation Status of RhoE

RhoE has a number of serine phosphorylation sites. The preliminary data indicate the differences in the phosphorylation status of nuclear RhoE when compared to cytoplasmic RhoE. The upper band RhoE in U87 glioblastoma cell is possibly phosphorylated and the validation was made using phosphatase enzyme to remove phosphate from 29kD RhoE. The U87 cell lysate underwent dephosphorylation by removing the phosphate groups from an organic compound via hydrolysis. Phosphatase enables the hydrolysis of phosphoric acid monoesters into a phosphate ion and a molecule with a free hydroxyl group. As a result, the hydrolysis of ATP to ADP and inorganic phosphate will release the protein to unbind with phosphate. However, the treatment of U87 cell lysate with calf intestinal phosphatase (CIP) as the main source of alkaline phosphatase (ALP) was unsuccessful. The attempt to remove upper band RhoE ended with the degradation of other proteins in U87 cell lysate. It was previously mentioned that RhoE appeared as double bands, 29 kD and 27 kD, in which 29kD is the phosphorylated form of RhoE; whereas 27kD is the non-phosphorylated form. The other application of polyacrylamide-bound Mn^{2+} -Phos-tag to SDS-PAGE was used to separate the phosphorylated proteins in the gel to make room for improvement

(Kinoshita et al. 2006). As an alternative, the analysis by mass spectrometry would be applicable to analyse the phosphorylation status of RhoE (McLachlin and Chait 2001).

6.2.4 Chromatin Immunoprecipitation (ChIP) of RhoE with DNA Helicase Protein

The accumulation of MCM3 in the nucleus during depletion of RhoE (see Section 5.2.5) has generated a fundamental knowledge on how RhoE regulates glioblastoma cells. The study on protein-DNA interaction using ChIP method for before and after the treatment with helicase loading inhibitor might offer better explanation on how RhoE could indirectly regulate DNA replication, which is consistent with the deregulation of cell cycle.

Besides that, the overexpression of MCM3 in U87 cell might also be beneficial to the study if the interaction with RhoE is direct. Instead of using pharmacological compound to inhibit DNA helicase loading, the site directed mutagenesis might be applicable to the gene encoded MCM3. It is important to consider whether to investigate either inhibition or mutation helicase loading followed by pull down MCM3 before determining the effect on RhoE interaction. It will be beneficial for future studies to investigate of ChIP as it might be able to completely remove RhoE from glioblastoma cells that bound to the chromatin.

APPENDIX 1

SEQUENCE AND ALIGNMENT OF PLASMID RhoEWT

(TRANSFECTED INTO 293T/U87 CELLS)

PLASMID pCMV5 RhoE Flag Vector (Amp^R)

CCS CSA WTK KGG GRG TYA WAT AGC AGA GCT CGT TTA
GTG AAC CGT CAG AAT TGC CAC CAT GGA CTA CAA GGA
CGA CGA TGA CAA GAA TTC GAA GGA GAG AAG AGC CAG
CCA GAA ATT ATC CAG TAA ATC TAT CAT GGA TCC TAA
TCA GAA CGT GAAATG CAA GAT AGT AGT AGT GGG CGA
CAG CCA GTG TGG GAA AAC CGC GCT GCT CCA CGT CTT
CGC CAA GGA CTG CTT CCC AGA AAA TTA CGT CCC TAC
GGT GTT TGA GAA TTA CAC TGC CAG TTT TGA AAT CGA
CAC ACA AAG AAT AGA GTT GAG CCT GTG GGA CAC TTC
AGG TTC TCC TTA CTA TGA CAA CGT CCG TCC ACT CTC
TTA CCC AGA TTC TGA TGC AGT GCT CAT TTG CTT TGA
CAT CAG TAG ACC AGA GAC TCT GGA CAG TGT CTT AAA
AAA GTG GAA AGG TGA GAT CCA GGA GTT TTG TCC CAA
TAC CAA GAT GCT GTT GGT GGG CTG CAA GTC TGA TCT
GCG GAC AGA TGT CAG CAC ATT AGT GGA ACT CTC AAA
TCA CAG GCA GAC TCC TGT GTC ATA TGA CCA GGG GGC
AAA TAT GGC CAA GCA GAT CGG AGC AGC CAC TTA CAT

AGA ATG CTC AGC TTT ACA GTC AGA AAA CAG CGT CAG
 AGA CAT TTT TCA CGT CGC CAC CTT GGC GTG TGT AAA
 TAA GAC AAA TAA AAA CGT TAA GCG GAA CAA ATC GCA
 GAG GGC CAC AAA GCG GAT TTC GCA CAT GCC TAG CAG
 ACC AGA ACT CTC AGC AGT TGC TAC GGA CTT ACG AAA
 GGA CAA AGC GAA GAG CTG TAC TGT GAT GTG AAA GCT
 TGG GTG GCA TCC CTG TGA CCC CTC CCC AGT GCC TCT
 CCT GGC CCT GGA AGT TGC CAC TCC AGT GCC CAC CAG
 CCT TGT CCT AAT AAA ATT AAG TTG CAT CAT TTT GTC
 TGA CTA GGT GTC CTT CTA TAA TAT TAT GGG GTG GAR
 GGG GGG TGG TAT GGA GCA AGG GCA AGT TGG GAA GAC
 AAC CTG TAG GGC CTG CGG GGT CTA TGG AAC AAG CTG
 GAG TGC AGT GGC ACA ATC TTG GCT CAC TGC ATC TCG
 CCT CTG GGT TCA AGC GAT CTC TGC TCA GCC TCC CGA
 GTT GTG GGA TTC CAG GCA TGC ATG ACA GCT CAG CTA
 ATT TTT GTT TTT GTA ARA CGG TTC ACG WAT TGG CAG
 CTG TCT CAT CCT ATY CAG TGA TCT ACC ACT GGC TCG
 ATG CTG ATW MGC KAA ACC AKG CTC CGT CCG TCT TCT
 GGA ATT AAG WAA YTW ATC ACC AGG A

> [ref|NM_005168.3](#) Homo sapiens Rho family GTPase 3 (RND3), mRNA
Length=2683

Score = 1068 bits (578), Expect = 0.0
Identities = 682/734 (93%), Gaps = 0/734 (0%)
Strand=Plus/Plus

```
Query 91 GAAGGAGAGAAGAGCCAGCCAGAAATTATCCAGTAAATCTATCATGGATCCTAATCAGAA 150
      |||
Sbjct 159 GAAGGAGAGAAGAGCCAGCCAGAAATTATCCAGCAAATCTATCATGGATCCTAATCAGAA 218

Query 151 CGTGAAATGCAAGATAGTAGTAGTGGGCGACAGCCAGTGTGGGAAAACCGCGCTGCTCCA 210
      |||
Sbjct 219 CGTGAAATGCAAGATAGTTGTGGTGGGAGACAGTCAGTGTGGAAAACTGCGCTGCTCCA 278

Query 211 CGTCTTCGCCAAGGACTGCTTCCCAGAAAATTACGTCCCTACGGTGTGTTGAGAATTACAC 270
      |||
Sbjct 279 TGTCTTCGCCAAGGACTGCTTCCCCGAGAATTACGTTCCCTACAGTGTGTTGAGAATTACAC 338

Query 271 TGCCAGTTTGAATCGACACACAAAGAATAGAGTTGAGCCTGTGGGACACTTCAGGTTTC 330
      |||
Sbjct 339 GGCCAGTTTGAATCGACACACAAAGAATAGAGTTGAGCCTGTGGGACACTTCGGGTTTC 398

Query 331 TCCTTACTATGACAACGTCCTCCACTCTCTTACCAGATTCTGATGCAGTGCTCATTTG 390
      |||
Sbjct 399 TCCTTACTATGACAATGTCCGCCCTCTCTTACCCTGATTCCGGATGCTGTGCTGATTTG 458

Query 391 CTTTGACATCAGTAGACCAGAGACTCTGGACAGTGTCTTAAAAAAGTGGAAAGGTGAGAT 450
      |||
Sbjct 459 CTTTGACATCAGTAGACCAGAGACCCTGGACAGTGTCTTAAAAAAGTGGAAAGGTGAAAT 518

Query 451 CCAGGAGTTTTGTCCCAATACCAAGATGCTGTGGTGGGCTGCAAGTCTGATCTGCGGAC 510
      |||
Sbjct 519 CCAGGAATTTTTGTCCCAATACCAAAATGCTCTTGGTGGGCTGCAAGTCTGATCTGCGGAC 578

Query 511 AGATGTCAGCACATTAGTGGAATCTCAATCACAGGCAGACTCCTGTGCATATGACCA 570
      |||
Sbjct 579 AGATGTTAGTACATTAGTAGAGCTCTCCAATCACAGGCAGACGCCAGTGTCTTATGACCA 638

Query 571 GGGGGCAAATATGGCCAAGCAGATCGGAGCAGCCACTTACATAGAATGCTCAGCTTTACA 630
      |||
Sbjct 639 GGGGGCAAATATGGCCAACAGATTGGAGCAGCTACTTATATCGAATGCTCAGCTTTACA 698

Query 631 GTCAGAAAACAGCGTCAGAGACATTTTTACGTCGCCACCTTGGCGTGTGTAATAAGAC 690
      |||
Sbjct 699 GTCGAAAATAGCGTCAGAGACATTTTTACGTTGCCACCTTGGCATGTGTAATAAGAC 758

Query 691 AAATAAAAACGTTAAGCGGAACAAATCGCAGAGGGCCACAAAGCGGATTTTCACACATGCC 750
      |||
Sbjct 759 AAATAAAAACGTTAAGCGGAACAAATCACAGAGAGCCACAAAGCGGATTTTCACACATGCC 818

Query 751 TAGCAGACCAGAATCTCAGCAGTTGCTACGGACTTACGAAAGGACAAAGCGAAGAGCTG 810
      |||
Sbjct 819 TAGCAGACCAGAATCTCGGCAGTTGCTACGGACTTACGAAAGGACAAAGCGAAGAGCTG 878

Query 811 TACTGTGATGTGAA 824
      |||
Sbjct 879 CACTGTGATGTGAA 892
```

ORIGIN

1 cagtcggctc ggaattggac ttgggaggcg cggtgaggag tcaggcttaa aacttgttgg
61 aggggagtaa ccagcctgct cctctcgcct tcctcctcgt ctgcgccgcg tttcagagag
121 aaaattcctg ttccaagaga aaataaggca acatcaatga aggagagaag agccagccag
181 aaattatcca gcaaatctat catggatcct aatcagaacg tgaaatgcaa gatagttgtg
241 gtgggagaca gtcagtgtgg aaaaactgcy ctgctccatg tcttcgccaa ggactgcttc
301 cccgagaatt acgttcctac agtgtttgag aattacacgg ccagttttga aatcgacaca
361 caaagaatag agttgagcct gtgggacact tcgggttctc cttactatga caatgtccgc
421 cccctctctt accctgattc ggatgctgtg ctgatttgct ttgacatcag tagaccagag
481 accctggaca gtgtcctcaa aaagtggaaa ggtgaaatcc aggaattttg tccaaatacc
541 aaaatgctct tggtcggctg caagtctgat ctgcggacag atgttagtac attagtagag
601 ctctccaatc acaggcagac gccagtgtcc tatgaccagg gggcaaatat ggccaaacag
661 attggagcag ctacttatat cgaatgctca gctttacagt cggaaaatag cgtcagagac
721 atttttcacg ttgccacctt ggcatgtgta aataagacaa ataaaaacgt taagcggaac
781 aaatcacaga gagccacaaa gcggatttca cacatgccta gcagaccaga actctcggca
841 gttgctacgg acttacgaaa ggacaaaagcg aagagctgca ctgtgatgtg aatctttcat
901 tatctttaat gaagacaaaag gaatctagtg taaaaaacia cagcaaacia aaaggtgaag
961 tctaaatgaa gtgcacagcc aaagtcatgt ataccagagg cttaggaggc gtttgagagg
1021 atactcatct ttttggaatc ctgaccttag gttcggcatg tagaccaagt gatgagaagt
1081 gaatacatgg aagagttttt aagtgtgact tgaaaaatat gccaaaaaat gagagataca
1141 aatgagctag aggaagatga ggggggatgc gactacctcc aagaagaaaa atcacactct
1201 gaatggtgct tgcatttttg ggtttttttt ttttgttata atctattcat ggatctccac
1261 tttgatttaa tttttaaatg ttttaatctc ctttcaaaa agtatacggt aatataccgt
1321 cctcaagggg gaactggcac tgtgacctta gcatttagtt ttctagagga tgtgatctaa
1381 tttctttcta gctcatcatt aaaaaggaaa ttgtatcagg acctatggga tatatccaga
1441 ggcaaacttt atgaggcttt gaaatcttgc cttcctgaag atagctgagt aggatggttc
1501 taaggaaagc ctttgcaatc ttgcaagatt tgtagaccag cactacaaag atcgcataga
1561 tcaaatagga aaaaaaatgt cgatttttat tcagtctgat ggttctgttc ttcattgtga
1621 ttgtcattaa aaagtggtaa attgctcaat gtaatatttt tgtgctgtg ttagaagttg

1681 tgtgattttt tgccatcggt gataaaaatg caaagtcaaa taaaaggtgt cttggtttga
1741 tgtcatagaa tgatccaagg agagaaaaaa ggtagttact gttttcacca gaaaaggtaa
1801 tgagtgaagg aaagaatagt agcagaaagc acagtttgtg agtaaagctg tctggaatta
1861 agttaccaa aatacaaagc aaaaggacta ttattttggg ttgaagctcc aaaactgaca
1921 gcatctgata atctgttggg ttatttcact tttcattaaa tgaacattga tgagagaaga
1981 tgccacttac ccaagcttta gagaatccct agtgaagat tatatgataa actttcagtc
2041 ctgacataac actagggcat ttctagagtg tcattgctaa aacctcactg aacagatgca
2101 gccaaggtct gtgttcagca cttggtctct gttgttacgt aaaataataa gcatttaaaa
2161 tagtttacag atatttttga ccagttcctt ttagagattc tttcagagaa gaaaccagat
2221 ctgacctggt tattgttggc gcttgttgaa aacgagcttt ctttcccatg atagtgcttc
2281 gtttttgaag tgttgaagct gtgctcccct taaatcgtgg caggagagat taaggtaatt
2341 acaacactca gttctatgtc ttacaagcac tttgtcttgt ctctgcaaga aaattcgatt
2401 ccagtcattt ccataaaat acagacattt taccaacata atatgctttg attgatgcag
2461 cattatgctt tgggcagtat tacaaaatag ctggcgagtg ctttctgtat ttaaatttg
2521 taaaaagaaa ataagttata actgttataa agcagaactt ttgttgatt ttttaaactg
2581 ttgaagtcac tgtgtatggt tgtttgtca atgtttccgc agtatttatt aaaacatact
2641 ttttttttct tcaaataaaa aagtaacctat gtctttgtct aaa

APPENDIX 2

SEQUENCE AND ALIGNMENT OF EMPTY VECTOR PLASMID (TRANSFECTED INTO 293T/U87 CELLS)

Plasmid pCMV EV Flag (KanR)

CSS CRA TKK GGG GYA TAT AGC AGA GCT GGT TTA GTG
AAC CGT CAG ATC CGC TAG CCG GAC TCA GAT CTC GAG
CTC AAG CTT GSC GCC ACC ATG GAC TAC AAG GAC GAC
GAT GAC AAG GGA TCC GGT ACC TCT AGA ATT CTG CAG
TCG ACG GTA CCG CGG GCC CGG GAT CGA TCC ACC GGA
TCT AGA TAA CTG ATC ATA ATC AGC CAT ACC ACA TTT
GTA GAG GTT TTA CTT GCT TTA AAA AAC CTC CCA CAC
CTC CCC CTG AAC CTG AAA CAT AAA ATG AAT GCA ATT
GTT GTT GTT AAC TTG TTT ATT GCA GCT TAT AAT GGT
TAC AAA TAA AGC AAT AGC ATC ACA AAT TTC ACA AAT
AAA GCA TTT TTT TCA CTG CAT TCT AGT TGT GGT TTG
TCC AAA CTC ATC AAT GTA TCT TAA CGC GTA AAT TGT
AAG CGT TAA TAT TTT GTT AAA ATT CGC GTT AAA TTT
TTG TTA AAT CAG CTC ATT TTT TAA CCA ATA GGC CGA
AAT CGG CAA AAT CCC TTA TAA ATC AAA AGA ATA GAC
CGA GAT AGG GTT GAG TGT TGT TCC AGT TTG GAA CAA

GAG TCC ACT ATT AAA GAA CGT GGA CTC CAA CGT CAA
 AGG GCG AAA AAC CGT CTA TCA GGG CGA TGG CCC ACT
 ACG TGA ACC ATC ACC CTA ATC AAG TTT TTT GGG GTC
 GAG GTG CCG TAA AGC ACT AAA TCG GAA CCC TAA AGG
 GAG CCC CCG ATT TAG AGC TTG ACG GGG AAA GCC GGC
 GAA CGT GGC GAG AAA GGA AGG GAA GAA GCG AAA GGA
 GCG GGC GCT AGG GCG CTG GCA AGT GTA GCG GTC ACG
 CTG CGC GTA ACC ACC ACA CCC GCC GCG CTT AAT GCG
 CCG CTA CAG GGC GCG TCA GTG GCA CTT TTC GGG GAA
 ATG TGC GCG GAA CCC CTA TTT GTT ATT TTT CTA ATA
 CAT TCA ATA TGT ATC CGC TCA TGA GAC ATA ACC CTG
 ATA ATG CTT CAT ATA TTG AAA AGG AGA GTC CTG AGC
 GGA AGACCA GCT GTG ATG TGT GTC AGT AGG TGT GAA
 AGT CCC AGC TCC CAG CAG CAG AGT ATG CAA GCA TGC
 ATC TCA TAG TCA GCA CAG KGK GAA GTC CCA GCT CCC
 AGC AGS MRA GTA TGC AAG CAT GCA TCT CAT TAG TMR
 CAA CAW AGT CCG CCC TA

> [gb|AF028239.1|AF028239](#) Mammalian expression vector pCMV-Script, complete sequence

Length=4278

Score = 1444 bits (744), Expect = 0.0

Identities = 786/792 (99%), Gaps = 6/792 (1%)

Strand=Plus/Plus

```
Query 191 TGATCATAATCAGCCATACCACATTTGTAGAGGTTTTACTTGCTTTAAAAAACCTCCCAC 250
      |||
Sbjct 965 TGATCATAATCAGCCATACCACATTTGTAGAGGTTTTACTTGCTTTAAAAAACCTCCCAC 1024

Query 251 ACCTCCCCTGAACCTGAAACATAAAATGAATGCAATGTTGTTGTTAACTTGTTTATTG 310
      |||
Sbjct 1025 ACCTCCCCTGAACCTGAAACATAAAATGAATGCAATGTTGTTGTTAACTTGTTTATTG 1084

Query 311 CAGCTTATAATGGTTACAAATAAAGCAATAGCATCACAAATTCACAAATAAAGCAtttt 370
      |||
Sbjct 1085 CAGCTTATAATGGTTACAAATAAAGCAATAGCATCACAAATTCACAAATAAAGCAtttt 1144

Query 371 tttCACTGCATTCTAGTTGTGGTTTGTCCAAACTCATCAATGTATCTTAACGCGTAAATT 430
      |||
Sbjct 1145 TTTCACTGCATTCTAGTTGTGGTTTGTCCAAACTCATCAATGTATCTTAACGCGTAAATT 1204

Query 431 GTAAGCGTTAATATTTTGTAAAAATTCGCGTTAAATTTTGTAAAAATCAGCTCATTTTTT 490
      |||
Sbjct 1205 GTAAGCGTTAATATTTTGTAAAAATTCGCGTTAAATTTTGTAAAAATCAGCTCATTTTTT 1264

Query 491 AACCAATAGGCCGAAATCGGCCAAAATCCCTTATAAATCAAAGAATAGACCGAGATAGGG 550
      |||
Sbjct 1265 AACCAATAGGCCGAAATCGGCCAAAATCCCTTATAAATCAAAGAATAGACCGAGATAGGG 1324

Query 551 TTGAGTGTGTTCCAGTTTGGAAACAAGAGTCCACTATTAAGAACGTGGACTCCAACGTC 610
      |||
Sbjct 1325 TTGAGTGTGTTCCAGTTTGGAAACAAGAGTCCACTATTAAGAACGTGGACTCCAACGTC 1384

Query 611 AAAGGGCGAAAAACCGTCTATCAGGGCGATGGCCACTACGTGAACCATCACCCTAATCA 670
      |||
Sbjct 1385 AAAGGGCGAAAAACCGTCTATCAGGGCGATGGCCACTACGTGAACCATCACCCTAATCA 1444

Query 671 AGTTTTTTGGGGTCGAGGTGCCGTAAAGCACTAAATCGGAACCCATAAGGGAGCCCCCGA 730
      |||
Sbjct 1445 AGTTTTTTGGGGTCGAGGTGCCGTAAAGCACTAAATCGGAACCCATAAGGGAGCCCCCGA 1504

Query 731 TTTAGAGCTTGACGGGGAAAGCCGGCGAACGTGGCGAGAAAGGAAGGAAG-AAGCGAAA 789
      |||
Sbjct 1505 TTTAGAGCTTGACGGGGAAAGCCGGCGAACGTGGCGAGAAAGGAAGGAAGAAAGCGAAA 1564

Query 790 GGAGCGGGCGCTAGGGCGCTGGCAAGTGTAGCGGTACGCTGCGCGTAACCACCACACCC 849
      |||
Sbjct 1565 GGAGCGGGCGCTAGGGCGCTGGCAAGTGTAGCGGTACGCTGCGCGTAACCACCACACCC 1624

Query 850 GCCGCGCTTAATGCGCCGCTACAGGGCGGTCA-GTGGCACTTTTCGGGGAAATGTGCGC 908
      |||
Sbjct 1625 GCCGCGCTTAATGCGCCGCTACAGGGCGGTCAAGTGGCACTTTTCGGGGAAATGTGCGC 1684

Query 909 GGAACCCCTATTTG-TTATTTTCT-AATACATTC-AATATGTATCCGCTCATGAGAC-A 964
      |||
Sbjct 1685 GGAACCCCTATTTGTTTATTTTCTAAATACATTCAAATATGTATCCGCTCATGAGACAA 1744

Query 965 TAACCCTGATAA 976
      |||
Sbjct 1745 TAACCCTGATAA 1756
```

ORIGIN

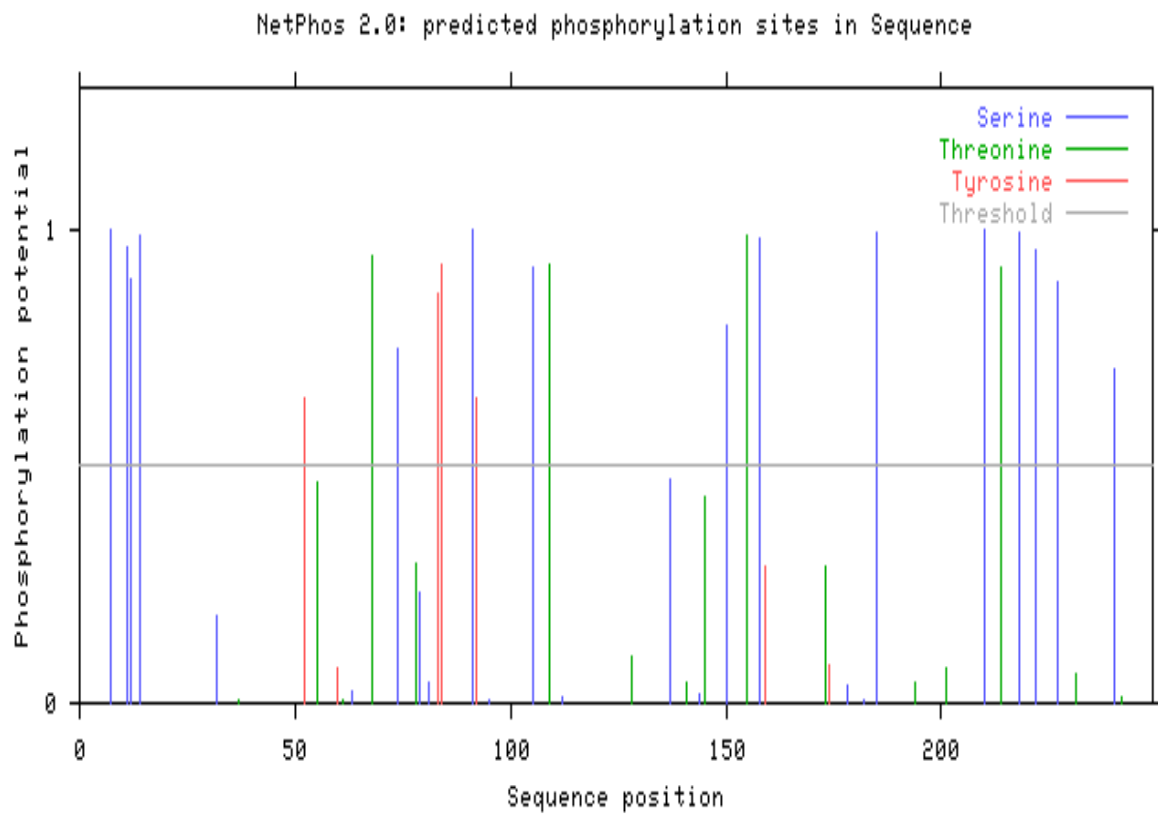
1 atgcattagt tattaatagt aatcaattac ggggtcatta gttcatagcc catatatgga
61 gttccgcggt acataactta cggtaaattg cccgcctggc tgaccgcca acgacccccg
121 ccattgacg tcaataatga cgtatgttcc catagtaacg ccaatagga ctttccattg
181 acgtcaatgg gtggagtatt tacggtaaac tgcccacttg gcagtacatc aagtgtatca
241 tatgccaagt acgcccccta ttgacgtcaa tgacggtaaa tggccccgct ggcattatgc
301 ccagtacatg accttatggg actttcctac ttggcagtac atctacgtat tagtcatcgc
361 tattaccatg gtgatgcggt tttggcagta catcaatggg cgtggatagc ggtttgactc
421 acggggattt ccaagtctcc accccattga cgtcaatggg agtttgtttt ggcacaaaa
481 tcaacgggac tttccaaaat gtcgtaacaa ctccgccccca ttgacgcaaa tgggcggtag
541 gcgtgtacgg tgggaggtct atataagcag agctggttta gtgaaccgtc agatccgcta
601 gcgattacgc caagctcgaa attaaccctc actaaaggga acaaaagctg gagctccacc
661 gcggtggcgg ccgctctagc ccgggcggat cccccgggct gcaggaattc gatatcaagc
721 ttatcgatac cgtcgacctc gagggggggc ccggtaccag gtaagtgtac ccaattcgcc
781 ctatagtgag tcgtattaca attcactcga tcgcccttcc caacagttgc gcagcctgaa
841 tggcgaatgg agatccaatt tttaagtgta taatgtgta aactactgat tctaattgtt
901 tgtgtatfff agattcacag tccaaggct catttcaggc ccctcagtcc tcacagtctg
961 ttcattgatca taatcagcca taccacattt gtagaggttt tacttgcttt aaaaaacctc
1021 ccacacctcc ccctgaacct gaaacataaa atgaatgcaa ttgttgttgt taacttgttt
1081 attgcagctt ataatggta caaataaagc aatagcatca caaatttcac aaataaagca
1141 tttttttcac tgcattctag ttgtggtttg tccaaactca tcaatgtatc ttaacgcgta
1201 aattgtaagc gttaatattt tgtaaaaatt cgcgttaaat ttttgtaaa tcagctcatt
1261 ttttaaccaa taggccgaaa toggcaaaat cccttataaa tcaaaagaat agaccgagat
1321 agggttgagt gttgttccag tttggaacaa gagtccacta ttaaagaacg tggactccaa
1381 cgtcaaaggc cgaaaaaccg tctatcaggc cgatggcca ctacgtgaac catcaccta
1441 atcaagtttt ttggggtcga ggtgccgtaa agcactaaat cggaacccta aaggagccc
1501 ccgatttaga gcttgacggg gaaagccggc gaacgtggcg agaaaggaag ggaagaaagc
1561 gaaaggagcg ggcgctaggg cgctggcaag tgtagcggtc acgctgcgcg taaccaccac
1621 acccgccgcg cttaatgcmc cgctacaggc cgcgtcaggt ggcacttttc ggggaaatgt
1681 gcgcggaacc cctatttgtt ttttttcta aatacattca aatatgtatc cgctcatgag

1741 acaataaccc tgataaatgc ttcaataata ttgaaaaag aagaatcctg aggcggaaag
1801 aaccagctgt ggaatgtgtg tcagttaggg tgtggaaagt cccagggctc cccagcaggc
1861 agaagtatgc aaagcatgca totcaattag tcagcaacca ggtgtggaaa gtccccaggc
1921 tccccagcag gcagaagtat gcaaagcatg catctcaatt agtcagcaac catagtccccg
1981 cccctaactc cgcccatccc gccctaact cgcggcagtt cgcggcattc tccgccccat
2041 ggctgactaa ttttttttat ttatgcagag gccgaggccg cctcggcctc tgagctattc
2101 cagaagtagt gaggaggctt ttttgaggc ctaggctttt gcaaagatcg atcaagagac
2161 aggatgagga tcgtttcgca tgattgaaca agatggattg cacgcaggtt ctccggccgc
2221 ttgggtggag aggctattcg gctatgactg ggcacaacag acaatcggt gctctgatgc
2281 cgccgtgttc cggctgtcag cgcagggcg cccggttctt tttgtcaaga ccgacctgtc
2341 cgggtgccctg aatgaactgc aagacgaggc agcgcggcta tcgtggctgg ccacgacggg
2401 cgttccttgc gcagctgtgc tcgacgttgt cactgaagcg ggaagggact ggctgctatt
2461 gggcgaagtg ccggggcagg atctcctgtc atctcacctt gctcctgcc agaaagtatc
2521 catcatggct gatgcaatgc ggggctgca tacgcttgat ccggctacct gccattcga
2581 ccaccaagcg aaacatcgca tcgagcgagc acgtactcgg atggaagccg gtcttgtcga
2641 tcaggatgat ctggacgaag aacatcaggg gctcgcgcca gccgaactgt tcgccaggct
2701 caaggcgagc atgcccgacg gcgaggatct cgtcgtgacc catggcgatg cctgcttgcc
2761 gaatatcatg gtggaaaatg gccgcttttc tggattcatc gactgtggcc ggctgggtgt
2821 ggcggaccgc tatcaggaca tagcgttggc taccctgat attgctgaag aacttggcgg
2881 cgaatgggct gaccgcttcc tcgtgcttta cggtatcgcc gctcccgatt cgcagcgc
2941 cgccttctat cgccttcttg acgagttctt ctgagcggga ctctggggtt cgaatgacc
3001 gaccaagcga cgcccaacct gccatcacga gatttcgatt ccaccgccgc cttctatgaa
3061 aggttgggct tcggaatcgt tttccgggac gccggctgga tgatcctcca gcgcggggat
3121 ctcatgctgg agttcttcgc ccaccctagg gggaggctaa ctgaaacacg gaaggagaca
3181 ataccggaag gaaccgcgc tatgacggca ataaaaagac agaataaac gcacggtgtt
3241 gggtcgtttg ttcataaacg cggggttcgg tcccaggct ggcactctgt cgataccca
3301 ccgagacccc attggggcca atacgcccgc gtttcttctt tttccccacc ccacccccca
3361 agttcgggtg aaggcccagg gctcgcagcc aacgtcgggg cggcaggccc tgccatagcc
3421 tcaggttact catatatact ttagattgat ttaaaacttc atttttaatt taaaaggatc
3481 taggtgaaga tcctttttga taatctcatg accaaaatcc cttaacgtga gttttcgttc

3541 cactgagcgt cagaccccggt agaaaagatc aaaggatctt cttgagatcc tttttttctg
3601 cgcgtaatct gctgcttgca aacaaaaaaaa ccaccgctac cagcgggtgtt ttgtttgccc
3661 gatcaagagc taccaactct ttttccgaag gtaactggct tcagcagagc gcagatacca
3721 aatactgtcc ttctagtgtg gccgtagtta ggccaccact tcaagaactc tgtagcaccg
3781 cctacatacc tcgctctgct aatcctgtta ccagtggctg ctgccagtgg cgataagtcg
3841 tgtcttaccg ggttggactc aagacgatag ttaccggata aggcgcagcg gtcgggctga
3901 acgggggggtt cgtgcacaca gccagcttg gagcgaacga cctacaccga actgagatac
3961 ctacagcgtg agctatgaga aagcgccacg cttcccgaag ggagaaaggc ggacaggtat
4021 ccggtaaagc gcagggctcg aacaggagag cgcacgaggg agcttccagg gggaaacgcc
4081 tggatcttt atagtctgt cgggtttcgc cacctctgac ttgagcgtcg atttttgtga
4141 tgctcgtcag gggggcggag cctatgaaa aacgccagca acgcggcctt tttacggttc
4201 ctggcctttt gctggccttt tgctcacatg ttctttcctg cgttatcccc tgattctgtg
4261 gataaccgta ttaccgcc

APPENDIX 3

PHOSPHORYLATION SITES PREDICTED IN RHOE



(A) Phosphorylation sites predicted in RhoE

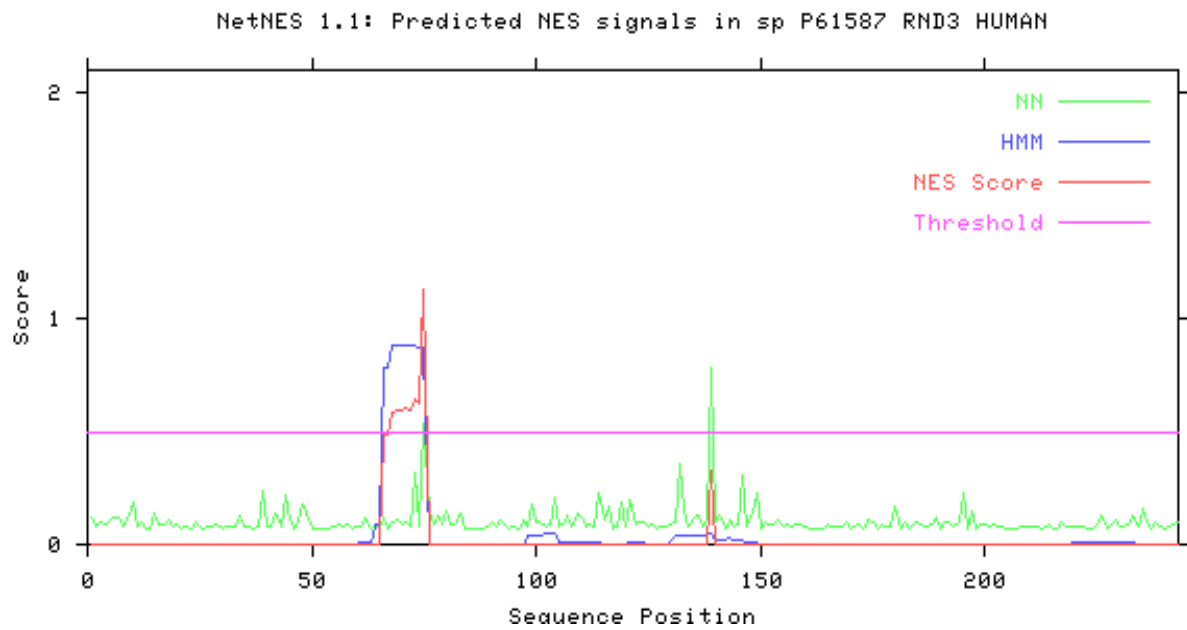
Serine predictions				
Name	Pos	Context	Score	Pred
		v		
Sequence	7	ERRASQKLS	0.998	*S*
Sequence	11	SQKLSSKSI	0.960	*S*
Sequence	12	QKLSSKSIM	0.893	*S*
Sequence	14	LSSKSIMDP	0.988	*S*
Sequence	32	VVGDSQCGK	0.185	.
Sequence	63	NYTASFEID	0.027	.
Sequence	74	RIELSLWDT	0.747	*S*
Sequence	79	LWDTSGSPY	0.230	.
Sequence	81	DTSGSPYYD	0.040	.
Sequence	91	VRELSYPDS	0.997	*S*
Sequence	95	SYPDSDAVL	0.006	.
Sequence	105	CFDISRPET	0.920	*S*
Sequence	112	ETLDSVLKK	0.012	.
Sequence	137	VGCKSDLRT	0.474	.
Sequence	144	RTDVSTLVE	0.018	.
Sequence	150	LVELSNHRQ	0.800	*S*
Sequence	158	QTPVSYDQG	0.981	*S*
Sequence	178	YIECSALQS	0.036	.
Sequence	182	SALQSENSV	0.008	.
Sequence	185	QSENSVRDI	0.996	*S*
Sequence	210	KRNKSQRAT	0.997	*S*
Sequence	218	TKRISHMPS	0.994	*S*
Sequence	222	SHMPSRPEL	0.957	*S*
Sequence	227	RPELSAVAT	0.891	*S*
Sequence	240	DKAKSCTVM	0.705	*S*
		^		
Threonine predictions				
Name	Pos	Context	Score	Pred
		v		
Sequence	37	QCGKTALLH	0.006	.
Sequence	55	NYVPTVFEN	0.469	.
Sequence	61	FENYTASFE	0.008	.
Sequence	68	FEIDTQRIE	0.946	*T*
Sequence	78	SLWDTSGSP	0.296	.
Sequence	109	SRPETLDSV	0.929	*T*
Sequence	128	FCPNTKMLL	0.096	.
Sequence	141	SDLRTDVST	0.042	.
Sequence	145	TDVSTLVEL	0.438	.
Sequence	155	NHRQTPVSY	0.985	*T*
Sequence	173	IGAATYIEC	0.288	.
Sequence	194	FHVATLACV	0.042	.
Sequence	201	CVNKTNKNV	0.076	.
Sequence	214	SQRATKRIS	0.919	*T*
Sequence	231	SAVATDLRK	0.060	.
Sequence	242	AKSCTVM--	0.010	.
		^		
Tyrosine predictions				
Name	Pos	Context	Score	Pred
		v		
Sequence	52	FPENYVPTV	0.645	*Y*
Sequence	60	VFENYTASF	0.073	.
Sequence	83	SGSPYYDNV	0.863	*Y*
Sequence	84	GSPYYDNVR	0.925	*Y*
Sequence	92	RPLSYPDSD	0.646	*Y*
Sequence	159	TPVSYDQGA	0.289	.
Sequence	174	GAATYIECS	0.081	.
		^		

(B) Phosphorylated peptide sequences in three (3) amino acids predicted in RhoE

APPENDIX 4

NUCLEAR EXPORT SIGNAL (NES) PREDICTED IN RHOE

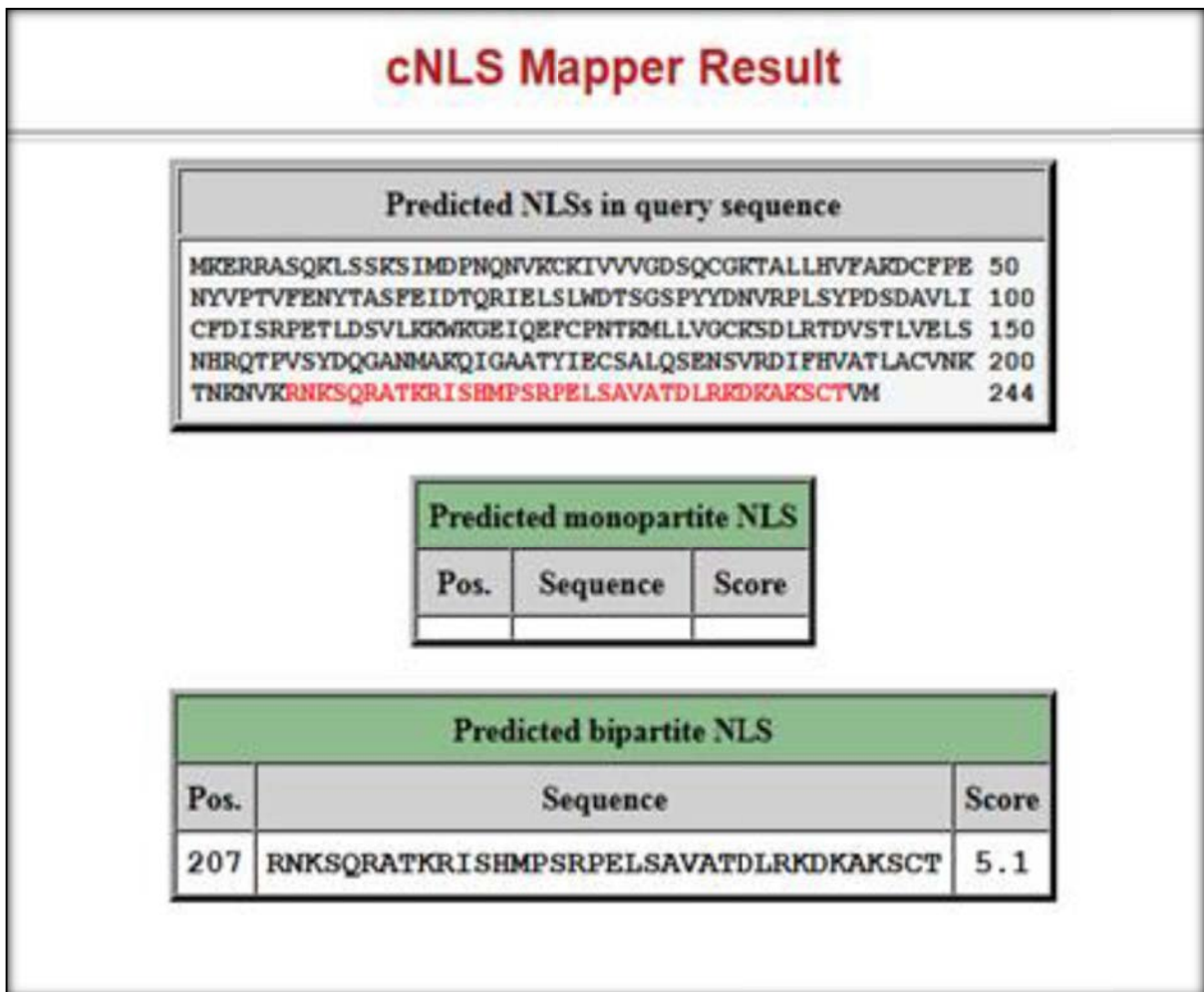
```
>sp_P61587_RND3_HUMAN - NetNES 1.1 prediction
```



sp_P61587_RND3_-68-T	0.096	0.886	0.588
sp_P61587_RND3_-69-Q	0.110	0.886	0.595
sp_P61587_RND3_-70-R	0.088	0.886	0.598
sp_P61587_RND3_-71-I	0.101	0.886	0.602
sp_P61587_RND3_-72-E	0.084	0.885	0.596
sp_P61587_RND3_-73-L	0.319	0.885	0.645
sp_P61587_RND3_-74-S	0.079	0.873	0.629
sp_P61587_RND3_-75-L	0.538	0.873	1.125

APPENDIX 5

NUCLEAR LOCALISATION SIGNAL (NLS) PREDICTED IN RHOE



207- RNKSQRATKRISHMPSRPELSAVATDLRKDKAKSCT -242

APPENDIX 6

LIST OF GENES FROM RHOE PULL DOWN ASSAY

- (A) List of genes obtained from U87 cells transfected with pCMV FLAG-RhoE^{WT}
- (B) List of genes obtained from U87 cells transfected with RhoE double mutants, pCMV
FLAG-RhoE^{T173R/V192R}

(A)

GENE CARDS	DAVID ID	GENE / PROTEIN DESCRIPTION
ACTBL2	797358	actin, beta-like 2 <i>Homo sapiens</i>
ALB	803627	albumin <i>Homo sapiens</i>
ALDH18A1	793882	aldehyde dehydrogenase 18 family, member A1 <i>Homo sapiens</i>
AP2M1	789199	adaptor-related protein complex 2, mu 1 subunit <i>Homo sapiens</i>
ARHGEF5	817871	Rho guanine nucleotide exchange factor (GEF) 5 <i>Homo sapiens</i>
ATAD3B	796501	similar to AAA-ATPase TOB3; ATPase family, AAA domain containing 3B <i>Homo sapiens</i>
ATPA1A	783032	ATPase, Na ⁺ /K ⁺ transporting, alpha 1 polypeptide <i>Homo sapiens</i>
ATR	806289	ataxia telangiectasia and Rad3 related; similar to ataxia telangiectasia and Rad3 related protein <i>Homo sapiens</i>
BAG1	798664	BCL2-associated athanogene <i>Homo sapiens</i>
C11ORF48	807064	chromosome 11 open reading frame 48 <i>Homo sapiens</i>
CAPRN1	820118	cell cycle associated protein 1 <i>Homo sapiens</i>
CAV1	798707	caveolin 1, caveolae protein, 22kDa <i>Homo sapiens</i>
CCDC47	779089	coiled-coil domain containing 47 <i>Homo sapiens</i>
CCT3	796391	chaperonin containing TCP1, subunit 3 (gamma) <i>Homo sapiens</i>
CDHR2	795714	protocadherin 24 <i>Homo sapiens</i>
CFL1	794115	cofilin 1 (non-muscle) <i>Homo sapiens</i>
CIRH1A	792420	cirrhosis, autosomal recessive 1A (cirhin) <i>Homo sapiens</i>
COL6A3	797879	collagen, type VI, alpha 3 <i>Homo sapiens</i>
COPA	787361	coatamer protein complex, subunit alpha <i>Homo sapiens</i>
COPB2	786977	coatamer protein complex, subunit beta 2 (beta prime) <i>Homo sapiens</i>
COX4NB	811425	COX4 neighbour <i>Homo sapiens</i>
CPNE5	777897	copine V <i>Homo sapiens</i>
CPT1A	783247	carnitine palmitoyltransferase 1A (liver) <i>Homo sapiens</i>
CSNK2A2	784435	casein kinase 2, alpha prime polypeptide <i>Homo sapiens</i>
CYFIP2	792857	cytoplasmic FMR1 interacting protein 2 <i>Homo sapiens</i>
DDX3Y	826174	DEAD (Asp-Glu-Ala-Asp) box polypeptide 3, Y-linked <i>Homo sapiens</i>
DDX47	808234	DEAD (Asp-Glu-Ala-Asp) box polypeptide 47 <i>Homo sapiens</i>
DNAJB11	793612	DnaJ (Hsp40) homolog, subfamily B, member 11 <i>Homo sapiens</i>
DSC1	825815	desmocollin 1 <i>Homo sapiens</i>
DSG1	802187	desmoglein 1 <i>Homo sapiens</i>
DSP	798372	desmoplakin <i>Homo sapiens</i>
EEF1A1	821677	eukaryotic translation elongation factor 1 alpha-like 7; eukaryotic translation elongation factor 1 alpha-like 3; similar to eukaryotic translation elongation factor 1 alpha 1; eukaryotic translation elongation factor 1 alpha 1 <i>Homo sapiens</i>
EEF1D	813345	eukaryotic translation elongation factor 1 delta (guanine nucleotide exchange protein) <i>Homo sapiens</i>
EEF1G	781923	eukaryotic translation elongation factor 1 gamma <i>Homo sapiens</i>
EIF2S1	815878	eukaryotic translation initiation factor 2, subunit 1 alpha, 35kDa <i>Homo sapiens</i>

GENE CARDS	DAVID ID	GENE / PROTEIN DESCRIPTION
EIF3A	795324	eukaryotic translation initiation factor 3, subunit A <i>Homo sapiens</i>
EIF3C	795748	eukaryotic translation initiation factor 3, subunit C <i>Homo sapiens</i>
EIF3E	818572	eukaryotic translation initiation factor 3, subunit E <i>Homo sapiens</i>
EIF3G	792561	eukaryotic translation initiation factor 3, subunit G <i>Homo sapiens</i>
EIF3H	788335	eukaryotic translation initiation factor 3, subunit H <i>Homo sapiens</i>
EIF3I	800360	eukaryotic translation initiation factor 3, subunit I <i>Homo sapiens</i>
EIF3J	812748	eukaryotic translation initiation factor 3, subunit J <i>Homo sapiens</i>
EIF4A1	778310	similar to eukaryotic translation initiation factor 4A; small nucleolar RNA, H/ACA box 67; eukaryotic translation initiation factor 4A, isoform 1 <i>Homo sapiens</i>
EIF5B	783097	eukaryotic translation initiation factor 5B <i>Homo sapiens</i>
EMG1	782397	EMG1 nucleolar protein homolog (S. cerevisiae) <i>Homo sapiens</i>
EPRS	788040	glutamyl-prolyl-tRNA synthetase <i>Homo sapiens</i>
ERLIN2	810009	ER lipid raft associated 2 <i>Homo sapiens</i>
EZR	816077	hypothetical protein LOC100129652; ezrin <i>Homo sapiens</i>
FAM120A	786904	family with sequence similarity 120A <i>Homo sapiens</i>
FAM98A	817972	family with sequence similarity 98, member A <i>Homo sapiens</i>
FARSA	785154	phenylalanyl-tRNA synthetase, alpha subunit <i>Homo sapiens</i>
FBL	785244	fibrillarlin <i>Homo sapiens</i>
FCGRT	821143	Fc fragment of IgG, receptor, transporter, alpha <i>Homo sapiens</i>
FLNA	786593	filamin A, alpha (actin binding protein 280) <i>Homo sapiens</i>
FMNL2	783204	formin-like 2 <i>Homo sapiens</i>
FMR1	787787	fragile X mental retardation 1 <i>Homo sapiens</i>
FNDC3B	802811	fibronectin type III domain containing 3B <i>Homo sapiens</i>
GANAB	806455	glucosidase, alpha; neutral AB <i>Homo sapiens</i>
GAPDH	801768	glyceraldehyde-3-phosphate dehydrogenase-like 6; hypothetical protein LOC100133042; glyceraldehyde-3-phosphate dehydrogenase <i>Homo sapiens</i>
GCN1L1	817738	GCN1 general control of amino-acid synthesis 1-like 1 (yeast) <i>Homo sapiens</i>
GNAS	809539	GNAS complex locus <i>Homo sapiens</i>
GTPBP4	810125	GTP binding protein 4 <i>Homo sapiens</i>
H2AFX	794356	H2A histone family, member X <i>Homo sapiens</i>
HADHA	789097	hydroxyacyl-Coenzyme A dehydrogenase/3-ketoacyl-Coenzyme A thiolase/enoyl-Coenzyme A hydratase (trifunctional protein), alpha subunit <i>Homo sapiens</i>
HIST1H2BC	820197	histone cluster 1, H2bi; histone cluster 1, H2bg; histone cluster 1, H2be; histone cluster 1, H2bf; histone cluster 1, H2bc <i>Homo sapiens</i>
HIST3H3	816461	histone cluster 3, H3 <i>Homo sapiens</i>
HIST4H4	784692	784692 histone cluster 1, H4l; histone cluster 1, H4k; histone cluster 4, H4; histone cluster 1, H4h; histone cluster 1, H4j; histone cluster 1, H4i; histone cluster 1, H4d; histone cluster 1, H4c; histone cluster 1, H4f; histone cluster 1, H4e; histone cluster 1, H4b; histone cluster 1, H4a; histone cluster 2, H4a; histone cluster 2, H4b <i>Homo sapiens</i>
HK1	777438	777438 hexokinase 1 <i>Homo sapiens</i>
HNRNPK	803294	803294 heterogeneous nuclear ribonucleoprotein K; similar to heterogeneous nuclear ribonucleoprotein K <i>Homo sapiens</i>

GENE CARDS	DAVID ID	GENE / PROTEIN DESCRIPTION
HNRNPM	791398	heterogeneous nuclear ribonucleoprotein M <i>Homo sapiens</i>
HNRNPR	822132	heterogeneous nuclear ribonucleoprotein R <i>Homo sapiens</i>
HNRNPU	817941	heterogeneous nuclear ribonucleoprotein U (scaffold attachment factor A) <i>Homo sapiens</i>
HRNR	779317	hornerin <i>Homo sapiens</i>
HSD17B4	785861	hydroxysteroid (17-beta) dehydrogenase 4 <i>Homo sapiens</i>
HSP90AA1	785761	heat shock protein 90kDa alpha (cytosolic), class A member 2; heat shock protein 90kDa alpha (cytosolic), class A member 1 <i>Homo sapiens</i>
HSP90B1	804644	heat shock protein 90kDa beta (Grp94), member 1 <i>Homo sapiens</i>
IGKV@	802175	immunoglobulin kappa variable group <i>Homo sapiens</i>
ILF3	810501	interleukin enhancer binding factor 3, 90kDa <i>Homo sapiens</i>
INTS7	809105	integrator complex subunit 7 <i>Homo sapiens</i>
IPO13	808279	importin 13 <i>Homo sapiens</i>
JUP	822268	junction plakoglobin <i>Homo sapiens</i>
KCTD10	790367	potassium channel tetramerisation domain containing 10 <i>Homo sapiens</i>
KIAA0776	810127	KIAA0776 <i>Homo sapiens</i>
KPNA2	813154	karyopherin alpha 2 (RAG cohort 1, importin alpha 1); karyopherin alpha-2 subunit like <i>Homo sapiens</i>
KPRP	773413	keratinocyte proline-rich protein <i>Homo sapiens</i>
KRT13	772288	keratin 13 <i>Homo sapiens</i>
KRT4	783234	keratin 4 <i>Homo sapiens</i>
KRT5	808801	keratin 5 <i>Homo sapiens</i>
KRT6C	815379	keratin 6C <i>Homo sapiens</i>
KRT78	784148	keratin 78 <i>Homo sapiens</i>
KRT80	814522	keratin 80 <i>Homo sapiens</i>
KRT9	811716	keratin 9 <i>Homo sapiens</i>
LARP1	813968	La ribonucleoprotein domain family, member 1 <i>Homo sapiens</i>
LARS	793517	leucyl-tRNA synthetase <i>Homo sapiens</i>
LCN1	810811	lipocalin 1-like 1; lipocalin 1 (tear prealbumin) <i>Homo sapiens</i>
LMNA	783908	lamin A/C <i>Homo sapiens</i>
LMNB2	779436	lamin B2 <i>Homo sapiens</i>
LOC100128226	782902	hypothetic protein <i>Homo sapiens</i>
LYZ	799441	lysozyme (renal amyloidosis) <i>Homo sapiens</i>
MACF1	788987	microtubule-actin crosslinking factor 1 <i>Homo sapiens</i>
MARS	818141	methionyl-tRNA synthetase <i>Homo sapiens</i>
MATR3	786723	matrin 3 <i>Homo sapiens</i>
MCM5	807548	minichromosome maintenance complex component 5 <i>Homo sapiens</i>
MRPS22	817976	mitochondrial ribosomal protein S22 <i>Homo sapiens</i>
MRPS7	804122	mitochondrial ribosomal protein S7 <i>Homo sapiens</i>
MTA1	800748	metastasis associated 1 <i>Homo sapiens</i>
MVP	801651	major vault protein <i>Homo sapiens</i>
MYO1C	795356	myosin IC <i>Homo sapiens</i>
MYOF	783835	myoferlin <i>Homo sapiens</i>

GENE CARDS	DAVID ID	GENE / PROTEIN DESCRIPTION
NACA2	820622	nascent polypeptide-associated complex alpha subunit 2 <i>Homo sapiens</i>
NAP1L1	821882	nucleosome assembly protein 1-like 1 <i>Homo sapiens</i>
NAT10	822057	N-acetyltransferase 10 (GCN5-related) <i>Homo sapiens</i>
NCAM2	795608	neural cell adhesion molecule 2 <i>Homo sapiens</i>
NCBP1	792438	nuclear cap binding protein subunit 1, 80kDa <i>Homo sapiens</i>
NCKAP1	804150	NCK-associated protein 1 <i>Homo sapiens</i>
NCL	792174	nucleolin <i>Homo sapiens</i>
NMNAT1	772256	nicotinamide nucleotide adenylyltransferase 1 <i>Homo sapiens</i>
NOL6	779120	nucleolar protein family 6 (RNA-associated) <i>Homo sapiens</i>
NOP2	821241	NOP2 nucleolar protein homolog (yeast) <i>Homo sapiens</i>
NPM3	793886	nucleophosmin/nucleoplasmin, 3 <i>Homo sapiens</i>
PAIP1	783127	poly(A) binding protein interacting protein 1; similar to poly(A) binding protein interacting protein 1 <i>Homo sapiens</i>
PARVB	825287	parvin, beta <i>Homo sapiens</i>
PCBP2	782567	poly(rC) binding protein 2 <i>Homo sapiens</i>
PGAM5	804781	phosphoglycerate mutase family member 5 <i>Homo sapiens</i>
PHB2	775357	prohibitin 2 <i>Homo sapiens</i>
PIK3CG	785330	phosphoinositide-3-kinase, catalytic, gamma polypeptide <i>Homo sapiens</i>
PML	807701	promyelocytic leukemia; similar to promyelocytic leukemia protein isoform 1 <i>Homo sapiens</i>
PRCKD	797767	protein kinase C, delta <i>Homo sapiens</i>
PRIM1	783798	primase, DNA, polypeptide 1 (49kDa) <i>Homo sapiens</i>
PRPF6	777887	similar to U5 snRNP-associated 102 kDa protein (U5-102 kDa protein); PRP6 pre-mRNA processing factor 6 homolog (<i>S. cerevisiae</i>) <i>Homo sapiens</i>
PRSS1	773661	protease, serine, 1 (trypsin 1); trypsinogen C <i>Homo sapiens</i>
PSMD2	793113	proteasome (prosome, macropain) 26S subunit, non-ATPase, 2 <i>Homo sapiens</i>
PSMD3	791833	proteasome (prosome, macropain) 26S subunit, non-ATPase, 3 <i>Homo sapiens</i>
PTPLAD1	784441	protein tyrosine phosphatase-like A domain containing 1 <i>Homo sapiens</i>
PWP2	782420	WP2 periodic tryptophan protein homolog (yeast) <i>Homo sapiens</i>
QARS	795667	glutamyl-tRNA synthetase <i>Homo sapiens</i>
RARS	819048	arginyl-tRNA synthetase <i>Homo sapiens</i>
RECQL	819070	similar to Werner syndrome protein; Werner syndrome, RecQ helicase-like <i>Homo sapiens</i>
RER1	783412	RER1 retention in endoplasmic reticulum 1 homolog (<i>S. cerevisiae</i>) <i>Homo sapiens</i>
RND3	789205	Rho family GTPase 3 <i>Homo sapiens</i>
RPL11	810885	ribosomal protein L11 <i>Homo sapiens</i>
RPL13	822027	ribosomal protein L13 pseudogene 12; ribosomal protein L13 <i>Homo sapiens</i>
RPL13A	791016	ribosomal protein L13a pseudogene 7; ribosomal protein L13a pseudogene 5; ribosomal protein L13a pseudogene 16; ribosomal protein L13a; ribosomal protein L13a pseudogene 18 <i>Homo sapiens</i>
RPL13AP25	792582	ribosomal protein L13a pseudogene 20; ribosomal protein L13a pseudogene 22; ribosomal protein L13a pseudogene 25 <i>Homo sapiens</i>

GENE CARDS	DAVID ID	GENE / PROTEIN DESCRIPTION
RPL15	779090	ribosomal protein L15 pseudogene 22; ribosomal protein L15 pseudogene 18; ribosomal protein L15 pseudogene 17; ribosomal protein L15 pseudogene 3; ribosomal protein L15 pseudogene 7; ribosomal protein L15 <i>Homo sapiens</i>
RPL18	776035	ribosomal protein L18 <i>Homo sapiens</i>
RPL18A	778688	ribosomal protein L18a pseudogene 6; ribosomal protein L18a <i>Homo sapiens</i>
RPL21	793235	ribosomal protein L21 pseudogene 134; ribosomal protein L21 pseudogene 80; ribosomal protein L21 pseudogene 20; ribosomal protein L21 pseudogene 46; ribosomal protein L21 pseudogene 45; ribosomal protein L21 pseudogene 131; ribosomal protein L21 pseudogene 16; ribosomal protein L21 pseudogene 53; ribosomal protein L21 pseudogene 120; ribosomal protein L21 pseudogene 37; ribosomal protein L21 pseudogene 93; ribosomal protein L21 pseudogene 39; ribosomal protein L21 pseudogene 29; ribosomal protein L21 pseudogene 28; ribosomal protein L21 pseudogene 14; ribosomal protein L21 pseudogene 98; ribosomal protein L21 pseudogene 105; ribosomal protein L21 pseudogene 87; ribosomal protein L21 pseudogene 128; ribosomal protein L21 pseudogene 69; ribosomal protein L21 pseudogene 97; ribosomal protein L21; ribosomal protein L21 pseudogene 119; ribosomal protein L21 pseudogene 125 <i>Homo sapiens</i>
RPL24	800698	ribosomal protein L24; ribosomal protein L24 pseudogene 6 <i>Homo sapiens</i>
RPL27	784332	ribosomal protein L27 <i>Homo sapiens</i>
RPL28	820040	ribosomal protein L28 <i>Homo sapiens</i>
RPL3	802424	ribosomal protein L3; similar to 60S ribosomal protein L3 (L4) <i>Homo sapiens</i>
RPL30	798725	ribosomal protein L30 <i>Homo sapiens</i>
RPL4	786754	ribosomal protein L4; ribosomal protein L4 pseudogene 5; ribosomal protein L4 pseudogene 4 <i>Homo sapiens</i>
RPL5	804383	ribosomal protein L5 pseudogene 34; ribosomal protein L5 pseudogene 1; ribosomal protein L5 <i>Homo sapiens</i>
RPL6	795791	ribosomal protein L6 pseudogene 27; ribosomal protein L6 pseudogene 19; ribosomal protein L6; ribosomal protein L6 pseudogene 10 <i>Homo sapiens</i>
RPL7	825605	ribosomal protein L7 pseudogene 26; ribosomal protein L7 pseudogene 16; ribosomal protein L7; ribosomal protein L7 pseudogene 32; ribosomal protein L7 pseudogene 23; ribosomal protein L7 pseudogene 24; ribosomal protein L7 pseudogene 20 <i>Homo sapiens</i>
RPL7L1	799659	ribosomal protein L7-like 1; ribosomal protein L7 pseudogene 14; ribosomal protein L7 pseudogene 21; ribosomal protein L7 pseudogene 22; ribosomal protein L7 pseudogene 46 <i>Homo sapiens</i>
RPL8	801125	ribosomal protein L8; ribosomal protein L8 pseudogene 2 <i>Homo sapiens</i>
RPLP0	796227	ribosomal protein, large, P0 pseudogene 2; ribosomal protein, large, P0 pseudogene 3; ribosomal protein, large, P0 pseudogene 6; ribosomal protein, large, P0 <i>Homo sapiens</i>
RPN2	791634	ribophorin II <i>Homo sapiens</i>
RPS12	800729	ribosomal protein S12; ribosomal protein S12 pseudogene 4; ribosomal protein S12 pseudogene 11; ribosomal protein S12 pseudogene 9 <i>Homo sapiens</i>
RPS14	817032	ribosomal protein S14 <i>Homo sapiens</i>

GENE CARDS	DAVID ID	GENE / PROTEIN DESCRIPTION
RPS15A	788428	ribosomal protein S15a pseudogene 17; ribosomal protein S15a pseudogene 19; ribosomal protein S15a pseudogene 12; ribosomal protein S15a pseudogene 24; ribosomal protein S15a pseudogene 11; ribosomal protein S15a <i>Homo sapiens</i>
RPS16	790706	ribosomal protein S16 pseudogene 1; ribosomal protein S16 pseudogene 10; ribosomal protein S16 <i>Homo sapiens</i>
RPS17	805465	ribosomal protein S17 <i>Homo sapiens</i>
RPS2	776216	ribosomal protein S2 pseudogene 8; ribosomal protein S2 pseudogene 11; ribosomal protein S2 pseudogene 5; ribosomal protein S2 pseudogene 12; ribosomal protein S2 pseudogene 51; ribosomal protein S2 pseudogene 17; ribosomal protein S2 pseudogene 55; ribosomal protein S2 pseudogene 20; ribosomal protein S2 <i>Homo sapiens</i>
RPS20	781689	ribosomal protein S20 <i>Homo sapiens</i>
RPS23	801872	ribosomal protein S23 <i>Homo sapiens</i>
RPS26	772335	ribosomal protein S26 pseudogene 38; ribosomal protein S26 pseudogene 39; ribosomal protein S26 pseudogene 35; ribosomal protein S26 pseudogene 31; ribosomal protein S26 pseudogene 20; ribosomal protein S26 pseudogene 54; ribosomal protein S26 pseudogene 2; ribosomal protein S26 pseudogene 53; ribosomal protein S26 pseudogene 25; ribosomal protein S26 pseudogene 50; ribosomal protein S26 pseudogene 6; ribosomal protein S26 pseudogene 8; ribosomal protein S26 <i>Homo sapiens</i>
RPS27	789083	ribosomal protein S27 pseudogene 29; ribosomal protein S27 pseudogene 9; ribosomal protein S27 pseudogene 23; ribosomal protein S27 pseudogene 13; ribosomal protein S27; ribosomal protein S27 pseudogene 21; ribosomal protein S27 pseudogene 7; ribosomal protein S27 pseudogene 6; ribosomal protein S27 pseudogene 19 <i>Homo sapiens</i>
RPS27L	783803	ribosomal protein S27-like <i>Homo sapiens</i>
RPS3	816191	ribosomal protein S3 pseudogene 3; ribosomal protein S3 <i>Homo sapiens</i>
RPS3A	789968	ribosomal protein S3A pseudogene 5; ribosomal protein S3a pseudogene 47; ribosomal protein S3a pseudogene 49; ribosomal protein S3A; hypothetical LOC100131699; hypothetical LOC100130107 <i>Homo sapiens</i>
RPS4X	791681	ribosomal protein S4X pseudogene 6; ribosomal protein S4X pseudogene 13; ribosomal protein S4, X-linked <i>Homo sapiens</i>
RPS6	808508	ribosomal protein S6 pseudogene 25; ribosomal protein S6; ribosomal protein S6 pseudogene 1 <i>Homo sapiens</i>
RPS7	773042	ribosomal protein S7; ribosomal protein S7 pseudogene 11; ribosomal protein S7 pseudogene 4; ribosomal protein S7 pseudogene 10 <i>Homo sapiens</i>
RPS9	798227	ribosomal protein S9; ribosomal protein S9 pseudogene 4 <i>Homo sapiens</i>
RRBP1	822623	ribosome binding protein 1 homolog 180kDa (dog) <i>Homo sapiens</i>
RSL1D1	781114	ribosomal L1 domain containing 1 <i>Homo sapiens</i>
RUVBL1	784165	RuvB-like 1 (E. coli) <i>Homo sapiens</i>
RUVBL2	813593	RuvB-like 2 (E. coli) <i>Homo sapiens</i>
SDCBP	799644	syndecan binding protein (syntenin) <i>Homo sapiens</i>
SEPT7	807411	septin 7 <i>Homo sapiens</i>
SEPT9	797163	septin 9 <i>Homo sapiens</i>
SF3B1	819770	splicing factor 3b, subunit 1, 155kDa <i>Homo sapiens</i>
SLC25A1	797071	solute carrier family 25 (mitochondrial carrier; citrate transporter), member 1 <i>Homo sapiens</i>

GENE CARDS	DAVID ID	GENE / PROTEIN DESCRIPTION
SLC25A11	802706	solute carrier family 25 (mitochondrial carrier; oxoglutarate carrier), member 11 <i>Homo sapiens</i>
SLC25A13	810512	solute carrier family 25, member 13 (citrin) <i>Homo sapiens</i>
SLC25A3	791524	solute carrier family 25 (mitochondrial carrier; phosphate carrier), member 3 <i>Homo sapiens</i>
SLC25A6	823629	solute carrier family 25 (mitochondrial carrier; adenine nucleotide translocator), member 6 <i>Homo sapiens</i>
SMARCA5	789548	SWI/SNF related, matrix associated, actin dependent regulator of chromatin, subfamily a, member 5 <i>Homo sapiens</i>
SMC1A	794773	structural maintenance of chromosomes 1A <i>Homo sapiens</i>
SMC2	798960	structural maintenance of chromosomes 2 <i>Homo sapiens</i>
SMC4	781161	structural maintenance of chromosomes 4 <i>Homo sapiens</i>
SMN1	773640	survival of motor neuron 1, telomeric; survival of motor neuron 2, centromeric <i>Homo sapiens</i>
SNRNP200	778808	similar to U5 snRNP-specific protein, 200 kDa; small nuclear ribonucleoprotein 200kDa (U5) <i>Homo sapiens</i>
SNRNP40	778964	small nuclear ribonucleoprotein 40kDa (U5) <i>Homo sapiens</i>
SNRNP70	777820	small nuclear ribonucleoprotein 70kDa (U1) <i>Homo sapiens</i>
SNRPD3	822931	small nuclear ribonucleoprotein D3 polypeptide 18kDa <i>Homo sapiens</i>
SPTBN1	802976	spectrin, beta, non-erythrocytic 1 <i>Homo sapiens</i>
SRPR	804747	signal recognition particle receptor (docking protein) <i>Homo sapiens</i>
SRPRB	826428	signal recognition particle receptor, B subunit <i>Homo sapiens</i>
SV2A	820568	synaptic vesicle glycoprotein 2A <i>Homo sapiens</i>
TBL2	798215	transducin (beta)-like 2 <i>Homo sapiens</i>
TCHH	793911	trichohyalin <i>Homo sapiens</i>
TECR	800114	glycoprotein, synaptic 2 <i>Homo sapiens</i>
TMEM109	822806	transmembrane protein 109 <i>Homo sapiens</i>
TMEM111	775532	transmembrane protein 111 <i>Homo sapiens</i>
TMEM214	775800	transmembrane protein 214 <i>Homo sapiens</i>
TSR1	801920	TSR1, 20S rRNA accumulation, homolog (<i>S. cerevisiae</i>) <i>Homo sapiens</i>
TUBA1B	802675	hypothetical gene supported by AF081484; NM_006082; tubulin, alpha 1b <i>Homo sapiens</i>
TUBB2B	799226	tubulin, beta 2B <i>Homo sapiens</i>
TXK	810008	TXK tyrosine kinase <i>Homo sapiens</i>
TXN	799188	thioredoxin <i>Homo sapiens</i>
UTP15	791589	UTP15, U3 small nucleolar ribonucleoprotein, homolog (<i>S. cerevisiae</i>) <i>Homo sapiens</i>
VARS	785609	valyl-tRNA synthetase <i>Homo sapiens</i>
VDAC1	798048	voltage-dependent anion channel 1; similar to voltage-dependent anion channel 1 <i>Homo sapiens</i>
VDAC2	785721	voltage-dependent anion channel 2 <i>Homo sapiens</i>
VIM	814359	vimentin <i>Homo sapiens</i>
WDR3	811278	WD repeat domain 3 <i>Homo sapiens</i>
XRCC5	809635	X-ray repair complementing defective repair in Chinese hamster cells 5 (double-strand-break rejoining) <i>Homo sapiens</i>

GENE CARDS	DAVID ID	GENE / PROTEIN DESCRIPTION
XRCC6	781592	X-ray repair complementing defective repair in Chinese hamster cells 6; similar to ATP-dependent DNA helicase II, 70 kDa subunit <i>Homo sapiens</i>
YWHAB	797325	tyrosine 3-monooxygenase/tryptophan 5-monooxygenase activation protein, beta polypeptide <i>Homo sapiens</i>
YWHAD	795546	tyrosine 3-monooxygenase/tryptophan 5-monooxygenase activation protein, delta polypeptide <i>Homo sapiens</i>
YWHAG	815903	tyrosine 3-monooxygenase/tryptophan 5-monooxygenase activation protein, gamma polypeptide <i>Homo sapiens</i>
YWHAQ	820893	tyrosine 3-monooxygenase/tryptophan 5-monooxygenase activation protein, theta polypeptide <i>Homo sapiens</i>
ZNF234	786428	zinc finger protein 234 <i>Homo sapiens</i>
ZNF622	787986	zinc finger protein 622 <i>Homo sapiens</i>

Note: Total of 229 genes recognised by DAVID

(B)

GENE CARDS	DAVID ID	GENE / PROTEIN DESCRIPTION
ABRA	811529	actin-binding Rho activating protein <i>Homo sapiens</i>
ACTG2	777533	actin, gamma 2, smooth muscle, enteric <i>Homo sapiens</i>
ALB	803627	albumin <i>Homo sapiens</i>
ANXA2	787053	annexin A2 pseudogene 3; annexin A2; annexin A2 pseudogene 1 <i>Homo sapiens</i>
AP2A1	797086	adaptor-related protein complex 2, alpha 1 subunit <i>Homo sapiens</i>
AP2M1	789199	adaptor-related protein complex 2, mu 1 subunit <i>Homo sapiens</i>
ATAD3A	799038	ATPase family, AAA domain containing 3A <i>Homo sapiens</i>
AZGP1	783250	alpha-2-glycoprotein 1, zinc-binding pseudogene 1; alpha-2-glycoprotein 1, zinc-binding <i>Homo sapiens</i>
BAZ1B	803680	bromodomain adjacent to zinc finger domain, 1B <i>Homo sapiens</i>
CALD1	799368	caldesmon 1 <i>Homo sapiens</i>
CAV1	798707	caveolin 1, caveolae protein, 22kDa <i>Homo sapiens</i>
CCDC47	779089	coiled-coil domain containing 47 <i>Homo sapiens</i>
CCT8	821074	similar to chaperonin containing TCP1, subunit 8 (theta); chaperonin containing TCP1, subunit 8 (theta) <i>Homo sapiens</i>
CDSN	795934	corneodesmosin <i>Homo sapiens</i>
CFL1	794115	cofilin 1 (non-muscle) <i>Homo sapiens</i>
CLCN3	784073	chloride channel 3 <i>Homo sapiens</i>
COL6A3	797879	collagen, type VI, alpha 3 <i>Homo sapiens</i>
COPA	787361	coatomer protein complex, subunit alpha <i>Homo sapiens</i>
CPNE5	777897	copine V <i>Homo sapiens</i>
CPT1A	783247	carnitine palmitoyltransferase 1A (liver) <i>Homo sapiens</i>
CSNK2A2	784435	casein kinase 2, alpha prime polypeptide <i>Homo sapiens</i>
DARS	778056	aspartyl-tRNA synthetase <i>Homo sapiens</i>
DCTPP1	776934	dCTP pyrophosphatase 1 <i>Homo sapiens</i>
DDX1	787752	DEAD (Asp-Glu-Ala-Asp) box polypeptide 1 <i>Homo sapiens</i>
DDX18	775239	DEAD (Asp-Glu-Ala-Asp) box polypeptide 18 <i>Homo sapiens</i>
DDX27	806668	DEAD (Asp-Glu-Ala-Asp) box polypeptide 27 <i>Homo sapiens</i>
DDX3Y	826174	DEAD (Asp-Glu-Ala-Asp) box polypeptide 3, Y-linked <i>Homo sapiens</i>
DFFA	815701	DNA fragmentation factor, 45kDa, alpha polypeptide <i>Homo sapiens</i>
DFFB	822769	DNA fragmentation factor, 40kDa, beta polypeptide (caspase-activated DNase) <i>Homo sapiens</i>
DMBT1	803041	deleted in malignant brain tumors 1 <i>Homo sapiens</i>
DNAJB11	793612	DnaJ (Hsp40) homolog, subfamily B, member 11 <i>Homo sapiens</i>
DSC1	825815	desmocollin 1 <i>Homo sapiens</i>
DSG1	802187	desmoglein 1 <i>Homo sapiens</i>
DSP	798372	desmoplakin <i>Homo sapiens</i>

GENE CARDS	DAVID ID	GENE / PROTEIN DESCRIPTION
EEF1D	813345	eukaryotic translation elongation factor 1 delta (guanine nucleotide exchange protein) <i>Homo sapiens</i>
EEF1G	781923	eukaryotic translation elongation factor 1 gamma <i>Homo sapiens</i>
EIF2S1	815878	eukaryotic translation initiation factor 2, subunit 1 alpha, 35kDa <i>Homo sapiens</i>
EIF3CL	787931	eukaryotic translation initiation factor 3, subunit C-like <i>Homo sapiens</i>
EIF3E	818572	eukaryotic translation initiation factor 3, subunit E <i>Homo sapiens</i>
EIF3F	803358	eukaryotic translation initiation factor 3, subunit F; similar to hCG2040283 <i>Homo sapiens</i>
EIF3G	792561	eukaryotic translation initiation factor 3, subunit G <i>Homo sapiens</i>
EIF3H	788335	eukaryotic translation initiation factor 3, subunit H <i>Homo sapiens</i>
EIF3M	798064	eukaryotic translation initiation factor 3, subunit M <i>Homo sapiens</i>
EIF4A1	778310	similar to eukaryotic translation initiation factor 4A; small nucleolar RNA, H/ACA box 67; eukaryotic translation initiation factor 4A, isoform 1 <i>Homo sapiens</i>
EPRS	788040	glutamyl-prolyl-tRNA synthetase <i>Homo sapiens</i>
ERLIN2	810009	ER lipid raft associated 2 <i>Homo sapiens</i>
EZR	816077	hypothetical protein LOC100129652; ezrin <i>Homo sapiens</i>
FBL	785244	fibrillarlin <i>Homo sapiens</i>
FHAD1	774513	forkhead-associated (FHA) phosphopeptide binding domain 1 <i>Homo sapiens</i>
FLNA	786593	filamin A, alpha (actin binding protein 280) <i>Homo sapiens</i>
FMNL2	783204	formin-like 2 <i>Homo sapiens</i>
FTL	793494	similar to ferritin, light polypeptide; ferritin, light polypeptide <i>Homo sapiens</i>
GBP1	783739	guanylate binding protein 1, interferon-inducible, 67kDa <i>Homo sapiens</i>
GCN1L1	817738	GCN1 general control of amino-acid synthesis 1-like 1 (yeast) <i>Homo sapiens</i>
GFPT2	810770	glutamine-fructose-6-phosphate transaminase 2 <i>Homo sapiens</i>
GNB2L1	793354	guanine nucleotide binding protein (G protein), beta polypeptide 2-like 1 <i>Homo sapiens</i>
GOLGA2	774455	golgi autoantigen, golgin subfamily a, 2 <i>Homo sapiens</i>
GRP	782874	gastrin-releasing peptide <i>Homo sapiens</i>
HADHA	789097	hydroxyacyl-Coenzyme A dehydrogenase/3-ketoacyl-Coenzyme A thiolase/enoyl-Coenzyme A hydratase (trifunctional protein), alpha subunit <i>Homo sapiens</i>
HDLBP	810749	high density lipoprotein binding protein <i>Homo sapiens</i>
HIST1H2BH	821062	histone cluster 1, H2bh <i>Homo sapiens</i>
HIST1H4C	784692	histone cluster 1, H4l; histone cluster 1, H4k; histone cluster 4, H4; histone cluster 1, H4h; histone cluster 1, H4j; histone cluster 1, H4i; histone cluster 1, H4d; histone cluster 1, H4c; histone cluster 1, H4f; histone cluster 1, H4e; histone cluster 1, H4b; histone cluster 1, H4a; histone cluster 2, H4a; histone cluster 2, H4b <i>Homo sapiens</i>
HNP1	787589	Hypertensive nephropathy <i>Homo sapiens</i>
HNRNPK	803294	heterogeneous nuclear ribonucleoprotein K; similar to heterogeneous nuclear ribonucleoprotein K <i>Homo sapiens</i>

GENE CARDS	DAVID ID	GENE / PROTEIN DESCRIPTION
HNRNPM	791398	heterogeneous nuclear ribonucleoprotein M <i>Homo sapiens</i>
HNRNPU	817941	heterogeneous nuclear ribonucleoprotein U (scaffold attachment factor A) <i>Homo sapiens</i>
HRNR	779317	hornerin <i>Homo sapiens</i>
HSP90AA1	785761	heat shock protein 90kDa alpha (cytosolic), class A member 2; heat shock protein 90kDa alpha (cytosolic), class A member 1 <i>Homo sapiens</i>
HSPA1A	775531	heat shock 70kDa protein 1A; heat shock 70kDa protein 1B <i>Homo sapiens</i>
IFI16	824993	interferon, gamma-inducible protein 16 <i>Homo sapiens</i>
IGHA1	824622	immunoglobulin heavy constant alpha 1 <i>Homo sapiens</i>
IMMT	772458	inner membrane protein, mitochondrial (mitofilin) <i>Homo sapiens</i>
KARS	785252	lysyl-tRNA synthetase <i>Homo sapiens</i>
KCTD10	790367	potassium channel tetramerisation domain containing 10 <i>Homo sapiens</i>
KIAA0090	825863	KIAA0090 <i>Homo sapiens</i>
KRT13	772288	keratin 13 <i>Homo sapiens</i>
KRT16	799223	keratin 16; keratin type 16-like <i>Homo sapiens</i>
KRT17	813039	keratin 17; keratin 17 pseudogene 3 <i>Homo sapiens</i>
KRT24	783507	keratin 24 <i>Homo sapiens</i>
KRT4	783234	keratin 4 <i>Homo sapiens</i>
KRT5	808801	keratin 5 <i>Homo sapiens</i>
KRT78	784148	keratin 78 <i>Homo sapiens</i>
KRT9	811716	keratin 9 <i>Homo sapiens</i>
KTN1	811040	kinectin 1 (kinesin receptor) <i>Homo sapiens</i>
LACRT	774749	lacritin <i>Homo sapiens</i>
LARS2	787847	leucyl-tRNA synthetase 2, mitochondrial <i>Homo sapiens</i>
LIMS1	786366	LIM and senescent cell antigen-like domains 1 <i>Homo sapiens</i>
LOC390714	790711	similar to Ig heavy chain V-III region VH26 precursor <i>Homo sapiens</i>
LOC391405	789246	similar to Ig kappa chain V-I region Walker precursor <i>Homo sapiens</i>
LTF	817740	lactotransferrin <i>Homo sapiens</i>
LYZ	799441	lysozyme (renal amyloidosis) <i>Homo sapiens</i>
MAP1B	785288	microtubule-associated protein 1B <i>Homo sapiens</i>
MARS	818141	methionyl-tRNA synthetase <i>Homo sapiens</i>
MAST2	798950	microtubule associated serine/threonine kinase 2 <i>Homo sapiens</i>
MCM3	815420	minichromosome maintenance complex component 3 <i>Homo sapiens</i>
MCM5	807548	minichromosome maintenance complex component 5 <i>Homo sapiens</i>
MLL	800385	myeloid/lymphoid or mixed-lineage leukemia (trithorax homolog, <i>Drosophila</i>) <i>Homo sapiens</i>
MPO	807542	myeloperoxidase <i>Homo sapiens</i>
MRPS22	817976	mitochondrial ribosomal protein S22 <i>Homo sapiens</i>
MRPS26	780064	mitochondrial ribosomal protein S26 <i>Homo sapiens</i>
MTHFD1	784198	methylenetetrahydrofolate dehydrogenase (NADP+ dependent) 1, methenyltetrahydrofolate cyclohydrolase, formyltetrahydrofolate synthetase <i>Homo sapiens</i>
MYBBP1A	805661	MYB binding protein (P160) 1a <i>Homo sapiens</i>

GENE CARDS	DAVID ID	GENE / PROTEIN DESCRIPTION
NCL	792174	nucleolin <i>Homo sapiens</i>
NOL6	779120	nucleolar protein family 6 (RNA-associated) <i>Homo sapiens</i>
NOP2	821241	NOP2 nucleolar protein homolog (yeast) <i>Homo sapiens</i>
NPM1	810988	nucleophosmin 1 (nucleolar phosphoprotein B23, numatrin) pseudogene 21; hypothetical LOC100131044; similar to nucleophosmin 1; nucleophosmin (nucleolar phosphoprotein B23, numatrin) <i>Homo sapiens</i>
PABPC1	788561	poly(A) binding protein, cytoplasmic pseudogene 5; poly(A) binding protein, cytoplasmic 1 <i>Homo sapiens</i>
PAIP1	783127	poly(A) binding protein interacting protein 1; similar to poly(A) binding protein interacting protein 1 <i>Homo sapiens</i>
PARP1	806958	poly (ADP-ribose) polymerase 1 <i>Homo sapiens</i>
PCBP2	782567	poly(rC) binding protein 2 <i>Homo sapiens</i>
PDIA5	795227	protein disulfide isomerase family A, member 5 <i>Homo sapiens</i>
PGAM5	804781	phosphoglycerate mutase family member 5 <i>Homo sapiens</i>
PHB2	775357	prohibitin 2 <i>Homo sapiens</i>
PKLR	793730	pyruvate kinase, liver and RBC <i>Homo sapiens</i>
PRKDC	791583	similar to protein kinase, DNA-activated, catalytic polypeptide; protein kinase, DNA-activated, catalytic polypeptide <i>Homo sapiens</i>
PRPF19	817432	PRP19/PSO4 pre-mRNA processing factor 19 homolog (<i>S. cerevisiae</i>) <i>Homo sapiens</i>
PRSS1	773661	protease, serine, 1 (trypsin 1); trypsinogen C <i>Homo sapiens</i>
PTRF	775001	polymerase I and transcript release factor <i>Homo sapiens</i>
QARS	795667	glutaminyl-tRNA synthetase <i>Homo sapiens</i>
RANBP2	823753	RAN binding protein 2 <i>Homo sapiens</i>
RECQL	784519	RecQ protein-like (DNA helicase Q1-like) <i>Homo sapiens</i>
RND3	789205	Rho family GTPase 3 <i>Homo sapiens</i>
RPL11	810885	ribosomal protein L11 <i>Homo sapiens</i>
RPL13	822027	ribosomal protein L13 pseudogene 12; ribosomal protein L13 <i>Homo sapiens</i>
RPL13A	791016	ribosomal protein L13a pseudogene 7; ribosomal protein L13a pseudogene 5; ribosomal protein L13a pseudogene 16; ribosomal protein L13a; ribosomal protein L13a pseudogene 18 <i>Homo sapiens</i>
RPL15	779090	ribosomal protein L15 pseudogene 22; ribosomal protein L15 pseudogene 18; ribosomal protein L15 pseudogene 17; ribosomal protein L15 pseudogene 3; ribosomal protein L15 pseudogene 7; ribosomal protein L15 <i>Homo sapiens</i>
RPL17	783997	ribosomal protein L17 pseudogene 22; ribosomal protein L17 pseudogene 36; ribosomal protein L17 pseudogene 20; similar to ribosomal protein L17; ribosomal protein L17 pseudogene 33; ribosomal protein L17 pseudogene 34; ribosomal protein L17 pseudogene 9; ribosomal protein L17; ribosomal protein L17 pseudogene 18; ribosomal protein L17 pseudogene 7; ribosomal protein L17 pseudogene 39 <i>Homo sapiens</i>
RPL18A	778688	ribosomal protein L18a pseudogene 6; ribosomal protein L18a <i>Homo sapiens</i>
RPL19	786531	ribosomal protein L19; ribosomal protein L19 pseudogene 12 <i>Homo sapiens</i>

GENE CARDS	DAVID ID	GENE / PROTEIN DESCRIPTION
RPL21	793235	ribosomal protein L21 pseudogene 134; ribosomal protein L21 pseudogene 80; ribosomal protein L21 pseudogene 20; ribosomal protein L21 pseudogene 46; ribosomal protein L21 pseudogene 45; ribosomal protein L21 pseudogene 131; ribosomal protein L21 pseudogene 16; ribosomal protein L21 pseudogene 53; ribosomal protein L21 pseudogene 120; ribosomal protein L21 pseudogene 37; ribosomal protein L21 pseudogene 93; ribosomal protein L21 pseudogene 39; ribosomal protein L21 pseudogene 29; ribosomal protein L21 pseudogene 28; ribosomal protein L21 pseudogene 14; ribosomal protein L21 pseudogene 98; ribosomal protein L21 pseudogene 105; ribosomal protein L21 pseudogene 87; ribosomal protein L21 pseudogene 128; ribosomal protein L21 pseudogene 69; ribosomal protein L21 pseudogene 97; ribosomal protein L21; ribosomal protein L21 pseudogene 119; ribosomal protein L21 pseudogene 125 <i>Homo sapiens</i>
RPL23	780689	ribosomal protein L23 pseudogene 6; ribosomal protein L23 <i>Homo sapiens</i>
RPL24	800698	ribosomal protein L24; ribosomal protein L24 pseudogene 6 <i>Homo sapiens</i>
RPL27	784332	ribosomal protein L27 <i>Homo sapiens</i>
RPL3	802424	ribosomal protein L3; similar to 60S ribosomal protein L3 (L4) <i>Homo sapiens</i>
RPL34	803929	ribosomal protein L34 <i>Homo sapiens</i>
RPL5	804383	ribosomal protein L5 pseudogene 34; ribosomal protein L5 pseudogene 1; ribosomal protein L5 <i>Homo sapiens</i>
RPL6	795791	ribosomal protein L6 pseudogene 27; ribosomal protein L6 pseudogene 19; ribosomal protein L6; ribosomal protein L6 pseudogene 10 <i>Homo sapiens</i>
RPL7A	823404	ribosomal protein L7a pseudogene 70; ribosomal protein L7a; ribosomal protein L7a pseudogene 30; ribosomal protein L7a pseudogene 66; ribosomal protein L7a pseudogene 27; ribosomal protein L7a pseudogene 11; ribosomal protein L7a pseudogene 62 <i>Homo sapiens</i>
RPL8	801125	ribosomal protein L8; ribosomal protein L8 pseudogene 2 <i>Homo sapiens</i>
RPL9	778568	ribosomal protein L9; ribosomal protein L9 pseudogene 25 <i>Homo sapiens</i>
RPN1	773182	ribophorin I <i>Homo sapiens</i>
RPN2	791634	ribophorin II <i>Homo sapiens</i>
RPS12	800729	ribosomal protein S12; ribosomal protein S12 pseudogene 4; ribosomal protein S12 pseudogene 11; ribosomal protein S12 pseudogene 9 <i>Homo sapiens</i>
RPS14	817032	ribosomal protein S14 <i>Homo sapiens</i>
RPS2	776216	ribosomal protein S2 pseudogene 8; ribosomal protein S2 pseudogene 11; ribosomal protein S2 pseudogene 5; ribosomal protein S2 pseudogene 12; ribosomal protein S2 pseudogene 51; ribosomal protein S2 pseudogene 17; ribosomal protein S2 pseudogene 55; ribosomal protein S2 pseudogene 20; ribosomal protein S2 <i>Homo sapiens</i>
RPS23	801872	ribosomal protein S23 <i>Homo sapiens</i>
RPS24	816407	ribosomal protein S24 <i>Homo sapiens</i>

GENE CARDS	DAVID ID	GENE / PROTEIN DESCRIPTION
RPS26	772335	ribosomal protein S26 pseudogene 38; ribosomal protein S26 pseudogene 39; ribosomal protein S26 pseudogene 35; ribosomal protein S26 pseudogene 31; ribosomal protein S26 pseudogene 20; ribosomal protein S26 pseudogene 54; ribosomal protein S26 pseudogene 2; ribosomal protein S26 pseudogene 53; ribosomal protein S26 pseudogene 25; ribosomal protein S26 pseudogene 50; ribosomal protein S26 pseudogene 6; ribosomal protein S26 pseudogene 8; ribosomal protein S26 <i>Homo sapiens</i>
RPS27	789083	ribosomal protein S27 pseudogene 29; ribosomal protein S27 pseudogene 9; ribosomal protein S27 pseudogene 23; ribosomal protein S27 pseudogene 13; ribosomal protein S27; ribosomal protein S27 pseudogene 21; ribosomal protein S27 pseudogene 7; ribosomal protein S27 pseudogene 6; ribosomal protein S27 pseudogene 19 <i>Homo sapiens</i>
RPS3	816191	ribosomal protein S3 pseudogene 3; ribosomal protein S3 <i>Homo sapiens</i>
RPS3A	789968	ribosomal protein S3A pseudogene 5; ribosomal protein S3a pseudogene 47; ribosomal protein S3a pseudogene 49; ribosomal protein S3A; hypothetical LOC100131699; hypothetical LOC100130107 <i>Homo sapiens</i>
RPS4X	791681	ribosomal protein S4X pseudogene 6; ribosomal protein S4X pseudogene 13; ribosomal protein S4, X-linked <i>Homo sapiens</i>
RPS6	808508	ribosomal protein S6 pseudogene 25; ribosomal protein S6; ribosomal protein S6 pseudogene 1 <i>Homo sapiens</i>
RPS7	773042	ribosomal protein S7; ribosomal protein S7 pseudogene 11; ribosomal protein S7 pseudogene 4; ribosomal protein S7 pseudogene 10 <i>Homo sapiens</i>
RPS8	821732	ribosomal protein S8; ribosomal protein S8 pseudogene 8; ribosomal protein S8 pseudogene 10 <i>Homo sapiens</i>
RPS9	798227	ribosomal protein S9; ribosomal protein S9 pseudogene 4 <i>Homo sapiens</i>
RRBP1	822623	ribosome binding protein 1 homolog 180kDa (dog) <i>Homo sapiens</i>
RSL1D1	781114	ribosomal L1 domain containing 1 <i>Homo sapiens</i>
S100A8	783621	S100 calcium binding protein A8 <i>Homo sapiens</i>
SART3	795024	squamous cell carcinoma antigen recognized by T cells 3 <i>Homo sapiens</i>
SEC62	793015	SEC62 homolog (<i>S. cerevisiae</i>) <i>Homo sapiens</i>
SF3B1	819770	splicing factor 3b, subunit 1, 155kDa <i>Homo sapiens</i>
SF3B3	792435	splicing factor 3b, subunit 3, 130kDa <i>Homo sapiens</i>
SFRS2B	784941	splicing factor, arginine/serine-rich 2B <i>Homo sapiens</i>
SGPL1	789498	sphingosine-1-phosphate lyase 1 <i>Homo sapiens</i>
SLC25A1	797071	solute carrier family 25 (mitochondrial carrier; citrate transporter), member 1 <i>Homo sapiens</i>
SLC25A10	796046	solute carrier family 25 (mitochondrial carrier; dicarboxylate transporter), member 10 <i>Homo sapiens</i>
SLC25A3	791524	solute carrier family 25 (mitochondrial carrier; phosphate carrier), member 3 <i>Homo sapiens</i>
SLC25A6	823629	solute carrier family 25 (mitochondrial carrier; adenine nucleotide translocator), member 6 <i>Homo sapiens</i>
SMC1A	794773	structural maintenance of chromosomes 1A <i>Homo sapiens</i>
SMC2	798960	structural maintenance of chromosomes 2 <i>Homo sapiens</i>
SMC3	793277	structural maintenance of chromosomes 3 <i>Homo sapiens</i>

GENE CARDS	DAVID ID	GENE / PROTEIN DESCRIPTION
SMC4	781161	structural maintenance of chromosomes 4 <i>Homo sapiens</i>
SND1	798687	staphylococcal nuclease and tudor domain containing 1 <i>Homo sapiens</i>
SNRNP35	820447	ATP-binding cassette, sub-family B (MDR/TAP), member 5; small nuclear ribonucleoprotein 35kDa (U11/U12) <i>Homo sapiens</i>
SRP54	787467	similar to signal recognition particle 54kDa; signal recognition particle 54kDa <i>Homo sapiens</i>
SRP72	816308	signal recognition particle 72kDa <i>Homo sapiens</i>
STAU1	822124	staufen, RNA binding protein, homolog 1 (<i>Drosophila</i>) <i>Homo sapiens</i>
STEAP3	799131	STEAP family member 3 <i>Homo sapiens</i>
SYNCRIP	811579	synaptotagmin binding, cytoplasmic RNA interacting protein <i>Homo sapiens</i>
TBL2	798215	transducin (beta)-like 2 <i>Homo sapiens</i>
TMEM109	822806	transmembrane protein 109 <i>Homo sapiens</i>
TOP2B	783488	topoisomerase (DNA) II beta 180kDa <i>Homo sapiens</i>
TTN	795630	titin <i>Homo sapiens</i>
TUBA1A	811901	tubulin, alpha 1a <i>Homo sapiens</i>
TUBB2C	776899	tubulin, beta 2C <i>Homo sapiens</i>
TXLNA	801671	taxilin alpha <i>Homo sapiens</i>
UBE2B	805624	ubiquitin-conjugating enzyme E2B (RAD6 homolog) <i>Homo sapiens</i>
VAR5	785609	valyl-tRNA synthetase <i>Homo sapiens</i>
VDAC2	785721	voltage-dependent anion channel 2 <i>Homo sapiens</i>
VIM	814359	vimentin <i>Homo sapiens</i>
YIPF5	778492	Yip1 domain family, member 5 <i>Homo sapiens</i>
YWHAG	815903	tyrosine 3-monooxygenase/tryptophan 5-monooxygenase activation protein, gamma polypeptide <i>Homo sapiens</i>
YWHAH	817322	tyrosine 3-monooxygenase/tryptophan 5-monooxygenase activation protein, eta polypeptide <i>Homo sapiens</i>
YWHAQ	820893	tyrosine 3-monooxygenase/tryptophan 5-monooxygenase activation protein, theta polypeptide <i>Homo sapiens</i>

Note: Total of 195 genes recognised by DAVID

REFERENCES

- Alberts, B., Johnson, A., Lewis, J., Raff, M., Roberts, K., & Walter, P. 2008, "The transport of molecules between the nucleus and the cytosol," *In Molecular Biology of The Cell*, 5th ed. Garland Science, Taylor and Francis Group, pp. 704-712
- Antonov, A.V. 2011. BioProfiling.de: analytical web portal for high-throughput cell biology. *Nucleic Acids Research*, 39, (suppl 2) W323-W327
- Arulanandam, R., Geletu, M., Feracci, H., & Raptis, L. 2010. Activated Rac1 requires gp130 for Stat3 activation, cell proliferation and migration. *Exp.Cell Res*, 316, (5) 875-886
- Azzarelli, R., Pacary, E., Garg, R., Garcez, P., van den Berg, D., Riou, P., Ridley, A.J., Friedel, R.H., Parsons, M., & Guillemot, F. 2014. An antagonistic interaction between PlexinB2 and Rnd3 controls RhoA activity and cortical neuron migration. *Nat Commun*, 5
- Bastos, R.N., Penate, X., Bates, M., Hammond, D., & Barr, F.A. 2012. CYK4 inhibits Rac1-dependent PAK1 and ARHGEF7 effector pathways during cytokinesis. *The Journal of Cell Biology*, 198, (5) 865-880
- Bilokapic, S. & Schwartz, T.U. 2012. 3D ultrastructure of the nuclear pore complex. *Curr Opin.Cell Biol*, 24, (1) 86-91
- Bohmer, R.M., Scharf, E., & Assoian, R.K. 1996. Cytoskeletal integrity is required throughout the mitogen stimulation phase of the cell cycle and mediates the anchorage-dependent expression of cyclin D1. *Mol.Biol.Cell*, 7, 101-111
- Boswell, S.A., Ongusaha, P.P., Nghiem, P., & Lee, S.W. 2007. The protective role of a small GTPase RhoE against UVB-induced DNA damage in keratinocytes. *J Biol Chem*, 282, (7) 4850-4858
- Boulter, E., Garcia-Mata, R., Guilluy, C., Dubash, A., Rossi, G., Brennwald, P.J., & BurrIDGE, K. 2010. Regulation of Rho GTPase crosstalk, degradation and activity by RhoGDI1. *Nat Cell Biol*, 12, (5) 477-483
- Boureaux, A., Vignal, E., Faure, S., & Fort, P. 2007. Evolution of the Rho Family of Ras-Like GTPases in Eukaryotes. *Molecular Biology and Evolution*, 24, (1) 203-216
- Brennan, C., Verhaak, R., McKenna, A., Campos, B., Noushmehr, H., Salama, S., Zheng, S., Chakravarty, D., Sanborn, J., Berman, S., Beroukhim, R., Bernard, B., Wu, C.J., Genovese, G., Shmulevich, I., Barnholtz-Sloan, J., Zou, L., Vegesna, R., Shukla, S., Ciriello, G., Yung, W.K., Zhang, W., Sougnez, C., Mikkelsen, T., Aldape, K., Bigner, D., Van-áMeir, E., Prados, M., Sloan, A., Black, K., Eschbacher, J., Finocchiaro, G., Friedman, W., Andrews, D., Guha, A., Iacocca, M., OğçÖNeill, B., Foltz, G., Myers, J., Weisenberger, D., Penny, R., Kucherlapati, R., Perou, C., Hayes, D., Gibbs, R., Marra, M., Mills, G., Lander, E., Spellman, P., Wilson, R., Sander, C., Weinstein, J., Meyerson, M., Gabriel, S., Laird, P., Haussler, D.,

- Getz, G., & Chin, L. 2013. The Somatic Genomic Landscape of Glioblastoma. *Cell*, 155, (2) 462-477
- Brewer, S. Designing primer for RhoE. Personal discussion with Sue. Laboratory 501, 5th floor Tower, School of Biosciences, University of Birmingham, U.K. 2011. Personal Communication
- Bustelo, X.R., Sauzeau, V., & Berenjano, I.M. 2007. GTP-binding proteins of the Rho/Rac family: regulation, effectors and functions in vivo. *Bioessays.Author Manuscript.*, 29, (4) 356-370
- Cao, S. & Buck, M. 2011. Optimization and stabilization of Rho small GTPase proteins for solution NMR studies: The case of Rnd1. *Small GTPases*, 2, (6) 295-304
- Champeris Tsaniras, S., Kanellakis, N., Symeonidou, I.E., Nikolopoulou, P., Lygerou, Z., & Taraviras, S. 2014. Licensing of DNA replication, cancer, pluripotency and differentiation: An interlinked world? *Seminars in Cell & Developmental Biology*, 30, (0) 174-180
- Chang, C.W., Counago, R.M., Williams, S.J., Boden, M., & Kobe, B. 2013. Distinctive conformation of minor site-specific nuclear localization signals bound to importin-alpha. *Traffic*, 14, (11) 1144-1154
- Chardin, P. 2006. Function and regulation of Rnd proteins. *Nature Review Molecular Cell Biology*, 7, 54-62
- Chen, J., Zhou, H., Li, Q., Qiu, M., Li, Z., Tang, Q., Liu, M., Zhu, Y., Huang, J., Lang, N., Liu, Z., Deng, Y., Zhang, S., & Bi, F. 2011. Epigenetic modification of RhoE expression in gastric cancer cells. *Oncol Rep.*, 25, (1) 173-180
- Chen, Z., Medina, F., Liu, M.y., Thomas, C., Sprang, S.R., & Sternweis, P.C. 2010. Activated RhoA Binds to the Pleckstrin Homology (PH) Domain of PDZ-RhoGEF, a Potential Site for Autoregulation. *Journal of Biological Chemistry*, 285, (27) 21070-21081
- Cherfils, J. & Zeghouf, M. 2013. Regulation of small GTPases by GEFs, GAPs and GDIs. *Physiology Review*, 93, 269-309
- Chuang, H.H., Yang, C.H., Tsay, Y.G., Hsu, C.Y., Tseng, L.M., Chang, Z.F., & Lee, H.H. 2012. ROCKII Ser1366 phosphorylation reflects the activation status. *Biochem.J*, 443, (1) 145-151
- Chubet, R.G. & Brizzard, B.L. 1996. Vectors for Expression and Secretion of FLAG Epitope-Tagged Proteins in Mammalian Cells. *BioTechniques*, 20, (1) 136-141
- Cinti, C., Trimarchi, C., & Giordano, A. G1 Phase Progression and Apoptosis. *Eurekah* , 199-235. 2003. Kluwer Academic / Prenum Publisher. Landes Bioscience. Johannes Boonstra. Serial (Book, Monograph)
- Clarke, K., Daubon, T., Turan, N., Soulet, F., Mohd Zahari, M., Ryan, K.R., Durant, S., He, S., Herbert, J., Ankers, J., Heath, J.K., Bjerkvig, R., Bicknell, R., Hotchin, N.A., Bikfalvi, A., & Falciani, F. 2015. Inference of Low and High-Grade Glioma Gene Regulatory Networks

- Delineates the Role of Rnd3 in Establishing Multiple Hallmarks of Cancer. *PLoS Genetics*, 11, (7) e1005325
- Cobrinik, D. 2005. Pocket proteins and cell cycle control. *Oncogene*, 24, (17) 2796-2809
- Coleman, M. L., Marshall, C. J., & Olson, M. F. 2004. RAS and RHO GTPases in G1-phase cell-cycle regulation. *Nature Review Molecular Cell Biology* [5], 355-366
- Coleman, M.L. & Olson, M.F. 2002. Rho GTPase signalling pathways in the morphological changes associated with apoptosis: A review. *Cell death and Differentiation*, 9, 493-504
- College of American Pathologists. (2011). *Brain Tumour - Glioblastoma*.
- Colyer, J. 1999, "Monitoring protein expression by Western blotting," *In Protein expression - a practical approach*, S. J. Higgins & B. D. Hames, eds., New York: Oxford University Press, pp. 232-236
- Cook, D.R., Rossman, K.L., & Der, C.J. 2014. Rho guanine nucleotide exchange factors: regulators of Rho GTPase activity in development and disease. *Oncogene*, 33, (31) 4021-4035
- Crawley, M. J. 2005, "Chapter 1: Fundamentals - p Values," *In Statistics: An Introduction using R*, John Wiley & Sons Ltd, London UK, pp. 1-14
- Croft, D.R. & Olson, M.F. 2011. Transcriptional regulation of Rho GTPase signaling. *Transcription.*, 2, (5) 211-215
- CRUK. Type of primary brain tumours. 2013. Online Source.
- Darenfed, H., Dayanandan, B., Zhang, T., Hsieh, S.H., Fournier, A.E., & Mandato, C.A. 2007. Molecular characterization of the effects of Y-27632. *Cell Motil.Cytoskeleton*, 64, (2) 97-109
- David, M., Petit, D., & Bertoglio, J. 2012. Cell cycle regulation of Rho signaling pathways. *Cell Cycle*, 11, (16) 3003-3010
- Dellinger, A.E. 2006. *Computational Biology of Ras Proteins*. Doctor of Philosophy North Carolina State University.
- Dermardirossian, C. & Bokoch, G.M. 2005. GDIs: central regulatory molecules in Rho GTPase activation. *Trends Cell Biol*, 15, (7) 356-363
- Evan, G. I. & Vousden, K. H. Proliferation, cell cycle and apoptosis in cancer. *Nature* 411, 342-348. 2001. California, USA, McMillan Magazine Ltd. Magazine Article.
- Fiegen, D., Blumenstein, L., Stege, P., Vetter, I.R., & Ahmadian, M.R. 2002. Crystal structure of Rnd3/RhoE: functional implications. *FEBS Lett.*, 525, (1-3) 100-104
- Fischer, A.H., Jacobson, K.A., Rose, J., & Zeller, R. 2008. Hematoxylin and Eosin Staining of Tissue and Cell Sections. *Cold Spring Harbor Protocols*, 2008, (5) db

- Flynn, P., Mellor, H., Casamassima, A., & Parker, P.J. 2000. Rho GTPase control of protein kinase C-related protein kinase activation by 3-phosphoinositide-dependent protein kinase. *J Biol Chem*, 275, (15) 11064-11070
- Fortin Ensign, S.P., Mathews, I.T., Symons, M.H., Berens, M.E., & Tran, N.L. 2013. Implications of Rho GTPase Signaling in Glioma Cell Invasion and Tumor Progression. *Front Oncol*, 3, 241
- Foster, R., Hu, K.Q., Lu, Y., Nolan, K.M., Thissen, J., & Settleman, J. 1996. Identification of a novel human Rho protein with unusual properties: GTPase deficiency and in vivo farnesylation. *Mol Cell Biol*, 16, (6) 2689-2699
- Franceschini, A., Szklarczyk, D., Frankild, S., Kuhn, M., Simonovic, M., Roth, A., Lin, J., Minguez, P., Bork, P., von Mering, C., & Jensen, L.J. 2013. STRING v9.1: protein-protein interaction networks, with increased coverage and integration. *Nucleic Acids Research*, 41, (D1) D808-D815
- Garavini, H., Riento, K., Phelan, J.P., McAlister, M.S., Ridley, A.J., & Keep, N.H. 2002. Crystal structure of the core domain of RhoE/Rnd3: a constitutively activated small G protein. *Biochemistry*, 41, (20) 6303-6310
- Gomez, O., Ballester-Lurbe, B., Guasch, R.M., Perez-Roger, I., Garcia-Rosello, E., & Terrado, J. 2014. Analysis of RhoE expression in the testis, epididymis and ductus deferens, and the effects of its deficiency in mice. *J Anat.*, 225, (6) 583-590
- Gottesbuhren, U., Garg, R., Riou, P., McColl, B., Brayson, D., & Ridley, A.J. 2012. Rnd3 induces stress fibres in endothelial cells through RhoB. *Biology Open*, 2, 210-216
- Guasch, R.M., Scambler, P., Jones, G.E., & Ridley, A.J. 1998. RhoE regulates actin cytoskeleton organization and cell migration. *Mol Cell Biol*, 18, (8) 4761-4771
- Hångerstrand, D., He, X., Bradic Lindh, M., Hoefs, S., Hesselager, G., Östman, A., & Nistér, M. 2011. Identification of a SOX2-dependent subset of tumor- and sphere-forming glioblastoma cells with a distinct tyrosine kinase inhibitor sensitivity profile. *Neuro-Oncology*, 13, (11) 1178-1191
- Hall, A. 2009. The cytoskeleton and cancer. *Cancer Metastasis Review*, 28, 5-14
- Hall, A. 2005. Rho GTPases and the control of cell behaviour. *Biochem.Soc.Trans.*, 33, (Pt 5) 891-895
- Hamada, M., Haeger, A., Jeganathan, K.B., van Ree, J.H., Malureanu, L., Walde, S., Joseph, J., Kehlenbach, R.H., & van Deursen, J.M. 2011. Ran-dependent docking of importin-beta to RanBP2/Nup358 filaments is essential for protein import and cell viability. *J Cell Biol*, 194, (4) 597-612
- Holmberg, J., He, X., Peredo, I., Orrego, A., Hesselager, G., Ericsson, C., Hovatta, O., Oba-Shinjo, S., Marie, S., Nister, M., & Muhr, J. 2011. Activation of Neural and Pluripotent Stem Cell Signatures Correlates with Increased Malignancy in Human Glioma. *PLOS ONE*, 6, (3) 1-10

- Huang, D.W., Sherman, B.T., & Lempicki, R.A. 2008. Systematic and integrative analysis of large gene lists using DAVID bioinformatics resources. *Nat.Protocols*, 4, (1) 44-57
- Huang, D.W., Sherman, B.T., & Lempicki, R.A. 2009. Bioinformatics enrichment tools: paths toward the comprehensive functional analysis of large gene lists. *Nucleic Acids Research*, 37, (1) 1-13
- Huang, D. W., Sherman, B. T., Zheng, X., Yang, J., Imamichi, T., Stephens, R., & Lempicki, R. A. 2002, "Extracting Biological Meaning from Large Gene Lists with DAVID," *In Current Protocols in Bioinformatics*, John Wiley & Sons, Inc..
- Hulsen, T., de Vlieg, J., & Alkema, W. 2008. BioVenn - a web application for the comparison and visualization of biological lists using area-proportional Venn diagrams. *BMC Genomics*, 9, (1) 488
- Ishizaki, T., Uehata, M., Tamechika, I., Keel, J., Nonomura, K., Maekawa, M., & Narumiya, S. 2000. Pharmacological properties of Y-27632, a specific inhibitor of Rho-Associated Kinases. *Molecular Pharmacology*, 57, 976-983
- Jie, W., Andrade, K.C., Lin, X., Yang, X., Yue, X., & Chang, J. 2015. Pathophysiological Functions of Rnd3/RhoE. *Comprehensive Physiology*, 6, (1) 169-186
- Kagawa, Y., Matsumoto, S., Kamioka, Y., Mimori, K., Naito, Y., Ishii, T., Okuzaki, D., Nishida, N., Maeda, S., Naito, A., Kikuta, J., Nishikawa, K., Nishimura, J., Haraguchi, N., Takemasa, I., Mizushima, T., Ikeda, M., Yamamoto, H., Sekimoto, M., Ishii, H., Doki, Y., Matsuda, M., Kikuchi, A., Mori, M., & Ishii, M. 2013. Cell cycle-dependent Rho GTPase activity dynamically regulates cancer cell motility and invasion in vivo. *PLOS ONE*, 8, (12) e83629
- Karlsson, R., Pedersen, E.D., Wang, Z., & Brakebusch, C. 2009. Rho GTPase function in tumorigenesis. *Biochim.Biophys.Acta*, 1796, (2) 91-98
- Kartalou, M. & Essigmann, J.M. 2001. Mechanisms of resistance to cisplatin. *Mutation Research*, 478, 23-43
- Kinoshita, E., Kinoshita-Kikuta, E., Takiyama, K., & Koike, T. 2006. Phosphate-binding tag, a new tool to visualize phosphorylated proteins. *Mol Cell Proteomics*, 5, (4) 749-757
- Kodiha, M. & Stochaj, U. 2012. Nuclear Transport: A switch for the Oxidative Stress-Signaling Circuit? *Journal of Signal Transduction*, 2012, 1-18
- Kolupaeva, V. & Janssens, V. 2013. PP1 and PP2A phosphatases--cooperating partners in modulating retinoblastoma protein activation. *FEBS J*, 280, (2) 627-643
- Komander, D., Garg, R., Wan, P.T.C., Ridley, A.J., & Barford, D. 2008. Mechanism of multi site phosphorylation from a ROCK I: RhoE complex structure. *The EMBO Journal*, 27, (23) 3175-3185
- Kong, J., Cooper, L.A., Wang, F., Gao, J., Teodoro, G., Scarpace, L., Mikkelsen, T., Schniederjan, M.J., Moreno, C.S., Saltz, J.H., & Brat, D.J. 2013. Machine-Based

Morphologic Analysis of Glioblastoma Using Whole-Slide Pathology Images Uncovers Clinically Relevant Molecular Correlates. *PLOS ONE*, 8, (11) 1-17

Kunz, M., Thon, N., Eigenbrod, S., Hartmann, C., Egensperger, R., Herms, J., Geisler, J., la Fougere, C., Lutz, J., Linn, J., Kreth, S., von Deimling, A., Tonn, J.C., Kretschmar, H.A., P+Äpperl, G., & Kreth, F.W. 2011. Hot spots in dynamic¹⁸FET-PET delineate malignant tumor parts within suspected WHO grade II gliomas. *Neuro-Oncology*, 13, (3) 307-316

Lal, A., Haynes, S.R., & Gorospe, M. 2005. Clean Western blot signals from immunoprecipitated samples. *Mol Cell Probes*, 19, (6) 385-388

Lemichez, E. & Aktories, K. 2013. Hijacking of Rho GTPases during bacterial infection. *Exp. Cell Res*, 319, (15) 2329-2336

Leverrier, Y. & Ridley, A.J. 2001. Requirement for Rho GTPases and PI 3-kinases during apoptotic cell phagocytosis by macrophages. *Curr Biol*, 11, (3) 195-199

Li, L., Gondi, C.S., Dinh, D.H., Olivero, W.C., Gujrati, M., & Rao, J.S. 2007. Transfection with anti-p65 intrabody suppresses invasion and angiogenesis in glioma cells by blocking nuclear factor-kappaB transcriptional activity. *Clin Cancer Res*, 13, (7) 2178-2190

Liacini, A., Sanger, D., & Forsyth, P. Small G-protein RhoE expressed in brain cancer and affects glioma morphology, motility and invasion, p. 2.

Liebig, T., Erasmus, J., Kalaji, R., Davies, D., Loirand, G., Ridley, A., & Braga, V.M. 2009. RhoE is required for keratinocyte differentiation and stratification. *Mol Biol Cell*, 20, (1) 452-463

Linch, M., Riou, P., Claus, J., Cameron, A.J., de, N.J., Larijani, B., Ng, T., McDonald, N.Q., & Parker, P.J. 2014. Functional implications of assigned, assumed and assembled PKC structures. *Biochem.Soc.Trans.*, 42, (1) 35-41

Lodge, J., Lund, P., & Minchin, S. 2007, "Bioinformatics," *In Gene Cloning - Principle and Application*, Taylor & Francis Group, pp. 207-247.

Loirand, G., Guerin, P., & Pacaud, P. 2006. Rho kinases in cardiovascular physiology and pathophysiology. *Journal of American Heart Association*, 98, 322-334

Lonjedo, M., Poch, E., Mocholi, E., Hernandez-Sanchez, M., Ivorra, C., Franke, T.F., Guasch, R.M., & Perez-Roger, I. 2013. The Rho family member RhoE interacts with Skp2 and is degraded at the proteasome during cell cycle progression. *J Biol Chem*, 288, (43) 30872-30882

Ludwig, K. & Parsons, S.J. 2011. The tumour suppressor, p190RhoGAP, differentially initiates apoptosis and confers doxorubicin sensitivity to breast cancer cells. *Genes & Cancer*, 2, (1) 20-30

Ma, W., Wong, C.C., Tung, E.K., Wong, C.M., & Ng, I.O. 2013. RhoE is frequently down-regulated in hepatocellular carcinoma (HCC) and suppresses HCC invasion through

antagonizing the Rho/Rho-kinase/myosin phosphatase target pathway. *Hepatology*, 57, (1) 152-161

Machacek, M., Hodgson, L., Welch, C., Elliott, H., Pertz, O., Nalbant, P., Abell, A., Johnson, G.L., Hahn, K.M., & Danuser, G. 2009. Coordination of Rho GTPase activities during cell protrusion. *Nature*, 461, (7260) 99-103

Madigan, J.P., Bodemann, B.O., Brady, D.C., Dewar, B.J., Keller, P.J., Leitges, M., Philips, M.R., Ridley, A.J., Der, C.J., & Cox, A.D. 2009. Regulation of Rnd3 localization and function by protein kinase C alpha-mediated phosphorylation. *Biochem.J*, 424, (1) 153-161

Madigan, J.P. 2008. *Regulation of localisation and function of the Rho family small GTPase, Rnd3*. PhD in Genetics and Molecular Biology University of North Carolina.

Marfori, M., Mynott, A., Ellis, J.J., Mehdi, A.M., Saunders, N.F.W., Curmi, P.M., Forwood, J.K., Bodmann, M., & Kobe, B. 2011. Molecular basis for specificity of nuclear import and prediction of nuclear localization. *Biochimica et Biophysica Acta (BBA) - Molecular Cell Research*, 1813, (9) 1562-1577

McCabe, M.T., Azih, O.J., & Day, M.L. 2005. pRb-Independent growth arrest and transcriptional regulation of E2F target genes. *Neoplasia*, 7, (2) 141-151

McCormack, J., Welsh, N.J., & Braga, V.M. 2013. Cycling around cell-cell adhesion with Rho GTPase regulators. *J Cell Sci.*, 126, (Pt 2) 379-391

McLachlin, D.T. & Chait, B.T. 2001. Analysis of phosphorylated proteins and peptides by mass spectrometry. *Current Opinion in Chemical Biology*, 5, 591-602

McMullan, R.J. 2002. *Regulation of keratinocytes function by Rho kinase*. Doctor of Philosophy. The University of Birmingham.

Mihlan, S., Reis, C., Thalheimer, P., Herterich, S., Gaetzner, S., Kremerskothen, J., Pavenstadt, H.J., Lewandrowski, U., Sickmann, A., & Butt, E. 2013. Nuclear import of LASP-1 is regulated by phosphorylation and dynamic protein-protein interactions. *Oncogene*, 32, (16) 2107-2113

Mingot, J.M., Bohnsack, M.T., Jakle, U., & Gorlich, D. 2004. Exportin 7 defines a novel general nuclear export pathway. *EMBO J*, 23, (16) 3227-3236

Moore, M.S. 1998. Ran and Nuclear Transport. *The Journal of Biological Chemistry*, 273, (36) 22857-22860

Morgan-Fisher, M., Wewer, U.M., & Yoneda, A. 2013. Regulation of ROCK Activity in Cancer. *Journal of Histochemistry & Cytochemistry*, 61, (3) 185-198

Newton, K., Matsumoto, M.L., Wertz, I.E., Kirkpatrick, D.S., Lill, J.R., Tan, J., Dugger, D., Gordon, N., Sidhu, S.S., Fellouse, F.A., Komuves, L., French, D.M., Ferrando, R.E., Lam, C., Compaan, D., Yu, C., Bosanac, I., Hymowitz, S.G., Kelley, R.F., & Dixit, V.M. 2008. Ubiquitin Chain Editing Revealed by Polyubiquitin Linkage-Specific Antibodies. *Cell*, 134, 668-678

NHS, UK. National Brain Tumour Registry. 2013. Online Source.

Ohgushi, M., Matsumura, M., Eiraku, M., Murakami, K., Aramaki, T., Nishiyama, A., Muguruma, K., Nakano, T., Suga, H., Ueno, M., Ishizaki, T., Suemori, H., Narumiya, S., Niwa, H., & Sasai, Y. 2010. Molecular pathway and cell state responsible for dissociation-induced apoptosis in human pluripotent stem cells. *Cell Stem Cell*, 7, (2) 225-239

Ongusaha, P. P., Kim, H. G., Boswell, S. A., Ridley, A. J., Der, C. J., Dotto, G. P., Kim, Y. B., Aaronson, S. A., & Lee, S. W. 2006. RhoE Is a Pro-Survival p53 Target Gene that Inhibits ROCK I-Mediated Apoptosis in Response to Genotoxic Stress. *Current biology : CB* 16[24], 2466-2472

Pacary, E., Heng, J., Azzarelli, R., Riou, P., Castro, D., Lebel-Potter, M., Parras, C., Bell, D.M., Ridley, A.J., Parsons, M., & Guillemot, F. 2011. Proneural transcription factors regulate different steps of cortical neuron migration through Rnd-mediated inhibition of RhoA signaling. *Neuron*, 69, (6) 1069-1084

Pecorino, L. *Molecular Biology of Cancer - Mechanisms, Targets and Therapeutics*. second[Chapter 7], 137-138. 2008. New York, Oxford University Press Inc., New York. Edited Book

Peris, B., Gonzalez-Granero, S., Ballester-Lurbe, B., Garcia-Verdugo, J.M., Perez-Roger, I., Guerri, C., Terrado, J., & Guasch, R.M. 2012. Neuronal polarization is impaired in mice lacking RhoE expression. *Journal of Neurochemistry* 1-12

Perona, R., Montaner, S., Saniger, L., Sanchez-Perez, I., Bravo, R., & Lacal, J.C. 1997. Activation of the nuclear factor-kappaB by Rho, CDC42, and Rac-1 proteins. *Genes Dev.*, 11, (4) 463-475

Poch, E., Minambres, R., Mocholi, E., Ivorra, C., Perez-Arago, A., Guerri, C., Perez-Roger, I., & Guasch, R.M. 2007. RhoE interferes with Rb inactivation and regulates the proliferation and survival of the U87 human glioblastoma cell line. *Exp. Cell Res*, 313, (4) 719-731

Poon, I.K.H. & Jans, D.A. 2005. Regulation of nuclear transport: Central role in development and transformation? *Traffic*, 6, 173-186

Rejman, J., Bragonzi, A., & Conese, M. 2005. Role of Clathrin- and Caveolae-Mediated Endocytosis in Gene Transfer Mediated by Lipo- and Polyplexes. *Mol Ther*, 12, (3) 468-474

Riento, K., Totty, N., Villalonga, P., Garg, R., Guasch, R.M., & Ridley, A.J. 2005a. RhoE function is regulated by ROCK I-mediated phosphorylation. *The EMBO Journal*, 24, (6) 1170-1180

Riento, K., Totty, N., Villalonga, P., Garg, R., Guasch, R.M., & Ridley, A.J. 2005b. RhoE function is regulated by ROCK I-mediated phosphorylation. *The EMBO Journal*, 24, (6) 1170-1180

Riento, K., Guasch, R.M., Garg, R., Jin, B., & Ridley, A.J. 2003. RhoE binds to ROCK I and inhibits downstream signaling. *Mol Cell Biol*, 23, (12) 4219-4229

- Riento, K., Villalonga, P., Garg, R., & Ridley, A. 2005c. Function and regulation of RhoE. *Biochem.Soc.Trans.*, 33, (Pt 4) 649-651
- Riera, A., Li, H., & Speck, C. 2013. Seeing is believing: the MCM2-7 helicase trapped in complex with its DNA loader. *Cell Cycle*, 12, (18) 2917-2918
- Riera, A. & Speck, C. 2014. Opening the gate to DNA replication. *Cell Cycle*
- Riera, A., Tognetti, S., & Speck, C. 2014. Helicase loading: how to build a MCM2-7 double-hexamers. *Semin.Cell Dev.Biol*, 30, 104-109
- Riou, P., Kjaer, S., Garg, R., Purkiss, A., George, R., Cain, R.J., Bineva, G., Reymond, N., McColl, B., Thompson, A.J., O'Reilly, N., McDonald, N.Q., Parker, P.J., & Ridley, A.J. 2013. 14-3-3 proteins interact with a hybrid prenyl-phosphorylation motif to inhibit G proteins. *Cell*, 153, (3) 640-653
- Riou, P., Villalonga, P., & Ridley, A.J. 2010. Rnd proteins: multifunctional regulators of the cytoskeleton and cell cycle progression. *Bioessays*, 32, (11) 986-992
- Robbins, D.E., Grueneberg, A., Deus, H.F., Tanik, M.M., & Almeida, J.S. 2013. A self-updating road map of The Cancer Genome Atlas. *Bioinformatics* 1-8
- Robertson, V.H. 2004. *A potential role for N-WASp in apoptosis of human epidermal keratinocytes*. Doctor of Philosophy. The University of Birmingham.
- Ryan, K. R. 2010. *Regulation of apoptosis and desmosomes by RhoE*. Doctor of Philosophy The University of Birmingham.
- Ryan, K.R., Lock, F.E., Heath, J.K., & Hotchin, N.A. 2012. Plakoglobin-dependent regulation of keratinocyte apoptosis by Rnd3. *J Cell Sci.*, 125, (Pt 13) 3202-3209
- Saad, I.I., Saha, S.B., & Thomas, G. 2014. The RAS subfamily Evolution - tracing evolution for its utmost exploitation. *Bioinformation*, 10, (5) 293-298
- Samson, R.Y. & Bell, S.D. 2013. MCM Loading-An Open-and-Shut Case? *Molecular Cell Previews*, 50, 457-458
- Samuel, M.S. & Olson, M.F. 2010. Dying alone: a tale of rho. *Cell Stem Cell*, 7, (2) 135-136
- Sathornsumetee, S., Reardon, D.A., Desjardins, A., Quinn, J.A., Vredenburgh, J.J., & Rich, J.N. 2007. Molecularly targeted therapy for malignant glioma. *Cancer*, 110, (1) 13-24
- Sebti, S.M. & Der, C.J. 2003. Searching for the elusive targets of farnesyltransferase inhibitors. *Nature Reviews*, 3, 945-951
- Senoo, H. & Iijima, M. 2013. Rho GTPase: A molecular compass for directional cell migration. *Commun Integr.Biol*, 6, (6) e27681
- Shimwell, N., Martin, A., Bruton, R.K., Blackford, A.N., Segwick, G.G., Gallimore, P.H., Turnell, A.S., & Grand, R.J.A. 2009. Adenovirus 5 E1A is responsible for increased

expression of insulin receptor substrate 4 in established adenovirus 5-transformed cell lines and interacts with IRS components activating the PI3 kinase/Akt signalling pathway A. *Oncogene*, 28, 686-697

Siddik, Z.H. 2003. Cisplatin: mode of cytotoxic action and molecular basis of resistance. *Oncogene*, 22, 7265-7279

Soffietti, R., Baumert, B.G., Bello, L., von, D.A., Duffau, H., Frenay, M., Grisold, W., Grant, R., Graus, F., Hoang-Xuan, K., Klein, M., Melin, B., Rees, J., Siegal, T., Smits, A., Stupp, R., & Wick, W. 2010. Guidelines on management of low-grade gliomas: report of an EFNS-EANO Task Force. *Eur.J Neurol.*, 17, (9) 1124-1133

Soling, A., Sackewitz, M., Volkmar, M., Schaarschmidt, D., Jacob, R.H.H.-J., & Rainov, N.G. 2005. Minichromosome maintenance protein 3 elicits a cancer-restricted immune response in patients with brain malignancies and is a strong independent predictor of survival in patients with anaplastic astrocytoma. *Clinical Cancer Research*, 11, 249-258

Sorokin, A.V., Kim, E.R., & Ovchinnikov, L.P. 2007. Nucleocytoplasmic transport of proteins. *Biochemistry (Mosc.)*, 72, (13) 1439-1457

Soulet, F., Kilarski, W.W., Antczak, P., Herbert, J., Bicknell, R., Falciani, F., & Bikfalvi, A. 2010. Gene signatures in wound tissue as evidenced by molecular profiling in the chick embryo model. *BMC Genomics*, 11, (495) 1471-2164

Spiering, D. & Hodgson, L. 2011. Dynamics of the Rho-family small GTPases in actin regulation and motility. *Cell Adh.Migr.*, 5, (2) 170-180

Stengel, K. & Zheng, Y. 2011. Cdc42 in oncogenic transformation, invasion, and tumorigenesis. *Cell Signal*, 23, (9) 1415-1423

Su, L., Agati, J.M., & Parsons, S.J. 2003. p190RhoGAP is cell cycle regulated and affects cytokinesis. *The Journal of Cell Biology*, 163, (3) 571-582

Symons, M. 2003. *Rho GTPases - Molecular Biology Intelligence Unit* Georgetown, Texas, USA, Kluwer Academic / Plenum Publishers.

Szklarczyk, D., Franceschini, A., Wyder, S., Forslund, K., Heller, D., Huerta-Cepas, J., Simonovic, M., Roth, A., Santos, A., Tsafou, K.P., Kuhn, M., Bork, P., Jensen, L.J., & von Mering, C. 2015. STRING v10: protein-protein interaction networks, integrated over the tree of life. *Nucleic Acids Res*, 43, (Database issue) D447-D452

Tamanoi, F., Kato-Stankiewicz, J., Jiang, C., Machado, I., & Thapar, N. 2001. Farnesylated proteins and cell cycle progression. *Journal of Cellular Biochemistry Supplement*, 37, 64-70

TCGA 2008. Comprehensive genomic characterization defines human glioblastoma genes and core pathways. *Nature*, 455, (7216) 1061-1068

Thompson, E. L. Cell Growth Protocol for U87 cell line. 2009. Myers Laboratory. Online Source.

Torigoe, T., Izumi, H., Ishiguchi, H., Yoshida, Y., Tanabe, M., Yoshida, T., Igarashi, T., Niina, I., Wakasugi, T., Imaizumi, T., Momii, Y., Kuwano, M., & Kohno, K. 2005. Cisplatin resistance and transcription factors. *Curr.Med.Chem.- Anti-Cancer Agents*, 5, (1) 15-27

Tran, E.J., King, M.C., & Corbett, A.H. 2014. Macromolecular transport between the nucleus and the cytoplasm: Advances in mechanism and emerging links to disease. *Biochim.Biophys.Acta*, 1843, (11) 2784-2795

Tu, D., Li, Y., Song, H.K., Toms, A.V., Gould, C.J., Ficarro, S.B., Marto, J.A., Goode, B.L., & Eck, M.J. 2011. Crystal Structure of a Coiled-Coil Domain from Human ROCK I. *PLOS ONE*, 6, (3) e18080

Ulrich, H., Bocsi, J., Glaser, T., & T+írnok, A. 2014. Cytometry in the brain: studying differentiation to diagnostic applications in brain disease and regeneration therapy. *Cell Proliferation*, 47, (1) 12-19

Vega, F. & Ridley, A.J. 2008. Rho GTPases in cancer cell biology - Minireview. *Federation of European Biochemical Societies Letters*, 582, 2093-2101

Verhaak, R.G.W., Hoadley, K.A., Purdom, E., Wang, V., Qi, Y., Wilkerson, M.D., Miller, C.R., Ding, L., Golub, T., Mesirov, J.P., Alexe, G., Lawrence, M., O'Kelly, M., Tamayo, P., Weir, B.A., Gabriel, S., Winckler, W., Gupta, S., Jakkula, L., Feiler, H.S., Hodgson, J.G., James, C.D., Sarkaria, J.N., Brennan, C., Kahn, A., Spellman, P.T., Wilson, R.K., Speed, T.P., Gray, J.W., Meyerson, M., Getz, G., Perou, C.M., & Hayes, D.N. 2010. Integrated Genomic Analysis Identifies Clinically Relevant Subtypes of Glioblastoma Characterized by Abnormalities in PDGFRA, IDH1, EGFR, and NF1. *Cancer Cell*, 17, (1) 98-110

Villalonga, P., Fernandez de Mattos, S., & Ridley, A.J. 2009. RhoE Inhibits 4E-BP1 Phosphorylation and eIF4E Function Impairing Cap-dependent Translation. *The Journal of Biological Chemistry*, 284, (51) 35287-35296

Villalonga, P., Guasch, R.M., Riento, K., & Ridley, A.J. 2004. RhoE inhibits cell cycle progression and Ras-induced transformation. *Molecular and Cellular Biology*, 24, (18) 7829-7840

Villalonga, P. & Ridley, A.J. 2006. Rho GTPases and cell cycle control. *Growth Factors*, 24, (3) 159-164

Visvikis, O., Maddugoda, M.P., & Lemichez, E. 2010. Direct modifications of Rho proteins: deconstructing GTPase regulation. *Biol Cell*, 102, (7) 377-389

Wickman, G.R., Julian, L., Mardilovich, K., Schumacher, S., Munro, J., Rath, N., Zander, S.A., Mleczak, A., Sumpton, D., Morrice, N., Bienvenut, W.V., & Olson, M.F. 2013. Blebs produced by actin-myosin contraction during apoptosis release damage-associated molecular pattern proteins before secondary necrosis occurs. *Cell Death Differ.*, 20, (10) 1293-1305

Williams, M.J. & Rottner, K. 2010. Introduction to *Small GTPases*. *Landes Biosciences* 1. Online Source.

- Wong, A.W., Scales, S.J., & Reilly, D.E. 2007. DNA Internalized via Caveolae Requires Microtubule-dependent, Rab7-independent Transport to the Late Endocytic Pathway for Delivery to the Nucleus. *Journal of Biological Chemistry*, 282, (31) 22953-22963
- Xia, H., Li, M., Chen, L., Leng, W., Yuan, D., Pang, X., Chen, L., Li, R., Tang, Q., & Bi, F. 2013. Suppression of RND3 activity by AES downregulation promotes cancer cell proliferation and invasion. *Int.J Mol Med.*, 31, (5) 1081-1086
- Xu, D., Farmer, A., Collett, G., Grishin, N.V., & Chook, Y.M. 2012. Sequence and structural analyses of nuclear export signals in the NESdb database. *Mol Biol Cell*, 23, (18) 3677-3693
- Yu, Z., Liu, M., Fu, P., Xie, M., Wang, W., & Luo, X. 2012. ROCK inhibition with Y27632 promotes the proliferation and cell cycle progression of cultured astrocyte from spinal cord. *Neurochem.Int.*, 61, (7) 1114-1120